10-30-2017 2:00 PM

Novel Night and Day Control of a PV Solar System as a STATCOM (PV-STATCOM) for Damping of Power Oscillations

Hesamaldin Maleki, *The University of Western Ontario*

Supervisor: Professor Rajiv K. Varma, *The University of Western Ontario*
A thesis submitted in partial fulfillment of the requirements for the Doctor of Philosophy degree in Electrical and Computer Engineering

Abstract

Installations of large scale PV solar farms are rapidly increasing, worldwide. This is causing a growing apprehension that inertialess power injections from these inverter based generators will result in a decline in power system stability. Instead, this thesis presents novel applications of a patent pending technology whereby the PV solar farms actually help significantly increase system stability. A novel 24/7 (night and day) control of a large-scale PV solar farm as a dynamic reactive power compensator STATCOM, termed PV-STATCOM, is presented for damping low-frequency electromechanical power oscillations resulting in a significant improvement in power transfer capability of existing power transmission systems. A new real and reactive power modulation based control of PV-STATCOM is demonstrated during daytime that combines the functionalities of both a STATCOM and a Battery Energy Storage System (BESS) to provide significantly enhanced levels of power oscillation damping than that achieved by either a STATCOM or a BESS.

The effectiveness of the proposed PV-STATCOM Power Oscillation Damping (POD) control techniques based on modulation of reactive power, real power or a combination of both is evaluated through both small signal and Electromagnetic Transients simulations studies. Participation factor analysis is utilized for selection of appropriate control signals and damping controllers. The POD controllers are designed through small signal Residue analysis and validated through Simplex Optimization technique in electromagnetic transient simulations. The efficacy of the proposed PV-STATCOM controls is demonstrated on three power systems: Single Machine Infinite Bus SMIB system, Two-Area system, and the 12 bus FACTS power system, which exhibit different power oscillation modes. New ramp up techniques for power restoration from solar farms are also presented, which are substantially faster than those specified by grid codes. A methodology for coordination of proposed PV-STATCOM controls with existing Power System Stabilizers (PSSs) on synchronous generators is further described for further damping enhancement.

This thesis thus presents a novel technology that can not only help increase the penetration of large scale PV solar farms but utilize them for reducing the need for construction of expensive new lines or use of costly Flexible AC Transmission systems for stability improvement.

Keywords

Photovoltaic (PV) Solar Farms, STATCOM, PV-STATCOM, Flexible AC Transmission System (FACTS), Power System Stabilizer (PSS), Optimization, Small Signal Analysis, Power Oscillation Damping (POD), Battery Energy Storage System (BESS), Reactive Power Compensation, Transmission Limits, Electromagnetic Transients Study (EMT), Real Power Restoration, Control Coordination.

Devoted to:

My parents, My beautiful wife Maedeh, and aunt Maryam

Acknowledgments

I would like to thank my supervisor Professor Rajiv K. Varma for his generous support, patience, motivation, and helpful guidance throughout my graduate studies at Western University. The contribution he made to my academic and social life is more than to be conveyed in words.

I would also like to thank Professor Vigna Kumaran Ramachandaramurthy for his continued support throughout my studies, for his trust in me and for giving me the chance to join his great team to enrich my industrial knowledge.

Special thanks to my friends that supported me throughout my studies with all means possible. Thank you Mohamad Ranjbaran for being my second brother and helping me with your great comments throughout my study. Thank you Alireza Arfa and Maryam Nikoonasiri for being my family here.

Last, and most importantly, I would like to express my sincere gratitude to my parents, my wife, my brother and his wife, and my aunt, Maryam. My hardworking father Mohamad Maleki and caring mother Ziba Shirazi who taught me the real meaning of life, faithfulness, and love. My brother Dr. Hosein Maleki and his wife, Dr. Mahsa Kaviani for their continuous encouragement and support. My wife, Maedeh Esmizadeh for her patience, unwavering love, countless sacrifices, and the faith she had in me. I also would like to thank my wife's family for their spiritual support, beautiful smiles, and kind considerations. Finally, my aunt Maryam Shirazi, there is no possible way to thank you for sacrifices from the first moment I was born.

List of Abbreviations

PV	Photo Voltaic
MW	Mega Watts
s	Second
Hz	Hertz
AVR	Automatic Voltage Regulator
PSS	Power System Stabilizer
STATCOM	STATic synchronous COMpensator
AC	Alternating Current
FACTS	Flexible AC Transmission System
POD	Power Oscillation Damping
TCSC	Thyristor Controlled Series Compensator
SVC	Static Var Compensator
IGBT	Insulated Gate Bipolar Transistor
GTO	Gate Turn-Off Thyristors
PCC	Point of Common Coupling
VSC	Voltage Source Converter
PWM	Pulse Width Modulation
SPWM	Sinusoidal Pulse Width Modulation
BESS	Battery Energy Storage System

DER	Distributed Energy Resources
DG	Distributed Generations
IEEE	Institute of Electrical and Electronics Engineers
SMIB	Single Machine Infinite Bus
Q-POD	Reactive power based Power Oscillation Damping
P-POD	Real power based Power Oscillation Damping
PQ-POD	Real and Reactive power based Power Oscillation Damping
OF	Objective Function
PF	Participation Factor
EMT	Electro Magnetic Transients
EMTDC	Electro Magnetic Transient Design and Control
PSCAD	Power System Computer Aided Design
MP	Maximum Power
DC	Direct Current
VRT	Voltage Ride Through
SG	Synchronous Generator
ONR	Off-Nominal Turn Ratio

List of Symbols

H	Generator inertia constant
I	Current
φ	Voltage Angle
λ	Complex eigenvalue
P	Active power
Q	Reactive Power
R	Resistance/Residue
V	Voltage
I	Current
T	Time
L	Inductance
C	Capacitance
F	Farad
X	Reactance
exp	Exponential
ϕ	Right eigenvector
ε	Error
τ	Settling time constant
ρ	Phase angle

θ	Voltage angle
ω	Speed/Modal Frequency
Δ	Delta transformer winding configuration/Variation
ξ	Damping Ratio
Ω	Sigma (Ohm unit)
μ	Mu (micro unit)
G	Compensator gain/Generator symbol

Table of Contents

List of Tables

List of Figures

List of Appendices

Chapter 1

1 Introduction

Environmental concerns related to power generation with fossil fuels on one hand and the limitation of hydro and gas power plants on the other have caused a surge of interest and investments in the integration of renewable energy sources. In theory, renewable energy sources are able to provide 3000 times more power than the current global energy needs [1]. Among all renewable energy sources such as Hydro, Geothermal, and Bioenergy, Wind and Photovoltaic (PV) power are seeing the maximum growth.

According to a Global Wind Energy Council (GWEC) 2014 report [2], the total wind power plant installation in 2014 has reached 51,473 MW with the highest contribution of 45.1% from China. Additionally, the price reduction in power generation with PV units [3] has resulted in a rapid increase in PV power generation around the world. Solar power generation is experiencing a rapid growth at a rate of almost 40% worldwide [4] with governmental organizations enforcing utilities to supply their demands by renewable energy sources. For example, states such as New Jersey and New York are planning to supply more than 20% of their electricity demand by 2021 through renewables. In addition, according to [5], 8% of all of Ontario's energy demand will be supplied by PV generation by 2025. To reach this goal, installation of utility-scale PV plants (in order of MWs) on the Ontario power network is predicted. Figure 1.1 illustrates the exponential growth in solar power generation globally [6]. An increase in the penetration of PV power plants, especially plants with utility-scale power rating, reduces the need for conventional sources of power, such as synchronous generators [7].

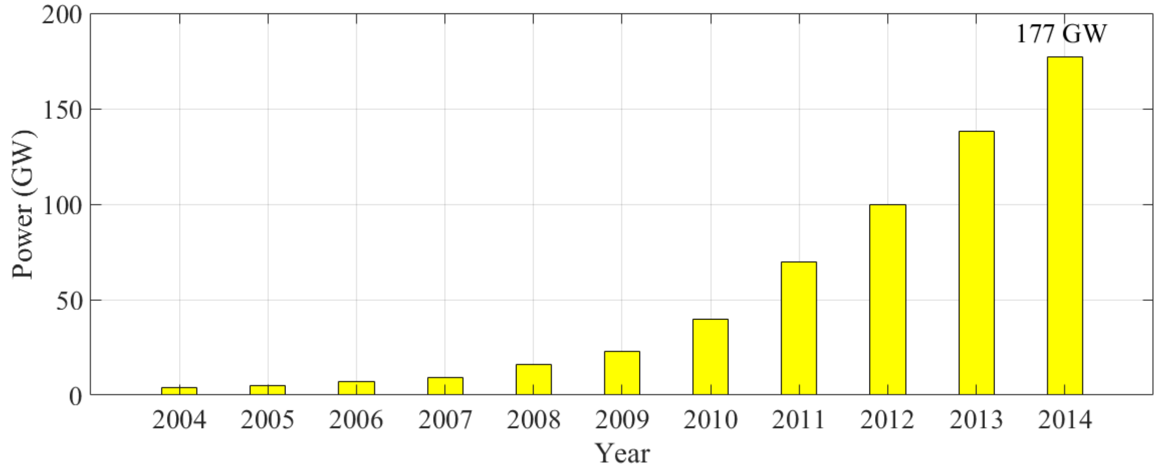

Figure 1.1Total solar power global capacity [6]

In this thesis, the main goal is to propose novel control techniques for utility-scale PV systems in order to overcome the stability challenges with the interconnection of large-scale PV power plants to existing power networks, as well as to further improve the stability performance of power systems through novel power oscillation damping controls for these large-scale power plants.

1.1 Large PV Solar Systems

Recently, large-scale PV solar farms with more than 100 MW capacity have been connected worldwide, such as: Kamuthi, in Tamil Nadu, India (648 MW) [8], Solar Star I and II (579 MW) in USA, Rancho Cielo Solar Farm (600 MW), Topaz Solar Farm (550 MW), Costas, Aquitaine project in France (300 MW) [9], Agua Caliente Solar Project (295 MW) in Arizona, USA, California Valley Solar Ranch Farm (250 MW), USA, Huanghe Hydropower Golmud Solar Park in China (200 MW) [10-12], Neuhardenberg Solar Park in Germany (145 MW)[13]. These sizes of solar farms are fast becoming comparable to conventional synchronous generators.

1.2 Power System Stability

The ability of a power system to remain in a state of equilibrium point during the normal power system operation and then regain the state of equilibrium after small and/or large disturbances is defined as the power system stability [14]. Power systems are subjected to small disturbances such as load switching and large disturbances such as line, generator or transformer outages due to faults. The power system needs to maintain its operation by properly responding to these disturbances without failure. As a power system expands and more loads and generation units are connected to the system, it is more likely that the number of disturbances will increase in the network. Power system stability is classified as follows:

1.2.1 Mid and Long-term Stability

Mid and long-term stability are defined as the dynamic response of the power system to severe contingencies which result in frequency deviation. The power system instability in the mid-to-long-term occurs within seconds to minutes in which the conventional power system governors and excitation units are not able to properly address the contingency due to their fast or slow response times [14-16].

1.2.2 Rotor Angle Stability

Rotor angle stability determines the ability of interconnected synchronous machines in the power system to maintain their synchronism. The rotor stability involves the electromechanical oscillations of power systems in which the power output of the synchronous generators varies with the generator rotor angle. These electromechanical oscillations are in the frequency range of 0.1 to 2 Hz [14] which are divided into two main categories:

- Local mode oscillations due to the oscillation of a single generator with respect to the rest of the power system with a frequency range of 1 to 2 Hz.

- Inter-area mode of oscillations resulting from the swing of a group of generators in one part and other groups of machines on another part of the power system. These oscillations have a relatively lower frequency range of 0.1 to 0.8 Hz.

1.2.3 Voltage Stability

Voltage stability refers to the ability of a power system to maintain voltages at all buses in an acceptable range. System instability occurs due to a lack of adequate reactive power support causing the bus voltages to decrease with increased loading, and eventually collapse. A good example of voltage instability is that which led to the 2003 blackout in North America as reported in [17]. The attempts from the operators to restore the voltage were unsuccessful and voltage continued decreasing following cascading line outages. In [18] voltage control techniques for voltage stability improvements of power systems are presented for an Italian power system. It is indicated that the proper response time is required to maintain the power system voltage stability during voltage drop in the power system.

1.2.3.1 Case Study

On August 10th 1996, following a series of disturbances, the Western System Coordinating Council (WSCC) grid in the USA broke up into four islanded regions affecting 7.5 million customers [19]. Figure 1.2 illustrates the line power flow from California-Oregon Intertie (COI).

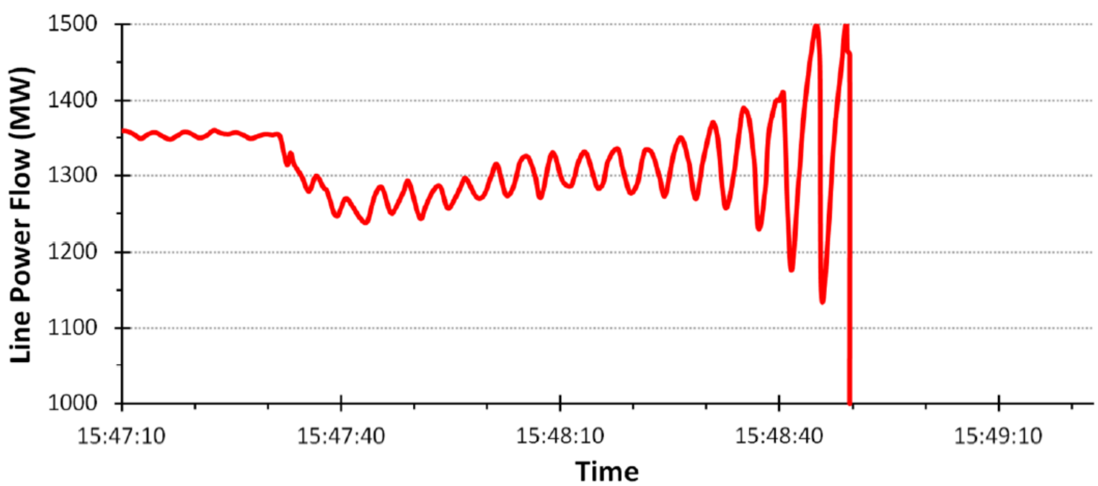

Figure 1.2 Line power flow from California-Oregon Intertie (COI) [19]

Illustrated in Figure 1.2 is the inter-area electromechanical mode of oscillation growth with an oscillation frequency of 0.24 Hz and damping ratio of -2.66% between northern and southern parts of the WSCC grid. This example is one of many occurrences of power oscillations in interconnected power systems. Other major examples include a 0.15 Hz oscillation through the synchronous interconnection of the Turkish Power System to the

European Network of Transmission System Operators for Electricity ENTSO-E [20], and 0.22 to 0.26 Hz oscillations in UCTE/CENTREL Power System [21]. These low-frequency power oscillations are a limiting factor for power transmission through long transmission lines [22] as shown in Figure 1.3.

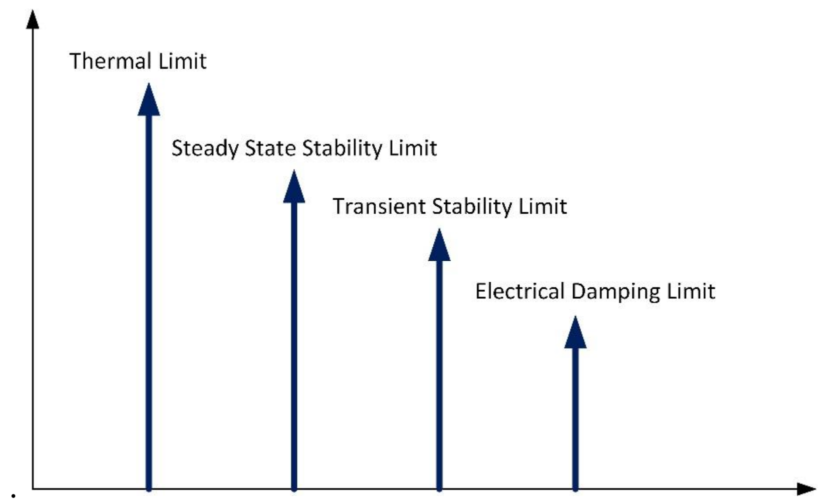

Figure 1.3 Power transmission limits.

Figure 1.3 [23] depicts that in order to increase the transmission capability of existing transmission lines, improvements in the electrical damping limit may be required. With regards to the increasing demand for transmitting larger amounts of power through existing transmission lines, this thesis presents improvements in inter-area power oscillations with a novel control concept of large-scale PV systems.

1.3 Impact of PV Solar Farms on Power Oscillations

Traditional power systems have full control over power generation by balancing variable demand and generation through controlling the active power generation in the power utilities. Whilst, future power systems with utility-scale solar power plant interconnections will experience not only variable power demand but also variability in generation caused by changes in the solar radiation and ambient temperature [24]. Table 1.1 illustrates the main advantages and disadvantages of various power generation units.

Table 1.1 Comparison among PV, Wind, and Conventional power plants[25]

Characteristics	PV	Wind	Conventional Generator
Fluctuation	High	Low	No
Cost for Large-scale	High	Moderate	Low to moderate
Maintenance cost	Minimal	High	Moderate
Inertia	No inertia	Low inertia	Large Inertia
Capacity factor	Very low	Low to moderate	High
Annual growth	Very high	High	High

As shown in Table 1.1, one of the concerns regarding large-scale PV power plants is the absence of inertia in these power units. Some reports have examined the effect of these large-scale solar power plants on power system stability. In [26] the effect of large-scale and distributed photovoltaic solar generation units on power system stability have been studied for the province of Ontario. Furthermore, in [25, 27, 28] the effect of increase in the PV power penetration on power system stability has been illustrated. According to [25], the replacement of existing synchronous generators with PV solar power plants will further reduce the power system stability by decommissioning the auxiliary synchronous generator controllers such as Automatic Voltage Controllers (AVR). It is therefore evident from the above studies that inertia-less PV power generation can adversely affect the power systems small signal and transient stability.

1.4 Power Oscillation Damping with FACTS Devices

Power System Stabilizer (PSS) units are traditionally installed on the generator exciter units for damping of these power oscillations, [14, 29]. On the other hand, Flexible AC Transmission System (FACTS) devices have demonstrated the capability to effectively damp both inter-area and local mode oscillations. Some practical examples can be found in [30] such as: stability improvement in Furnas/Brazil with 500 kV Thyristor Controlled Series Compensator TCSC, where TCSC damping function is activated hundreds of times a day to stabilize the power system, [30] and Raipur 71 MVar TCSC in India in which the inter-area mode of oscillations for a 412 km long transmission line between Eastern and Western regions of the Indian grid is dampened [31]. Voltage Source Converter based FACTS devices such as STATic synchronous COMpensator (STATCOM) can be used to further improve the power system stability. In [32], a comparative study between various FACTS devices for Power Oscillation Damping (POD) is presented. As shown in [32], STATCOM devices can significantly increase the stability margins of the power system, especially during the contingencies. The other advantage of STATCOM devices compared to series FACTS devices, such as TCSC, is the voltage profile improvement whereby STATCOMs can improve the voltage stability of the power system. Power system stability improvements with STATCOMs have been studied widely in the literature [33-36]. Although the advantages of STATCOM equipped with Power Oscillation Damping (POD) controllers for damping low-frequency power oscillations are illustrated in these studies, STATCOMs are more expensive in comparison to other FACTS devices such as TCSCs and Static Var Compensators (SVC). The price range for these devices per kW can be found in [37]. Hence, a cost-benefit analysis has to be done to evaluate the suitability of these expensive devises for POD [32].

1.4.1 STATCOM

STATCOM is a shunt-connected reactive power compensation device which mainly consists of a DC link capacitor bank, solid-state switches such as Gate Turn-Off Thyristors (GTO) or Insulated Gate Bipolar Transistor (IGBT). An AC filter is used to eliminate the high order harmonic frequencies and interfacing transformer. The main purpose of installing a STATCOM on the power system is to enhance the power system performance with a very fast response time (in order of a few cycles).

A difference in the magnitude of the voltage at the STATCOM terminal and Point of Common Coupling (PCC) results in bi-directional reactive power flow from STATCOM to PCC and vice versa. Whenever the voltage at the STATCOM terminal is greater than the PCC voltage, STATCOM injects reactive power into the PCC. This behavior of the STATCOM is the same as the behavior of the shunt capacitor. On the other hand, if the voltage at the STATCOM terminal is less than the voltage of the PCC, the STATCOM absorbs the reactive power from the PCC and behaves like an inductor.

The advantage of STATCOMs over fixed capacitor banks and shunt inductors connected to the grid is the rapidity of its control. Since the STATCOMs exchange reactive power using semiconductor devices, power losses are incurred in the operation of these devices. Hence, in order to keep the capacitor voltage at its desired value, a small amount of active power is absorbed from the grid by the STATCOM to keep the capacitor charged during its operation.

The basic configuration of a STATCOM is a two-level 3-phase Voltage Source Converter (VSC). A Pulse Width Modulation (PWM) technique is used to generate the *On* and *Off* firing signals for IGBTs or GTOs. Different PWM techniques have been presented in the literature, such as Sinusoidal PWM (SPWM) and Space-Vector PWM. Comparative studies of the performance efficiencies of different PWM techniques are presented in [38] and [39]. The specific technique of PWM is mainly selected based on the inverter application. Among PWM techniques, SPWM technique, as a basic and common technique, has shown acceptable results in most of the power system studies.

In SPWM, by comparing three sinusoidal signals with three carrier signals, firing pulses for IGBT or GTO units are generated. It is shown that the switching of semiconductor devices results in harmonic injection to the PCC [40]. Hence, for higher voltage applications, STATCOMs with multilevel inverter features have been proposed in [41-43].

1.4.1.1 Control Characteristics

Despite different STATCOM topologies, the operating characteristic of the STATCOMs is the same. The Voltage-Current Characteristic of STATCOMs is presented in Figure 1.4. It is noted that the STATCOM can provide rated capacitive current even at very low voltages, which is not the case with Static Var Compensators (SVCs) [22].

1.4.1.2 Control Techniques with Case Studies

STATCOMs have been installed on various power systems, such as a 140 MVAR STATCOM in Carro Navia [44], a 140 MVAR STATCOM in the Zhangjiagang plant, Eastern China [45] and a 16 MVAR STATCOM in Evron, France [46]. According to [44] to [46], it is shown that the actual installation of STATCOMs can help the power system in different ways. For example, in [44], the STATCOM is used for voltage stability and an increase in the power transfer capability of the network; in [45], the STATCOM is used for

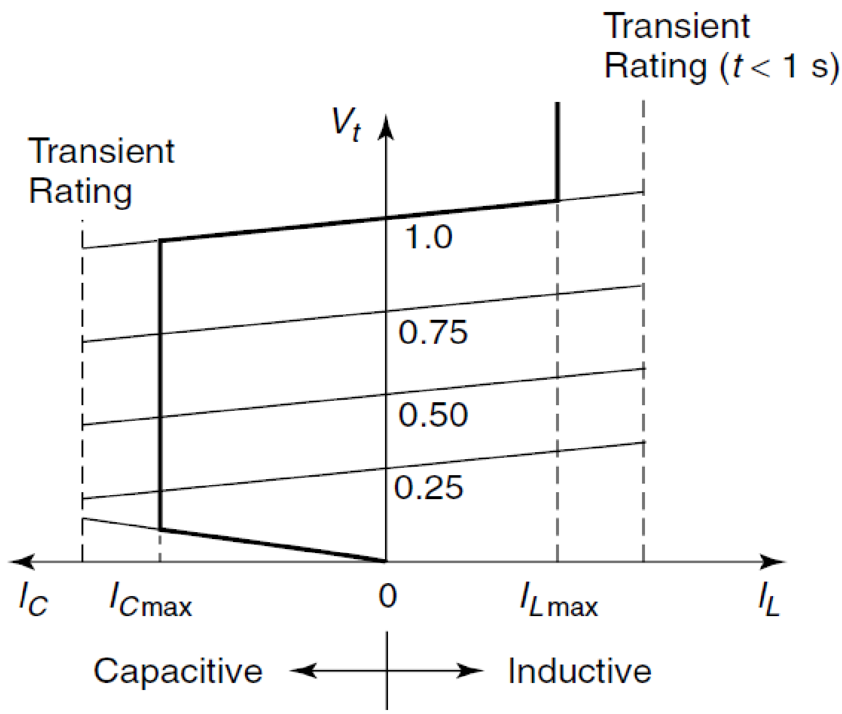

Figure 1.4 The voltage-current characteristic of the STATCOM [22]

power factor correction in a very large arc furnace in a steel company. The dynamic control of the positive, negative and zero sequence currents due to the existence of an unbalanced load from a railway company is presented in [46]. Besides these actual installations of STATCOMs, many studies have presented various other control strategies for STATCOM devices such as the mitigation of Sub-Synchronous Resonance [47] and an increase in fault ride-Through capability of wind farms [48]. The main idea behind all the aforementioned control strategies is to control the voltage at the PCC by rapidly exchanging reactive power from the STATCOM with the grid.

1.4.1.3 Optimized Coordinated Controller Design

Although improvements in power system stability with POD controllers in FACTS devices have been shown in the literature, the adverse interaction between POD controllers and existing PSS units in the power system has been addressed in [49, 50]. Hence, FACTS devices need to be coordinated with PSSs to avoid any adverse interaction [51]. A technique for controller coordination of PSS and FACTS has been proposed in [50, 52, 53]. In [52], the optimization is done based on minimizing the dynamic oscillations of the line power. In [53], optimization based on a pole placement approach has been adopted. The pole placement technique which is used in most of the literature is performed based on a linearized model of the power system. In addition, according to [54], other objective functions, including PSS gain, should also be minimized in order to reduce the excessive controller effort of PSS. After the controllers are designed based on power system linearized model, additional studies are required to evaluate the performance of the controllers in detailed EMT-type simulation studies. In this thesis, a simple though effective technique for coordination between PSS and POD controllers is presented in which the entire coordination and optimization of controllers are performed in detailed EMT-type simulation studies.

1.4.1.4 Placement of FACTS Devices for POD

The location of FACTS devices has a major impact on their performance in the power system. In [55] the optimal location of FACTS devices based on enhancement of steady-state stability of the power systems is presented. In [56], the placement of FACTS devices to increase the loadability of a power system is described. In [57-59], the techniques to determine optimal locations of FACTS devices for damping low-frequency power oscillations are proposed. Since FACTS devices mainly operate based on reactive power modulation, the optimal location selection is based on the effectiveness of reactive power controllers on the power system. In [58], the placement technique based on residue analysis for energy storage devices is presented. In this thesis, the effect of location of the PV power system based on its real and reactive power output is presented.

1.4.2 Energy Storage Devices

Large scale energy storage devices such as Flywheel Energy Storage Systems (FESS) and Battery Energy Storage Systems (BESS) can effectively improve the performance of power systems. Some examples are: AES Energy Storage Angamos Battery Energy Storage System (BESS), in which 20 MW/5MWh BESSs are used for frequency regulation purposes and 36 MW BESS for improving grid stability and integrating wind energy in Younicos Battery Park [60]. In [61-63] POD with energy storage devices is presented. Although it is demonstrated that the POD based energy storage devices can increase the damping ratio of selected mode of oscillations, the comparison between these devices with other FACTS devices for POD has not been studied. Furthermore, the battery models are simple voltage source with a converter in which other BESS dynamics are not considered during the transients.

1.5 Control of PV Solar Farms as STATCOM (PV-STATCOM)

1.5.1 Smart Inverters

In 2009, EPRI's Photovoltaic & Storage integration program started a new set of studies for high penetration of Distributed Energy Resources (DER) [6]. The term "Smart Inverter" was proposed for any inverter-based Distributed Generation (DG) that is facilitated with any real or reactive power controller features. The goal of this project was to enable high-penetration scenarios in which different energy resources such as PV and BESS operate in a smart and beneficial way [6]. This initiative involved many inverter manufacturers, utilities, universities and other research organizations. The results from the research have provided valuable inputs for Standards developed by the National Institute of Standards and Technology (NIST) and the International Electronics Commission (IEC), including IEEE 1547 and California Rule 21. Recently many papers have used the term Smart-Inverter for any active control strategy related to DG inverters. These control strategies mainly refer to reactive power modulation with remnant DG inverter capacity [25, 64-66]. Based on Rule 21, future smart PV inverters can have the ability to regulate the PV real power as well.

1.5.2 Updates in Standards for PV Interconnections

The DERs have been widely installed on the distribution systems. Besides all the benefits of DER interconnection to the power systems, such as improvement in voltage profile, reduction in the line and transformer losses, reduction in environmental impact and enhancement in power quality, [67] many studies have shown the adverse effects of DER interconnection to the distribution systems. To minimize many of the aforementioned problems, standards such as IEEE 1547-2003 have been established. Based on IEEE Std 1547-2003, "the DER shall not actively regulate the PCC voltage". According to this standard, voltage regulation by DERs may conflict with other areas of Electrical Power Systems. In the meantime, some studies have shown the drawback of this non-active DG power control and proposed new control strategies to overcome these challenges by active control strategies for DG inverters [68-70]. On the other hand, current standards such as IEEE 1547 [71], VDE-AR-N 4105: 2011 [72] (low voltage) BDEW-2008 [73] (medium/high voltage) in European standard, AS 4777-2005 in New Zealand and IEC 61727-2004 [17] for PV interconnections provide the specifications of reactive power regulation for inverter based DGs [74]. According to [74], it is seen that European standards provide more flexibility in reactive power modulation from DG inverters than IEEE 1547. For example, the VDE and BDEW both addressed the voltage support from the DG inverters by reactive power injection or absorption, while in IEEE 1547, DGs shall not actively regulate the PCC voltages. It can be inferred that current standards need to be further reviewed to permit the DG controllers to actively participate in power system issues at their PCC. Hence, new regulations have been presented for DG operations such as Rule No. 21. In Rule 21, it has been stated that “the smart inverters may actively regulate the voltage at the PCC while in parallel with Distribution Provider’s Distribution system”. Along with development in Rule 21, IEEE 1547 series have presented a new version of IEEE 1547 as IEEE 1547a which allows the DG inverters to control the voltage at PCCs.

1.5.3 POD with PV-STATCOM

A novel patented control of PV solar farms as STATCOM (PV-STATCOM) was presented for enhancing the connectivity of wind farms in the night [75] and for increasing power transfer capacity through damping of power oscillations both during night and day [76]. This control technique utilized the entire inverter capacity in the nighttime and the inverter capacity remaining after real power generation during daytime for power oscillation damping. An eighth-order POD controller for large PV solar farm was proposed in [77], whereas an energy function based design of POD controller was presented in [78]. Both these controllers are relatively complex in design. All the POD controls in the above papers [75-78] are based on remaining inverter capacity during daytime. Hence, the proposed POD capability of solar farm is limited during daytime, in fact becoming zero during hours of full sun. Further, the effectiveness of the proposed control technique with different possible PV plant locations has not been studied.

In [79], the real and reactive power POD controller for PV system is proposed. The study is done for a Single Machine Infinite Bus (SMIB) system. In this study, the effect of different PV real power generation levels has not been investigated. Furthermore, the proposed controller only addresses one mode of oscillations. It is noted from the studies that the effect of variation of PV real power on POD effectiveness needs to be further investigated. In addition, a comparison between the effect of real and reactive power based POD controllers for PV systems needs to be performed.

1.6 Scope and Objectives of the Thesis

The objective and the scope of this thesis are as follows:

1. Examine the effectiveness of novel, patent-pending, real and reactive power based power oscillation damping (POD) controls of PV-STATCOM in various study systems exhibiting multiples oscillatory modes. These controls include real power based power oscillation damping controller (P-POD), reactive power based controller (Q-POD) and the combined real and reactive power based controller (PQ-POD).

2. Compare the performance of real power based on POD (P-POD) controller of varying sizes of a Battery Energy Storage System (BESS) with the Reactive power based POD (Q-POD) controller of PV-STATCOM.

3. Study of a coordinated optimized control of Power System Stabilizers (PSSs) with POD controllers of PV-STATCOM utilizing inverter capacity remaining after real power generation during daytime.

4. Examine the performance of a novel reactive power based POD Control of a PV-STATCOM utilizing the full capacity of the inverter at any time during day and night.

5. Study the effectiveness of combined real and reactive power based power oscillation damping control (PQ-POD) of the PV-STATCOM together with the influence of PV-STATCOM location in systems exhibiting both local and interarea oscillatory modes.

6. Investigate the performance of the novel PV-STATCOM POD controllers in a multimachine system exhibiting several oscillatory modes utilizing Wide Area Measurement control signals which are impacted by communication delays.

1.7 Outlines of Chapters

1. Chapter 2: presents power systems and components modeling for detailed EMTDC and small signal in PSCAD/EMTDC and Matlab Simulink software. The concept of PV-STATCOM in Partial and Full STATCOM mode of operation is discussed. Controllers design procedure and PV-STATCOM placement technique based on residue analysis are presented in this chapter.

2. Chapter 3: Presents POD with Full PV-STATCOM mode during the night time based on inverter reactive power output control Q-POD. In addition, real power based power oscillation damping P-POD control with BESS is presented. A comparative study is done to achieve the similar damping of 100 MW PV-STATCOM with BESS. This study has been performed on SMIB power system in which only one mode of oscillation is observed. To perform the comparative study, the controllers are optimized in PSCAD/EMTDC software.

3. Chapter 4: Presents the optimized coordination between PV-STATCOM POD controllers with existing PSS units. Two-Area power system is selected as the study system in which local and interarea modes of oscillations are observed. In this chapter, the partial power oscillation damping with generators PSS units and PV-STATCOM in partial mode of operation is studied. Coordination is performed in detailed EMT-type simulation in PSCAD software with Master/Slave simulation.

The performance of the PV-STATCOM in partial mode is compared with the same size actual STATCOM.

4. Chapter 5: presents novel control concept for Q-POD with PV-STATCOM in which the entire PV inverter capacity is utilized during the day and night. Two-Area power system is selected as the study power system. This POD control technique provides 24/7 POD ability from PV system regardless of the time of the day. Furthermore, novel fast ramp and nonlinear PV real power restoration with Q-POD is presented.

5. Chapter 6: presents novel combined real and reactive power POD control technique for PV systems. The controllers are design based on residue technique and further optimized in PSCAD/EMTDC software. The effect of the location of PV-STATCOM on the POD is investigated based on the small signal analysis. In addition, the effect of sudden variation in PV real power generation on power system frequency is illustrated.

6. Chapter 7: The effect of proposed PQ-POD controller on power system with multiple modes of oscillations is investigated. The effect of Q-POD and P-POD controller on each mode of oscillations are presented and controller signal selection based on available PV system real power is presented. Both EMT-Type simulation and small signal studies were conducted to justify the results. The control signal selection based on the Participation Factor analysis is presented. The effect of the PV real power injection on the power system stability with and without proposed techniques were presented.

Chapter 2

2 Power System Modeling and Controller Design

2.1 Introduction

In this chapter, the concept of PV-STATCOM is presented. The models of different power system components including transmission lines, transformers, synchronous generators, and loads for stability studies are presented. Detailed models of PV system and its various conventional and PV-STATCOM controllers are presented. The design procedures of various PV system controllers are explained. The need for detailed EMT-type and small signal study is discussed. The PV-STATCOM operation in both the domains is described. A comparison is performed between the small signal model simulation and PSCAD/EMTDC detailed model simulation of the proposed PV-STATCOM system. The POD controller design techniques and the effect of PV-STATCOM location on power system stability are explained in this chapter. Embedded Simplex optimization technique for PV-STATCOM controller design in PSCAD/EMTDC software based on Master/Slave simulation is presented. In addition, a detailed model of aggregated Battery Energy Storage System (BESS) is developed in PSCAD/EMTDC software.

2.2 PV-STATCOM Concept

The power output from the PV system during a sunny day is shown in Figure 2.1. From Figure 2.1, it is shown that even during a full sunny day, in 24 hours operation, more than 70% of overall time the PV system operates below its rated power output. A patent-pending technology has been proposed [80], according to which the PV system can be controlled as a STATCOM, termed PV-STATCOM, in different modes of operation as described below:

2.2.1 Partial STATCOM Operation Mode

In the Partial STATCOM operation mode, the PV inverter capacity remaining after real power generation is utilized for STATCOM mode of operation during daytime. In this mode, which is depicted in Figure 2.1, the priority of the controller is to convert the PV system Maximum Power (MP) from Direct Current (DC) to Alternating Current (AC), and only the remaining capacity of the inverter can be utilized for reactive power control. Hence, the capability of Partial STATCOM mode of operation is limited during noon hours when the entire inverter capacity is used up for real power generation.

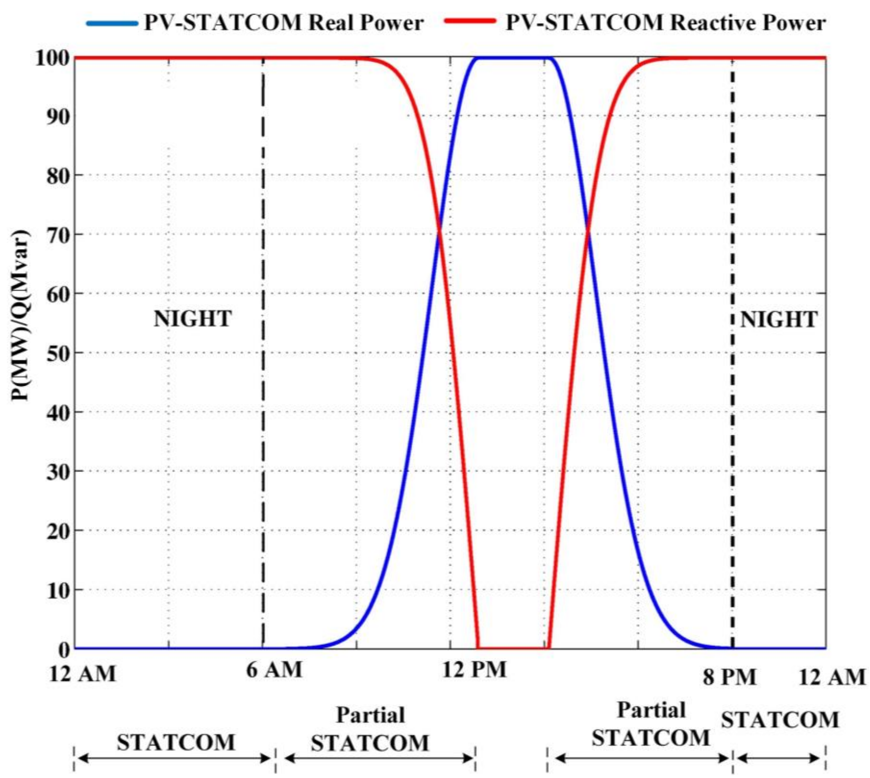

Figure 2.1 Power output of a 100MW PV system versus time on a sunny day (Partial STATCOM operation mode)

2.2.2 Full STATCOM Operation Mode

In this mode, the entire PV solar farm inverter capacity is utilized for STATCOM mode of operation. The full inverter capacity is continuously available during night time. During daytime, as soon as any unacceptable low-frequency power oscillations due to any system disturbance are detected, the real power generation function is discontinued for a brief period (typically less than a minute) and the solar inverter transforms into a STATCOM with the entire inverter capacity for power oscillation damping. If the low-frequency oscillations are damped, the real power generation function is reinstated.

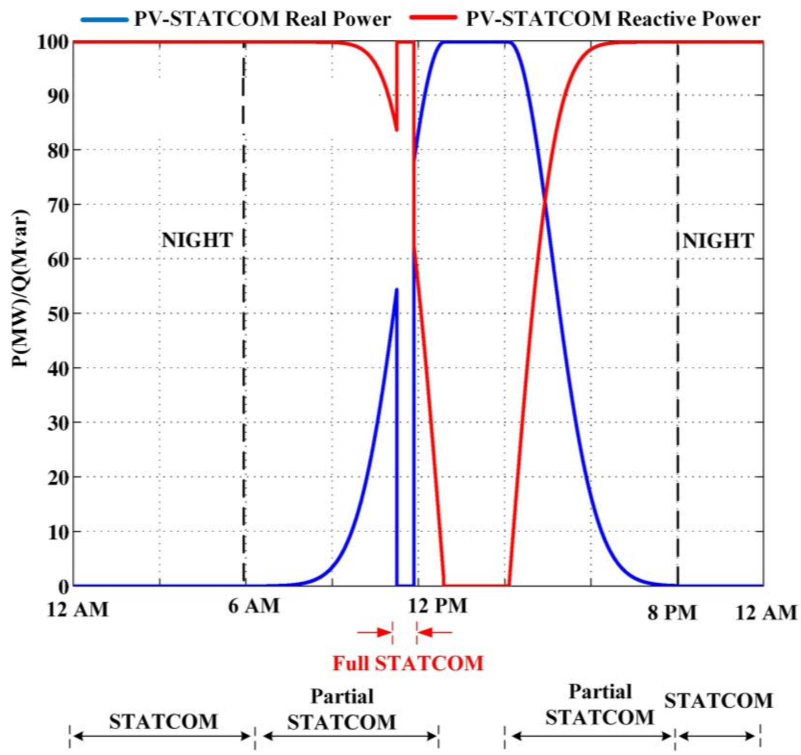

Figure 2.2 Power output of a 100MW PV system versus time on a sunny day (Full STATCOM Operation mode)

There is another mode of Full PV-STATCOM operation in which the revenue making real power generation function for the grid is discontinued for a brief period. However, during this period both real and reactive power output of PV system are controlled to damp power oscillation. This mode has been proposed in Patent [80], which will be discussed later in *Section 5.4.1*.

2.3 Power System Studies

Proposed POD controllers for PV-STATCOM system are tested on three well-known power systems to ensure the functionality of the controllers. Power systems used in this thesis are as follows:

2.3.1 Study System 1: Single Machine Infinite Bus (SMIB) System

The Single Machine Infinite Bus (SMIB) power system [81] is used as the initial system for POD controller design. Figure 2.3 illustrates the SMIB power system. A large synchronous generator is connected to an infinite bus through a 600-km line. Since SMIB power system contains one synchronous generator, during the contingencies such as a fault on the transmission line, only one electromechanical mode of oscillation will appear after the contingency. Hence, SMIB power system is suitable for first step development of POD controllers in which only one mode of oscillation is addressed. The data for this system is given in Appendix A.

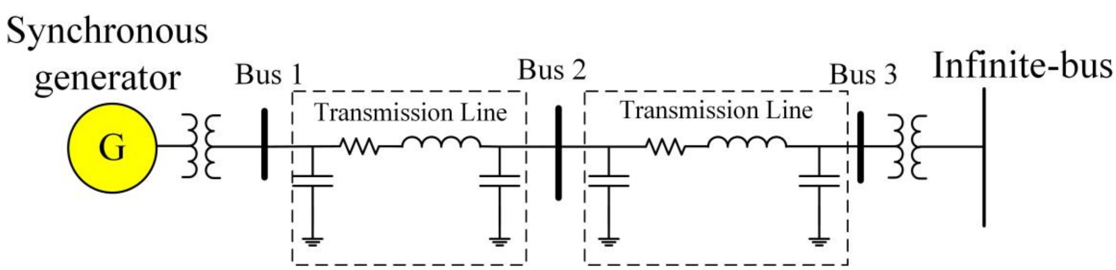

Figure 2.3 Single-line diagram of an SMIB system with a 100 MW PV plant connected to the midline.

2.3.2 Two-Area Power System

The Two-Area power system with four machines connected with 220 km tie-line [14, 44] is depicted in Figure 2.4 This power system is widely used in literature due to the existence of local and interarea modes of oscillations [33, 44, 82]. The different modes of oscillations with respect to various generators are as follows:

a) Generators 1 and 2 oscillate against each other (Local mode 1)

b) Generators 3 and 4 oscillate against each other (Local mode 2)

c) Generators 1 and 2 oscillate against Generators 3 and 4 (Inter area mode)

The data for this system is given in Appendix B.

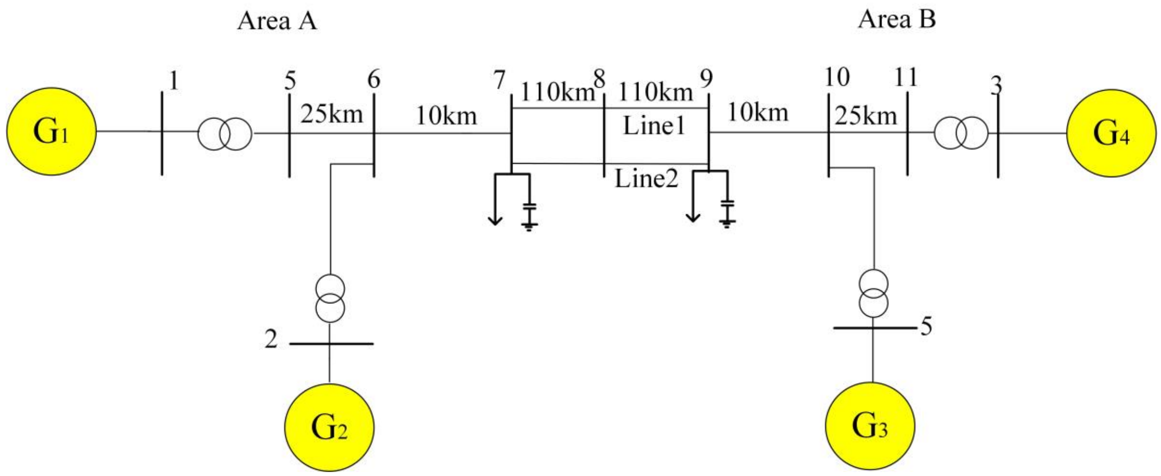

Figure 2.4 Single-line diagram of a Two-Area power system.

2.3.3 12 Bus Power System

The 12 bus FACTS power system has been proposed and is being widely used for studying the impact of FACTS controls [83-85]. This system is utilized in this thesis for study of PV-

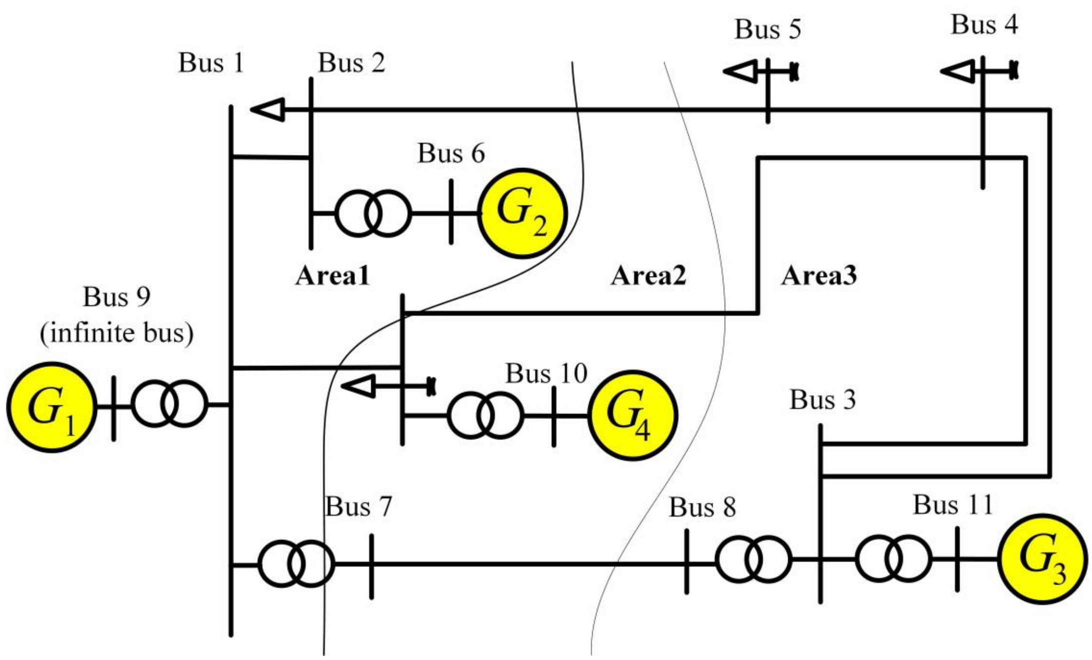

Figure 2.5 Single-line diagram of the 12-bus FACTS power system

STATCOM damping controls through both EMTDC/PSCAD software for EMT-type simulation and Matlab Simulink software for small signal studies Figure 2.5 portrays the single line diagram of 12 bus FACTS benchmark power system. This power system consists of 12 buses (six 230 kV, Two 345-kV and four 22 kV buses). As illustrated in Figure 2.5, the power system is divided into three geographical Areas 1, 2, and 3. Area 1 is mainly a generation area where most of the power is generated through hydropower. Area 2 is located between the generation area (Area 1) and the load Area (Area 3). In Area 2, one hydro generation unit is available in which the generated power is only sufficient for its local demand. Since in Area 2 the generation is limited, the system demand often must be met through 230 kV transmission lines. Area 3 which contains most of the loads is located 500 km away from Area 1. A thermal generator is available in Area 3. There is one 345 kV line connecting Area 1 to Area 3 (Bus 7 to Bus 8).

According to [83], the power system has poorly damped interarea oscillations in addition to three local modes of oscillations for each generator. Thus, this study system is considered suitable for both transient and small signal stability studies considering FACTS devices connected to the different location of the power system. The system data is given in Appendix C

2.4 Modeling of Power System Components

Many advanced simulations software currently are available to perform power system studies with detailed modeling of each component such as PSCAD/EMTDC [86], Matlab Simulink, PSS®E [87], etc. In this chapter modeling of all necessary component for stability studies are presented. These models are used throughout this thesis.

2.4.1 Synchronous Generator Modeling

Synchronous generators are the main sources of real power generation in the power system and can be modeled with a different level of complexity [14]. In this thesis, the 6-order model of synchronous generators considering the leakage reactance [14] is modeled in detailed EMT type simulation in PSCAD/EMTDC. The same generator is modeled in small signal in Matlab Simulink software assuming all phases are balanced [16].

2.4.2 Generator Excitation Modeling

Various forms of excitation systems such as DC, AC, and Static Excitation systems [88] have been used for generator voltage regulation. In this thesis, a fast DC 1 A type excitation [89] is used to regulate the generator voltage at the desired value. The general form of DC 1 A exciter system suitable for stability studies is presented in Figure 2.6 [90].

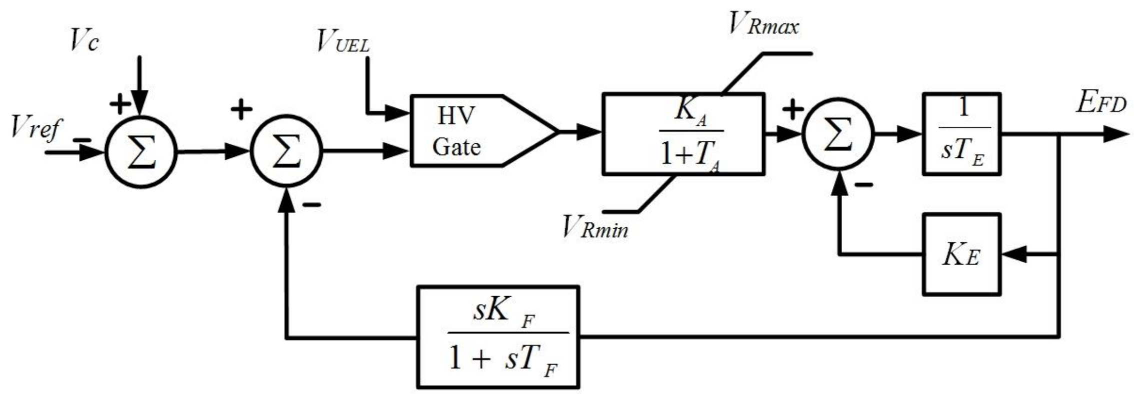

Figure 2.6 IEEE DC 1 A Excitation system model

As shown in Figure 2.6 the reference voltage (V_{ref}) is compared with the PCC voltage V_c and a compensated feedback signal from field voltage E_{FD} having a feedback rate K_F and feedback time constant T_F. High-Value (HV) gate is used only in extreme or unusual conditions to limit the output below the under-excitation signal V_{UEL}. K_A and T_A present the regulating gain and time constant, respectively. V_{Rmax} and V_{Rmin} limit the regulator output. K_E represent the exciter constant rate to field. It is common that station operators manually adjust the voltage regulator though periodically trimming rheostat set point in order to set the voltage error to zero. This action can be simulated by selecting the value of K_E. According to [90], in power system programing tools, if K_E is set to zero, program itself has to calculate the value for K_E else, K_E can be set by the programmer. T_E represents the exciter time constant. Appendix A illustrates exciter parameters for each power system.

2.4.3 Power System Stabilizer (PSS)

Figure 2.7 illustrates the block diagram of PSS used in this thesis.

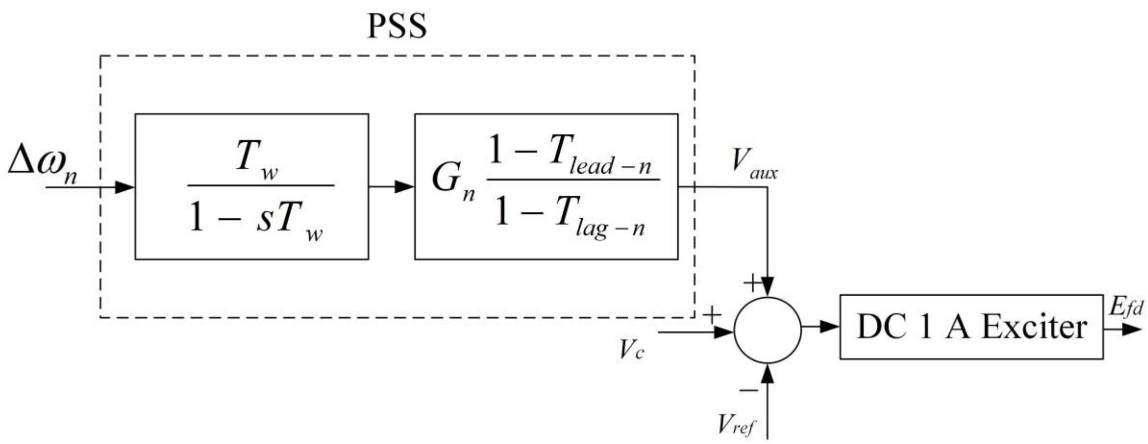

Figure 2.7 Block diagram of the PSS

In this block diagram, T_w is the washout filter time constant, while G_n, T_{lead-n}, and T_{lag-n} are the stabilizer gain, lead and lag controller for the n^{th} generator, respectively. Since the aim of PSS is to damp the local mode of oscillations the speed deviation of the generator ω_n is used as the control signal. The design procedure for washout filter and the compensator is discussed later in *Section* 2.7.

2.4.4 Governor

The primary function of a governor is to control the generator speed to meet the frequency stability requirements of the grid [91, 92] by matching the generation with demand. In this thesis, since the small signal and transient stability studies are addressed, the frequency stability of the power system with regards to governor response is not covered in detail. Hence, the simplified classical model of the hydro governor with a constant droop is used. Figure 2.8 represents the governor simplified model. T_W is referred to water starting time, which normally in full load condition lies between 0.5 and 4*s* [14]. *R* represents the droop feedback gain. SG stands for the synchronous generator model. Governor data for study systems are presented in Appendix A.

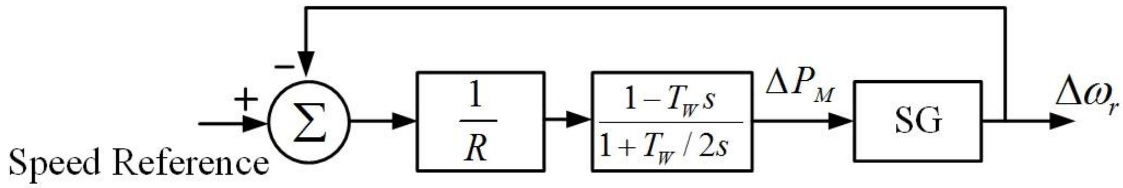

Figure 2.8 Governor simplified model

2.4.5 Transformers

Transformers are representated by the Π-model of a two-winding transformer [14] as shown in Figure 2.9.

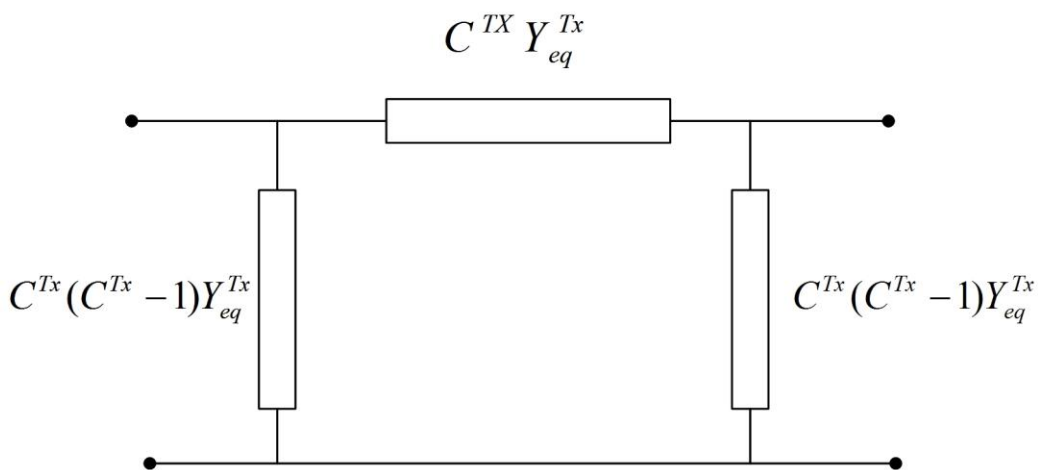

Figure 2.9 Π-model representation of a two-winding transformer

Z_{eq}^{Tx} is the equivalent leakage reactance of the transformer. Hence the transformer admittance is calculated as:

$$Y_{eq}^{Tx} = \frac{1}{Z_{eq}^{Tx}} \tag{2.1}$$

and

$$C^{Tx} = \frac{1}{ONR} \tag{2.2}$$

ONR represents the Off-Nominal Turn Ratio of the transformer.

2.4.6 Loads

Load modeling has a significant effect on power oscillation damping simulation studies. In this thesis, constant impedance load model is used which is adequate for stability studies [93]. Although different loads can be used for further investigation of power system dynamic response, in this thesis the methodology does not include various load models. The concept of the proposed controllers are presented with constant impedance load which is acceptable for stability studies in this thesis [16].

The constant impedance load model is described as:

$$Y_i^{load} = \frac{P_i^{load} - jQ_i^{load}}{V_i} \tag{2.3}$$

where, Y_i^{load} is the shunt admittance connected to i^{th} load bus.

2.4.7 Transmission Lines

Figure 2.10 illustrates the π model of the line used in this thesis [14].

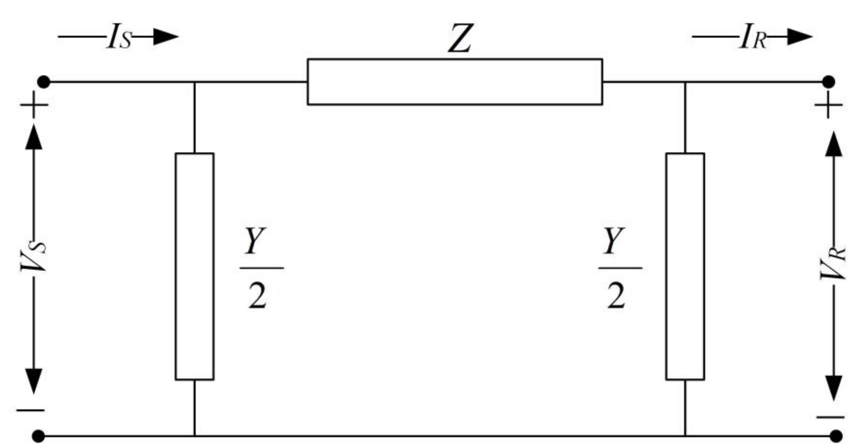

Figure 2.10 Line π model

Z and *Y* represent the series impedance and shunt admittance of the line, respectively. The relation between sending end voltage V_s, receiving end current I_R and receiving end voltage V_R is given by:

$$V_s = Z\left(\frac{Y}{2}V_R + I_R\right) + V_R \tag{2.4}$$

2.5 Modeling of a Grid Connected PV Solar System

Figure 2.11 portrays the grid connected aggregated model of 100 MW solar farm including 6-pulse 3-phase inverter, controllers, AC filter, and delta-star step-up transformer. The solar farm is connected to the power system at a bus called the Point of Common Coupling (PCC).

Maximum Power Point Tracing (MPPT) unit is used to harvest the maximum available DC power. A large DC link capacitor is used to maintain the PV solar farm DC side voltage at the desired value. The main duty of the PV inverter is to transform the available DC power to AC. The inverter consists of IGBT semiconductor devices which provide the *On*/*Off*

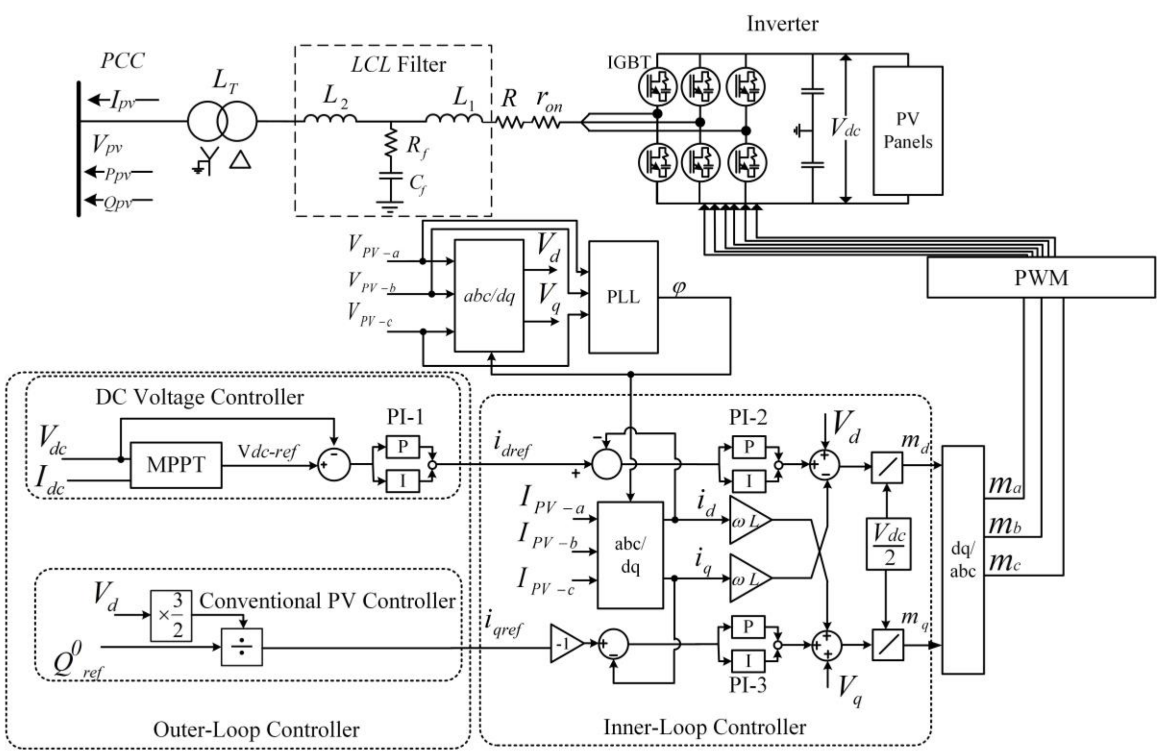

Figure 2.11 Detailed PV power plant modeled in PSCAD/EMTDC

switching states for inverter function. In order to maintain the required PV system power output quality, AC filter is designed to filter the high-frequency harmonics caused by high-frequency switching of inverter semiconductors. A step-up coupling transformer is used to connect the large-scale utility size PV solar farm to the high voltage transmission network. The details of each subsystem are presented below:

2.5.1 PV Solar Panel

PV solar panels are power generating devices which can convert the solar radiation to electric power. The power output of these single PV modules is nonlinearly affected by the solar radiation and temperature. To illustrate the behavior of PV modules power output, the Voltage and Current (VI) characteristics of these units with regards to solar radiation and temperature are used [94]. In large scale PV solar power system, a substantial number of PV modules are connected in series and parallel to realize the required current and voltage. To achieve the required DC voltage, PV modules are connected in series to form a String. Furthermore, the desired current is achieved through the interconnection of these Strings in parallel which forms an Array. Through parallel and series interconnection of solar modules, the PV solar farm capacity can reach to tens or hundreds of Megawatts. Figure 2.12 illustrates the I-V and P-V characteristics of the simulated 100 MW_{pk} solar power system with regards to different solar radiation and constant temperature.

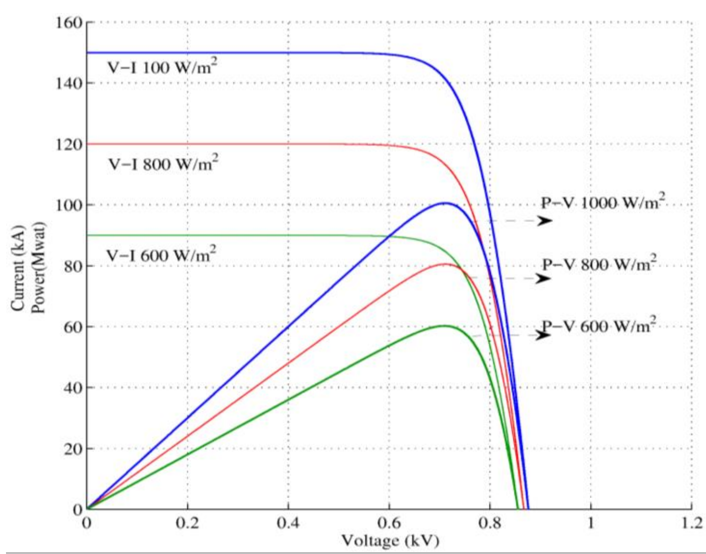

Figure 2.12 The effect of solar radiation on I-V and P-V characteristic of a 100 MW_{pk} solar power plant

The effect of temperature on solar power output is illustrated in Figure 2.13.

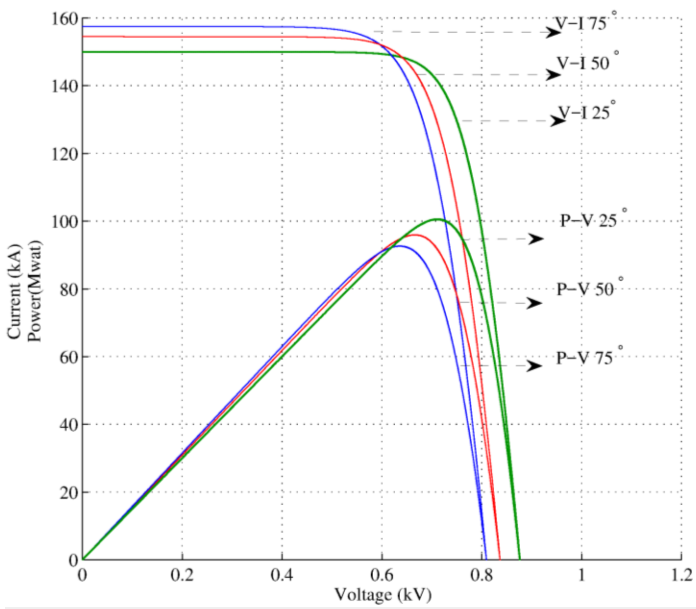

Figure 2.13 The effect of ambient temperature on V-I and V-P characteristic of a 100 MW_{pk} solar power plant for (25, 50, and 75 °C)

It is shown that the increase in temperature results in a nonlinear reduction in solar power output. From Figure 2.12 and Figure 2.13 it is noted that with regards to both different solar radiation and temperature, there is a peak point for PV system real power which can be determined by inverter DC voltage. The voltage associated with maximum PV power output is called Maximum Power Point Voltage V_{mpp}..

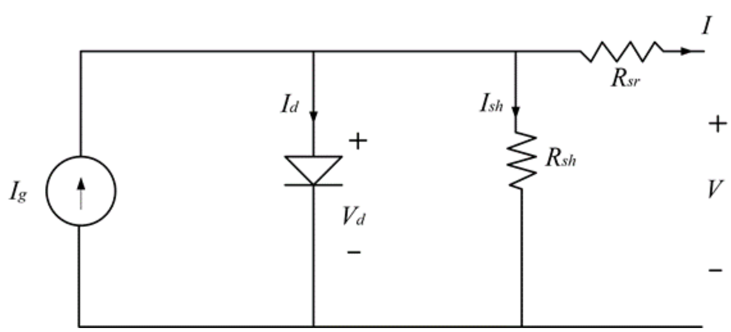

Figure 2.14 Single line diagram of an aggregated PV solar farm

The modeling of PV solar farm is commonly performed through an aggregated PV system model as shown in Figure 2.14. I_g is the current generated by the solar cells exposed to the light. I_d is the current following through the antiparallel diode [95, 96]. This current contains the nonlinear characteristics of the individual solar cell. R_{sr} and R_{sh} represent the series and shunt resistances respectively. I_{sh} represents the shunt current passes through the shunt resistor R_{sh}. According to Kirchhoff's law:

$$I = I_g - I_d - I_{sh} \tag{2.5}$$

By substituting the relevant expressions for I_d and I_{sh} [23]

$$I = I_g - I_0\left[\exp\left(\frac{q(V_d + IR_{sr}}{nkT}\right) - 1\right] - \left(\frac{V + IR_{sr}}{R_{sh}}\right) \tag{2.6}$$

where q is the electronic charge ($q = 1.1602 \times 10^{-19}\ C$). K is the Boltzman constant of $1.3806503 \times 10^{-23}\ J/K$. n represents the ideality factor of the diode. T represents the cell temperature. I_0 is the diode saturation current.

As mentioned earlier, to achieve higher voltage and current outputs for large PV solar farm applications, the aggregated simulation model is commonly used. If N_p number of cells are connected in parallel and N_s number of cells in series, the output current I_A and voltage output voltage V_A form the following equation:

$$I_A = N_pI_g - N_pI_0\left[\exp\left(\frac{q(V_A + I_A\frac{N_s}{N_p}R_{sr}}{N_snkT}\right) - 1\right] - \left(\frac{V_A + I_A\frac{N_s}{N_p}R_{sr}}{\frac{N_s}{N_p}R_{sh}}\right) \tag{2.7}$$

With regards to different solar radiation and temperature, I_0 and I_g are:

$$I_g = I_{gref}\left(\frac{G}{G_{ref}}\right)\left[1 + K_v\left(T - T_{ref}\right)\right] \tag{2.8}$$

$$I_{0=}I_{0ref}\left[\frac{T}{T_{ref}}\right]^3 exp\left[\frac{E_{g,ref}}{KT_{ref}} - \frac{E_g}{KT}\right] \tag{2.9}$$

where, G and G_{ref} are solar radiation and reference value for solar radiation, respectively. T_{ref} is the reference cells temperature, E_g is the bandgap energy of the solar cell material and K_v is the temperature coefficient of photocurrent. Appendix D presents the electrical specification for FS 272 PV module that is used in this thesis.

2.5.2 Inner Loop Controller

The inner loop controller provides decoupled *d*-*q* axis control of real and reactive power based on the *d* axis reference current I_{dref} and *q* axis reference current I_{qref}, respectively [97]. The details of controller decoupling and controller design for each component are described below.

2.5.2.1 *abc* to *dq* Transformation

Three phase electrical variables such as voltage, current, flux linkage can be represented in two-dimensional frame *dq*-frame [98]. In *dq* frame, under the steady-state condition, signals are assumed to be DC waveforms which result in simpler compensator, controller analysis and design. Transformation of three *abc* to *dq* frame is shown in Figure 2.15.

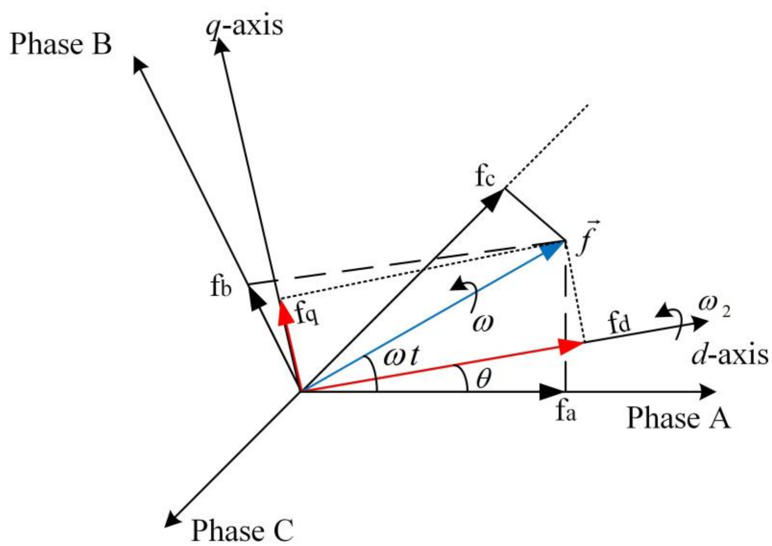

Figure 2.15 *abc* to *dq* transformation

$\vec{f}$ is an electrical space vector with rotational speed ω= 377 rad/sec $2\pi f$. Its phase components f_a, f_b, and f_c are as follows:

$$f_a = Acos(\omega t)$$

$$f_a = Acos(\omega t - \frac{2\pi}{3})$$

$$f_a = Acos\left(\omega t - \frac{4\pi}{3}\right) \tag{2.10}$$

These variables f_a, f_b, and f_c can be transformed to dq frame as f_d and f_q with rotational frame in which the speed of the rotation is the same as ω. The transformation is given as:

$$\begin{bmatrix} f_d \\ f_q \end{bmatrix} = \frac{2}{3}\begin{bmatrix} \cos(\omega t) & \cos(\omega t - \frac{2\pi}{3}) & \cos(\omega t + \frac{2\pi}{3}) \\ -\sin(\omega t) & -\sin(\omega t - \frac{2\pi}{3}) & -\sin(\omega t + \frac{2\pi}{3}) \end{bmatrix}\begin{bmatrix} f_a(t) \\ f_b(t) \\ f_c(t) \end{bmatrix} \tag{2.11}$$

The space vector $\vec{f}(t)$ can be represented as

$$\vec{f}(t) = \left(f_d + jf_q\right) \tag{2.12}$$

Figure 2.16 presents $\vec{f}(t)$ in *abc* and *dq* frame. In Figure 2.15, θ represents the angle between phase A-axis and d-axis in *dq* frame.

2.5.2.2 Phase Locked Loop (PLL)

In order to synchronize the *d*-axis rotational reference frame of ABC to DQ reference frame in Section 2.5.2.1, a PLL [97] is utilized as shown in Figure 2.16. The Voltage-Controlled Oscillator (VCO) is used to generate the phase shift ρ and is realized as a resettable integrator. The integrator resets if the output reaches to 360°. Saturation block is used to ensure that controller signal ω remains within ±377°. The aim is to keep V_q to zero to ensure that the phase shift ρ is equal to $\omega t + \theta$ in Figure 2.15 [99].

With regards to an integrator in the feedback loop, ρ tracks the constant components with zero steady state error. To ensure that the controller is also able to track the ramp components with zero steady-state error, at least one additional integrator is required in compensator H(s) at s=0. Based on the design requirements higher order compensator can

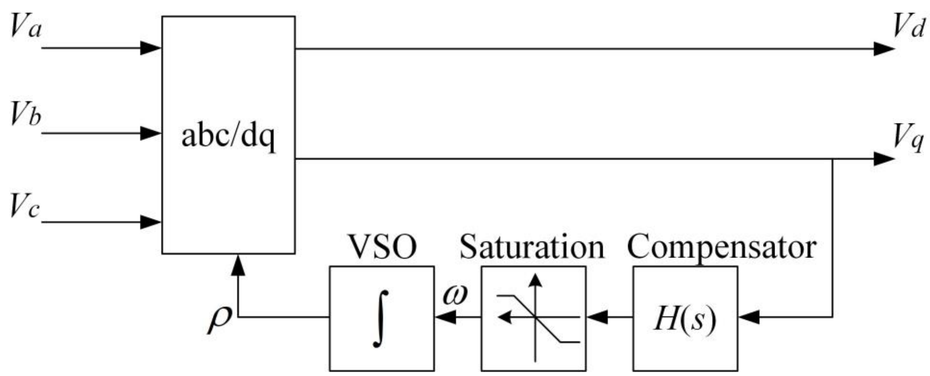

Figure 2.16 PLL block diagram

be developed [97]. In this thesis, a Proportional and Integral (PI) controller with constant k_p and T_i is used as compensator. The parameters of PI controller are given in Appendix E.

2.5.2.3 PWM Modeling

To generate three phase triggering pulses for IGBT units, sinusoidal PWM is used [100]. Firing pulses are generated through comparison between 5 kH triangular signals with the sinusoidal reference signal. A 5 kH switching frequency is selected to avoid excessive losses and minimize the noise in the audible range [23].

2.5.2.4 Decoupled Control of Real And Reactive Power

Assuming steady state operation, according to Figure 2.11, *dq* frame representation of PV-STATCOM inverter current and voltage is given by:

$$L\frac{di_d}{dt} = L\omega i_q - (R + r_{on})i_d + \frac{V_{DC}}{2}m_d - V_d \qquad (2.13)$$

$$L\frac{di_q}{dt} = L\omega i_d - (R + r_{on})i_q + \frac{V_{DC}}{2}m_q - V_q \qquad (2.14)$$

where R is line reactance, r_{on} is the switched-on resistance of the IGBT units, L represents the line inductance, V_{DC} is DC side voltage, V_d and V_q are direct and quadrant voltages, respectively. A full derivation of (2.13) and (2.14) can be found in [97].

To eliminate the coupling terms $L\omega i_q$ and $L\omega i_d$, m_d and m_q are determined as

$$m_d = \frac{2}{V_{DC}}\left(u_d - L\omega_0 i_q + V_{sd}\right) \quad (2.15)$$

$$m_q = \frac{2}{V_{DC}}\left(u_q + L\omega_0 i_d + V_{sq}\right) \quad (2.16)$$

where u_d and u_q are new control inputs. Hence, substituting (2.15) and (2.16) in (2.13) and (2.14) we get

$$L\frac{di_d}{dt} = -(R + r_{on})i_d + u_d(2.26) \quad (2.17)$$

$$L\frac{di_q}{dt} = -(R + r_{on})i_q + u_q(2.27) \quad (2.18)$$

Hence, by controlling u_d and u_q, i_d and i_q can be controlled in a decoupled manner. Figure 2.17 illustrates the *dq* current control loops.

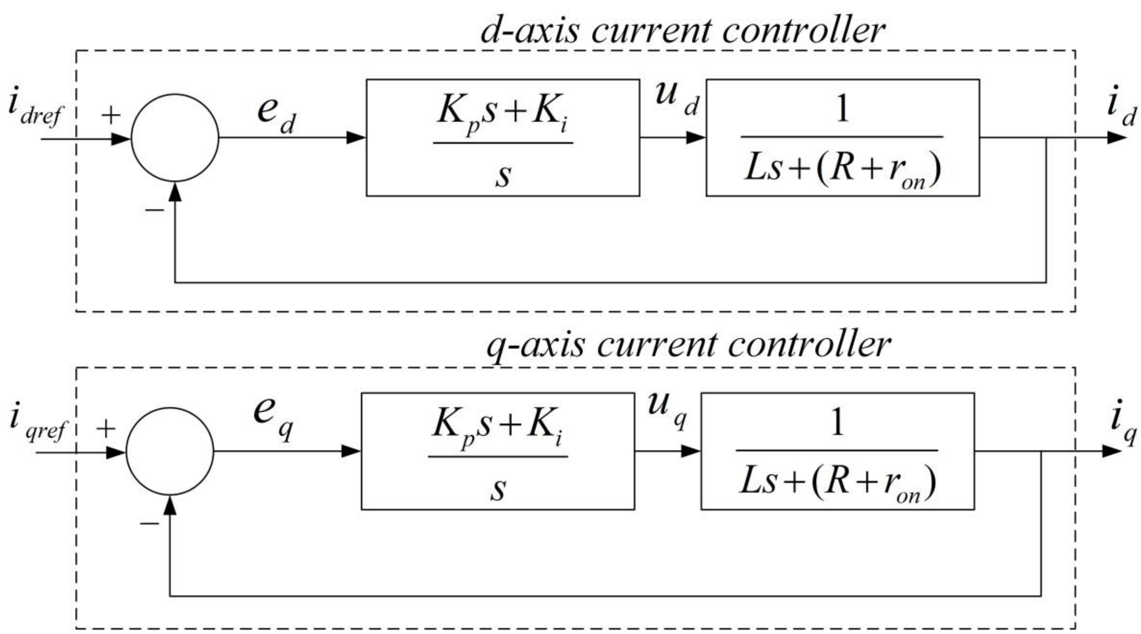

Figure 2.17 Block diagram of i_d and i_q control loops

To achieve the desired time constant τ_i for the closed-loop system, following parameters are selected [97]:

$$k_p = {}^{L}/_{\tau_i} \tag{2.19}$$

$$k_i = (R + r_{on})\tau_i \tag{2.20}$$

The parameters of PI controllers for PV system are given in Appendix E. The step responses for i_d and i_q controllers are illustrated in Figure 2.18 assuming 100 MW_{pk} PV system is connected to the Two-Area power system. It is evident from Figure 2.18 that i_d and i_q are controlled in a decoupled manner. The settling time is 1 *ms*, and no overshoot is seen in the step response. The decoupled i_d/i_q controller is at least 10 times faster than outer-loop controllers i.e. 10 times faster than DC voltage controller and 100 times faster than POD controllers, which results in decoupled inner and outer loop control design [97].

In addition, the designed controller has bandwidth of $1/\tau_i$=1000 which is 5 times slower than the switching frequency of 5kH as per required in [97].

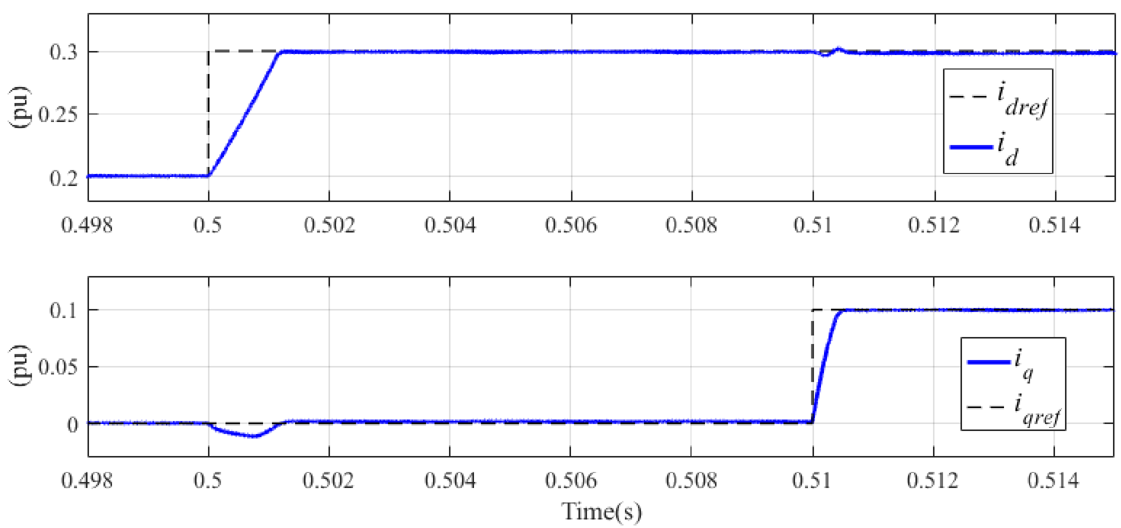

Figure 2.18 Step response for i_d/i_q controller

The i_d and i_q reference signals are generated from outer-loop controllers. In *dq* frame three phase real and reactive power are:

$$P_s(t) = \frac{3}{2}\left[V_{sd}(t)i_d(t) + V_{sq}(t)i_q(t)\right] \tag{2.21}$$

$$Q_s(t) = \frac{3}{2}\left[-V_{sd}(t)i_q(t) + V_{sq}(t)i_d(t)\right] \quad (2.22)$$

Having PLL, in a steady state, V_{sq}= 0, (2.21) and (2.22) can be rewritten as

$$i_{dref}(t) = \frac{2}{3V_{sd}(t)} \; P_s(t) \quad (2.23)$$

$$i_{qref}(t) = -\frac{2}{3V_{sq}(t)} Q_s(t) \quad (2.24)$$

2.5.3 LCL Filter Design

LCL filter configuration is widely used in literature for smoothing the output current of Voltage Source Converter (VSC) units [98]. Through proper design of *LCL* filter, the switching frequency of the inverter unit can be reduced which results in less switching losses along with cost saving and reduction in component sizes [101]. To design the *LCL* filter, following considerations are required;

1. The capacitor size has to be limited in order to absorb less that 5% of VSC rated power output for maintenance of unity power factor.

2. The resonance frequency should be 10 times greater than the grid frequency and be less than half of the switching frequency ($10f_g < f_{res} < 1/2f_{sw}$)

3. The current ripple is assumed to be 10% of the rated current and needs to be attenuated through LCL filter by 20%. Hence, the current ripple is limited to 2% after the LCL filter.

Figure 2.19 illustrates the single phase of delta connected LCL filter

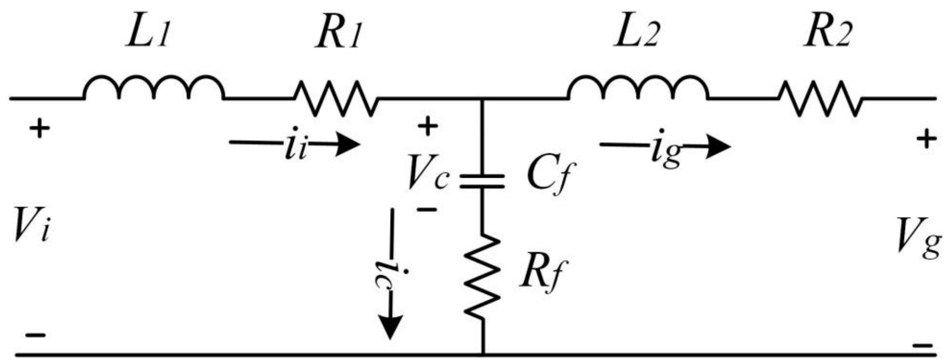

Figure 2.19 Single phase *LCL* filter

L_1, R_1, L_2, R_2, R_f, and C_f are inverter side inductor, inverter side inductor resistance, grid side inductor, grid side inductor resistance, damping resistance, and filter capacitor, respectively. V_i is input voltage and V_g is the grid side voltage.

The transfer function associated with LCL filter in Figure 2.19 with and without damping resistance are

$$H_{LCL}(s) = \frac{1}{L_1 C_f L_2 s^3 + (L_1 + L_2)s} \tag{2.25}$$

$$H_{LCL}(s) = \frac{C_f R_f s + 1}{L_1 C_f L_2 s^3 + C_f (L_1 + L_2) R_f s^2 + (L_1 + L_2)s} \tag{2.26}$$

The effect of R_f on the filter response will be shown later in this subsection. The base impedance Z_b and capacitance C_b for LCL filter design are

$$Z_b = \frac{E_n^2}{P_n} \tag{2.27}$$

$$C_b = \frac{1}{\omega_g Z_b} \tag{2.28}$$

where, P_n and E_n are rated power and voltage, and $\omega_g = 2\pi f_g$. The maximum current ripple ΔI_{max} is given as

$$\Delta I_{max} = \frac{V_{DC}}{6f_{sw}L_1} \tag{2.29}$$

where V_{dc} is the inverter DC side voltage. The max current I_{max} is

$$Imax = \frac{\sqrt{2}P_n}{3V_{ph}} \tag{2.30}$$

where, $V_{ph}$is the phase voltage.

Hence from (2.28) and (2.29) we get

$$L_1 = \frac{V_{DC}}{6f_{sw}\Delta I_{Lmax}} \tag{2.31}$$

The ratio between the grid current at switching harmonic $i_g(h_{sw})$ and the switching current output from the inverter $i(h_{sw})$ is

$$\frac{i_g(h_{sw})}{i(h_{sw})} = \frac{1}{[1 + r(1 - CL_1\omega_{sw}^2)]} \tag{2.32}$$

where r is the constant ratio between grid side inductor L_2 and inverter side inductor L_1. In this thesis, r is selected to be 0.1. Hence L_2=0.1L_1.

The resonance frequency is given by

$$\omega_{res} = \sqrt{\frac{L_1 + L_2}{L_1L_2C_f}} \tag{2.33}$$

and it must satisfy

$$10f_g < f_{res} < 1/2f_{sw} \tag{2.34}$$

The damping resistance is calculated as

$$R_f = \frac{1}{3\omega_{res}C_f} \tag{2.35}$$

The Matlab code for *LCL* filter design considering PV-STATCOM connected to the different study systems is given in Appendix F.

Figure 2.20 illustrates the Bode plot for LCL filter with and without damping resistance for PV-STATCOM in a Two-Area power system where, L_1= 7.511μH, L_2=0.7511μH, C_f=20 μF, R_f=0.052 Ω to illustrate the effect of damping resistance on the LCL filter response. It is observed from Figure 2.20 that the damping resistance eliminates the gain spike and smoothens the overall response of the LCL filter. Moreover, the resonance frequency of 3.72 kH is well within required limit.

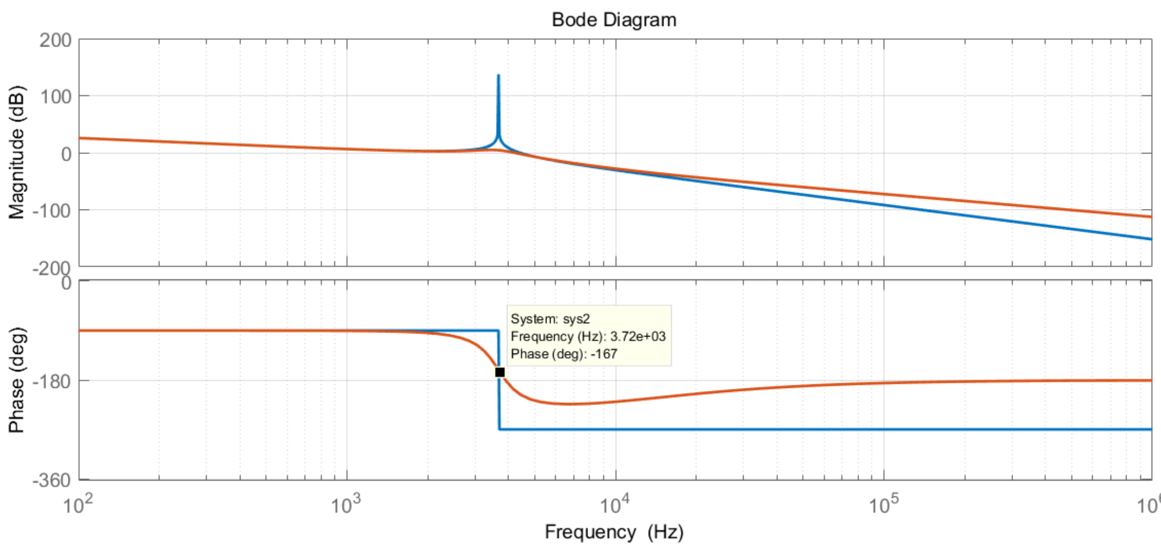

Figure 2.20 Bode plot for designed *LCL* filter for 100 MW$_{pk}$ PV system connected to Two-Area power system at 230 kV bus.

2.5.4 MPPT Algorithm

As described earlier in *Section* 2.5.1, the PV power output of the solar panels has a nonlinear relation with irradiance and cell temperature. Since the aim is to harvest the maximum available power from the PV solar farm, Maximum Power Point Tracking (MPPT) unit is used to generate the reference DC voltage (V_{dref}) in which the maximum available power is achieved. The MPPT flowchart is presented in Figure 2.21. The MPPT unit monitors the actual current and voltage and generates the reference voltage V_{dref} based on the predefined algorithms of Incremental Conductance (IC) [102]. Two possible scenarios are examined in this algorithm [103]. In the first scenario, when there is no change in voltage, the algorithm examines the changes in the current. If the current deviation is zero, the algorithm assumes that the PV is operating at its MPP. Hence, no voltage step change is required. If the deviation is observed in current, a small deviation as *delV* is applied to the MPPT voltage output. By changing the DC voltage, the current also varies. This process continues until the PV reaches to its MPP operation.

In the second scenario, if there is a change in the V_{dc} [103], the MPPT evaluates

$$\frac{dI}{dV} = -\frac{I_{PV}}{V_{DC}} \tag{2.36}$$

If (2.36) is satisfied, the change in the voltage is due to the change in insolation or temperature but PV system is operating at MPPT. Hence, no voltage change is applied. On the other hand, if the relation is not satisfied, PV system is not operating at MPP and a voltage change is applied to V_{dc}. The process continues until MPP is achieved. In this thesis, the sampling interval is set to 0.1 sec, V_{op}=840 V, and I_{sc}=120 kA as shown in Figure 2.12 for 100 MW_{pk} solar power plant.

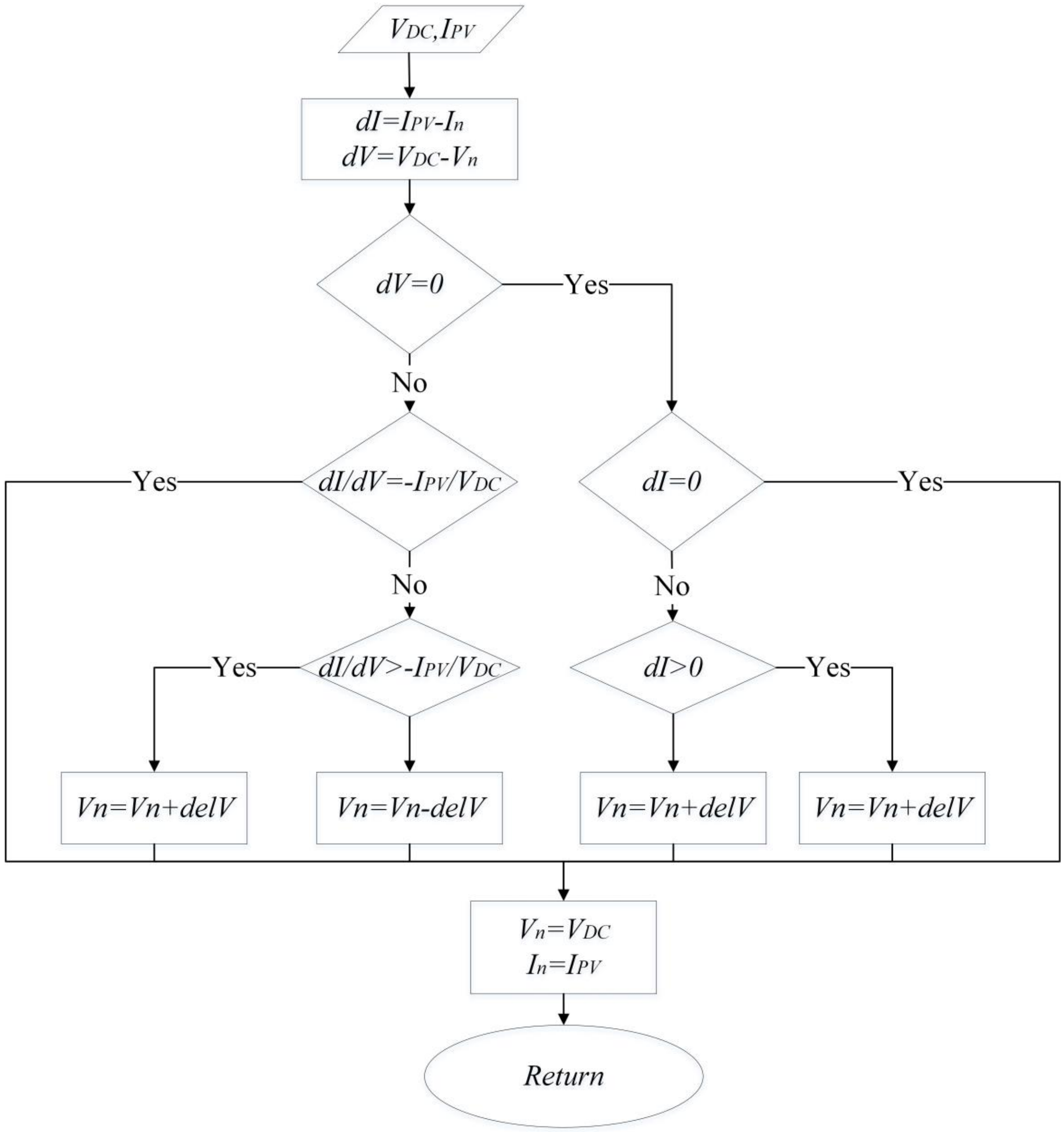

Figure 2.21 MPPT block diagram [23]

2.5.5 DC Voltage Controller

The DC voltage of the PV system needs to be controlled to maintain the DC capacitor voltage based on the reference voltage (V_{dref}) from the MPPT unit. The DC link voltage V_{dc} is controlled to inject the balance of generated PV power and DC link voltage absorbed power to the grid. The DC side voltage dynamics considering inverter losses and capacitor real power absorption is as follows [23]:

$$C_{dc}\frac{\partial V_{dc}}{\partial t} = i_{PV} - i_{loss} - i_{dc} \tag{2.37}$$

where, i_{PV} is the PV system output current, i_{dc} represents the VSC DC side current, i_{loss} is the loses current, and C_{dc} is the DC side capacitor. Equation (2.37) can be rewritten in Laplace form as:

$$sV_{dc}C_{dc} = I_{PV} - I_{loss} - I_{dc} = -\frac{3}{4}\left(m_d I_d + m_q I_q\right) \tag{2.38}$$

Since in decoupled dq transformation, the real power is mainly controlled through i_d, (2.38) can be rewritten as

$$sV_{DC}C_{DC} = -\frac{3}{4}(m_d I_d) \tag{2.39}$$

Hence, the compensator for V_{dc} can be expressed as a PI controller as follows:

$$I_{dref} = -\frac{4sV_{dc}C_{dc}}{3m_d} = -K_{dc}\left(V_{dc} - V_{dc-ref}\right) \tag{2.40}$$

where the compensator K_{dc} can be modeled as

$$K_{dc} = K_{pdc} + \frac{K_{idc}}{s} \tag{2.41}$$

This controller is used throughout this thesis for all modes of PV system operation. As discussed earlier, the reference DC voltage V_{dc-ref} in PV mode of operation is generated through MPPT algorithm. In addition, during off-MPPT operation mode which is described later in *Section* 2.6.3, this controller is used to reduce the real power output to zero by setting V_{dc-ref} to PV system open circuit voltage V_{op}. Controller parameters are tuned to be 10 times slower than inner-loop controller, with overshoot less than 10%. In addition, controllers are tuned to be 10 times faster than sampling MPPT sampling time i.e. MPPT algorithm sampling rate is 0.1 Sec hence, the V_{dc} controller are tuned with τ=0.01 sec. The controller parameters are given in Appendix E.

2.5.6 Conventional Reactive Power Controller

In normal PV system operation, the aim is to convert DC power to AC with unity power factor. According to (2.24), the Q_{ref} is set to zero. Hence, the i_{qref} is set to zero.

2.6 PV-STATCOM Modeling

As discussed earlier in this chapter, if low-frequency power oscillations with a frequency range of 0.1 to 2 Hz are detected in the power system, the conventional operation mode of PV system is disabled and STATCOM mode of operation is activated. By activation of STATCOM mode, the aim is to increase the damping of the power system by controlling reactive or/and the real power of PV solar power plant. Note that the inner loop controllers, inverter, filters, and transformer remain the same as those in PV conventional mode of operation. Figure 2.22 illustrates the real and reactive power controller of PV-STATCOM. The specific controllers can be selected through switches S_1, S_2, and S_3.

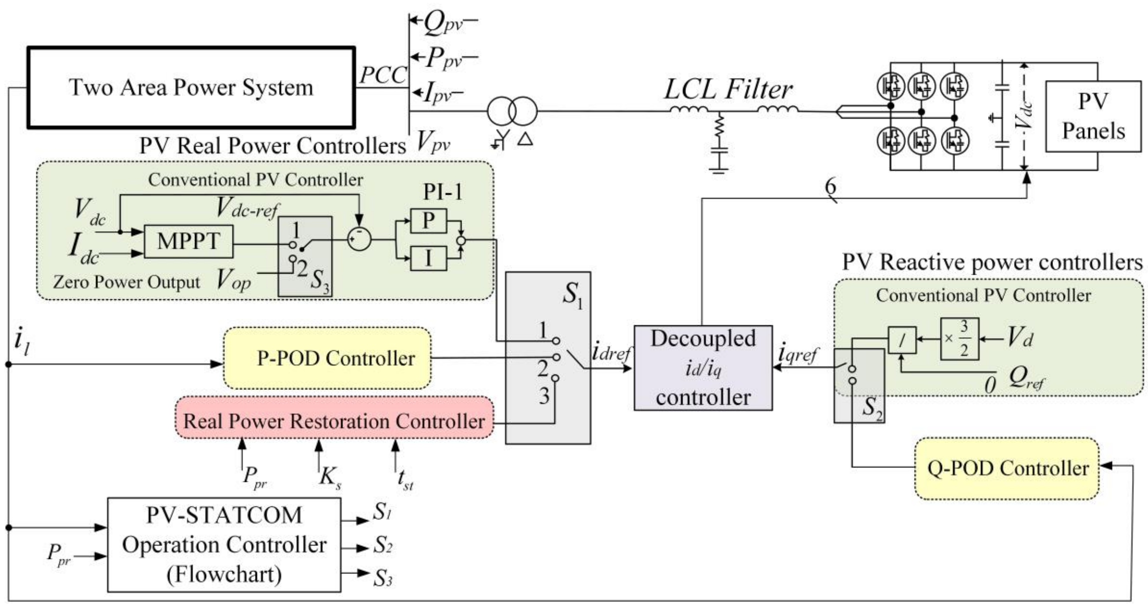

Figure 2.22 PV-STATCOM detailed modeling in PSCAD/EMTDC

2.6.1 Zero Power Output

This controller is activated if the full capacity of PV inverter is required for reactive power based POD. Hence, the i_d reference signal is generated through controlling DC voltage at

V_{op}. As shown in Figure 2.12, by controlling the V_{dc} at 840 V, the real power output of the PV can be controlled to zero.

2.6.2 Reactive Power Based POD (Q-POD) Controller

As shown in Figure 2.2, PV inverter capacity is fully available during the night time. If the power oscillations appear in the power system, PV-STATCOM reactive power is controlled to damp the power oscillations. This technique is available in full and partial STATCOM mode of operation.

2.6.3 Real Power Based POD (P-POD) Controller

In addition to Q-POD controller, in this thesis, during the day time, additional POD controller based on the PV-STATCOM real power controller is presented. If the P-POD is activated, the real power setpoint is set to half of the pre-fault value of PV real power. Furthermore, in this mode, PV-STATCOM real power is controlled through an off-MPPT technique by controlling the i_{dref} to modulate the PV-STATCOM real power output for damping the low electromechanical power oscillations.

2.6.4 Real Power Restoration Controller

If the power oscillations are damped, the PV real power is restored to its pre-fault value P_{pr} with a ramp rate K_{st} or in a nonlinear function. If the restoration is completed, PV controllers switch back to conventional PV control mode.

2.7 POD Controller Design

Figure 2.23 illustrates the general form of FACTS stabilizer in power system,

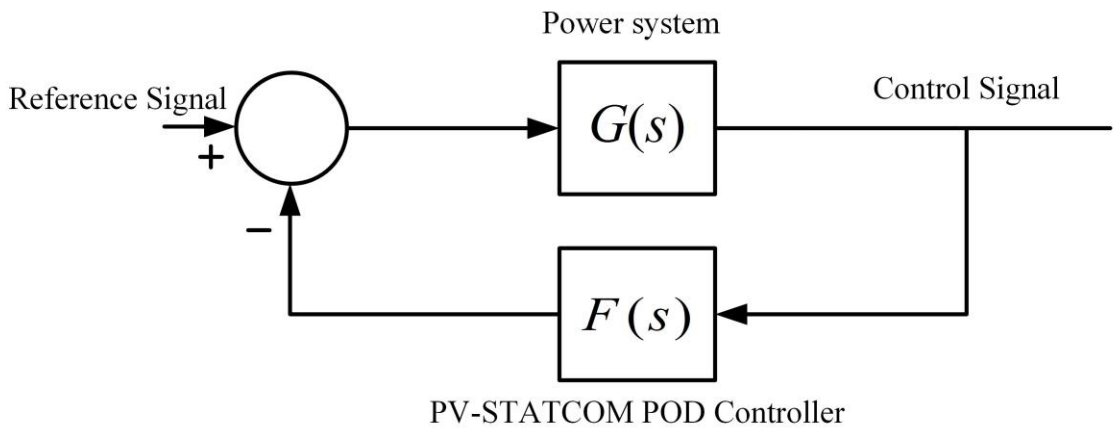

Figure 2.23 Block Diagram of POD controller

$G(s)$ represents the power system transfer function and $F(s)$ models the PV-STATCOM POD controllers as:

$$F_{(s)} = KH(s) = KG_{POD}(s).G_W \tag{2.42}$$

$$G_w(s) = \frac{s\,T_w}{1 + sT_w} \tag{2.43}$$

$$G_{POD}(s) = \left[\frac{1 + T_{lead}s}{1 + T_{lag}s}\right]^m \tag{2.44}$$

$G_W(s)$ represents the washout filter transfer function, $G_{POD}(s)$ is the POD transfer function and K represents for the feedback gain. T_w denotes the washout filter time constant. T_{lead} and T_{lag} are Lead and Lag time constants, respectively. The objective of designing the POD lead-lag controller is to determine the appropriate values for T_w, T_{lead}, T_{lag}, and K in order to add adequate lead or lag phase compensation to the feedback control loop at a certain frequency [104].

2.7.1 Washout Filter Design

Washout filter is used in PV-STATCOM POD controller to ensure that the steady-state error in the control signal will not result in a steady state error in the POD controller. As shown in (2.43), (knowing that $s = j\omega_f$), as ω_f reduces, $G_w(s)$ moves towards zero. Hence, the transfer function is appropriate for blocking DC-offset or steady-state signals. It can also be shown that for higher frequencies than the washout filter corner frequency $1/T_w$, $G_w(s)$ becomes almost $1\angle 0^{\circ}$. To design the washout filter, corner frequency $1/T_w$ is set about a decade below the lowest frequency mode of oscillation [104].

Assuming the frequency mode of oscillation to be 2 Hz, T_w is set to 5 s (i.e corner frequency is 0.2 Hz). The Bode plot for this washout filter is presented in Figure 2.24.

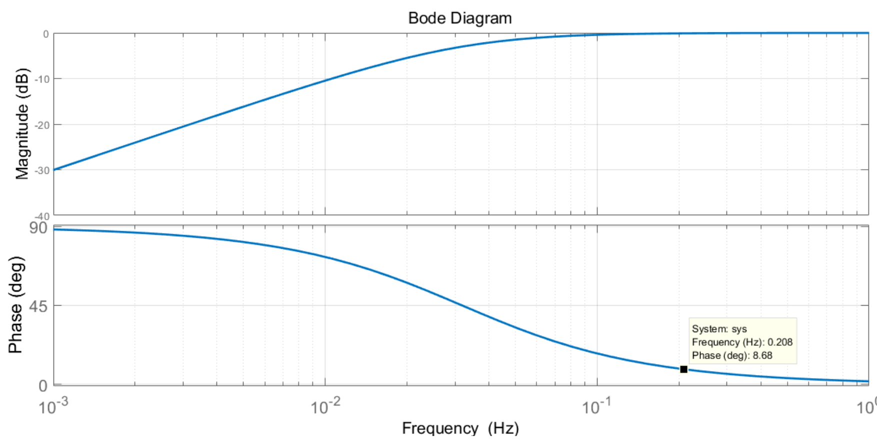

Figure 2.24 Frequency response of washout filter with T_w=5s

As shown in Figure 2.24 for 2 Hz frequency range, the phase shift is almost equal to 8.86° which is considered negligible.

2.7.2 Participation Factor (PF) Analysis

PF analysis is used in this thesis to select the control signals in which the selected modes of low-frequency power oscillations have higher participation. To determine the participation of an individual state in selected mode of oscillation, PF analysis provides dimensionless relation between the states and modes [14, 104]. The concept of PF analysis which is used in this thesis is as follows:

For a given state-space system with $n \times n$ matrix A, λ_h is h^{th} eigenvalue in which

$$A\nu_h = \lambda_h \nu_h \tag{2.45}$$

where, ν_h is the *right eigen vector* of *A* matrix associated to λ_h

$$\nu_h = [\nu_{1h} \upsilon_{2h} \dots \dots . \upsilon_{nh}]^T \tag{2.46}$$

Likewise, the *left eigenvector* $w_h = [w_{h1} w_{h1} \dots \dots . w_{hn}]$ is determined to satisfy

$$w_h A = w_h \lambda_h \tag{2.47}$$

$$w_h \nu_h = 1 \tag{2.48}$$

Having right and left eigenvectors of matrix *A*, PF matrix can be formed as

$$P_{hk} = w_{hk} \nu_{kh} \tag{2.49}$$

where, P_{hk} provides a measure in which λ_h contributes in the k^{th} state.

Note that from (2.48);

$$\sum_{k=1}^{n} P_{hk} = \sum_{k=1}^{n} w_{kh}\, \nu_{kh} = 1 \tag{2.50}$$

To calculate the participation of each state, small signal simulation of the power system is required. In this thesis, Matlab simulation is used for small signal simulation and is presented in *Section 2.9*. The linearized model of the power system is obtained through the linearization function in Matlab with proper selection of input and output signals [105].

2.7.3 PV-STATCOM POD Design Based on Residue Analysis

To design the POD controller for small signal stability, Residue technique is used in this thesis [104]. The residue technique is performed based on modal analysis in Matlab Simulink. Consider the Two-Area Power system with PV-STATCOM interconnection to bus 8 as shown in Figure 2.25.

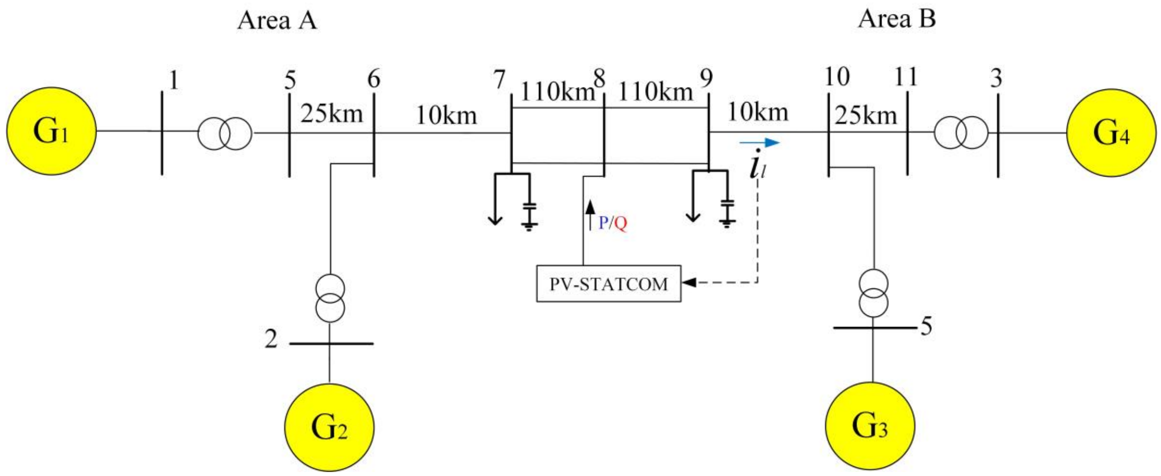

Figure 2.25 Two-Area Power system with PV-STATCOM connected at bus 10.

The line current between buses 9 and 10 is selected as the best control signal (i.e. i_l has the highest Participation in the electro mechanical oscillatory mode) [14]. The transfer function from the PV-STATCOM reference reactive power ΔQ and the line current i_l is $G_s(s) = \Delta i_l/\Delta Q$. To determine the compensation controller for POD, the interarea mode phase shift when POD controller feedback loop is switched from open to closed is considered.

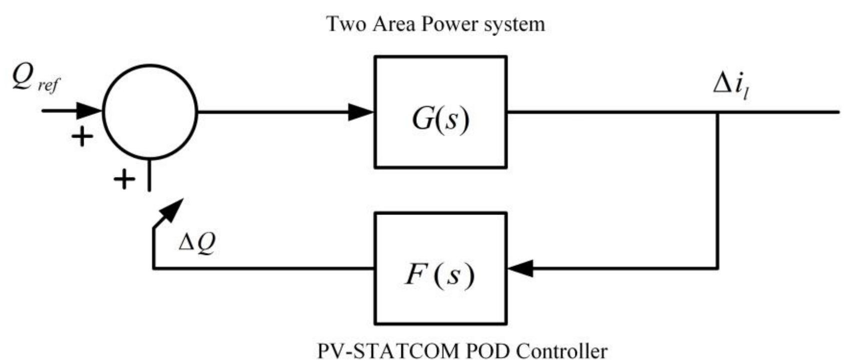

Figure 2.26. Insertion of a Feedback Loop with a Small Gain in a System

A transfer function $G(s)$ can be described by its partial fractions as:

$$G(s) = \frac{r_1}{s - P_1} + \frac{r_2}{s - P_2} + \cdots + \frac{r_i}{s - P_i} + \cdots + \frac{r_n}{s - P_n} \tag{2.56}$$

where, r_i represents the residue of the distinct pole P_i. To determine the compensation controller for POD, the interarea mode phase shift when POD feedback circuit is switched from open position to closed position is considered.

The Transfer function of Two-Area power system with PV-STATCOM, assuming the feedback loop is closed, is:

$$W(s) = \frac{G_s(s)}{1 - G_s(s)F_s(s)} = \frac{G_s(s)}{1 - kG_s(s)H(s)} \tag{2.57}$$

Hence, the closed-loop poles are derived as:

$$1 - G_s(s)F_s(s) = 0 \tag{2.58}$$

Assuming that the open loop transfer function where the G_s(s) is excited by the eigenvalue λ_h is:

$$G_s(\lambda_h) = \frac{r_h}{s - \lambda_h} \tag{2.59}$$

where r_h is the residue of eigenvalue λ_h of the forward-loop transfer function $G_s(\lambda_h)$ [104]. The characteristic equation of (2.59) associated to λ_h is:

$$1 - \frac{r_h}{s - \lambda_h} F(\lambda_h) = 0, or\ s = \lambda_h + k_R r_h H(\lambda_h) \tag{2.60}$$

After closure of feedback loop, the mode λ_h is shifted by small amount $\Delta\lambda_h$ from the open-loop pole. The root for the new characteristic equation is s= (λ_h+$\Delta\lambda_h$). Equation (2.60) then becomes:

$$(\lambda_h + \Delta\lambda_h) - \lambda_h - k_R r_h H(\lambda_h + \Delta\lambda_h) = 0 \tag{2.61}$$

If the mode shift is small enough, then the transfer function H(s) around s=λ_h can be represented by first-order Taylor series as:

$$H(\lambda_h + \Delta\lambda_h) = H(\lambda_h) + \left(\frac{\partial H(s)}{\partial s}\bigg|_{s\,=\,\lambda_h}\right)\Delta\lambda_h \tag{2.62}$$

Substituting (2.62) in (2.61) leads to;

$$\Delta\lambda_h = \frac{Kr_h H(\lambda_h)}{1 - Kr_h \frac{\partial H(\lambda_h)}{\partial \lambda_h}} \tag{2.63}$$

If *K* is small enough to satisfy $\left|Kr_h \frac{\partial H(\lambda_h)}{\partial \lambda_h}\right| \ll 1$, (2.63) can be rewritten as:

$$\Delta\lambda_h = Kr_h H(\lambda_h) \tag{2.64}$$

The residue r_h of the eigenvalue λ_h is a complex number with $\theta_h = arg\{r_h\}$. To achieve the mode shift to be $\pm180°$, the POD controllers must be designed with compensation angle ϕ:

$$\phi = \pm180 - arg\{r_h\} \tag{2.65}$$

Note that according to Figure 2.24, the phase shift of washout filter around the frequency of the selected mode (0.1-2 Hz) is around 8.26° which is considered negligible.

2.7.4 Optimization of PV-STATCOM Controllers

The POD controllers are first designed using small signal residue analysis to obtain the optimized controller parameters - *Gain, Lead* and *Lag* time constants. In order to account for system nonlinearities, these optimized parameters are subsequently tuned using the *Simplex Optimization* technique [105] embedded in the electromagnetic transients software PSCAD/EMTDC [106]. The *Nonlinear-Simplex* optimization method is an optimization technique based on geometric consideration in which desired *Objective Function* (OF) is achieved through a heuristic procedure.

A *Simplex* is a geometric object which is formed by *N+1* points in an *N*-dimensional space. The optimization starts with an initial value of the random or predefined variable. During the optimization process, the worst vertex is discarded and the new vertex which is the reflection of the discarded vertex with regards to the centroid of remaining vertices is selected. The same procedure continues in each iteration and OF moves towards the lower

OF value. The process can speed up if, during the optimization, the vertex of OF is very large. The procedure continues until the OF comes within the predefined error limit from the optimum point of operation.

In PSCAD/EMTDC software, an optimization is performed through *Master*/*Slave* simulation programming as shown in Figure 2.27.

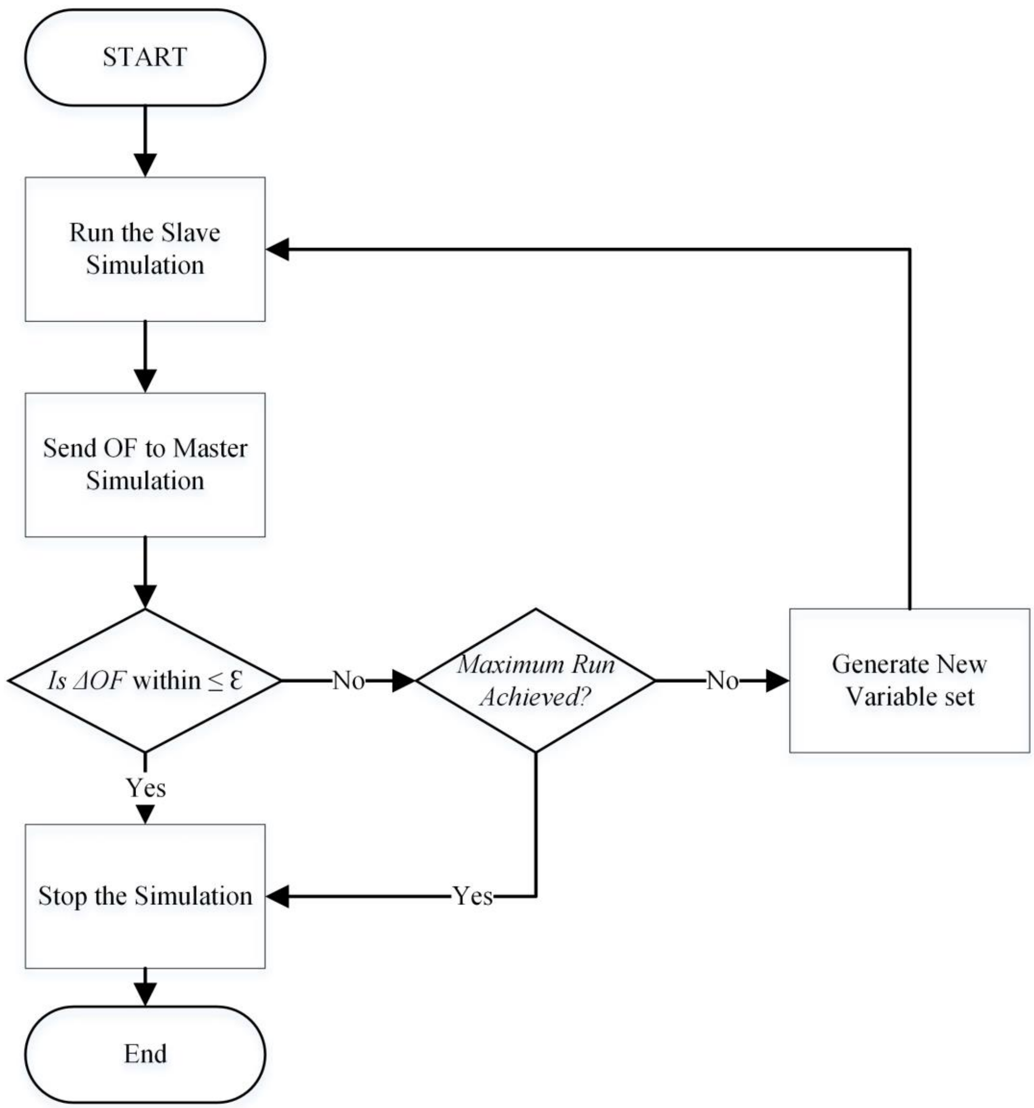

Figure 2.27 *Simplex* Optimization Flowchart

The main function is placed in *Slave* simulation and the simulation runs for predefined run time (depending on the simulation study). After the simulation is done in *Slave* project, OF will be generated and sent to the *Master* project in which the optimization technique is performed and new sets of variables will be generated. These new parameters will be sent back to *Slave* project for a new simulation run. This process continues until the desired OF is achieved and deviation in the objective function (ΔOF) remains in predefined error limit Ɛ or the maximum number of iterations is achieved. For better illustration of this technique, a numerical example of simplex optimization procedure in PSCAD/EMTDC is provided in Appendix G.

2.8 Placement of PV-STATCOM – Residue Analysis

The effect of PV-STATCOM interconnection to the power system is studied based on its potential to stabilize the selected mode of oscillation. Participation analysis is used to determine the control signal which has the highest participation in the oscillatory mode to be damped. This signal is used as the input control signal for POD controllers at all locations of PV solar system and for all types of controllers used (real power, reactive power or combined real and reactive power based). However the effectiveness of a specific type of POD controller at a given location of PV solar farm is determined from Residue Analysis [108]. According to (2.56), assuming that all zeros and poles of $G(s)$ and $H(s)$ are distinct, the closure of the feedback loop of the POD controllers results in a change in the selected eigenvalue λ_i as

$$\Delta\lambda_h = K r_h H(\lambda_h) \tag{2.64}$$

According to [107], the magnitude of r_h is a proper indicator of suitability of the POD controller. Hence, the magnitude of the residue associated with control signal can be determined by calculation of $\Delta\lambda$ with regards to closure of the feedback loop. The higher the magnitude of the reside the better the location of PV-STATCOM for POD.

2.9 Small-signal Modeling of PV-STATCOM

Although PSCAD/EMTDC software is suitable for detailed simulation studies, it does not have a platform for modal analysis. In addition, fast switching of power electronic devices such as IGBTs or GTOs requires a very small simulation time step in the EMT-Type simulations (5 to 15μs). This very short simulation time step results in a very long simulation time. Hence, to perform the small signal studies and to design controllers, a simplified small signal PV model has been developed in Matlab software [108]. This model is useful if the aim is to study the stability of power system with respect to changes in magnitude and phases of all voltages and currents. Hence, there is no need to solve all differential equations resulting from the interaction between *R*, *C*, and *L* elements [16]. Figure 2.28the simplified small signal model of PV-STATCOM.

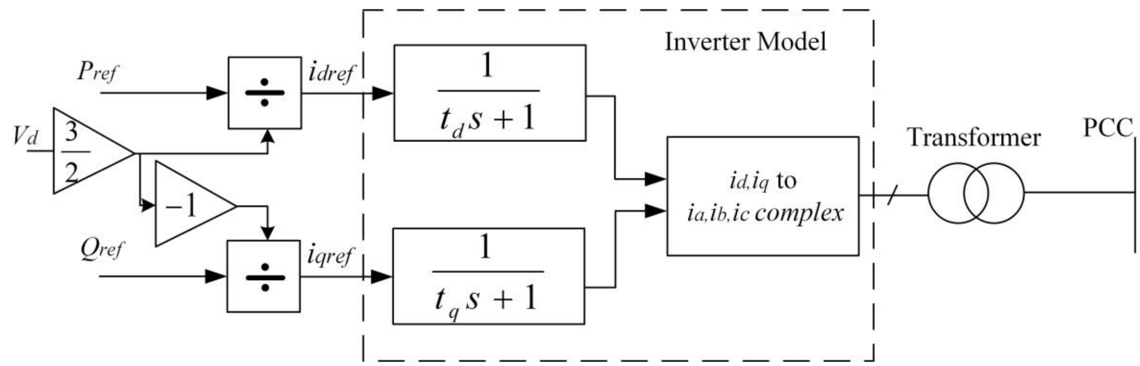

Figure 2.28 PV-STATCOM small signal model

Both real and reactive power can be controlled by controlling real and reactive power reference signals P_{ref} and Q_{ref} as follow:

$$\begin{bmatrix} id \\ iq \end{bmatrix} = 3/2 \begin{bmatrix} Vd & Vq \\ Vq & -Vd \end{bmatrix}^{-1} \begin{bmatrix} P \\ Q \end{bmatrix} \tag{2.65}$$

(2.65) can be simplified further utilizing (2.24) where V_q is controlled to zero through proper design of PLL as:

$$\begin{bmatrix} id \\ iq \end{bmatrix} = 3/2 \begin{bmatrix} Vd & 0 \\ 0 & -Vd \end{bmatrix}^{-1} \begin{bmatrix} P \\ Q \end{bmatrix} \tag{2.66}$$

The inverter is modeled as a first order transfer function with unity steady-state gain at t_d,t_q=15 ms [26]. According to [109], inverter modeling with a first order function having time constant of the dominant pole of the closed loop transfer function has an acceptable response except for some differences during high frequency transients. For power oscillation damping studies performed in this thesis, the high frequency transients do not play a role in the damping of electromechanical modes which have frequencies in the range 0.1-2 Hz (time periods of 10 sec – 0.5 sec). Hence the first order model of the inverter is considered to be adequate. Figure 2.29 illustrates the comparison between the step response of the detailed model of PV-STATCOM in PSCAD/EMTDC and small signal PV-STATCOM model in Matlab Simulink.

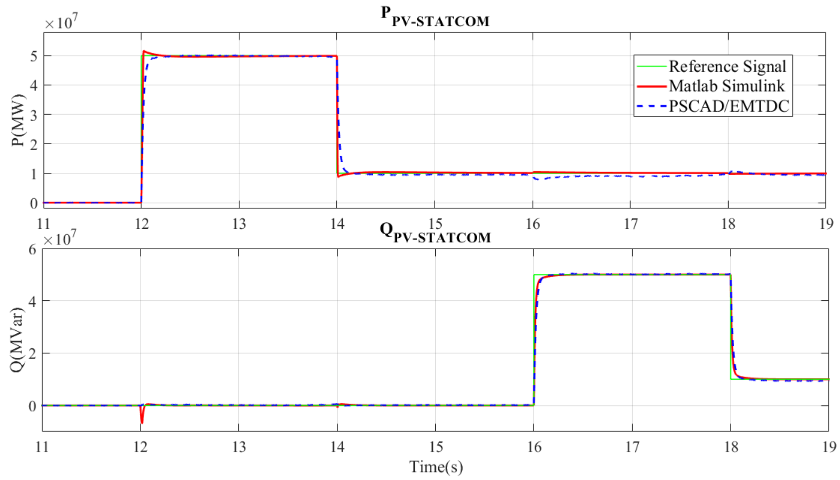

(a)

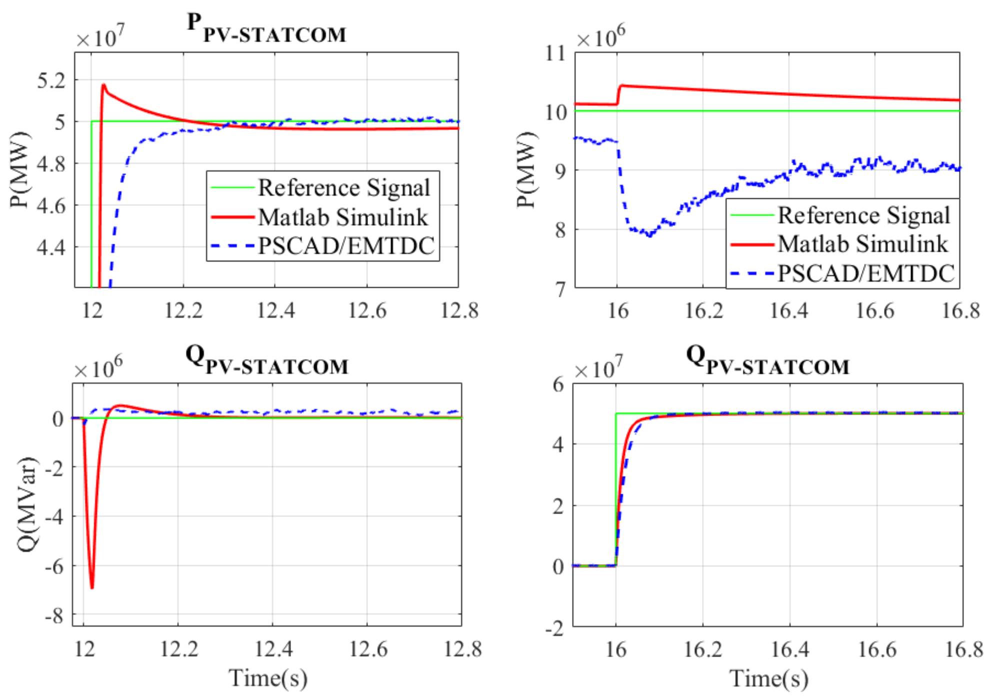

(b)

Figure 2.29 (a) Comparison of decoupled controller for PV-STATCOM in PSCAD/EMTDC and Matlab Simulink (b) Magnified results

It is seen from Figure 2.29, the simplified model of PV-STATCOM in Matlab provides similar steady state responses as the detailed model simulation in PSCAD/EMTDC software. There are differences in the transients from both the models. However, as explained above, these differences are not expected to impact the power oscillation damping behavior. It is noted when there is a step change in the PV real power output, the reactive power is not affected. Meanwhile, it is observed that the PV real power is not influenced by changing the PV system reactive power. Hence, both real and reactive of PV-STATCOM can be controlled in decoupled manner.

2.10 BESS Modeling

Where the performances of BESS P-POD controller and PV-STATCOM Q-POD controller need to be compared for damping purposes, a detailed model of BESS is required. For this reason, the BESS is presented here. Figure 2.30 presents the aggregated BESS model developed in PSCAD and the connection principle of energy storage system for different BESS capacities.

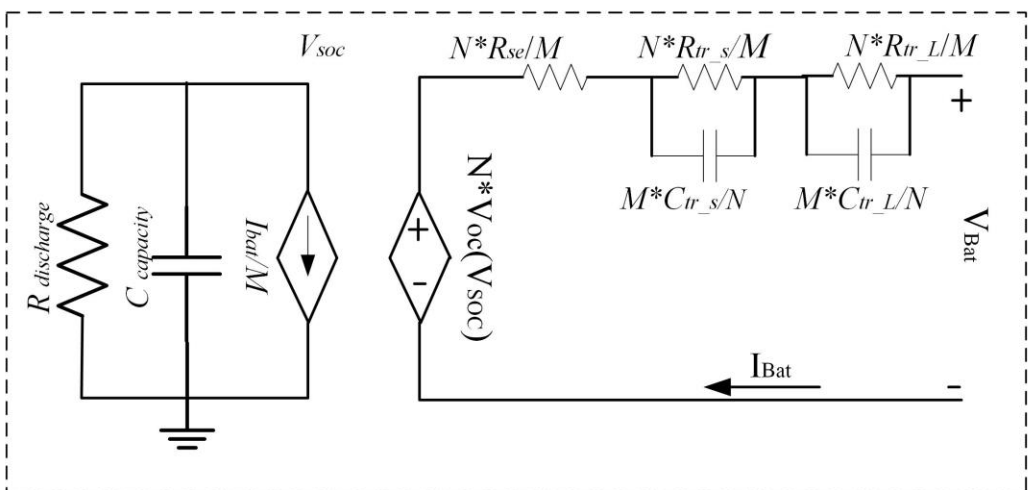

Figure 2.30 Aggregated BESS modeling in PSCAD/EMTDC

$C_{Capacity}$ stands for the battery usable capacity. $R_{dicharge}$ is the self-discharge resistor. R_{se} denotes the series resistor R_{Series} which is responsible for the instantaneous voltage drop during step response. The internal parameter of the battery can be simulated by RC networks. Short term transients are represented by R_{tr_s} and C_{tr_s} as $R_{Transient\_S}$, $C_{Transient\_S}$. In addition, long-term transients can be modeled by *RC* network with R_{tr_l} and C_{tr_l} as $R_{Transient\_L}$, and $C_{Transient\_L}$. By connecting *N* battery cells in series, the voltage output of the energy storage system can be increased up to *N* times of the individual battery voltage. Meanwhile, to increase the rated current of the BESS, *M* batteries are connected in each branch in parallel. The behavior of entire energy storage system will then follow the same behavior for single battery model [110]. Since in [110] it is shown that the discharge current has a negligible effect on the battery parameter, in this thesis, the single-variable function model of each variable is used in PSCAD/EMTDC modeling.

An aggregated BESS system based on series and parallel connection of accurate 4.1-V, 850-*mAh TCL PL-383562* Li-ion batteries model [111] is simulated in PSCAD/EMTDC software. The FORTRAN code for the battery model in PSCAD/EMTDC is included in

Appendix **H**. Figure 2.31 illustrates the simulated results of single battery parameters based on the different level of State Of Charge (SOC).

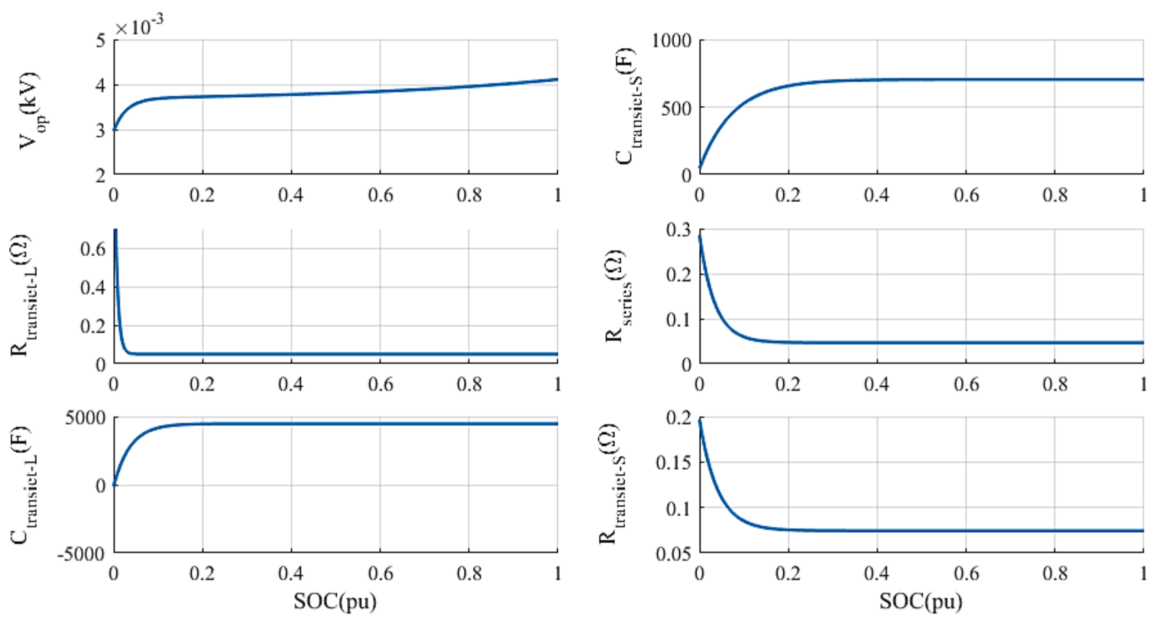

Figure 2.31 BESS *RLC* components variation based on SOC

2.11 Conclusion

In this chapter, the concepts of PV-STATCOM in both partial and full STATCOM modes of operation are presented. Three study power systems – the Single Machine Infinite Bus (SMIB) system, Two-Area system, and the 12 Bus FACTS power systems which will be utilized in this thesis are described. The models of different power system components and the constituents of the PV solar system are presented. The procedures for designing different PV system controllers are illustrated.

The selection of POD control signal based on Participation Factor analysis is enunciated. The design of power oscillation damping controllers based on *Simplex* Optimization technique and Residue analysis is further presented.

Residue analysis is described as an effective technique to determine the most effective location of PV-STATCOM for power oscillation damping. The performance of PV-STATCOM models in small signal and EMTDC/PSCAD simulations is compared. A model of large scale BESS in PSCAD/EMTDC is also presented and the behavior of internal variables are illustrated based on State of Charge of the BESS.

Chapter 3

3 Power Oscillation Damping in Single Machine Infinite Bus (SMIB) System with PV-STATCOM and Battery Energy Storage System (BESS)

3.1 Introduction

The objective of this Chapter is to investigate the effectiveness of real power modulation on power oscillation damping. This real power control is provided by a Battery Energy Storage System (BESS). This work is expected to provide insights for designing the real power modulation based control of a PV-STATCOM in Chapter 6 and 7. This chapter also presents a comparison between the performance of a PV-STATCOM and (BESS) for damping the inertial mode oscillations in Single Machine Infinite Bus (SMIB) power system. The performance of Real Power Modulation based Power Oscillation Damping (P-POD) for BESS is compared with Reactive Power Modulation based Power Oscillation Damping (Q-POD) controller of a PV-STATCOM while operating in Full STATCOM mode of operation. The BESS is modeled in PSCAD/EMTDC software. The effect of BESS size on damping of electromechanical oscillations of the generator is further investigated using EMTDC/PSCAD software. The POD controllers are optimized to justify the comparison between the different POD techniques.

3.2 Study System Model

The SMIB system depicted in Figure 3.1 is selected as the study system for the present study. Figure 3.1 illustrates the SMIB power system in which the BESS and PV-STATCOM are connected at its midpoint. The BESS and PV solar system share the same inverter, *LCL* filter and inner loop controllers. During Q-POD with PV-STATCOM, PV modules are connected to the DC bus. However, the P-POD control with BESS is activated by connecting the battery bank to the inverter DC bus. The red lines illustrate the controller during P-POD control with BESS. The blue lines represent the controller signals during Q-POD control.

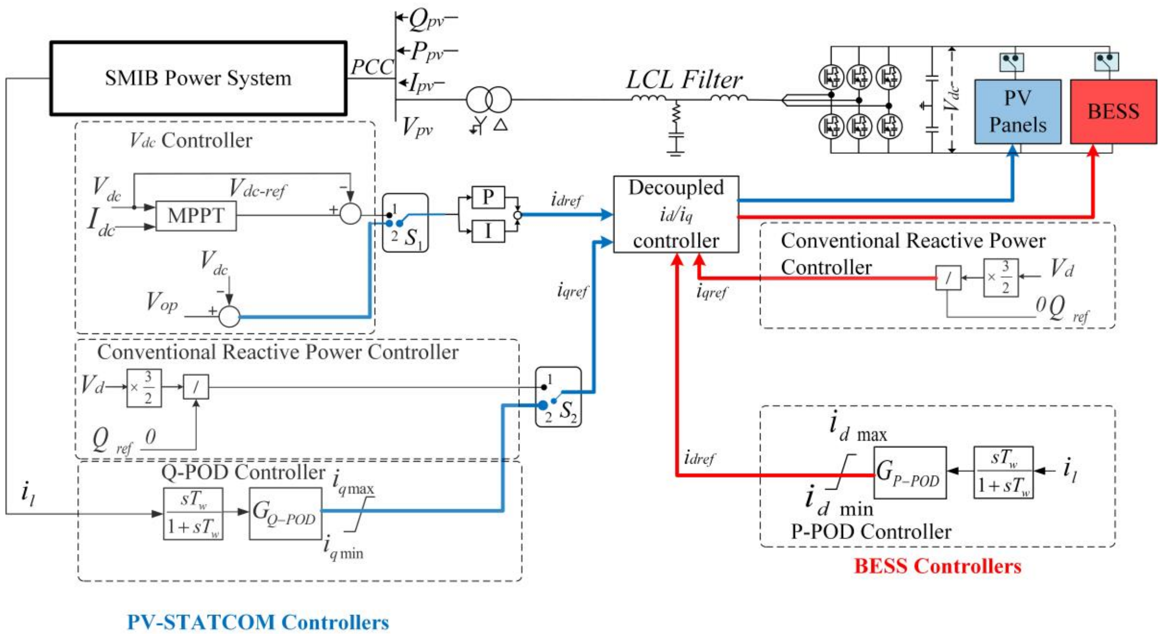

Figure 3.1 SMIB power system with PV-STATCOM and BESS

The generator power is transferred to the infinite bus through a transmission line, which in this study is considered to be 400 km. No PSS is considered for the generator excitation unit. It is noted that for this operating condition, the power system is poorly stable. To compare the effectiveness of P-POD with BESS and Q-POD with PV-STATCOM, the location of BESS and PV-STATCOM is kept the same for both studies. The solar farm is assumed to be of 100 MW rating.

3.3 PV-STATCOM Components

The PV-STATCOM system and its associated controllers are depicted in Figure 3.1. As shown in Figure 3.1 the conventional PV mode of operation is achieved by connecting the PV modules to DC bus. The models of different components of the PV-STATCOM have been described earlier in the thesis, i.e., PV solar panels (*Section* 2.5.1), Decoupled i_d/i_q controller (*Section* 2.5.2), LCL filter (*Section* 2.5.3), MPPT algorithm (*Section* 2.5.4), DC Voltage controller (*Section* 2.5.5), and Conventional Reactive Power Controller (*Section* 2.5.6). The new added outer loop controllers are designed as follows:

3.3.1 Q-POD controller for PV-STATCOM

The midline current i_l is selected as the control signal for POD. Since in this power system only 1 synchronous generator exists, i_l has high participation factor in the electro mechanical mode of oscillation [23]. Moreover, utilizing a local signal avoids any delay between the control signal and the Q-POD controller for PV-STATCOM. The washout filter is designed based on the technique described in Section 2.7.1 with $T_W = 5$. The Q-POD controller with $G_{Q-POD}(s)$ transfer function is as:

$$G_{Q-POD}(s) = G\left[\frac{1 + T_{lead}s}{1 + T_{lag}s}\right] \tag{3.1}$$

where, T_{lead}, T_{lag} and the G are lead, lag time constants and the gain of the controller, respectively. The controller parameters are optimized through embedded simplex technique in Section 0. The Q-POD generates the i_{qref} current for the inner-loop controller.

To activate the POD controller of PV-STATCOM, S_2 is set to position 2.

3.4 BESS Modeling

Figure 3.1 further illustrates the BESS connected to the same inverter as the PV-STATCOM. To perform POD with BESS, the PV panels are disconnected and BESS is connected to the DC bus. The BESS can provide a bi-directional power flow control at its PCC. Various sizes of BESS are used in which the maximum power input/output of the BESS is controlled through a hard-limiter on i_{dref} signal. The overall BESS model is based on the aggregation of 850 *mAh TCL PL-383562* Li-ion battery models described in Section 2.10. The number of battery modules in series is kept constant at N=240. Hence, DC voltage of all sizes of BESS remains constant within 40%-100% SOC of the battery.

It is assumed that BESS is in 90% of its SOC during POD. This assumption is acceptable for this study since the aim is to compare the fully charged BESS with PV-STATCOM. Furthermore, the POD is performed for less than 10 *s* during which period the SOC of the battery will not get affected considerably.

3.4.1 Conventional Reactive Power Controller

Since in this chapter, the aim is to compare the effectiveness of P-POD controller in BESS and Q-POD controller in PV-STATCOM, the reactive power output of the BESS is controlled to zero during the period of POD. To control the reactive power output to zero, i_{qref} is set to zero and is controlled through inner-loop controller, as described in *Section* 2.5.2.4.

3.4.2 P-POD Controller design for BESS

In this chapter, POD is performed with BESS real power modulation through the proposed P-POD controller. i_l signal is used as the control signal to perform P-POD. i_l is passed through the washout filter with T_w=5 *s* and is fed to the $G_{P\text{-}POD}$ compensator:

$$G_{p-POD}(s) = G\left[\frac{1 + T_{lead}s}{1 + T_{lag}s}\right] \tag{3.2}$$

where, T_{lead}, T_{lag} and the G are lead, lag time constants and the gain of the controller, respectively. The controller parameters are optimized with the *Simplex* optimization technique described in Section 2.7.4.

3.5 Optimization of Q-POD and P-POD Controllers

In this study, the size of both PV-STATCOM and BESS is assumed to be equal. The PV-STATCOM has ±100 MVar inverter capacity and the BESS has ±100 MW_{pk} capacity. Optimization of controllers is performed considering a 3-phase to ground fault to be initiated at generator bus for a duration of 5 cycles. The SMIB power system, PV-STATCOM, and BESS are simulated in *Slave* project and simulation runs for 20 seconds to encompass a minimum of 10 cycles of low frequency oscillations (1 Hz to 2 Hz). The aim is to minimize the low-frequency power oscillations after the fault. Hence, the objective function (OF) for this study is

$$OF = \int_{T_1}^{T_2} \left(i_{mid} - i_{mid-ref}\right)^2 dt \tag{3. 3}$$

where T_1 and T_2 are the start and end time of *Slave* simulation, i_{mid} is the midline current and $i_{mid\text{-}ref}$ is the reference midline current. Figure 3.2 presents the optimization of controller parameters for P-POD and Q-POD in PV-STATCOM and BESS system as the number of iterations progress.

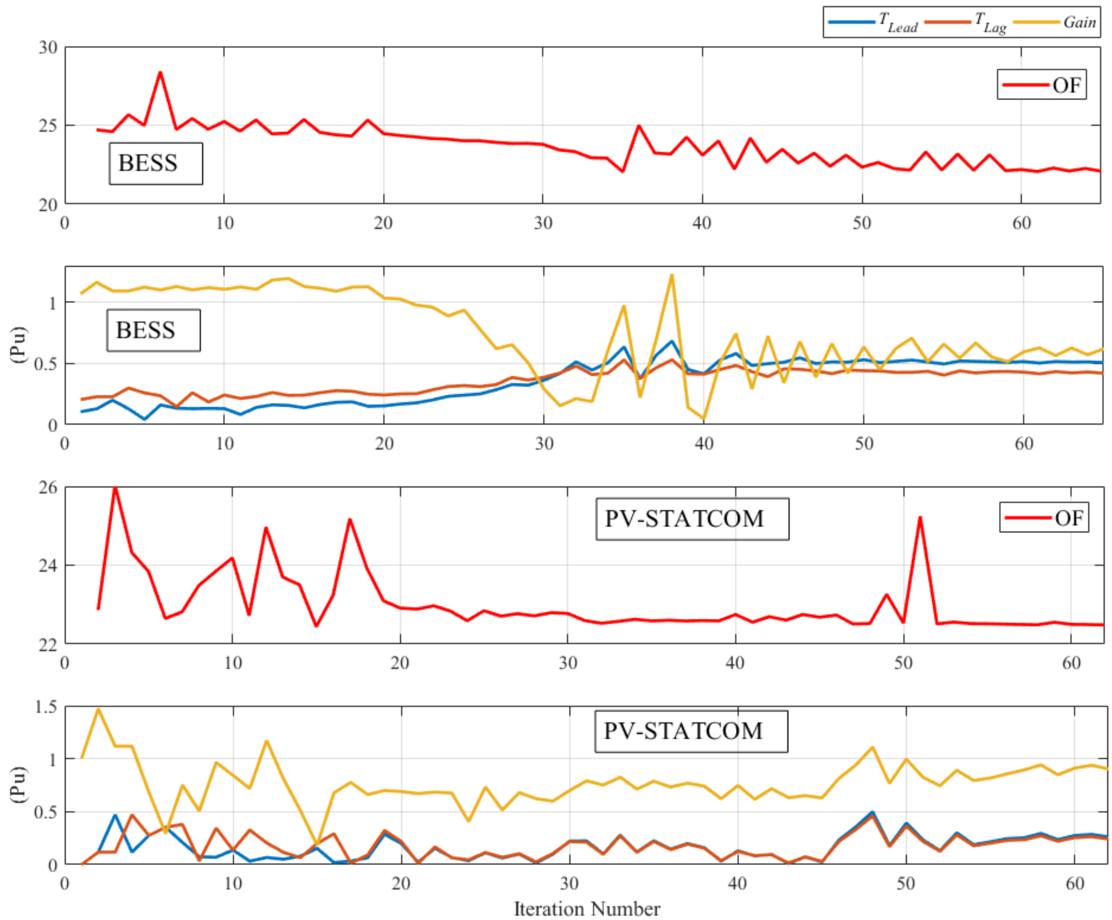

Figure 3.2 Objective Function, T_{lead}, T_{lag}, and *Gain* for P-POD and Q-POD in PV-STATCOM and BESS

It is seen from Figure 3.2 that the OFs for both Q-POD and P-POD converge within 62 iterations to the desired limit ε which in this study selected as 1.

3.6 Case Studies

3.6.1 No POD Controller

It is assumed that the PV-STATCOM inverter capacity is fully available for Q-POD controller and no real power is generated from the PV system during the night time. In steady-state operation condition, 527 MW real power transfers from the generator to the grid. At *t*= 5 sec, a 3-phase to ground fault is initiated at the generator bus, which is cleared after 5 cycles. Due to the fault, growing low frequency electro mechanical oscillations appear in the power system. Figure 3.3 illustrates the midline power oscillations after the fault. In this study, no POD controller is activated. Both the PV system and BESS stay idle during the contingency.

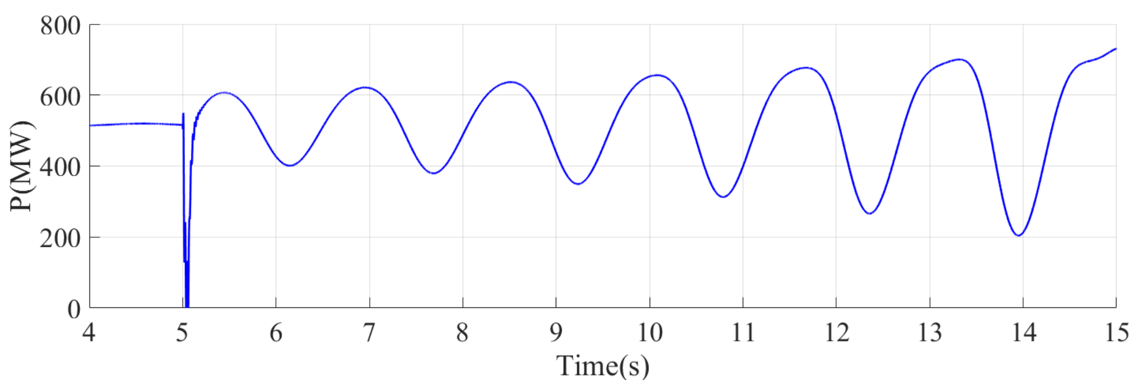

Figure 3.3 SMIB midline real power with no POD controller

3.6.2 Q-POD with PV-STATCOM Reactive Power

Figure 3.4 depicts the results for midline real power and PV-STATCOM reactive power after the fault, considering the Q-POD controller for PV-STATCOM to be activated. As shown in Figure 3.4 (a) the oscillations get damped after 3 sec. Figure 3.4 (b) illustrates that after the fault clearance, the Q-POD controller modulates the PV-STATCOM reactive power output to damp the power oscillations. Furthermore, the entire PV-STATCOM inverter capacity is utilized to damp the power oscillations.

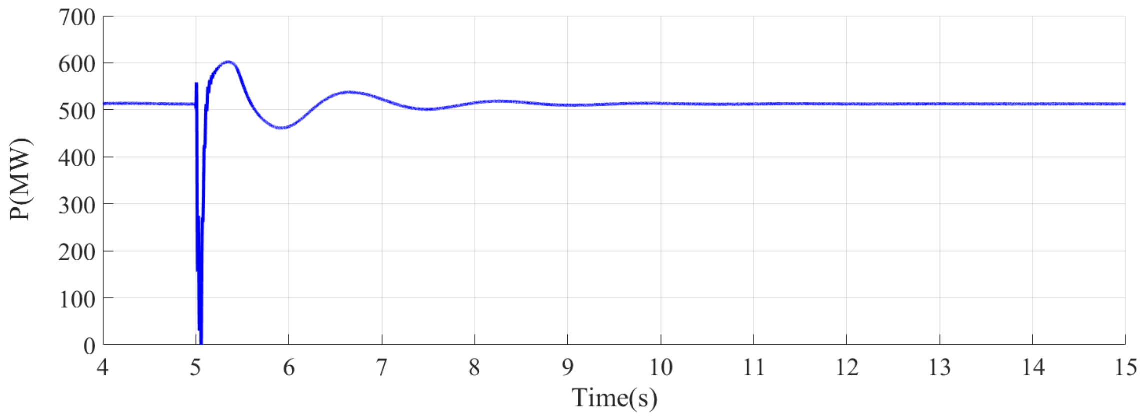

(a)

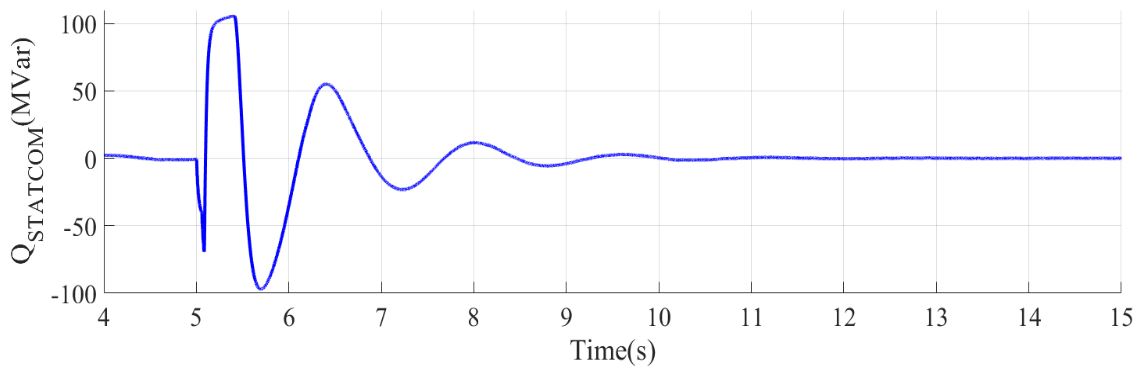

(b)

Figure 3.4 (a) SMIB midline real power, (b) PV-STATCOM reactive power in Q-POD mode of operation

3.6.3 P-POD with BESS Real Power

In this study, power oscillations are damped with BESS real power controller. Different BESS sizes are used such as ±10, ±25, and ±50 MW_{max} in order to compare the effect of POD with BESS and Q-POD with PV-STATCOM. Figure 3.5 shows the results for SMIB system midline and BESS real power after the fault for three BESS sizes. The effectiveness of P-POD controller increases by increasing the size of the BESS from 10 to 50 MW_{pk}. The results show that even the ±10 MW_{pk} BESS can improve power oscillation damping. However, to achieve the desired 5% minimum damping ratio, a minimum of ±25 MW_{pk} capacity is required i.e. a settling time less than 10 sec for 1.7 Hz oscillations [22]. As shown in Figure 3.5, if ±50 MW_{pk} BESS is selected for P-POD the damping of power oscillations are further improved and become similar to results achieved through Q-POD control of PV-STATCOM.

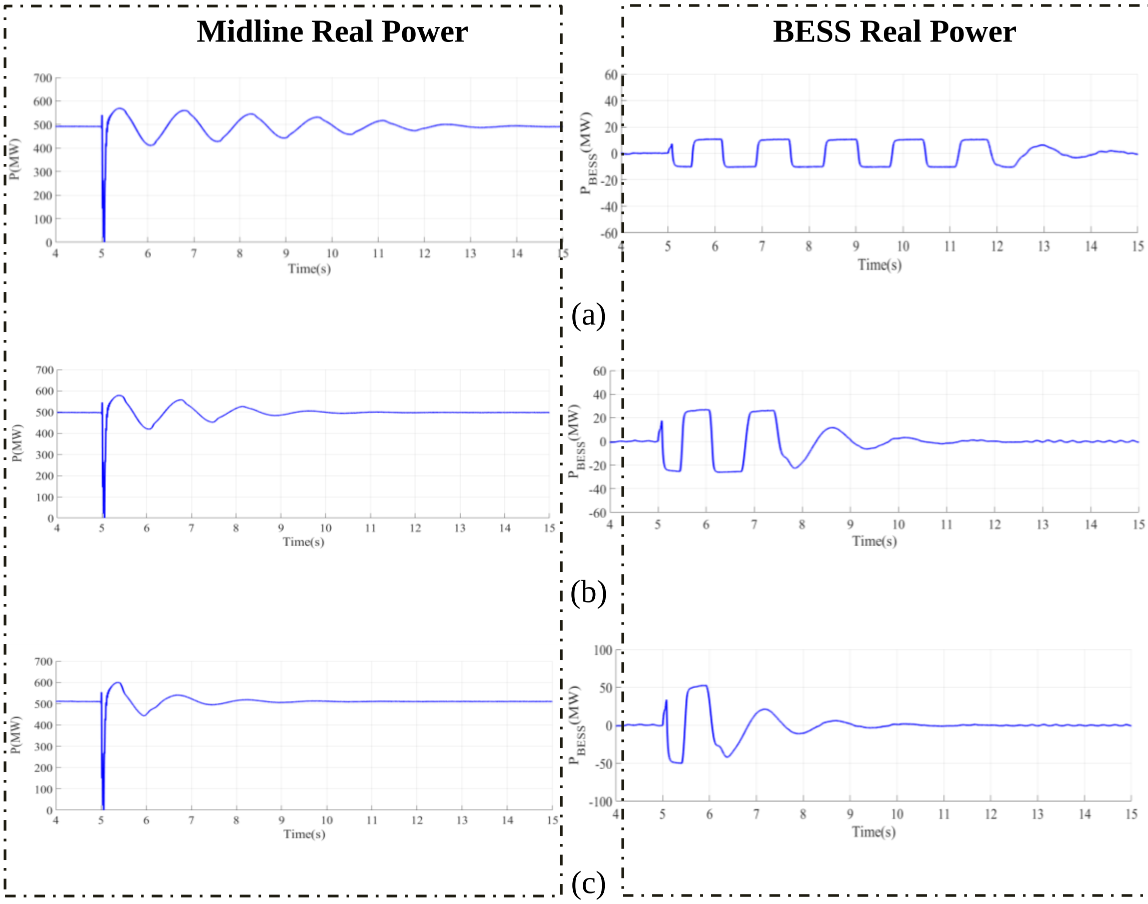

Figure 3.5 SMIB midline real power considering P-POD with ±10, ±20, and ±50 MW_{max} BESS

In Figure 3.6 (a), the SMIB system midline power for No-POD, Q-POD with PV-STATCOM, and P-POD with BESS are illustrated for comparison of all scenarios. Figure 3.6 (b) depicts the PV-STATCOM reactive power and BESS real power. Figure 3.6 (c) portrays the midline voltage during POD with PV-STATCOM and BESS. It is clear from Figure 3.6 (a) and Figure 3.6 (b) that a BESS of half the size of a PV-STATCOM is sufficient to perform the same level of POD. According to Figure 3.6 (c) the small difference is observed for midline voltage between P-POD with BESS and Q-POD with PV-STATCOM. In both cases, the voltage remains within acceptable range based on the E.On and NERC grid codes [112, 113].

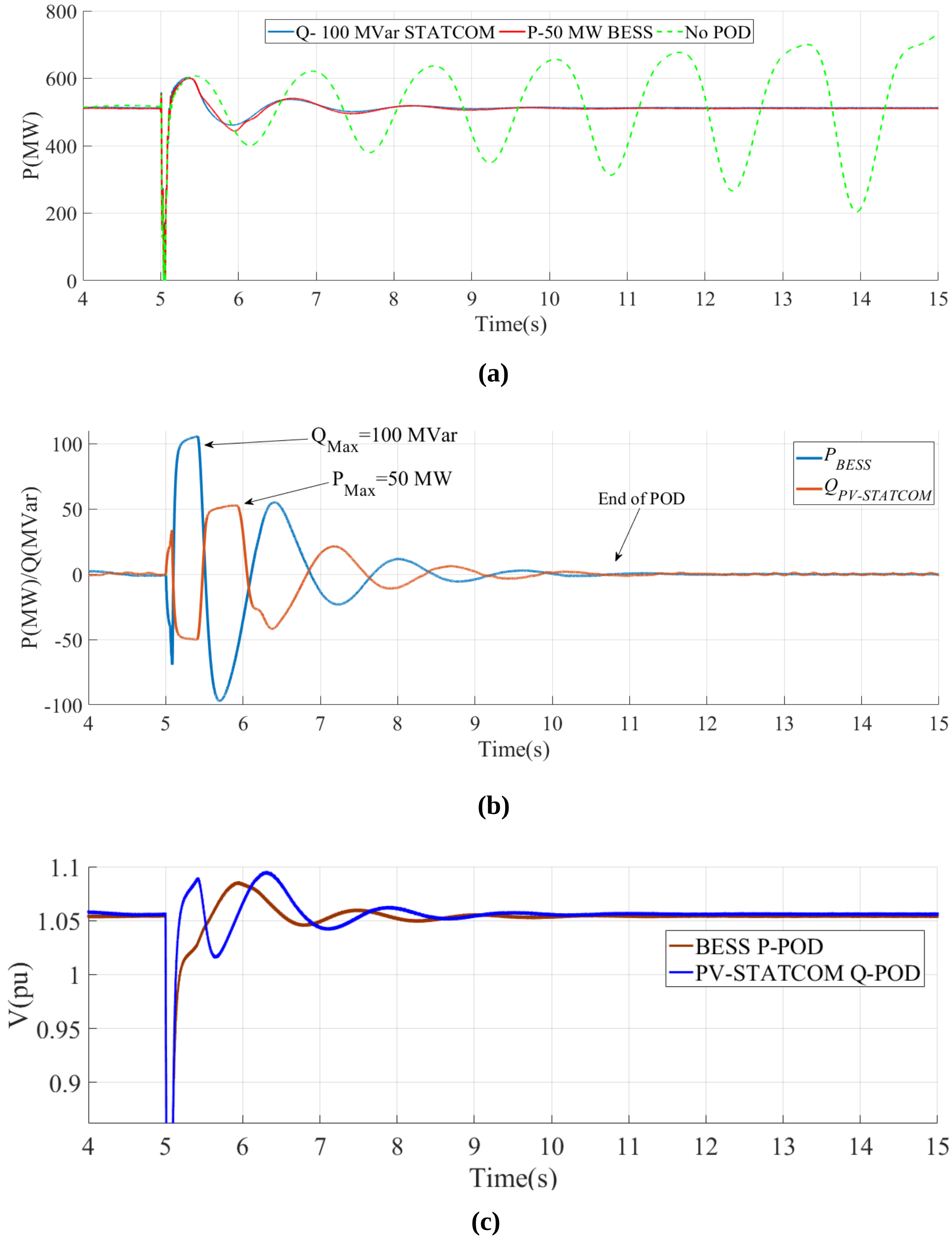

Figure 3.6 Comparison between P-POD and Q-POD for BESS and PV-STATCOM

3.7 Conclusion

A comparative study of Q-POD control with PV-STATCOM and P-POD control with BESS is performed in this Chapter. The POD controllers are optimized in EMT-type detailed simulation studies to achieve maximal damping for both P-POD and Q-POD. The effectiveness of P-POD control with BESS is dependent on the size of BESS. Case studies for P-POD controller with various sizes of BESS are presented and results are compared with Q-POD with PV-STATCOM. It is shown that a BESS of half the size of PV-STATCOM is needed to achieve the same level of power oscillation damping.

The studies in this chapter illustrate that real power modulation based POD controller can be effectively employed for damping electromechanical oscillations. Based on this conclusion, such P-POD control is implemented on a PV-STATCOM during daytime in Chapter 6 and Chapter 7.

Chapter 4

4 Coordinated Control of PV Solar System as STATCOM (PV-STATCOM) and Power System Stabilizers for Power Oscillation Damping

4.1 Introduction

The objective of this chapter is to examine if a coordination of traditionally used power system stabilizers (PSS) and reactive power modulation based PV-STATCOM control can provide increased levels of power oscillation damping than with either one of them acting alone. Hence, this chapter presents an optimized coordinated control of PV-STATCOM with Power System Stabilizers (PSS) for Power Oscillation Damping (POD) in the Two-Area power system. All the four synchronous generators are considered to be equipped with PSS whereas a large-scale PV solar power plant is connected at the midpoint of the tie-line connecting the two areas. The capacity of the PV inverter remaining after real power generation is utilized for dynamic reactive power exchange to damp power oscillations caused by a disturbance. The master-slave simulation technique based on simplex optimization in PSCAD/EMTDC software is utilized for performing the optimization and controller coordination.

4.2 Study System Model

Figure 4.1 illustrates the Two-Area power system utilized in this study. The PSS units are added in the excitation systems of all four generators. The different components of Two-Area power system are described in *Section* 2.3.2. The PSS block diagram is presented in Section 2.4.3. The speed of individual generator is used as the control signal for the PSS resident on that generator. A large PV solar system rated at 150 MW is connected at the midline of the power system. It is assumed that during steady state conditions, 430 MW real power transfers from Area A to Area B. The system data is presented in Appendix B

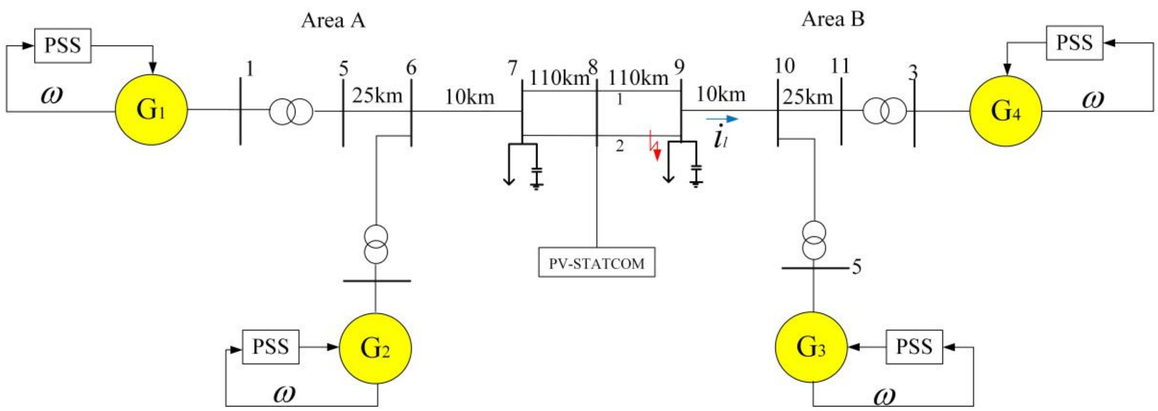

Figure 4.1 Two-Area Power System with PV-STATCOM

4.3 Model of PV-STATCOM in Partial STATCOM mode

An aggregated 150 MW solar power plant controlled as STATCOM (PV-STATCOM) is simulated in PSCAD/EMTDC software. Figure 4.2 depicts the controllers for the proposed PV-STATCOM.

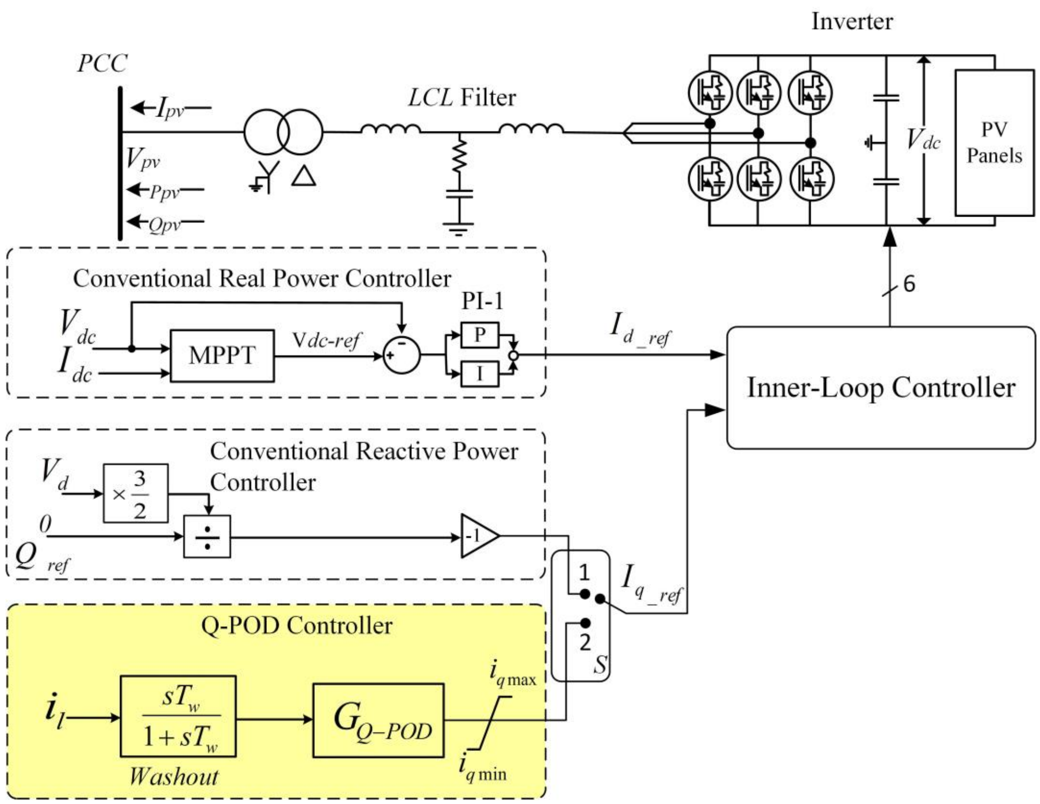

Figure 4.2 PV-STATCOM components and controllers

The models of different components of the PV-STATCOM have been described earlier in the thesis, i.e., PV solar panels (*Section* 2.5.1), Decoupled i_d/i_q controller (*Section* 2.5.2), LCL filter (*Section* 2.5.3), MPPT algorithm (*Section* 2.5.4), DC Voltage controller (*Section* 2.5.5), and Conventional Reactive Power Controller (*Section* 2.5.6). The additional Q-POD controller is added in order to perform the POD with PV-STATCOM remnant inverter capacity.

4.3.1 Q-POD Controller in Partial STATCOM mode

The Q-POD controller controls the reactive power output of the PV-STATCOM to damp the low-frequency electromechanical oscillations. i_L represents the line current between buses 9 and 10, which has the highest participation factor in interarea mode of oscillation [14]. The i_L signal is passed through washout filter to remove its DC component. The washout filter design is described in *Section* 2.7.1. The damping controller transfer function is selected as:

$$G_s(t) = G \times \frac{1 + sT_{lead}}{1 + sT_{lag}} \tag{4.1}$$

where, G represents the controller gain; and T_{lead} and T_{lag} model the *lead* and *lag* time constants, respectively.

This controller generates the I_{qref} reference current for PV inverter inner loop controller to control the PV reactive power. The real power production is not affected during Q-POD control, implying that real power production is given priority during the POD operation. Consequently, MPPT unit continues to be activate and i_{dref} is not influenced during POD. If the low frequency electromechanical oscillations appear in the power system, switch S is changed from position 1 to position 2. Thus, i_{qref} is controlled through Q-POD controller.

4.4 Optimized Coordinated Controller Design

PSS controllers for synchronous generators and Q-POD controllers for PV-STATCOM are designed with the *Simplex* optimization technique implemented in the EMTDC/PSCAD software. This optimization is implemented based on the Master/Slave simulation described in *Section* 2.7.4. It is assumed that 3-phase to ground fault is initiated near the bus 9 and faulted line 2 is disconnected after 5 cycles. Optimization of PSSs and Q-POD controller is performed based on minimization of low frequency oscillation in the line power after the line 2 disconnection, as follows:

4.4.1 Optimized Q-POD Controller Design

If all PSSs are out of service, POD is entirely performed by the Q-POD control of PV-STATCOM in Partial STATCOM mode of operation. Q-POD controller is designed to damp the interarea mode of oscillation together with the local modes of oscillation. It is assumed that the PV solar system is generating 100 MW. The remaining PV inverter capacity is calculated as:

$$Q = \sqrt{S^2 - P^2} \tag{4.2}$$

where, P is the PV real power output, S represent the inverter rating, and Q represent the remaining inverter capacity.

According to (4.2), for a 150 MW solar power plant producing 100 MW real power, 111 Mvar PV inverter remnant capacity is available for Q-POD. Since line current i_l between buses 9 and 10 has the highest participation factor (PF) in the interarea mode of oscillation [14], i_l is selected as the control signal for Q-POD controller. To optimize the Q-POD controller, OF is defined as

$$OF = \int_{T_1}^{T_2} \left(P_{mid} - P_{mid-ref}\right)^2 dt \tag{4.3}$$

where, P_{mid} and $P_{mid\text{-}ref}$ are midline power and midline power reference, respectively. T_1 and T_2 are the start and the end times of the power oscillations caused by the line outage. The washout filter with T_w=10 sec is designed to block the steady state components and pass the interarea mode oscillatory component having frequency less than 1 Hz. Figure 4.3 illustrates the OF and Q-POD controller parameters during the optimization process.

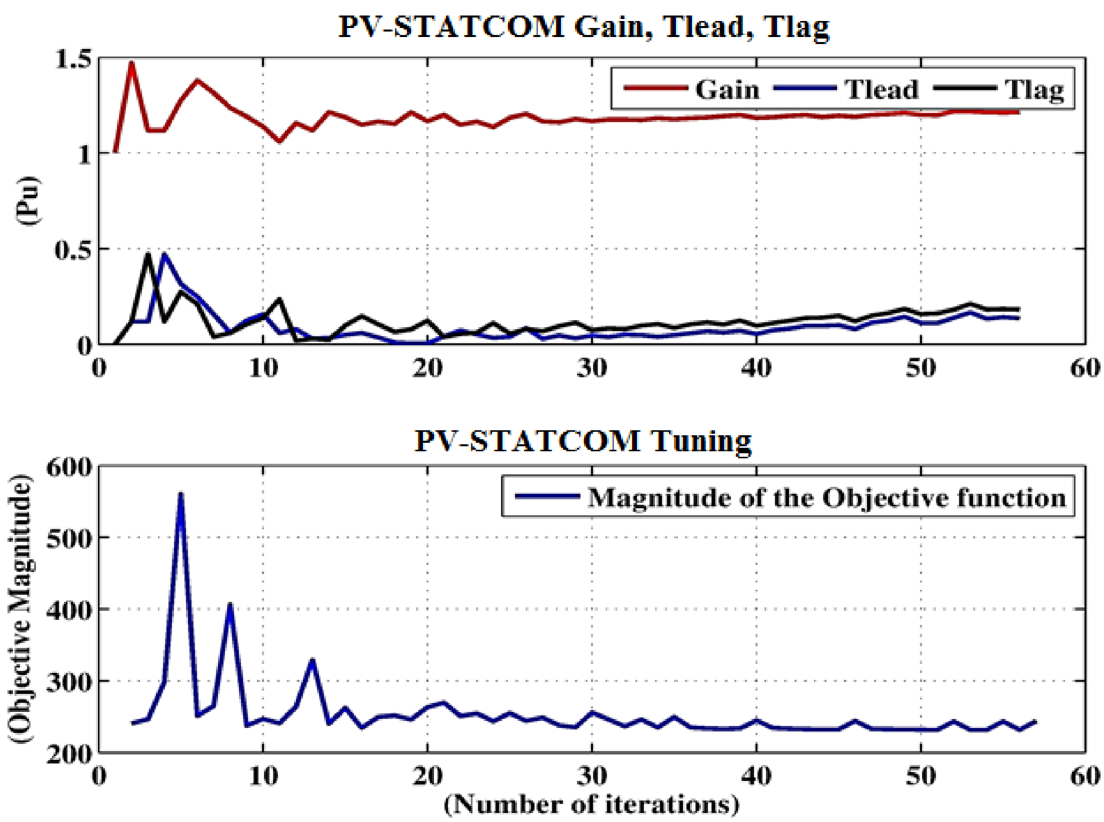

Figure 4.3 *Lead, and Lag* time constants and *Gain* of the Q-POD controller and the Objective Function (OF) during the optimization process.

4.4.2 Power Oscillation Damping with PSS

Lead-Lag controllers of the PSS (*Section* 2.4.3) are designed based on the *Simplex* optimization technique in PSCAD/EMTDC software. It is desired to minimize the local mode of oscillations for each generator during the contingencies. Hence, the OF for PSSs variables optimization is;

$$OF = \sum_{n=1}^{4} \int_{T_1}^{T_2} (P_n - P_{n_{ref}})^2 \, dt \tag{4.4}$$

where, P_n and P_{nref} are the power output and power output reference, respectively, for the n_{th} generator. The power output reference is the generator power output during the steady-state operation. Figure 4.4 illustrates the optimization process for design of PSS controllers.

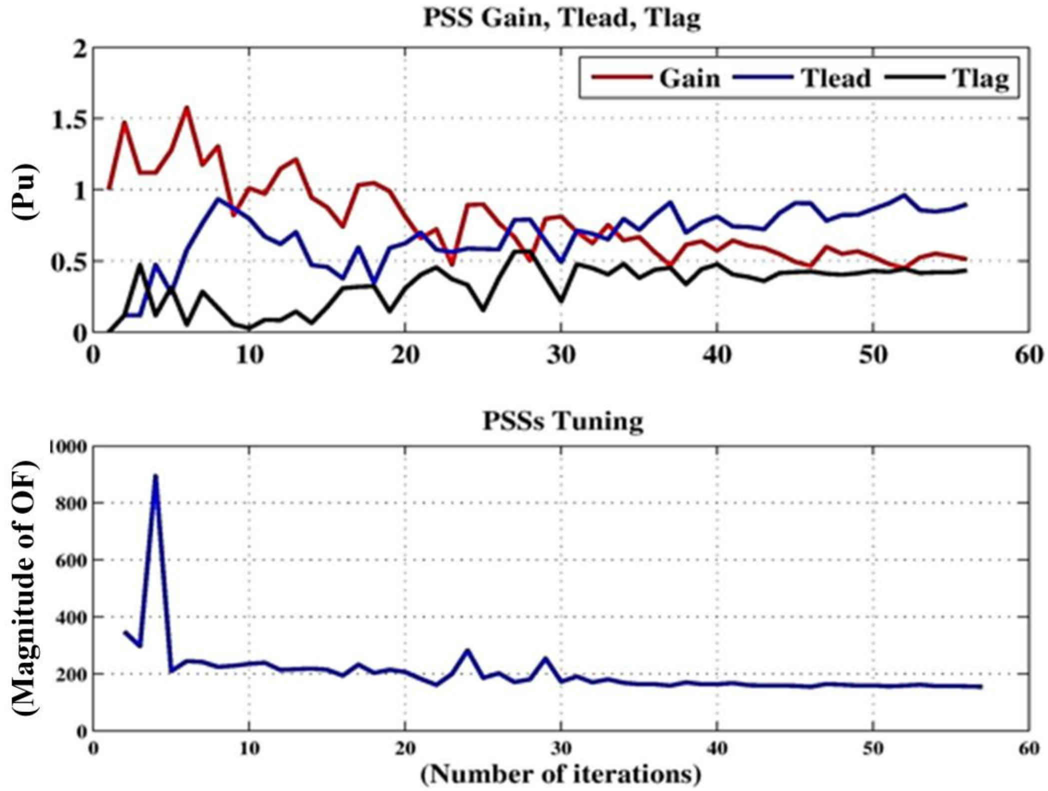

Figure 4.4 ***Lead, and Lag*** **time constants and** ***Gain*** **of the PSS and The OF during the optimization process**

4.4.3 PSS and Q-POD Coordination

The objectives of the coordinated design of Q-POD controller of PV-STATCOM with the PSS of generators are as to:

1) increase the damping of local modes of oscillation,

2) increase the damping of inter-area mode of oscillation

Based on the requirements of the coordination, the OF is determined as follows:

$$OF = w_1 \int_{T_1}^{T_2} \left(P_{midline} - P_{midline_{ref}}\right)^2 dt + w_2 \int_{T_1}^{T_2} (P_{G_1} - P_{G_1 ref})^2\, dt$$
$$+ w_3 \int_{T_1}^{T_2} (P_{G_2} - P_{G_2 ref})^2\, dt + w_4 \int_{T_1}^{T_2} (P_{G_3} - P_{G_3 ref})^2\, dt$$
$$+ w_5 \int_{T_1}^{T_2} (P_{G_4} - P_{G_4 ref})^2\, dt \quad (4.4)$$

The weighting function *w* is dependent on the objectives of the optimization process, i.e. to minimize the inter-area oscillations, and local power oscillations. The weighting function for each objective function is calculated based on the PF analysis of different generators in the interarea mode of oscillation.

The participation of rotor speeds for G_1 to G_4 in the inter area oscillation are 15%, 17%, 31% and 32%, respectively based on PF technique presented in *Section* 2.7.3. It is therefore concluded that a larger weight function needs is needed for generators 3 and 4.

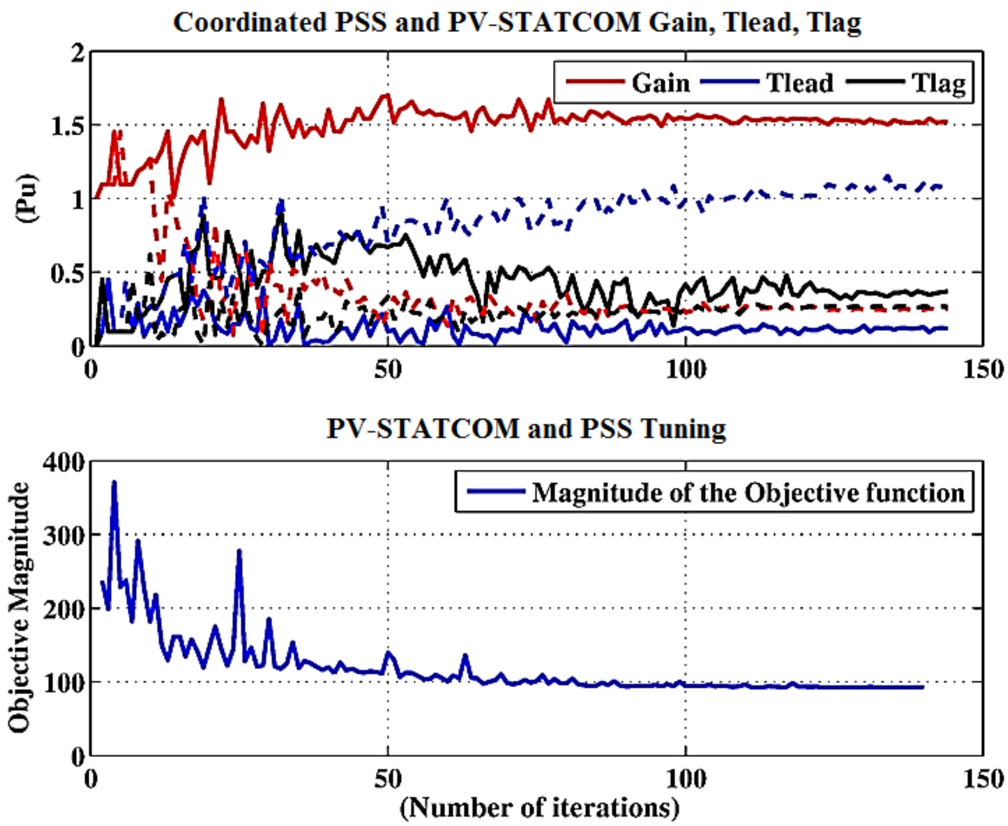

Figure 4.5 ***Lead, and Lag*** **time constants and** ***Gain*** **of the PSSs and Q-POD controller and The OF during the optimization process (dashed lines represent the PSS compensator parameters)**

Since the main objective is to reduce the oscillation in interarea mode of oscillation, w_1 is selected as 80% (note that based on specific requirements different values can be selected). The rest 20% is divided between other weight functions as w_2=3.5%, w_3=4.5%, w_4=6%, and w_5=6%. Figure 4.5 illustrates the simultaneous optimization process for coordination between PSS and PV-STATCOM Q-POD controllers.

Comparing Figure 4.4 and Figure 4.5 it is seen that during the coordination process, the PSS gains are reduced from 0.5 to 0.25 which results in a lower control effort from PSS controllers during the POD process. This gain reduction is due to participation of PV-STATCOM in POD in which reduces the need for excessive PSS effort.

4.5 Case Studies

It is assumed that in steady state condition, 430 MW real power transfers from Area A to B through line 1 and 2 (215 MW each). At *t*=5 sec, a 3-phase to ground fault is initiated at line 2 near the bus 9 for 5 cycles. The faulted line 2 is cleared after 5 cycles and the entire 430 MW power is transferred through line 1. The performances of the proposed PSS and Q-POD controllers are tested for damping the low frequency oscillations due to the fault and subsequent outage of line 2.

4.5.1 No PSS and No Q-POD Controller

In this study, the generators PSSs are deactivated and the Q-POD controller of PV-STATCOM is also disabled. The PV system is assumed to be generating 100 MW real power. Figure 4.6 illustrates the result for this study. It is seen that the growing oscillations occur both in the midline power and PV system real power. The system soon becomes unstable.

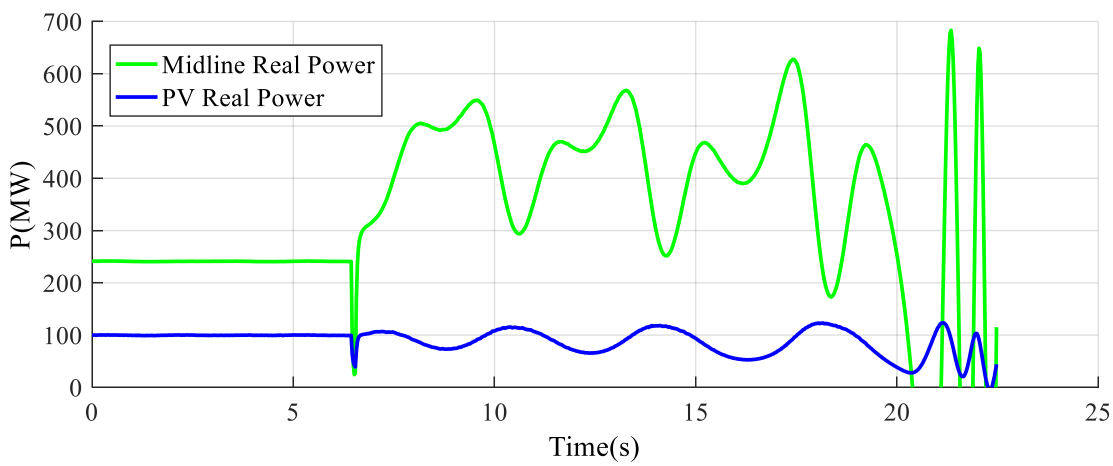

Figure 4.6 Midline real power for No Q-POD and PSS controller

4.6 PSS only

In this study, all 4 PSSs are activated to damp the power oscillations. Figure 4.7 depicts the midline real power during the above-described contingency. The oscillations get damped in 10 seconds and power system operates in a stable manner.

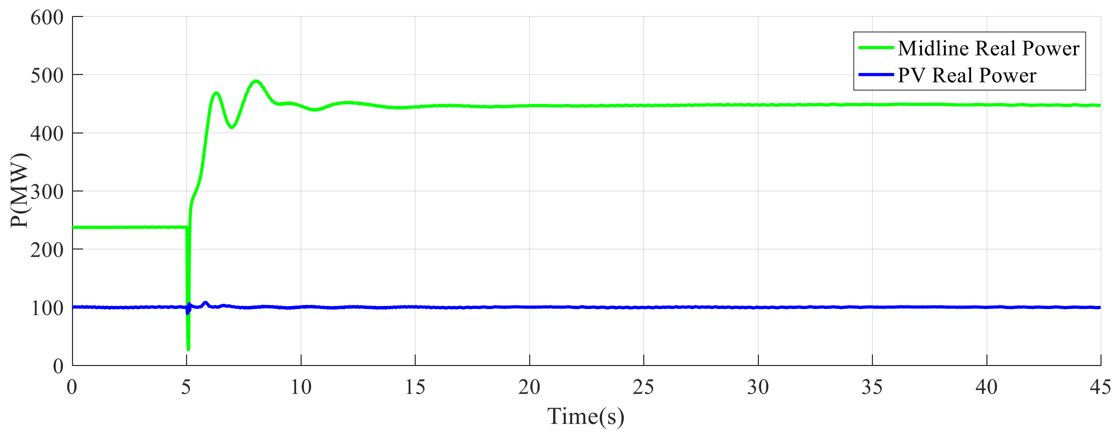

Figure 4.7 Midline real power and PV power output (PSS activated)

4.7 Q-POD with PV-STATCOM only in Partial STATCOM mode

All PSSs are deactivated and power oscillation damping is done with the remnant PV inverter capacity (±111 MVar) in Partial-STATCOM mode of the PV-STATCOM. Figure 4.8 (a) depicts the midline power and PV system real power for this study. Figure 4.8 (b) illustrates the PV-STATCOM reactive power output during Q-POD, while Figure 4.8 (c) depicts the midline voltage.

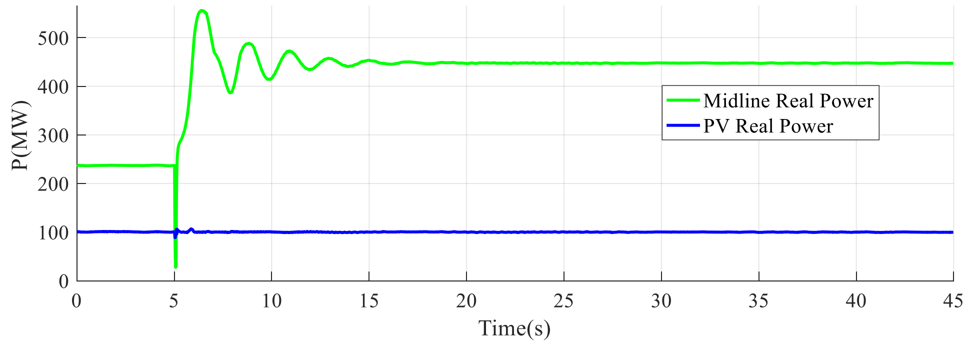

(a)

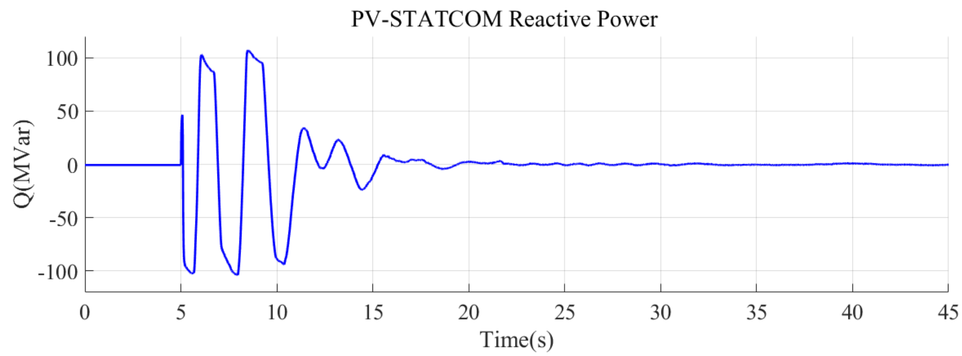

(b)

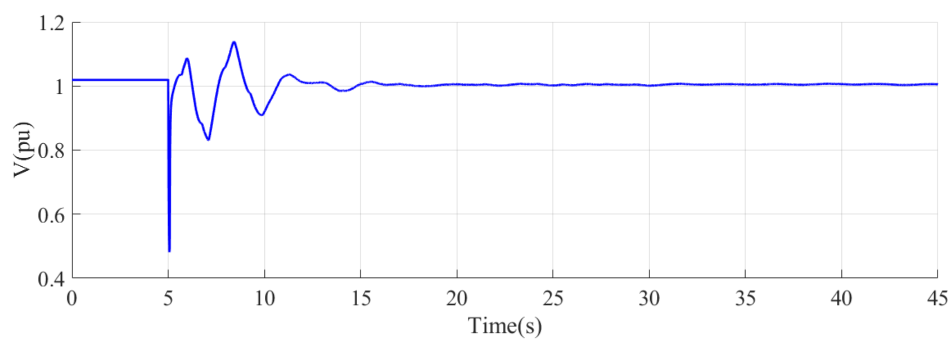

(c)

Figure 4.8 (a)Midline real power and PV-STATCOM power output during Q-POD (b) PV-STATCOM reactive power, (c) Midline voltage

The Q-POD control by PV-STATCOM damps the inter area power oscillations in 13 sec. However, this power oscillation damping takes longer time than that achieved with the activation of PSSs only. The PCC bus voltage is modulated based on PV-STATCOM reactive power output.

4.7.1 Coordinated PSSs and Q-POD Controller

In this study both PSSs and the Q-POD controller of PV-STATCOM are activated. The controllers are coordinated and optimized.

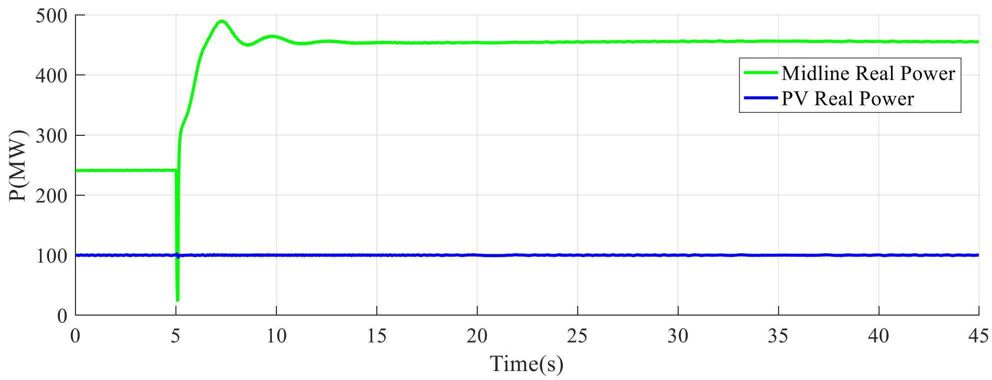

(a)

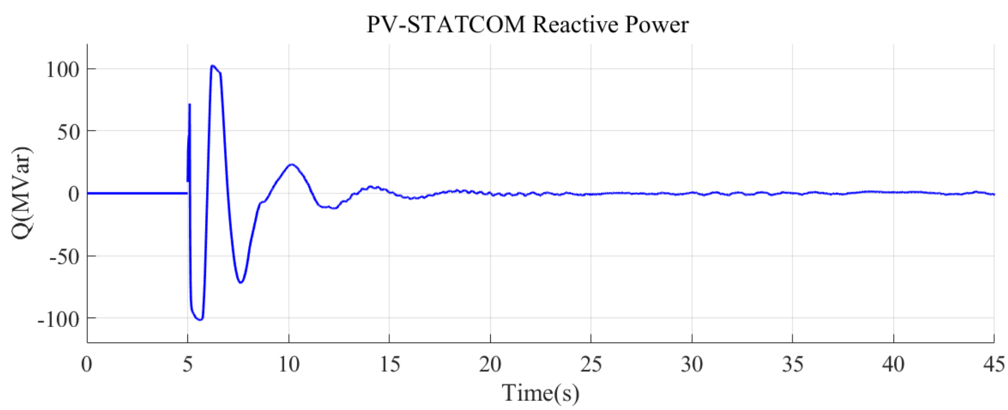

(b)

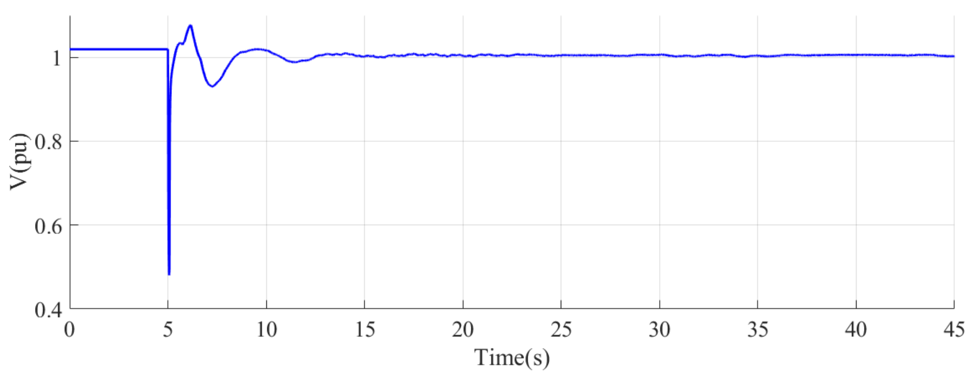

(c)

Figure 4.9 (a)Midline real power and PV-STATCOM power output during coordinated Q-POD and PSS (b) PV-STATCOM reactive power, (c) Midline voltage

Figure 4.9 (a) illustrates the result for midline real power. Figure 4.9 (b) depicts PV-STATCOM reactive power output. Figure 4.9 (c) illustrates the midline voltage for this study. The power oscillations are damped in 4 seconds which is much lower than those achieved with PSSs or Q-POD with PV-STATCOM, acting alone. The midline voltage variations are also considerably smaller in this case comparing to the case of Q-POD with PV-STATCOM.

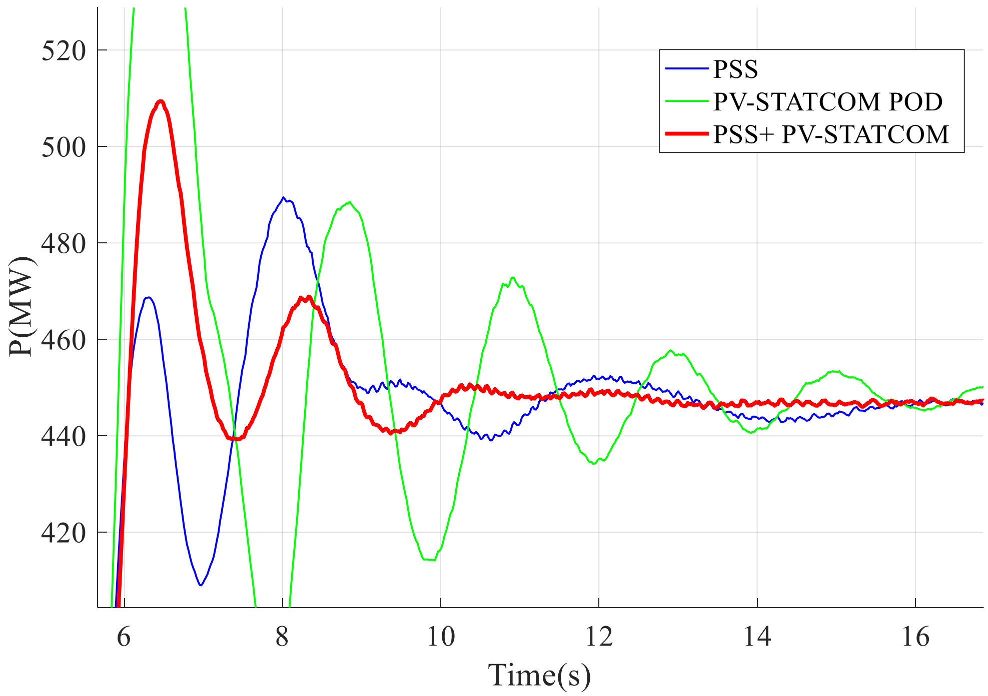

Figure 4.10 Midline real power for proposed control techniques

In Figure 4.10 the performances of proposed controllers for PSSs, Q-POD, and coordinated PSSs and Q-POD for PV-STATCOM are compared. The most effective and fastest damping is achieved when both Q-POD and PSS are activated in coordinated manner.

4.8 Comparison Between PV-STATCOM and Actual STATCOM

The damping performance of an actual 111 Mvar STATCOM connected together with a 150 MW PV solar farm generating 100 MW is now compared with the 150 MW PV solar farm controlled as PV-STATCOM. The proposed PV-STATCOM controller described in

Section 4.3.1 is used in the actual STATCOM. The STATCOM is considered to be connected at the same PCC point of the PV system, although not shown in Figure 4.1. In this study, the PV system remains connected and generates 100 MW real power in the conventional mode (i.e. it does not operate in PV-STATCOM mode). Figure 4.11 (a) depicts the midline and PV system real power for both the above cases. Figure 4.11 (b) shows the PV system real power for both studies in a magnified manner. It is evident that the PV-STATCOM demonstrates the same effectiveness in damping power oscillations as an actual STATCOM of the same rating. The only difference between PV-STATCOM and STATCOM in this study is a small variation in the PV real power during the power oscillation damping process. This is due to a slight interaction between the real and reactive power controllers (imperfect decoupling) in PV-STATCOM. In any case, this does not reduce the effectiveness of the PV-STATCOM.

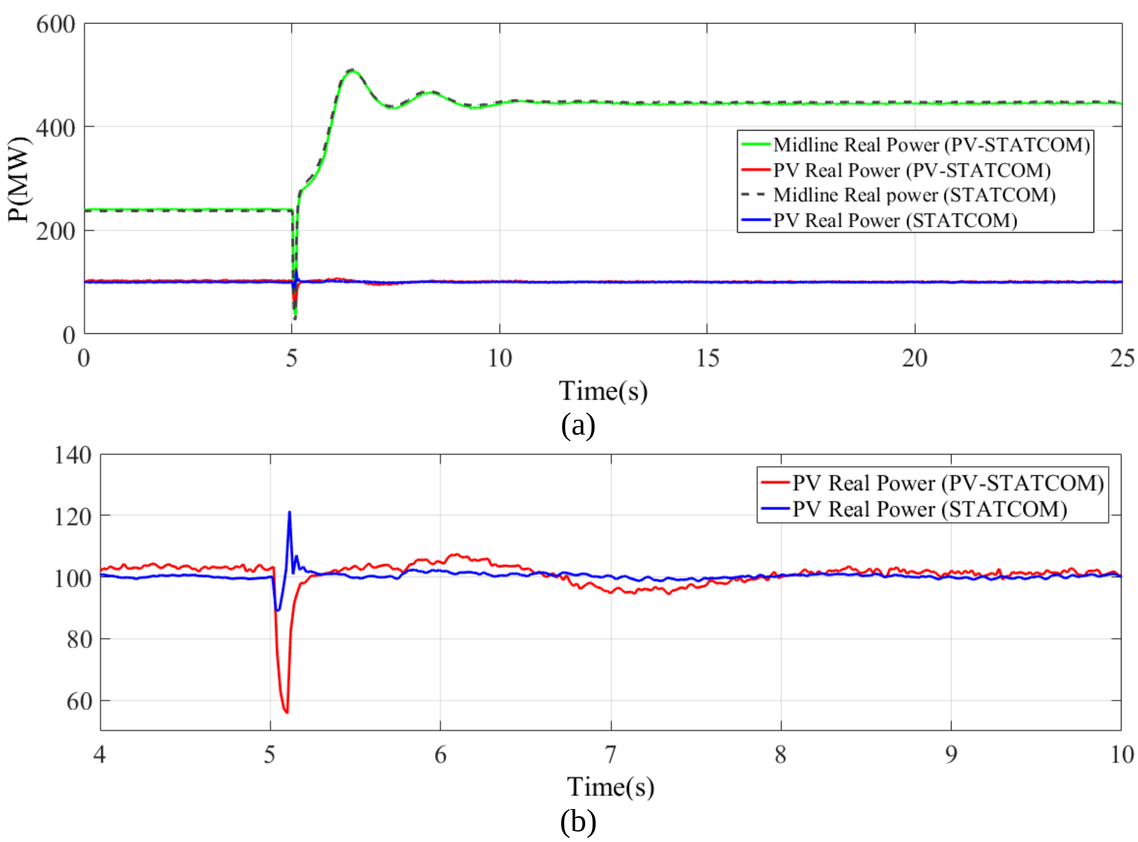

Figure 4.11 (a) Midline, PV system, and PV-STATCOM real power. (b) PV system and PV-STATCOM real power (Magnified)

4.9 Conclusion

This Chapter demonstrates an optimized coordinated control of PV solar farm as STATCOM (PV-STATCOM) and PSSs for damping power oscillations in a multi-machine power system. The optimized coordination of controllers for PSS units and PV-STATCOM is performed using the Simplex method embedded in the EMTDC/PSCAD software. The following conclusions are made:

i) A coordinated control of PV-STATCOM and PSSs results in a much higher damping than that achievable with either PSS or PV-STATCOM acting alone.

ii) The performance of a PV-STATCOM utilizing the remaining inverter capacity (after real power generation) is similar to that of an actual STATCOM of the same capacity rating.

Since large PV solar farms are being increasingly connected at transmission levels, worldwide, such utilization of PV systems as PV-STATCOMs in a coordinated manner with the existing PSSs can greatly enhance the power oscillation damping and lead to increased power transfers in transmission lines. This novel control will result in a more optimal utilization of the PV system asset for grid stabilization.

Chapter 5

5 Power Oscillation Damping with Reactive Power Control in Full PV-STATCOM

5.1 Introduction

This chapter presents a novel Power Oscillation Damping (POD) control for PV-STATCOM system in Full STATCOM mode of operation during the day time. In the proposed control, as soon as power oscillations due to a system disturbance are detected, the solar farm discontinues its real power generation function very briefly (few seconds) and releases its entire inverter capacity to operate as a STATCOM for POD.

After the oscillations are damped, the solar farm restores real power output to its pre-disturbance level in a ramped manner, while keeping the damping function activated resulting in a much faster restoration than that specified in grid codes [114, 115].

During nighttime, the solar farm performs POD with its entire inverter capacity. It is shown from EMTDC/PSCAD simulations that the proposed control provides significant increase in power transfer capacity on a 24/7 basis in systems which exhibit both local inertial and inter-area modes. Another novel contribution of this chapter is that the POD function is kept activated during the ramp up of power to its pre-disturbance value utilizing the inverter capacity remaining after real power generation. This prevents any recurrence of power oscillations and also allows a much faster ramp-up than prescribed by grid codes [114] where such a damping function during ramp-up is not envisaged. The proposed novel smart PV inverter control as PV-STATCOM thus allows a 24/7 capability of power oscillation damping with full inverter capacity. Furthermore, this POD function is accomplished with a simple first order controller.

The effectiveness of the proposed PV-STATCOM for POD is demonstrated on a Single Machine Infinite Bus (SMIB) system [116] and the Two-Area system [14] through detailed electromagnetic transients studies using PSCAD/EMTDC software. The *Simplex* optimization method embedded in PSCAD/EMTDC [106] is utilized to design the POD controller.

5.2 Concept of PV-STATCOM in Full STATCOM mode

The proposed smart inverter PV-STATCOM has two modes of operation – Partial STATCOM and Full STATCOM modes, illustrated in *Section* 2.2. As discussed in Chapter 2, the remnant PV inverter capacity during the day time and full PV inverter capacity during the nighttime can be utilized for POD as soon as low frequency power oscillations are detected in the power system. This technique is however limited during periods around noontime when the inverter capacity is largely or completely taken up for PV real power production. Hence, in this chapter, the Full STATCOM mode of operation is proposed wherein the PV real power injection function is disabled and entire PV inverter capacity is made available for POD.

5.3 Power System Studies

The performance of the proposed Q-POD in Full STATCOM mode is studied using two power systems – the Single Machine Infinite Bus (SMIB) system and the Two-Area power system, utilizing the PSCAD/EMTDC software. The PV-STATCOM is connected at the midpoint of both study systems as shown in Figure 5.1. The modeling of each power system is presented in *Section* 2.3.

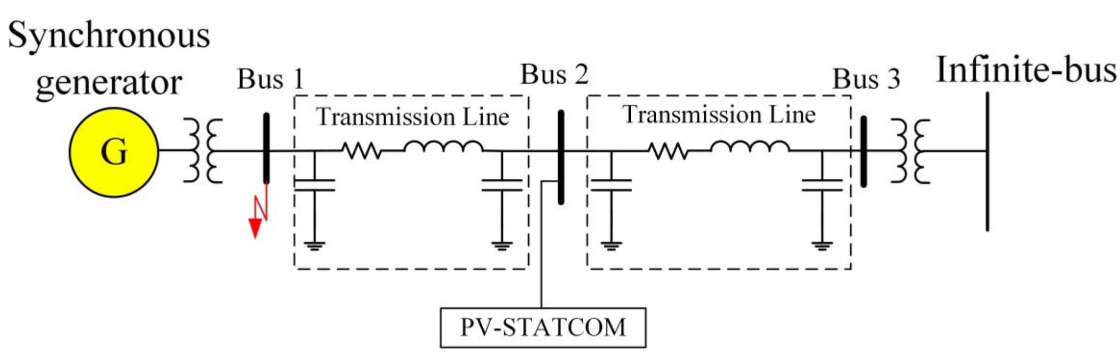

(a)

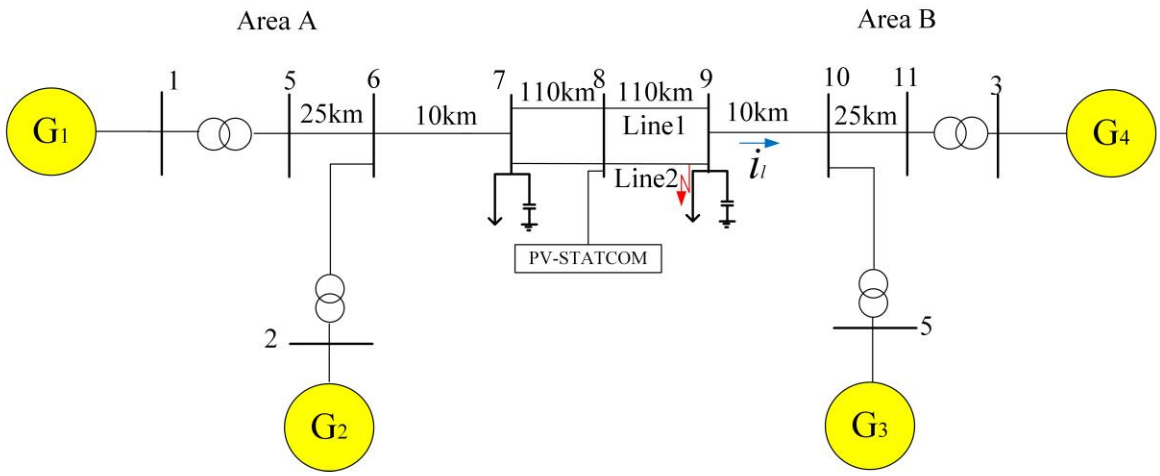

(b)

Figure 5.1(a) SMIB power system, (b) Two-Area Power system

5.4 Modeling of the PV-STATCOM in Full PV-STATCOM mode

Figure 5.2 illustrates the proposed 100 MW PV-STATCOM power system. The models of different components of the PV-STATCOM have been described earlier in the thesis, i.e., PV solar panels (*Section* 2.5.1), Decoupled i_d/i_q controller (*Section* 2.5.2), *LCL* filter (*Section* 2.5.3), MPPT algorithm (*Section* 2.5.4), DC Voltage controller (*Section* 2.5.5), and Conventional Reactive Power Controller (*Section* 2.5.6). In this chapter, additional controllers are proposed to perform POD with PV-STATCOM utilizing full PV inverter capacity as Q-POD controller. PV real power controllers are introduced for PV real power restoration. An Oscillation Detection Unit (ODU) is presented to detect the low frequency oscillatory modes and select the proper mode of PV-STATCOM operation. The ODU unit, Q-POD controller, and PV real power controllers are described below:

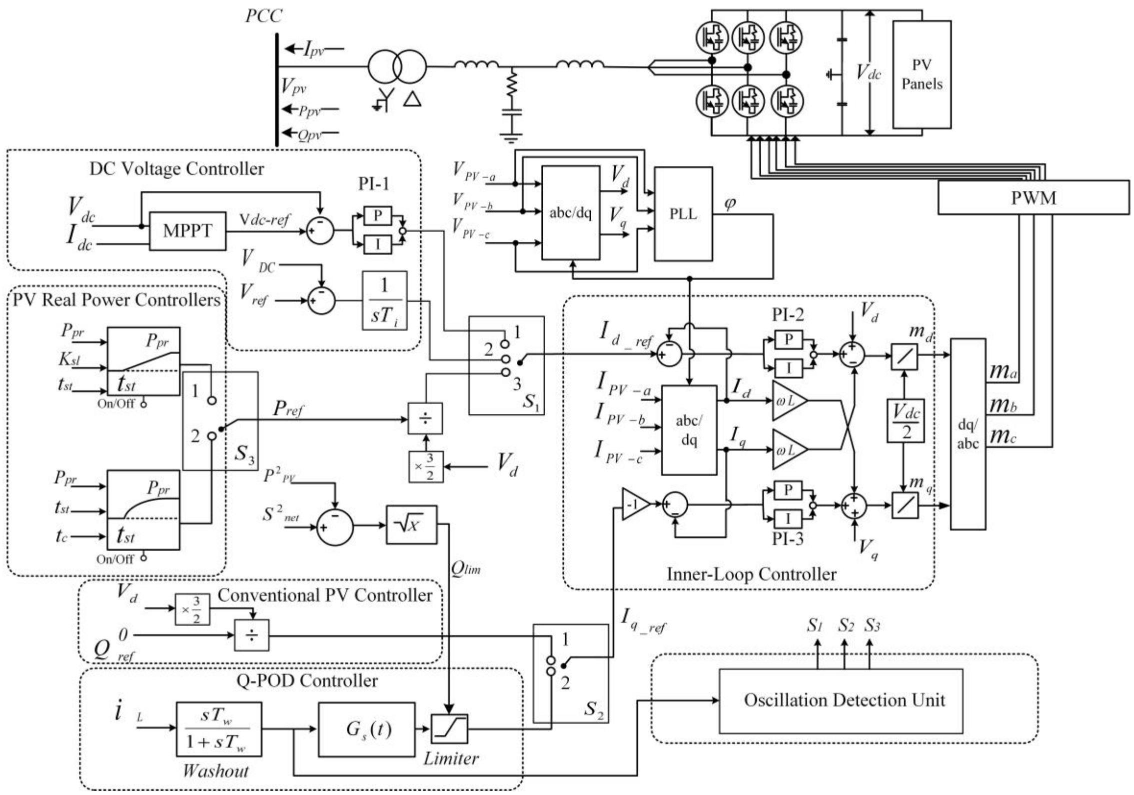

Figure 5.2 Block Diagram of 100 MW PV-STATCOM Components and Controllers

5.4.1 Q-POD Controller

The Q-POD controller based on the line current i_L at the PCC controls the reactive power output of the PV-STATCOM to damp the low-frequency electromechanical oscillations. In Study System 1 (SMIB), i_L represents the midline current where the PV system is connected. Meanwhile, in Study System 2 (Two-Area), i_L represents the line current between buses 9 and 10, which has the highest participation factor in interarea mode of oscillation [14]. The i_L signal is fed to the washout filter to remove its steady state component. The washout filter design is described in *Section* 2.7.1. The damping controller transfer function is selected as:

$$G_s(t) = G \times \frac{1 + sT_{lead}}{1 + sT_{lag}} \tag{5.1}$$

where, G represents the controller gain; and T_{lead} and T_{lag} model the *lead* and *lag* time constants, respectively.

This controller generates the I_{qref} reference current for PV inverter inner loop controller to control the PV reactive power. This controller remains activated during the PV real power restoration interval.

5.4.2 PV Real Power Controllers

These controllers are responsible for the restoration of the real power output of the PV solar farm to its pre-disturbance value after power oscillation damping is achieved in the Full STATCOM mode. Grid codes [115, 117] do not allow the power to be restored in a step manner as this may cause undesirable voltage and power oscillations. Instead these codes require the solar farms to restore their power with a prespecified ramp rate so that the above oscillations can be prevented. No damping function is envisaged in these grid codes during the process of power ramp-up.

In this chapter, a novel power restoration technique is proposed, according to which the solar farm continues to perform power oscillation damping during the entire power restoration process in the Partial STATCOM mode. This new mode of operation prevents the recurrence of power oscillations while the power is being restored to its pre-disturbance level. The proposed technique allows a much faster ramp rate to be achieved since power oscillations continue to be damped during the entire restoration process.

Two types of power restoration techniques are implemented in the PV Real Power Controllers depicted in Figure 5.1, and described below.

5.4.2.1 Power Restoration in a Ramped Manner

In this mode, the controller changes the PV real power output from zero to the pre-disturbance PV power level in a ramped manner with a ramp rate of K_{sl} starting at time $t = t_{st}$. This is the normal recommended mode for restoration of solar farms by grid codes. No damping function is envisaged during the ramp-up.

5.4.2.2 Proposed Power Restoration in the Partial STATCOM Mode with POD Control Active

In this mode, the controller changes the PV real power output from zero to the pre-disturbance PV power level in a ramped manner with a ramp rate of K'_{sl} starting at time $t = t_{st}$. The solar farm is operated in the Partial STATCOM mode with POD control kept active.

A variant of this technique is also shown in this chapter, according to which the power is restored from zero to the pre-disturbance level in a nonlinear mode starting at $t = t_{st}$ with an exponential time constant t_c. This time constant can be determined based on the decay time constant of the ambient power oscillatory modes. This technique is only demonstrated as an alternate technique which is shown to be quite effective.

During the real power restoration process, solar farm performs POD in Partial STATCOM mode with the reactive power capacity available after real power generation at that time instant. The reactive power limit Q_{lim} which continuously keeps declining as the real power gets restored to its original pre-disturbance level is given by

$$Q_{lim} = \sqrt{S^2 - P^2} \tag{5.2}$$

where, S represents the total inverter capacity, P is the inverter real power output and Q_{lim} is the maximum available inverter capacity during power restoration. Based on (2.24) the limitation in i_{qref} signal is applied on the output of POD controller.

5.4.3 Oscillation Detection Unit

The ODU autonomously detects the occurrence of unacceptable low-frequency electromechanical power oscillations caused by any grid disturbance such as faults. The ODU operates based on the flow chart depicted in Figure 5.3 and generates the ON/OFF status signals for switches S_1, S_2, and S_3. The magnitude of the line current at the PCC of solar farm is selected as the control signal for POD [76]. The oscillatory component of line current Δi_l is compared with a predefined value ε which in this study is chosen as 5%.

This ODU detects any oscillations in the control signal, which are caused by system disturbances such as faults. The ODU will also respond to system oscillations caused by sudden changes in the load, and will activate the Full PV-STATCOM operation. This aspect of load change, however, has not been considered in this thesis.

If the variation is more than ε the Full STATCOM mode is activated for POD control and PV real power is reduced to zero. If the oscillations stabilize and remain within the acceptable range, the selected power restoration mode (Ramp, or Nonlinear) is activated at $t=t_{st}$. A 2 *sec* delay is incorporated as a factor of safety. As soon as the PV real power P_{pv} reaches its pre-disturbance value P_{pr}, the STATCOM operation mode changes to the conventional PV controller mode of operation.

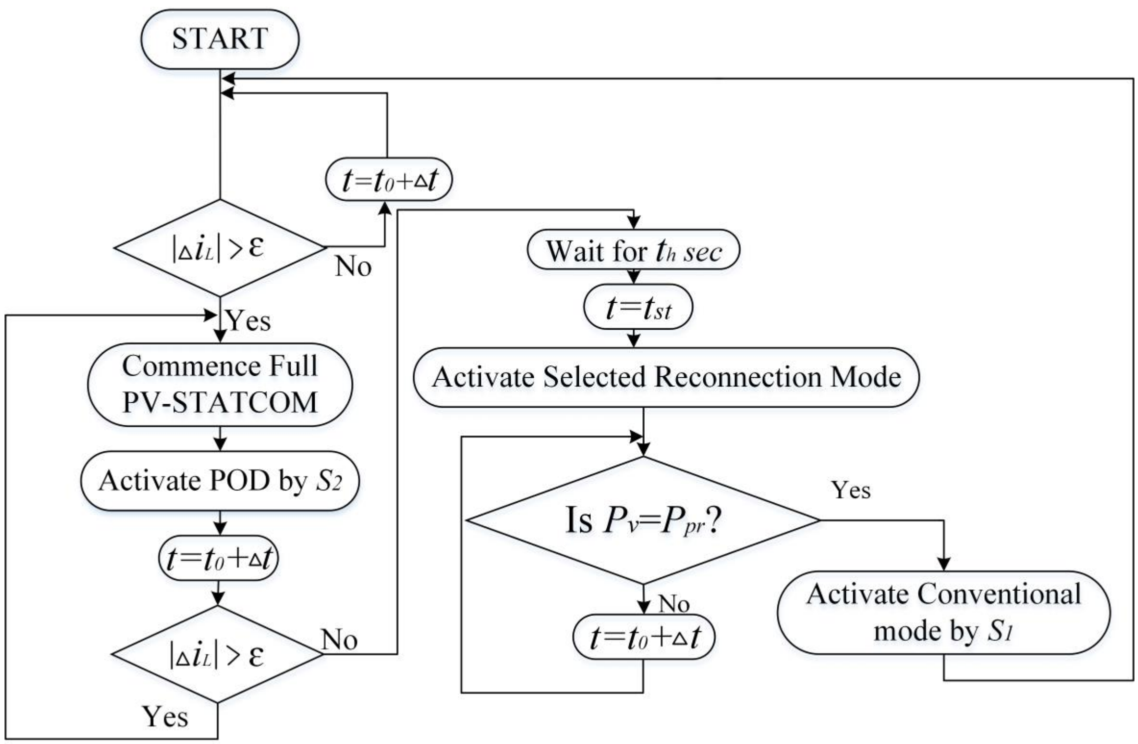

Figure 5.3 Flowchart of the operation of Oscillation Detection Unit

5.5 Optimized POD Controller Design

The POD controller parameters - *Gain*, *Lead* and *Lag* time constant are determined by the *Simplex* optimization technique [105] embedded in the PSCAD/EMTDC software [106]. The procedure and implementation of the optimization technique in PSCAD software is discussed in *Section* 2.7.4 . In this study, the aim is to minimize the low frequency power oscillations in line current. The corresponding Objective Function (OF) is defined as:

$$OF = \int_{T_1}^{T_2} \left(i_l - i_{l\_ref}\right)^2 dt \tag{5.3}$$

where, i_{l_ref} is the reference value of the midline current i_l. T_1 and T_2 are the start and end time of the current oscillations after the fault, respectively.

Figure 5.4 presents the OF, *Gain*, T_{lead} and T_{lag} for PV-STATCOM damping controllers design in SMIB and the Two-Area power systems. The OF converges in about 40 runs for the SMIB system and 59 runs for the Two-Area power system.

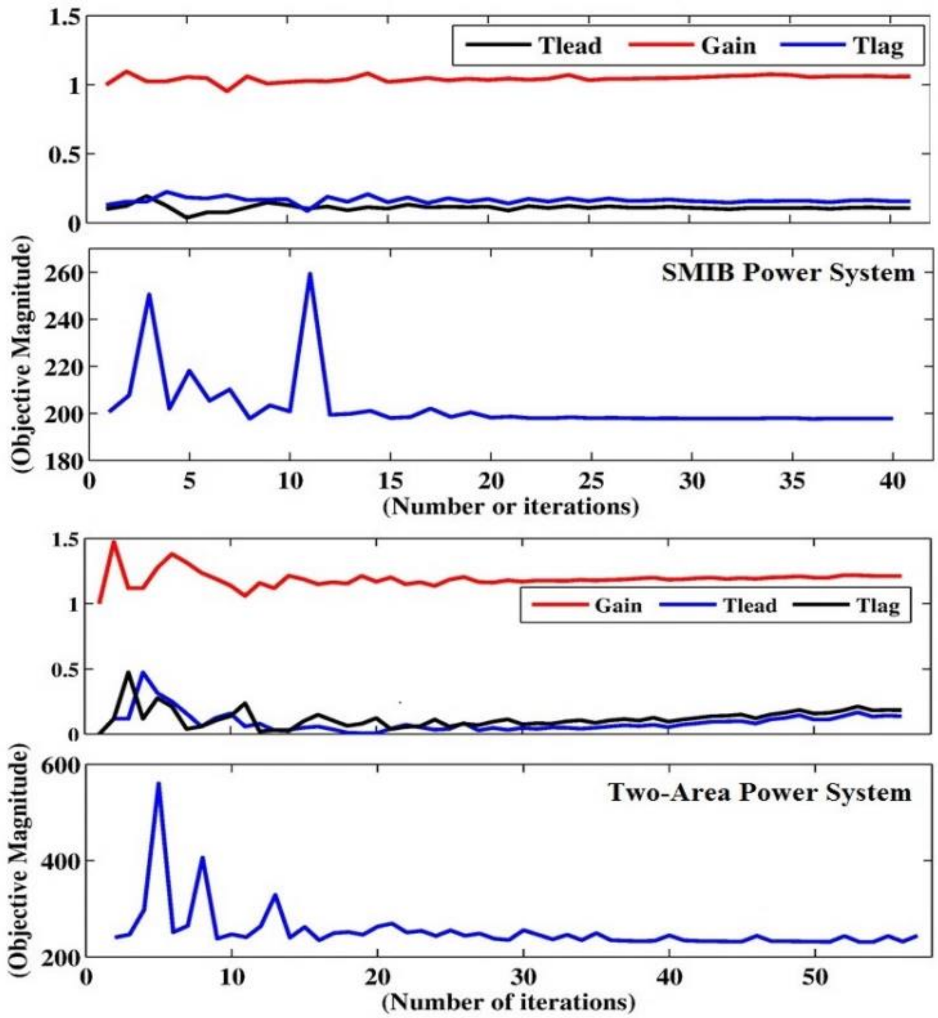

Figure 5.4 The OF, *Gain*, T_{lead} and T_{lag} for damping controllers for PV-STATCOM in SMIB and Two-Area power systems.

5.6 CASE STUDY 1: THE SMIB SYSTEM

This case study presents the improvement in power transfer capability in Study System 1 (SMIB System) through power oscillation damping with the proposed PV-STATCOM control. A three phase to ground fault is initiated at generator bus at t = 2 sec for 5 cycles in the different studies to examine the performance of the proposed control. The simulation studies are performed using the PSCAD/EMTDC software.

5.6.1 Power Transfer without PV-STATCOM Control

Figure 5.5 depicts the mid-line real power flow at the PCC bus of the PV solar farm as well as the power output of the solar farm. In this case, as soon as the fault occurs, the PV solar farm is disconnected thereby reducing its power output from 100 MW to zero. In order to ensure that the power oscillations have a damping ratio of at least 5% [102, 118] the oscillations should stabilize in about 10 sec for the considered oscillatory mode.

The SMIB system can transfer at most 200 MW power from the synchronous generator in addition to the 100 MW power generated by the PV solar farm. To examine the effect of increased power transfer in the study system, a similar fault study as above is conducted with 430 MW generator power. This results in unacceptably high-power oscillations as shown in Figure 5.5.

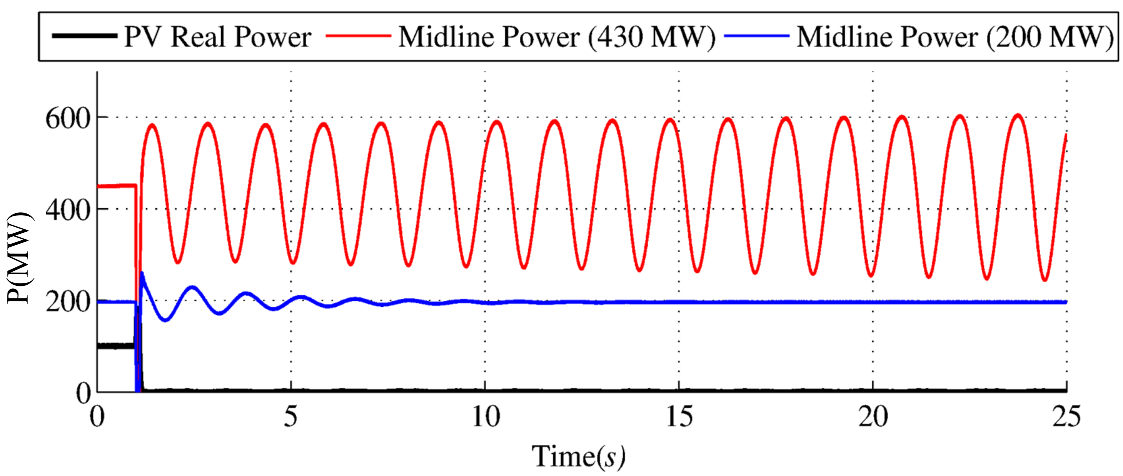

Figure 5.5 Maximum power transfer capability of the SMIB system

5.6.2 Study 2: Power Transfer of SMIB with PV-STATCOM POD Mode and Step PV Reconnection

In this study, the same fault as the one in Study 1 is applied at the SMIB system generator side. During the fault, ODU changes the PV operation mode to PV-STATCOM mode of operation. Figure 5.6 demonstrates that with the proposed POD technique, the maximum power transfer capability limit of the SMIB system is increased to 433 MW from the synchronous generator (damping ratio higher than 5%).

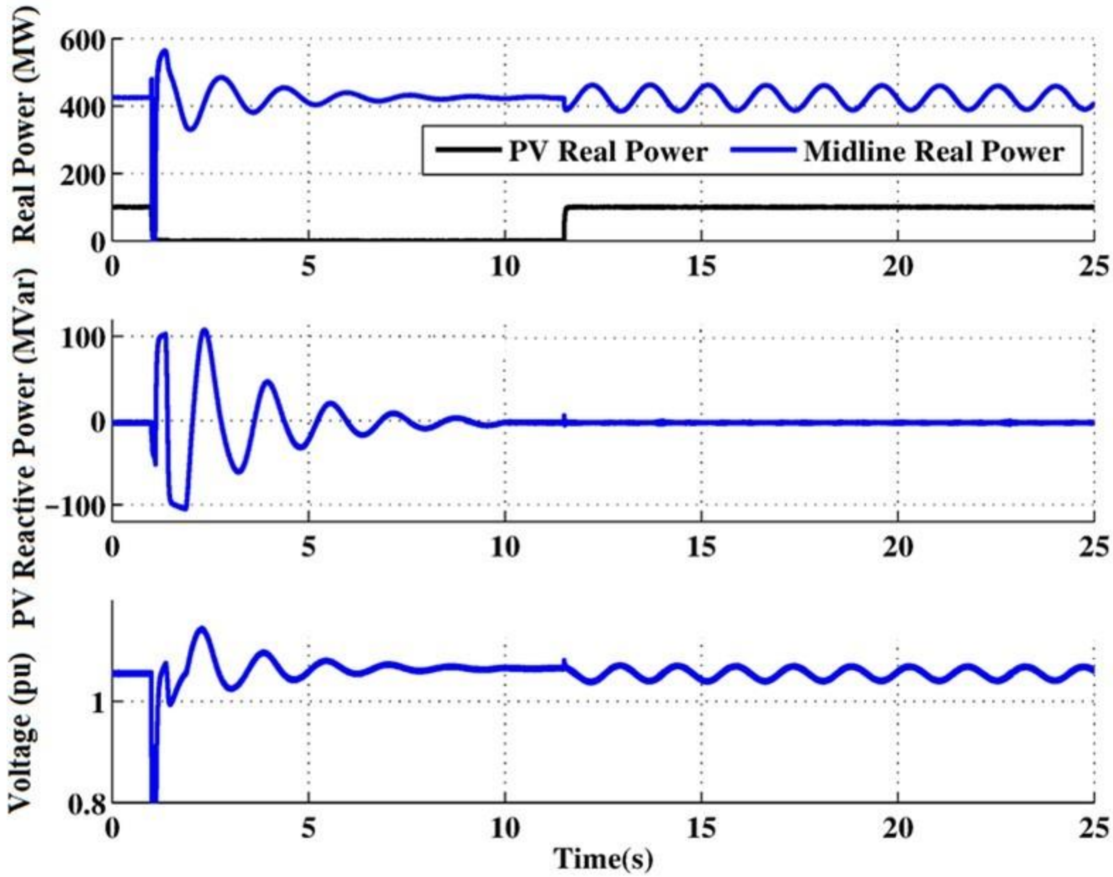

Figure 5.6 Midline and PV real power, PV reactive power and Midline voltage in SMIB system (Study 2), Step PV reconnection.

After the oscillations are damped, the ODU changes the mode of operation to *Step* reconnection control and 100 MW PV power is injected into the line in a *Step* function mode. It is shown that the sudden increase in the power results in an additional low power oscillations.

This mode of reconnection is not advised by the grid codes, but is described here only to illustrate its negative impact

5.6.3 Power Transfer with Full PV-STATCOM Damping Control and Power Restoration in Normal Ramped Manner

This study is conducted with a generator power of 430 MW and PV solar farm producing its rated power output of 100 MW at mid-noon with maximum solar irradiance. For this case, Figure 5.7 (a) depicts the midline power flow and the PV solar power output, whereas

Figure 5.7 5.7(b) and Figure 5.7 (c) demonstrate the reactive power of the PV-STATCOM and PCC voltage, respectively.

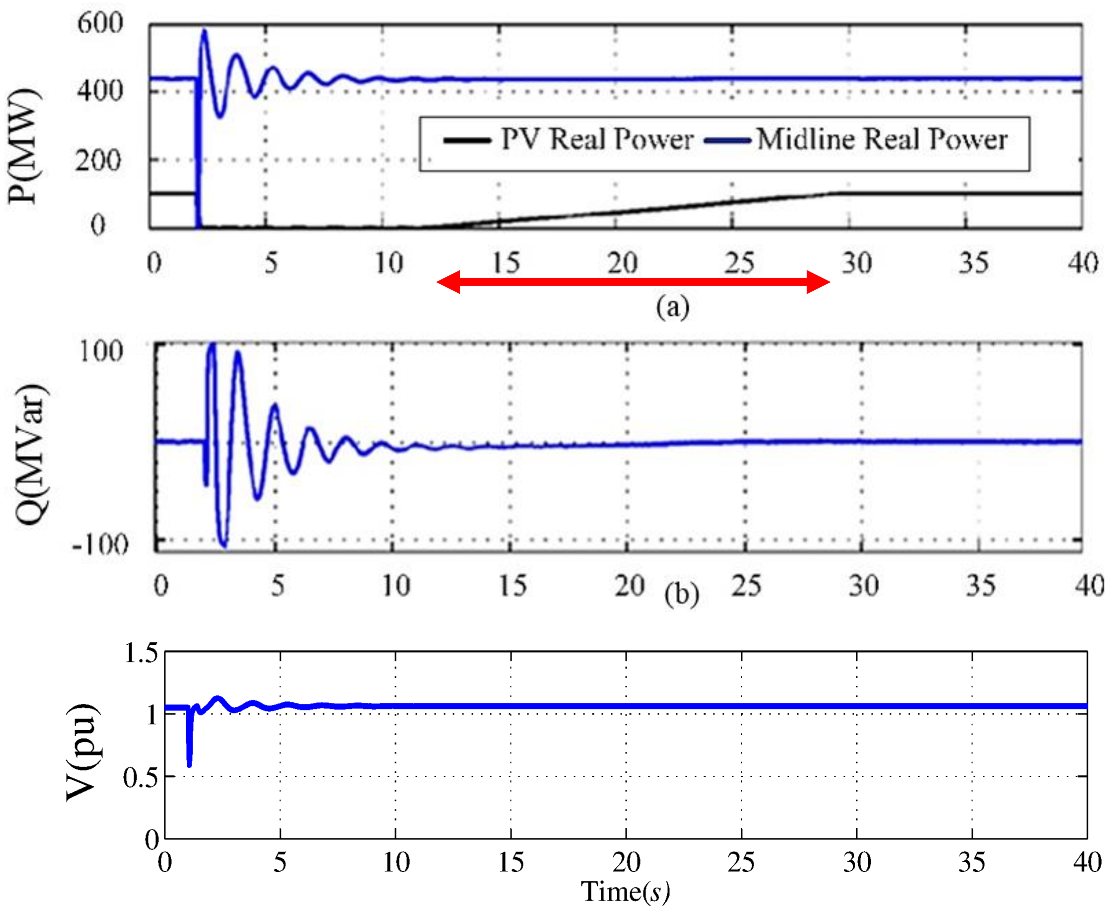

(c)

Figure 5.7(a) Midline and PV system real powers, (b) PV-STATCOM reactive power, (c) Midline voltage during POD and normal ramped power restoration.

The proposed Full PV-STATCOM control utilizes the entire inverter capacity for reactive power modulation to successfully damp the power oscillations to within acceptable limits in 8 seconds. The PCC voltage is also rapidly stabilized. Grid codes such as [119] specify that power restoration from a PV solar farm from zero to its rated level may be done with a typical ramp rate of 10% of rated capacity in 1 minute to avoid any power oscillations. In this case study, the fastest ramp rate which will expectedly not cause any resurrection of power oscillations is determined from simulations to be 5.5 MW/sec. Therefore, after power oscillations stabilize, the restoration of PV solar power output to its pre-disturbance value is commenced at t = 12 sec (incorporating the 2 sec factor of safety) with the above-obtained ramp rate of 5.5 MW/sec. It is noted that the power is completely restored in a time period of 18 *sec*, with no ensuing power oscillations.

5.6.4 Power Transfer with Full PV-STATCOM Damping Control and Ramped Power Restoration with POD Control Active in Partial STATCOM Mode

This study is performed to demonstrate the effectiveness of the proposed restoration technique for the same system operating conditions as in previous Case. Figure 5.8 (a) depicts the midline power flow and the PV solar power output whereas Figure 5.8 (b) and (c) illustrate the reactive power of the PV- STATCOM and PCC voltage, respectively.

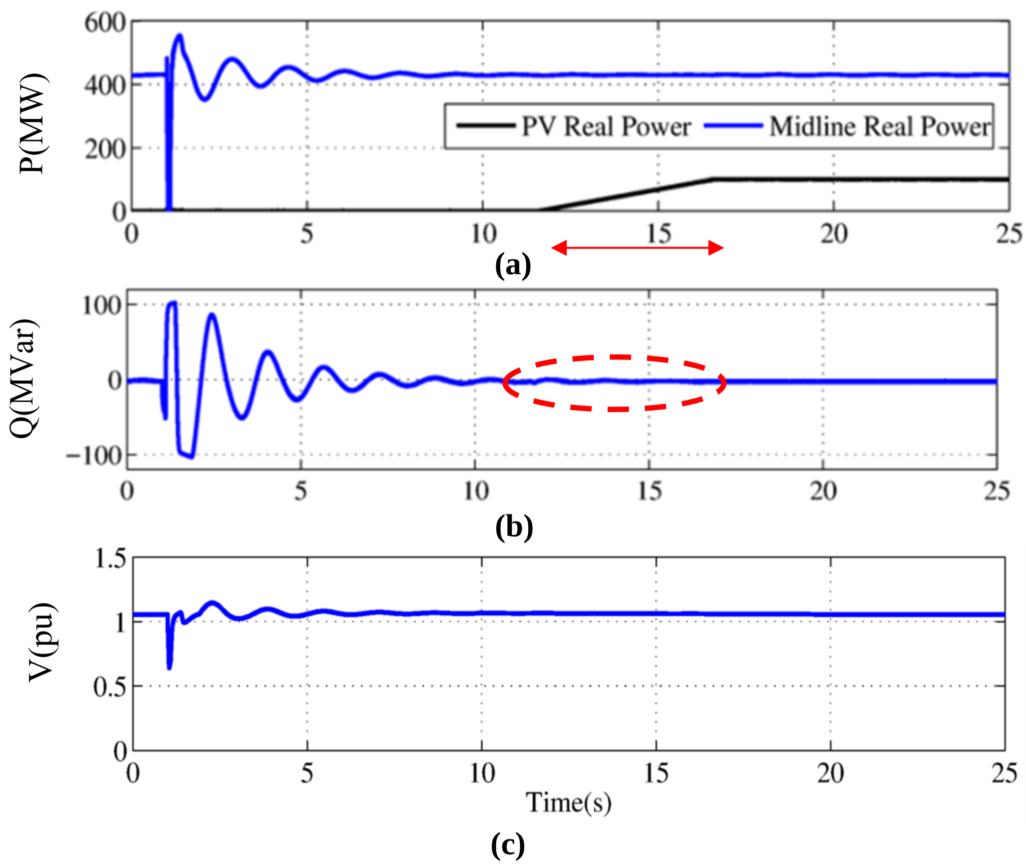

Figure 5.8 (a) Midline and PV system real power, (b) PV-STATCOM reactive power, (c) Midline voltage during POD and power restoration in Partial PV-STATCOM damping mode.

The PV real power is restored in a ramp manner with power oscillation damping continually being performed in the Partial STATCOM mode during the ramp-up. For better illustration, the reactive power modulation during the restoration period is indicated in a red dashed circle. It is evident from Figure 5.8 that with this novel restoration technique, the restoration of power to the pre-disturbance value is achieved in only 5 sec as compared to 18 sec in the previous case. This technique successfully prevents any recurrence of both power and voltage oscillations.

5.6.5 Nighttime Power Transfer Enhancement with Full PV-STATCOM Power Oscillation Damping Control

The same 5 cycle fault at t = 2 sec is initiated for a generator power output of 430 MW at nighttime. Figure 5.9 (a) portrays the behavior of 430 MW power flow in the tieline with and without the PV-STATCOM POD control. Figure 5.9 (b) illustrates the generator reactive power of the PV-STATCOM. It is seen that the solar farm with the proposed Full PV-STATCOM POD control successfully enables the same increase in power transfer from 200 MW to 430 MW in the nighttime, as in daytime.

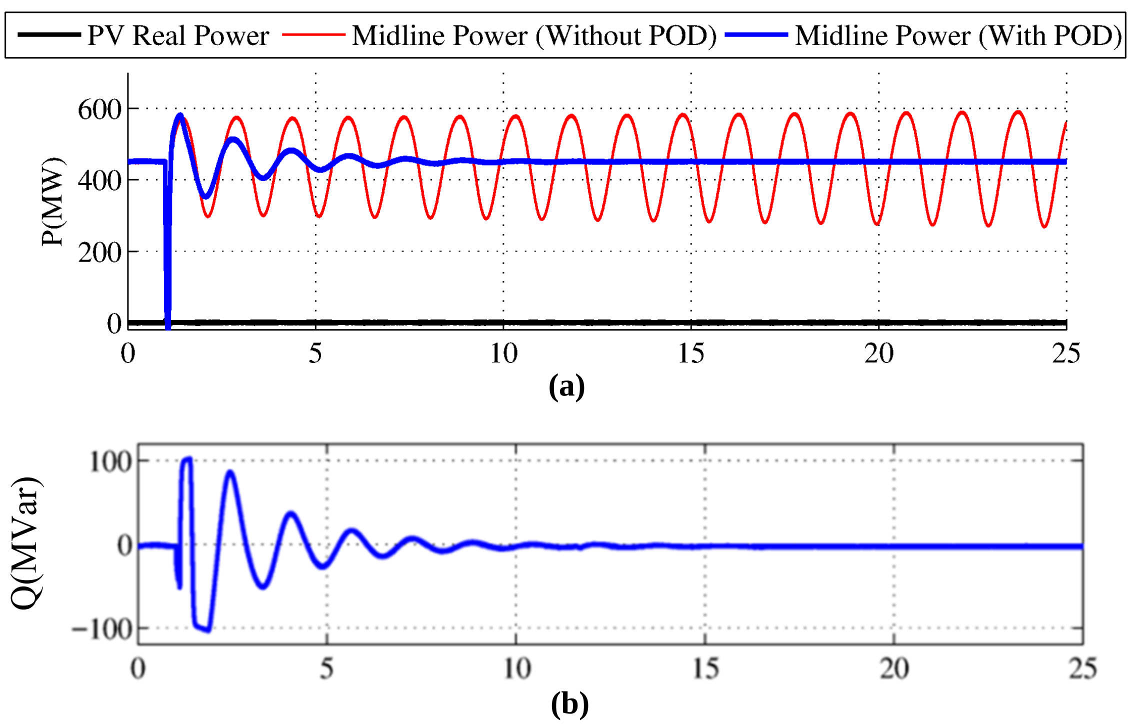

Figure 5.9 Nighttime (a) Midline real power with and without POD with PV-STATCOM control, (b) PV-STATCOM reactive power during POD.

5.7 Case Study 2: Two-Area Power System

5.7.1 Power Transfer without PV-STATCOM Control

In the Two-Area power system depicted in Figure 5.1 (b), power is transferred from Area *A* to Area *B* equally through tie-lines 1 and 2 under normal operation. A three phase to ground fault is initiated at *t* =2 sec for 5 cycles in Line 2 close to Bus 9. The circuit breakers disconnect the faulted line 2 and the entire tie line power is subsequently transferred through Line 1. The midline connected PV solar farm is considered to produce its rated 100 MW power at noon under maximum solar irradiance. As soon as the fault occurs the PV solar farm is disconnected. Figure 5.10 shows the midline real power and the PV solar power for this study. In this case, the maximum tie line power that can be stabilized with a damping ratio of 5% subsequent to the fault is 230 MW.

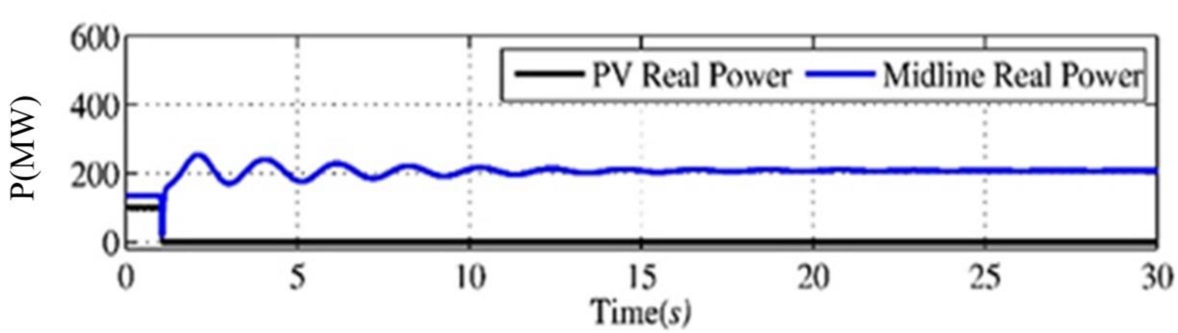

Figure 5.10 Midline and PV real power in Two-Area system (230 MW)

In this study, the objective is to increase the line power transfer limit from 230 MW to 430 MW. Figure 5.11 (a) illustrates the midline power and PV solar power output, whereas Figure 5.11 (b) depicts the PCC voltage for the case of 430 MW power transfer in the tie-line. The considered fault is seen to cause severe oscillations both in tieline power and the bus voltage.

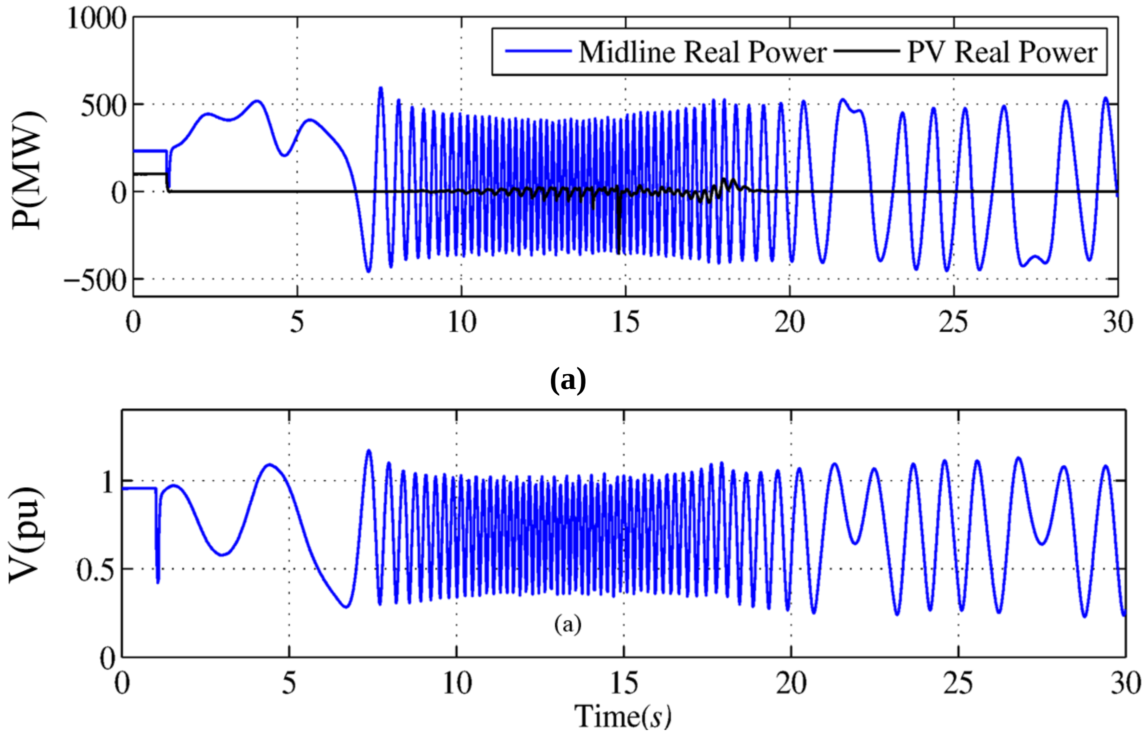

(b)

Figure 5.11 Midline and PV real power and Midline voltage in Two-Area system (430 MW power transfer).

5.7.2 Power Transfer with Full PV-STATCOM Damping Control and Power Restoration in Normal Ramped Manner

As soon as power oscillations are initiated, the solar power output is reduced to zero and the solar farm is transformed to Full PV-STATCOM with POD control. It is noted that according to the Voltage Ride Through criteria of grid codes [114, 115], the PV solar farm must be anyway disconnected due to the large voltage excursions caused by the fault. The proposed PV-STATCOM control goes a step further and instead of staying idle in disconnected mode, utilizes its entire inverter capacity for POD to increase the power transfer.

Figure 5.12 (a) illustrates the midline power and the PV real power. Figure 5.12 (b) and (c) show the PV-STATCOM reactive power and PCC bus voltage, respectively.

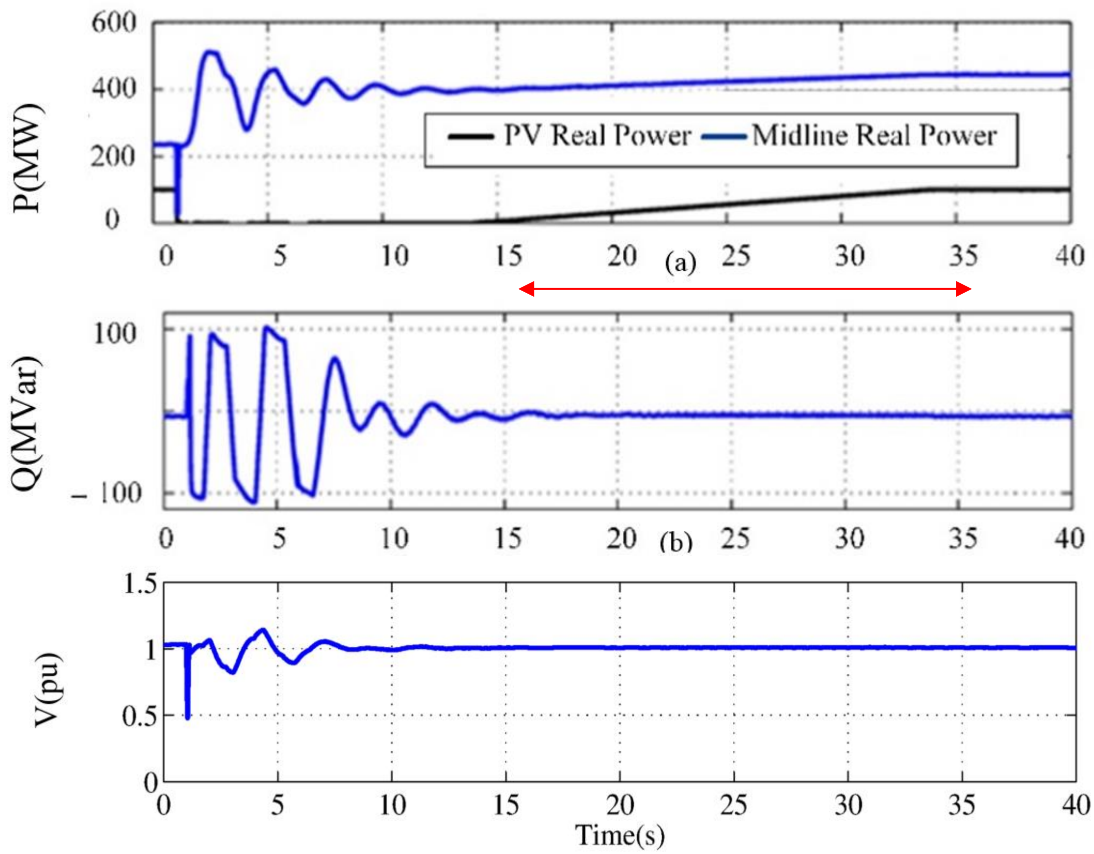

(C)

Figure 5.12(a) Midline and PV real power, (b) PV reactive power, (c) Midline voltage during POD and power restoration in a normal ramped manner.

The PV-STATCOM POD function successfully stabilizes the power oscillations to within acceptable limits in about 10 sec (just before t = 12sec). The PCC voltage oscillations are also mitigated rapidly. The power restoration is commenced at t=15 sec, after a 2 sec delay for safety purpose. The solar power is ramped up to its pre-disturbance level of 100 MW at a rate of 5.5 MW/sec, as determined earlier, in about 18 sec.

5.7.3 Power transfer with Full PV-STATCOM Damping Control and Ramped Power Restoration with POD Control Active in Partial STATCOM Mode

This study is performed to illustrate the efficacy of the proposed restoration technique for the same system operating conditions as in the previous

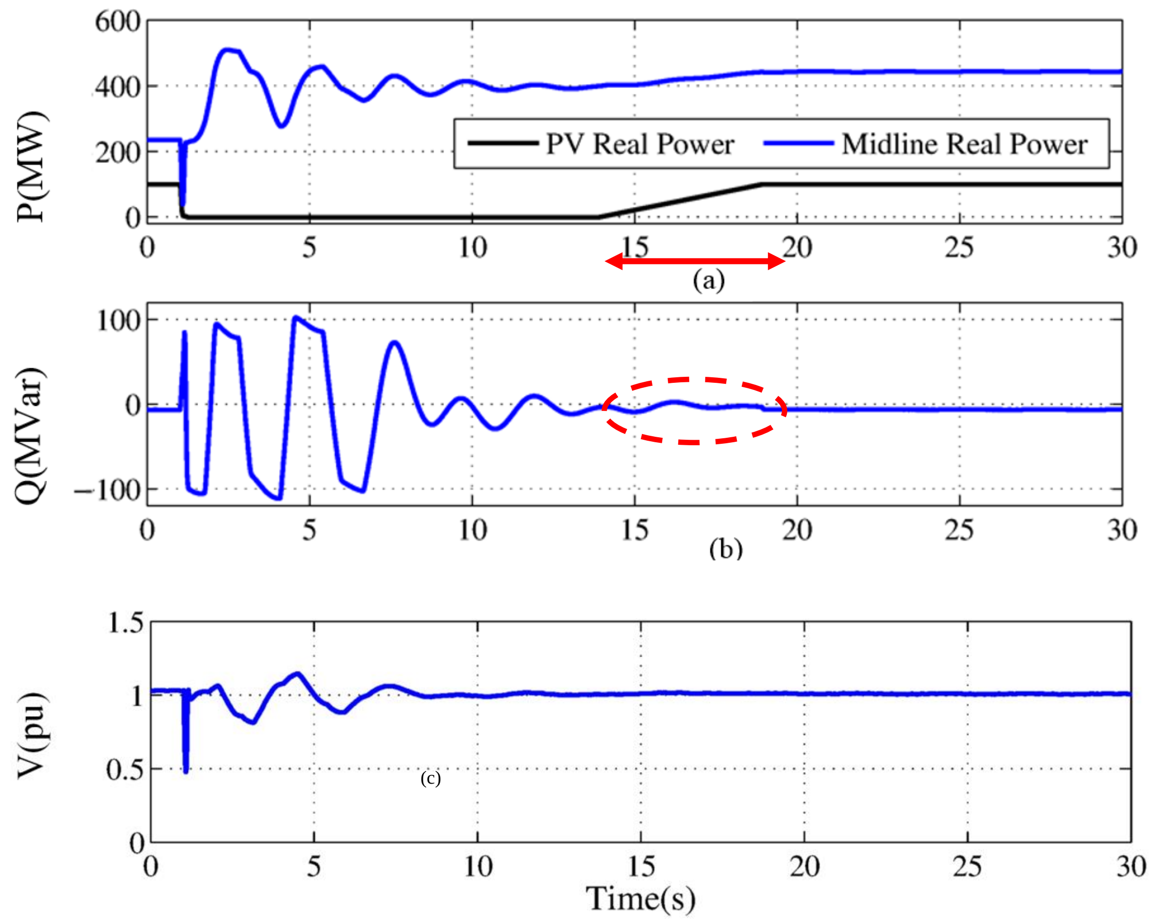

(c)

Figure 5.13 (a) Midline and PV real power, (b) PV reactive power, (c) Midline voltage during POD and power restoration in a fast ramped manner.

Case. Figure 5.13 (a) depicts the midline power flow and the PV solar power output whereas Figure 5.13 (b) and (c) demonstrate the reactive power of the PV-STATCOM and PCC voltage, respectively. It is evident that POD with Partial PV-STATCOM operating mode activated reduces the time of PV power restoration to its pre-disturbance level of 100 MW in just 5 sec. This is about 3.5 times faster than without the proposed restoration technique.

5.7.4 Power transfer with Full PV-STATCOM Damping Control and Nonlinear Power Restoration with POD Control Active in Partial STATCOM Mode

This study is presented to show the effectiveness of an alternate technique of power restoration in a nonlinear (exponential) manner, after the power oscillations have been damped through POD control in Full STATCOM mode of operation. The time constant of the exponential restoration is determined from a hit and trial process. During the restoration period, the POD function remains activated in Partial STATCOM mode to damp the power oscillations. Figure 5.14 illustrates the midline power flow and the PV solar power output for this case. In this case, 95% of entire pre-disturbance PV real power is restored within 2 *sec* and the remaining 5% is restored in 1 *sec.* The nonlinear PV restoration technique thus significantly reduces the restoration interval from 18 *s* to 3 *s*. This is presented just an initial study. More work is needed to systematically determine the time constant of the

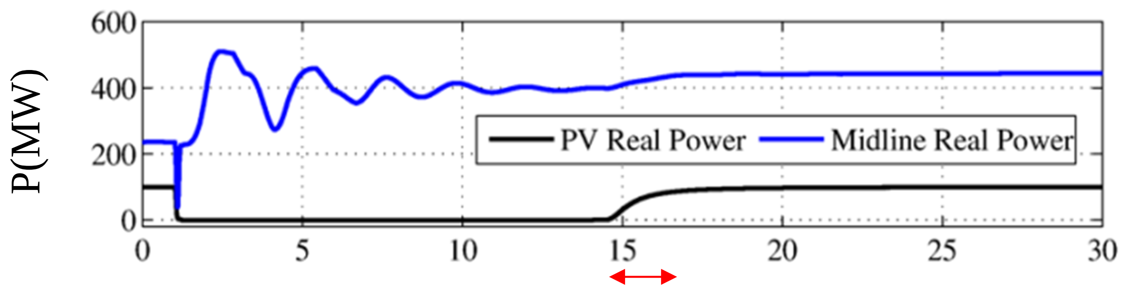

Figure 5.14 Midline and PV real power when power is restored nonlinearly

exponential ramp-up, which is outside the scope of this thesis. To compare the effect of Ramp and Nonlinear restoration techniques, Figure 5.15 illustrates the midline real power after restoration with both restoration techniques. As shown in Figure 5.15, in the ramp restoration technique, undamped low frequency power oscillations appear in the midline real power. The occurrence of these oscillations can be eliminated by proposed nonlinear restoration. Further investigation is required to justify the best effective ramp rate for nonlinear restoration.

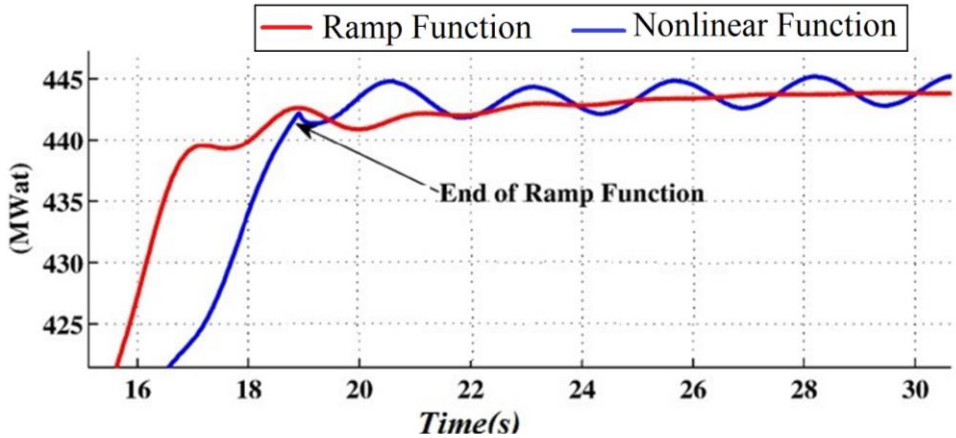

Figure 5.15 Midline real power after power restoration with Ramp and Nonlinear function

5.8 Nighttime Power Transfer Enhancement with Full PV-STATCOM Power Oscillation Damping Control

The effectiveness of the proposed Full PV-STATCOM based POD control subsequent to the same fault as in *Section* 5.7.1 is presented in this study. Figure 5.16 (a) portrays the behavior of 230 MW and 430 MW of power flow in the tieline without the PV-STATCOM control. Figure 5.16 (b) and (c) demonstrate the tieline power and PV system reactive power during POD in Full STATCOM mode of operation. The maximum power transfer in the tie line is only 230 MW. The proposed power oscillation damping in Full STATCOM mode of operation, utilizing the full inverter capacity during nighttime increases the power transfer capability of the tieline from 230 MW to 430 MW, i.e., by 200 MW.

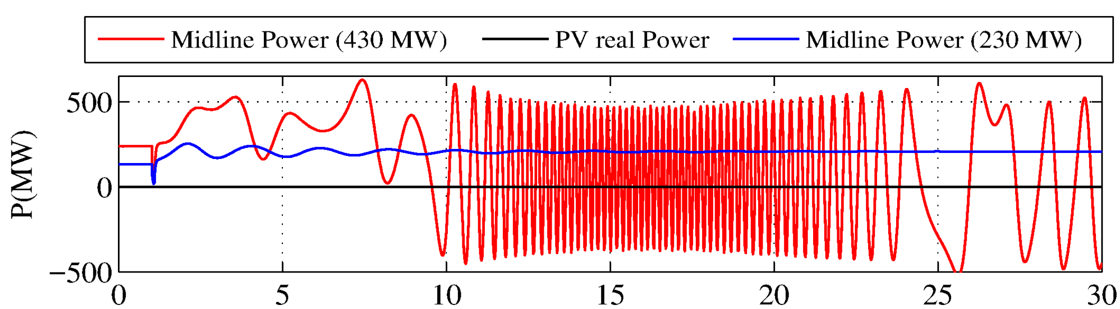

(a)

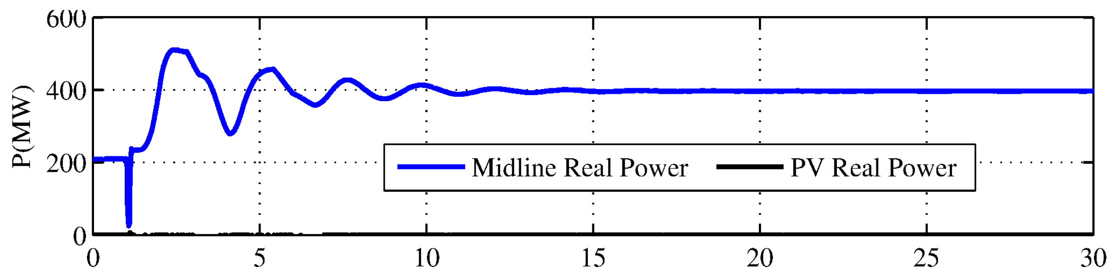

(b)

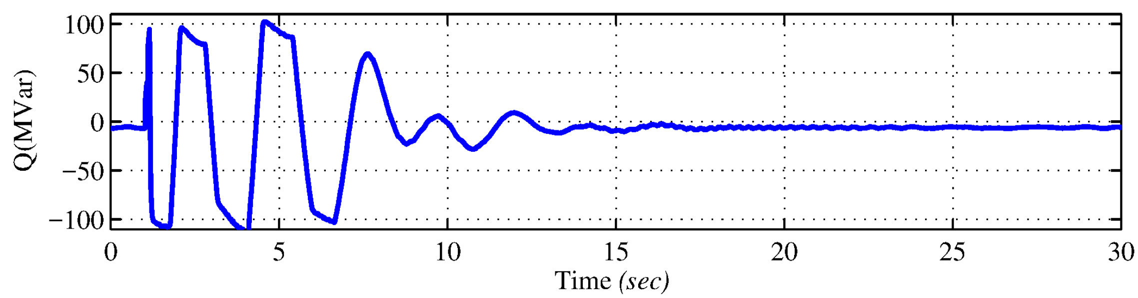

Figure 5.16 Nighttime (a) Midline real power without POD with PV-STATCOM control, (b) Midline real power with Full PV-STATCOM POD Control, (c) PV-STATCOM reactive power

5.9 The Effect of Proposed POD Controls on Power System Frequency

One of the potential concerns regarding the discontinuation of PV real power is its likely effect on the power system frequency. Figure 5.17 depicts the power system frequency with and without PV-STATCOM POD controller. It is shown that even with the proposed fast restoration of PV real power in which the entire POD and restoration is performed in 18 *sec*, the power system frequency continues to be remain stable. In fact the proposed PV-STATCOM control substantially reduces the oscillations in frequency that would be caused with the solar farm in the absence of PV-STATCOM control.

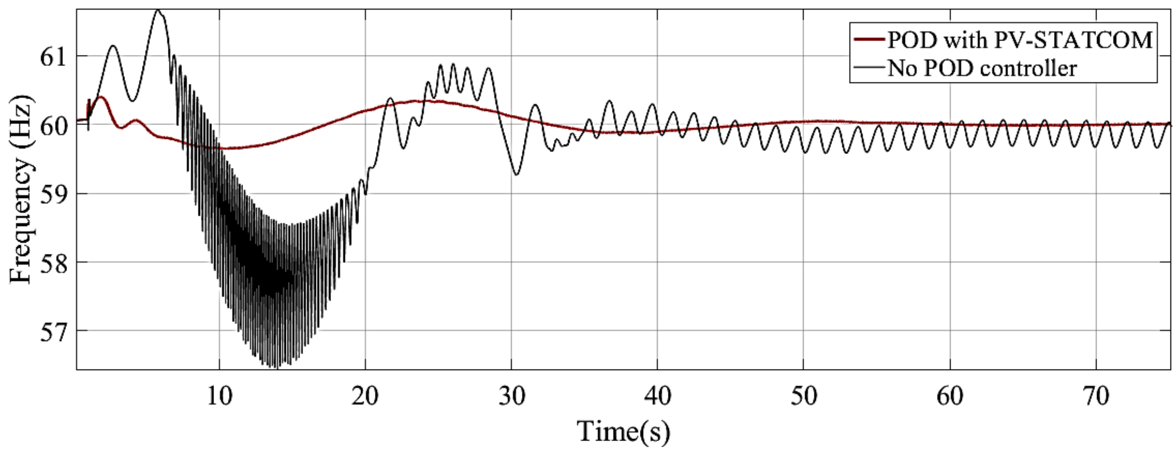

Figure 5.17 The effect of proposed controller on power system frequency

5.10 Conclusion

This chapter presents a novel control of transmission line connected large PV solar system as a STATCOM, termed PV-STATCOM, for damping power oscillations and thereby substantially increasing the power transfer capacity of that transmission line. The proposed control provides POD utilizing its entire inverter capacity during nighttime. During daytime it discontinues its real power generation function very briefly (about 15 sec) and utilizes its entire capacity for POD. It subsequently restores power generation to its pre-disturbance level in a gradual manner while keeping the POD function activated utilizing the remaining inverter capacity. EMTDC/PSCAD simulation studies are performed to demonstrate the effectiveness of the proposed PV-STATCOM control in a single machine infinite bus (SMIB) system which demonstrates local inertial oscillatory mode and the Two-Area system which exhibits both local inertial and inter-area modes of oscillations.

In SMIB system, a 100 MW midline connected PV solar system increases the power transfer capacity by 230 MW, whereas in the Two-Area system a 100 MW PV solar system increases the power transmission limit by 200 MW. Moreover, the proposed power restoration technique keeping POD activated is more than 3 times faster than that specified by grid codes (without POD function).

The temporary (about 18 sec) shutdown of real power production function for POD is not seen to cause any adverse impact on system frequency.

The proposed PV-STATCOM provides 24/7 functionality of an equivalent STATCOM for POD at the same location. This PV-STATCOM is expected to be about 50-100 times lower in cost than an equivalent STATCOM as it utilizes the existing infrastructure (substation, bus-work, transformers, circuit breakers, protection systems, etc.) of a PV solar farm to transform it into a full scale STATCOM of similar size.

The PV-STATCOM as an alternate FACTS device is expected to bring significant savings for utilities seeking to increase their power transmission capacity. It also opens a new revenue making opportunity for transmission connected solar farms to provide 24/7 STATCOM functionality at substantially lower cost. The implementation of this technology of course requires appropriate agreements among utilities, system regulators, solar farm developers and inverter manufacturers.

Chapter 6

6 Novel Combined Real and Reactive Power Control of PV Solar Farm as STATCOM (PV-STATCOM) for Power Oscillation Damping

6.1 Introduction

This chapter presents a novel day-and-night control of a large-scale PV solar farm as PV-STATCOM system for damping low-frequency power oscillations. Three different Power Oscillation Damping (POD) control strategies for PV-STATCOM are presented: i) Reactive power based POD (Q-POD), ii) Real power based POD (P-POD), and iii) Combined Real and Reactive power based POD (PQ-POD). The influence of the PV-STATCOM location on its effectiveness for POD is presented. Small signal and detailed electromagnetic transients model of the Two-Area power system and a 100 MW PV-STATCOM are developed in Matlab and PSCAD/EMTDC software, respectively. POD controllers are designed in two stages. In small signal studies, the controllers are designed based on small signal disturbance around the steady state operating point. Subsequently, these controller parameters are used for optimized controller design for the electromagnetic transient studies of the power system. The effectiveness of the proposed PV-STATCOM POD controllers on damping the power oscillations is demonstrated for various levels of PV power generation and locations of PV solar farm. In addition, the influence of the proposed POD control techniques on power system frequency is studied.

6.2 Concept of PV-STATCOM PQ-POD control mode

Figure.6.1 presents the typical pattern of large-scale PV solar farm real power output on a sunny day and the corresponding inverter remaining capacity during a 24-hour period.

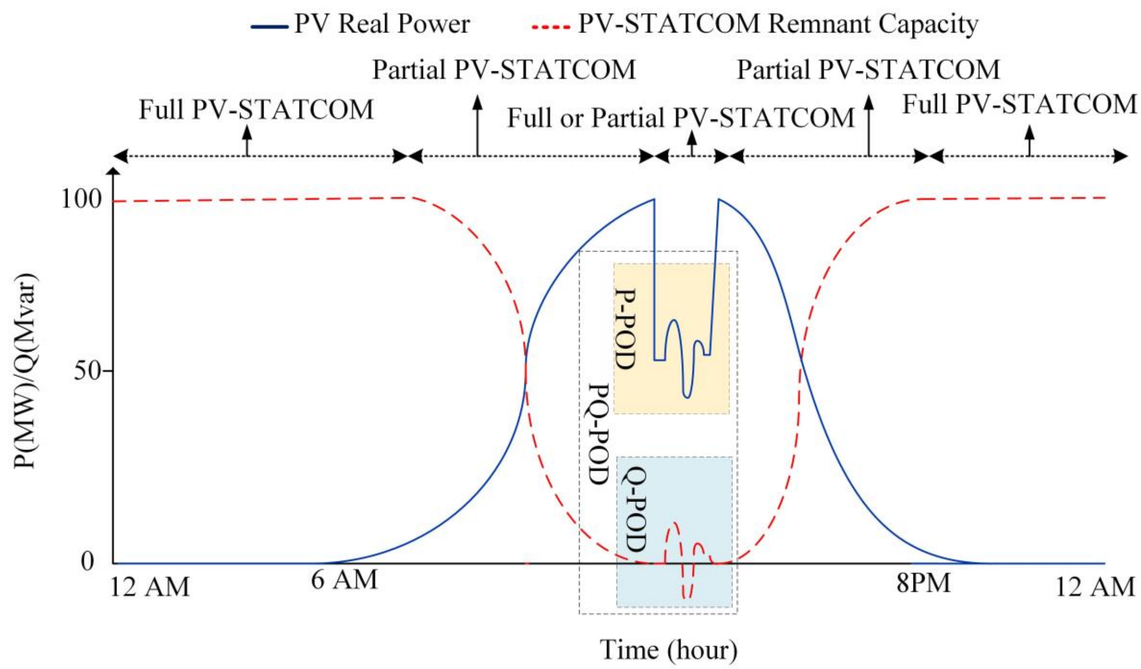

Figure.6.1 PV-STATCOM inverter remaining capacity, PV real, and reactive power during 24 hours.

Figure.6.1 depicts both PV real power modulation and reactive power modulation which can be utilized either individually or in combination for power oscillation damping. Correspondingly, three modes of POD control are proposed as below:

i) Reactive Power Modulation based POD Control (Q-POD Control)

The reactive power is modulated between zero and the remaining inverter capacity (Partial STATCOM mode), or between zero and the rated inverter capacity (Full STATCOM mode) to accomplish POD. No real power modulation is involved. This mode is available both during day and night.

ii) Real Power Modulation based POD Control (P-POD Control)

The maximum real power production based on available solar irradiance is reduced to half and the real power is modulated between zero and the maximum value for POD. No reactive power modulation is involved. This mode is available during daytime.

iii) Combined Real and Reactive Power Modulation based POD Control (PQ-POD Control)

The maximum real power production based on available solar irradiance is reduced to half and the real power is modulated between zero and the maximum value for POD. Simultaneously reactive power is also modulated between zero and the inverter capacity remaining after real power modulation. This mode is available during daytime.

In cases of P-POD or PQ-POD activated after a system disturbance, whenever the real power is reduced for modulation purpose, after the low-frequency power oscillations are damped to within acceptable limits, the real power is restored to its pre-disturbance level in a ramped manner. It is noted that during the ramp-up period, POD function using available reactive power is kept activated to prevent any subsequent onset of power oscillations while power is restored.

6.3 Study System

In this chapter, the effectiveness of the proposed PV-STATCOM POD controllers is demonstrated in the Two-Area power system described in *Section* 2.3.2. PSSs are not considered in the generator excitation units for this study. Figure 6.2 illustrates the Two-Area power system in which the PV-STATCOM is connected at bus 10. This study system is simulated in Matlab Simulink and PSCAD for small signal and detailed electromagnetic transients studies.

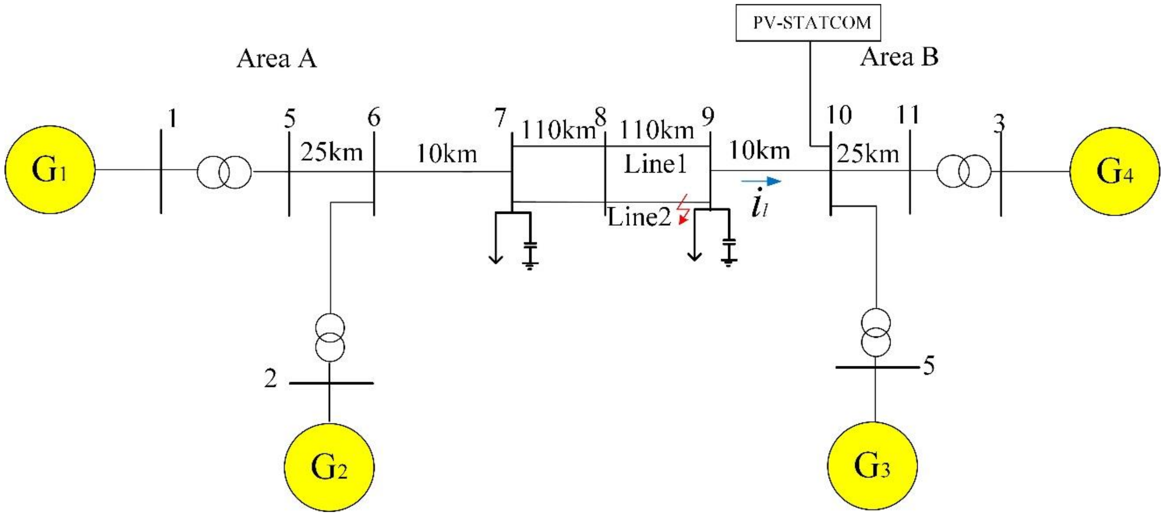

Figure 6.2 Single-line diagram of Two-Area power system with PV-STATCOM connected to bus 10.

6.4 PV-STATCOM in EMT and Small Signal

Figure 6.3 presents the model of PV-STATCOM, which is utilized in both the small signal studies and detailed EMTDC/PSCAD electromagnetic transients (EMT) simulation studies.

6.4.1 PV-STATCOM EMT Model

Figure 5.2 illustrates the proposed 100 MW PV-STATCOM power system. The models of different components of the PV-STATCOM have been described earlier in the thesis, i.e., PV solar panels (*Section* 2.5.1), Decoupled i_d/i_q controller (*Section* 2.5.2), LCL filter (*Section* 2.5.3), MPPT algorithm (*Section* 2.5.4), DC Voltage controller (*Section* 2.5.5), and Conventional Reactive Power Controller (*Section* 2.5.6). The remaining constituents are described below:

6.4.1.1 Q-POD Controller

The Q-POD controller operation in Full STATCOM mode is described in *Section* 5.4.1. In this mode, the entire PV inverter capacity is released by reducing the PV-STATCOM real.

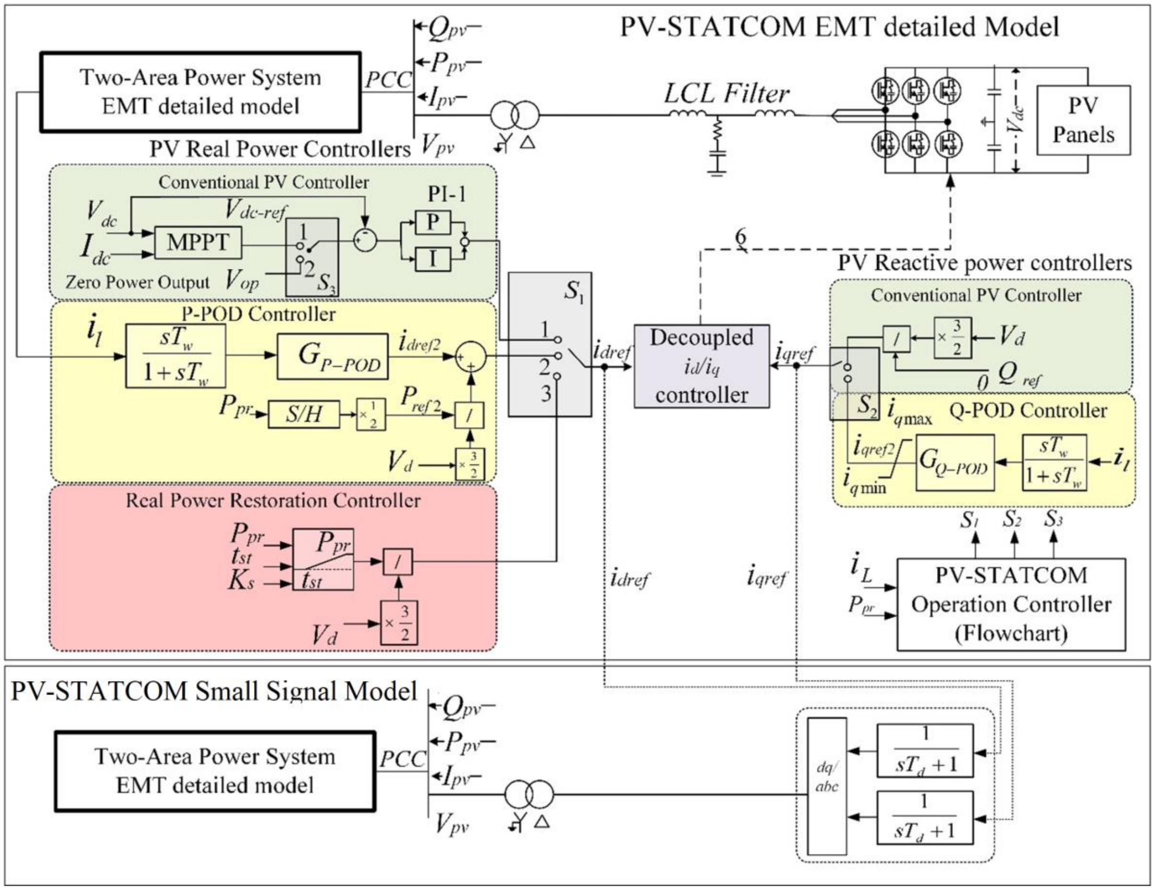

Figure 6.3 PV-STATCOM Controllers in detailed and small signal simulation

power output to zero. Hence, POD can be performed by controlling the PV-STATCOM reactive power output utilizing the entire inverter capacity. The magnitude of the line current signal from bus 9 to bus 10 i_l which has the highest participation factor in selected interarea mode of oscillation is used as a control signal. i_l is subsequently passed through the washout filter. The oscillatory component of i_l is fed as the input signal for compensator with $G_{Q\text{-}POD}$ transfer function *Section* 5.4.1. A hard limiter is used on the compensator output to limit the $i_{q\text{-}ref}$ based on (5.2). To release the entire PV system inverter capacity, $V_{dc\text{-}ref}$ changes to V_{op} by changing S_3 to position 2. Further, i_{qref} changes to i_{qref2} by switching S_2 to position 2 to change the PV-STATCOM reactive power control mode from conventional to Q-POD control mode.

6.4.1.2 P-POD Controller

In this mode, the POD is performed only by controlling the PV-STATCOM real power output. The i_{dref} is controller at i_{dref2}. To activate P-POD controller, the real power set point is reduced to half of its pre-fault value (P_{pr}) using Sample and Hold (S/H) and divider block. The real power is controlled around the P_{ref2} through P-POD controller. I_{dref2} is calculated as:

$$i_{dref2} = \frac{2}{3 \times V_d} P_{ref2} + i_{P-POD} \tag{6.1}$$

where $i_{P\text{-}POD}$ represents the current output from P-POD controller with $G_{P\text{-}POD}$ transfer function:

$$G_{p\_POD}(t) = G \times \frac{1 + sT_{lead}}{1 + sT_{lag}} \tag{6.2}$$

i_l passes through washout filter with T_w time constant to filter its steady state component and is used as the control signal.

6.4.1.3 PQ-POD controller

In this mode of operation, both P-POD and Q-POD are activated to enhance the PV-STATCOM POD performance. The i_{dref} is controllered at i_{dref2} and i_{qref} changes to i_{qref2}. The generated i_{qref2} from Q-POD controller is limited through the hard limit block based on the available PV system inverter capacity. During the day time, PQ-POD can be activated by switching S_1 to position 3 and S_2 to position 2.

6.4.2 PV-STATCOM Small Signal Model

Figure 6.3 illustrates the small signal model of the PV solar farm [109], inverter, and current controllers. This model is described in detail in *Section* 2.9. In this chapter, the reference i_{dref} and i_{qref} signals are the same as PV-STATCOM in EMT model.

6.4.3 Selection of PV-STATCOM Operation Mode

The flowchart for PV-STATCOM operation mode selection is illustrated in Figure 6.4. The specific mode of operation is selected based on the power system conditions.

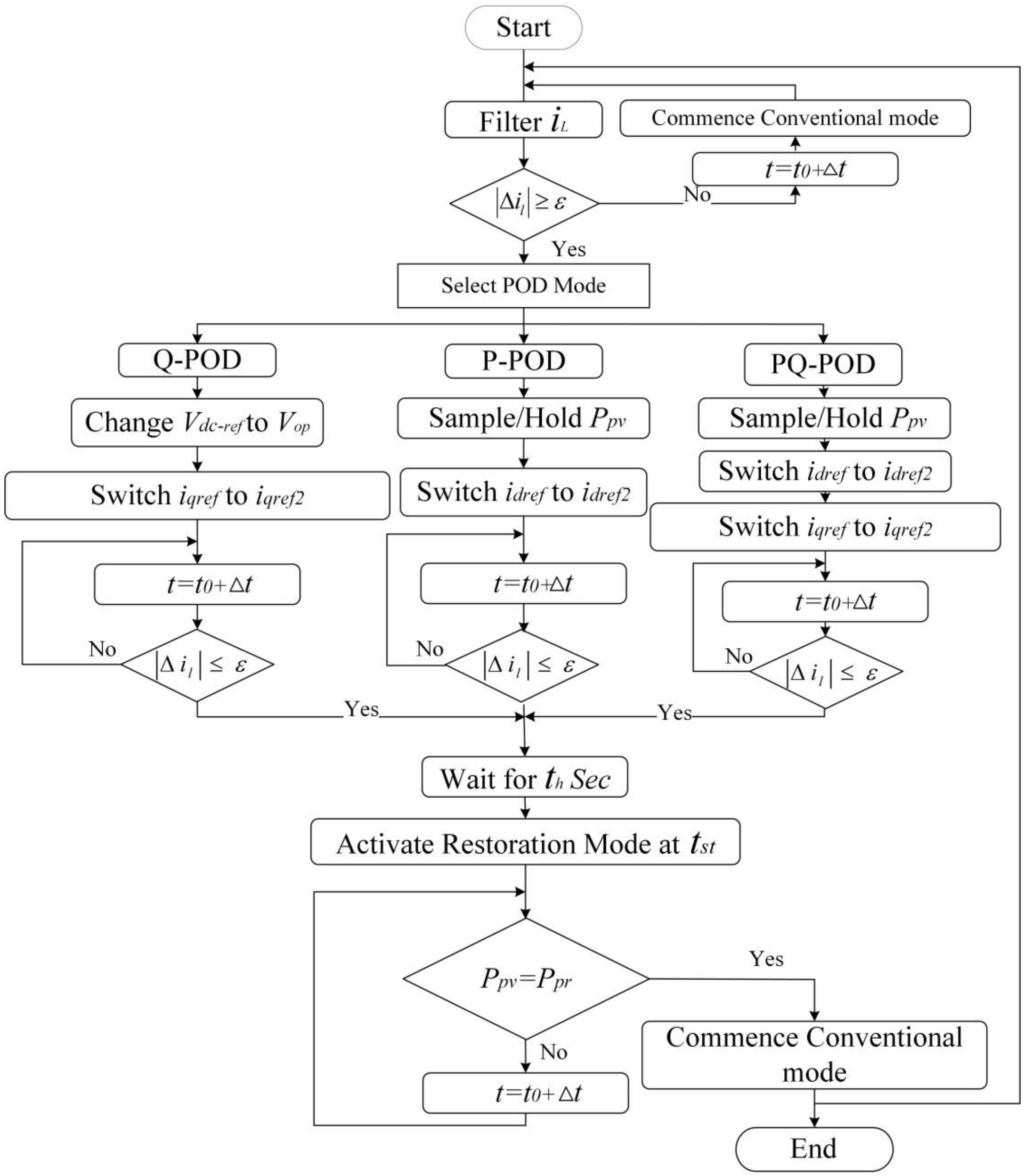

Figure 6.4 Flowchart of PV-STATCOM operation mode selection.

As described earlier, to detect the occurrence of low frequency oscillations, i_l is passed through washout filter (*Section* 2.7.1) to filter the steady state components of the signal.

The magnitude of i_l deviation is compared with a predefined limit ε. If the oscillations in i_l signal are within the limit ε, which in this chapter is selected as 5%, the conventional PV mode of operation is activated. If the oscillations are more than ε, POD mode is activated as follows:

a) Q-POD is activated by changing V_{dcref} to V_{op} , i_{qref} changes to i_{qref2}.

b) P-POD is activated by changing i_{dref} to i_{dref2}. The reactive power is controller through conventional controller.

c) PQ-POD is activated by changing V_{dcref} to V_{op} , i_{qref} changes to i_{qref2}, and i_{dref} changes to i_{dref2}.

In the POD techniques, if the magnitude of oscillations in i_l stabilizes within ε, after a 2 *sec* safety delay, the real power restoration mode is activated. It is emphasized that the POD function is kept activated in the Partial STATCOM mode while the real power is restored to its pre-disturbance value P_{pr}. If the P_{pv} reaches P_{pr}, the conventional PV mode of operation is reactivated.

6.4.4 PQ-POD Controller Design

The controllers are designed based on the residue analysis technique presented in *Section 2.7.3* and further optimized in PSCAD/EMTDC software based on the embedded *Simplex* Optimization technique described in Section 2.7.4. The POD controller parameters are given in Appendix I.

6.5 Placement of PV-STATCOM in Two-Area power system

The effectiveness of the PV-STATCOM control at different locations is examined using the residue analysis technique described in *Section* 2.8.

In the Two-Area power system, five different locations are considered for PV system placement as buses 6, 7, 8, 9, and 10, respectively. It is assumed that the PV system is generating half of its available power (50 MW). This power generation level gives adequate

PV inverter remaining capacity to perform the residue analysis for Q-POD controller while there is enough real power available for P-POD controller. The input and output signals for the Q-POD feedback loop are the variation in PV-STATCOM reactive power (ΔQ) and variation in midline current (Δi_l), respectively. For P-POD controller, the input is the variation in PV-STATCOM real power (ΔP) and Δi_l.

6.5.1 Residue Analysis for PV-STATCOM with Q-POD

Figure 6.5 presents the results for residue analysis for PV-STATCOM interconnection at the different buses for different levels of power transfer from Area A to B vice versa. The highest residue associated with PV-STATCOM in Q-POD control mode is achieved considering the midline power transfer is at its maximum (430 MW) and PV-STATCOM is connected to bus 10.

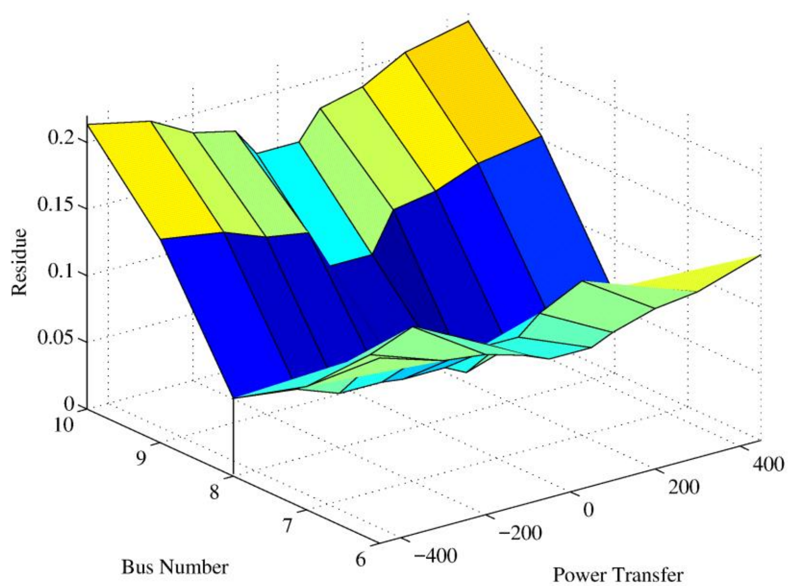

Figure 6.5 Residue analysis for PV-STATCOM Q-POD controller.

6.5.2 Residue analysis for PV-STATCOM with P-POD

The results of the residue analysis for PV-STATCOM with P-POD controller are presented in Figure 6.6. If the PV-STATCOM is connected at the midline of the Two-Area power system (Bus 8), PV real power does not have a significant effect on the interarea mode of oscillations. The highest residue for this study is achieved when the PV-STATCOM is connected at bus 6 or 10.

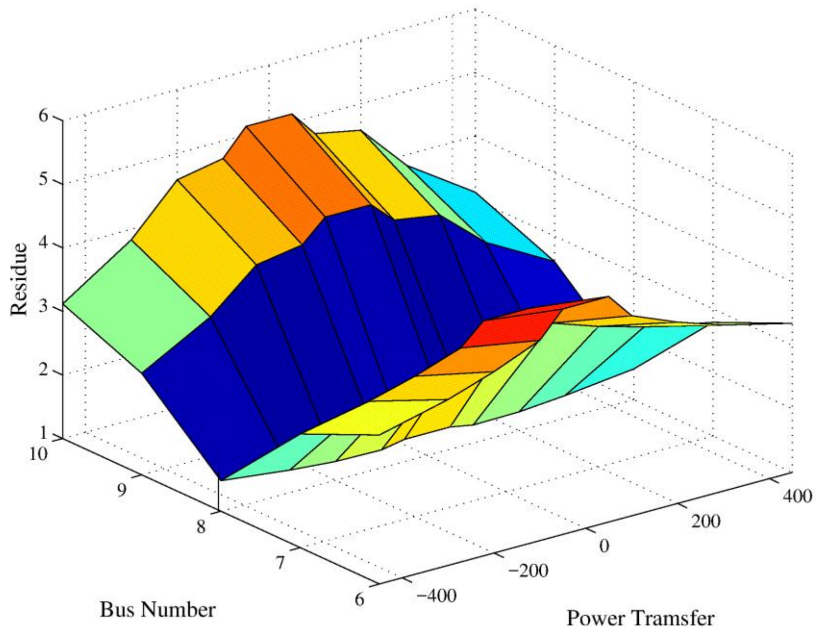

Figure 6.6 Residue analysis for PV-STATCOM P-POD controller.

Based on the results obtained in Figure 6.5 and Figure 6.6, the best location to perform PQ-POD controller is bus 10 in which both Q-POD and P-POD have the highest residue magnitude on the interarea mode of oscillation.

6.6 Case Studies

Three Case Studies based on the location of PV-STATCOM are presented in this chapter. In Case Study I, the PV-STATCOM is connected at bus 10 which is the best bus candidate for PQ-POD control. The performances of the proposed POD control techniques are tested in detailed EMT simulation studies. In addition, the effect of various PV real power generation on each POD technique is evaluated. In Case Studies 2 and 3, the PV-STATCOM location is changed from bus 10 to bus 8 and 6, respectively. The effect of the location of PV-STATCOM on the performance of the proposed POD techniques is examined and results are compared with those obtained in residue analysis;

6.6.1 Power Oscillation Damping by PV-STATCOM Interconnected at the Best Location

In this study, it is assumed that the PV-STATCOM is connected at bus 10 and 430 MW power is being transferred from Area A to B and. A three-phase to ground fault is initiated at *t*=1 sec for 5 cycles near bus 9. Due to the fault, growing low-frequency power oscillations occur in the line current. Figure 6.7 illustrates the power transfer capability of the Two-Area power system after three phase fault initiation. It is seen that the maximum power capability of the line is 250 MW. The aim is now to increase the power transfer capability of the same line to 430 MW with the proposed POD controllers.

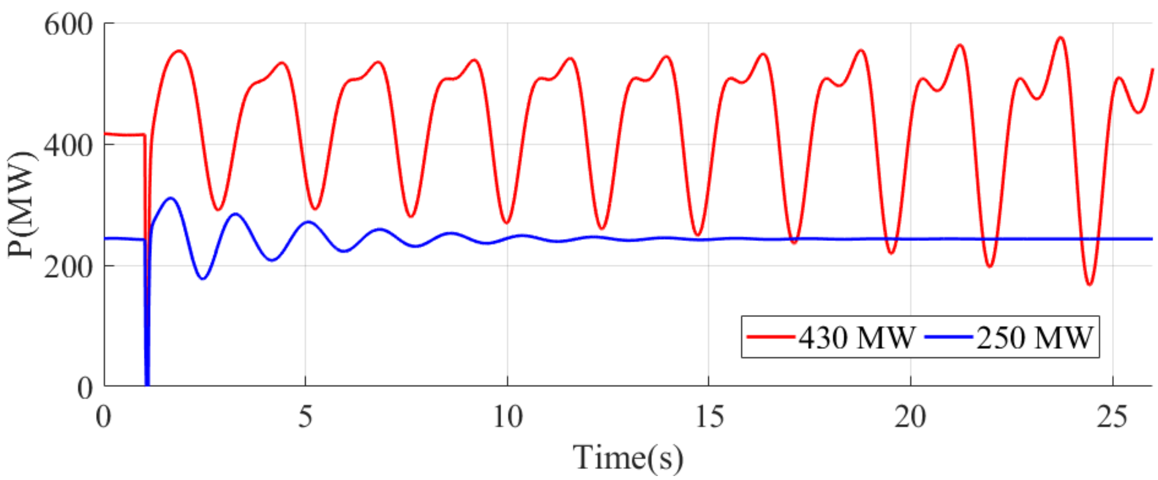

Figure 6.7 Maximum power transfer capability of Two-Area power system.

Figure 6.8 depicts the results of power oscillation damping achieved by different POD techniques. It is observed that the Q-POD, P-POD and PQ-POD controllers damp the power oscillations to within acceptable limits in 12 *sec*, 12 *sec*, and 7 *sec*, respectively. This implies that the best POD is achieved by the PQ-POD control.

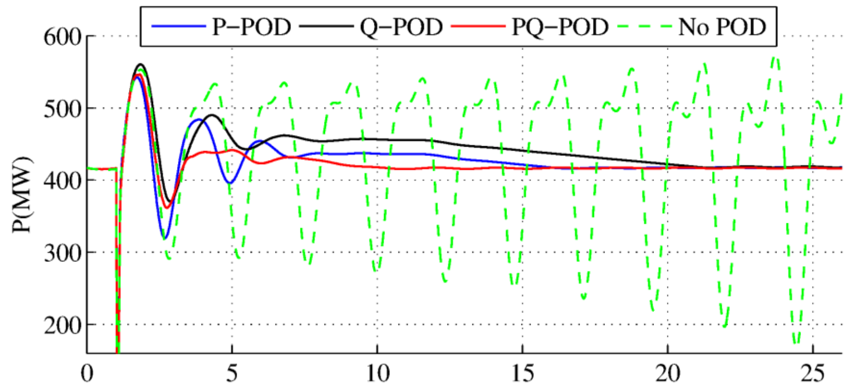
P−POD
Q−POD
PQ−POD
No POD
P(MW)
600
500
400
300
200
0
5
10
15
20
25

(a)

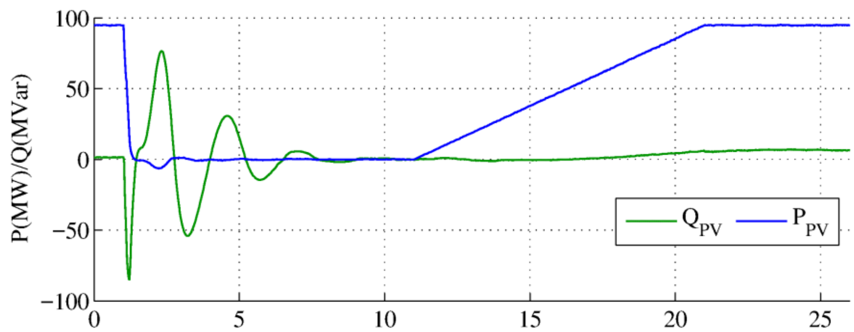
P(MW)/Q(MVar)
100
50
0
−50
−100
0
5
10
15
20
25
Q_PV
P_PV

(b)

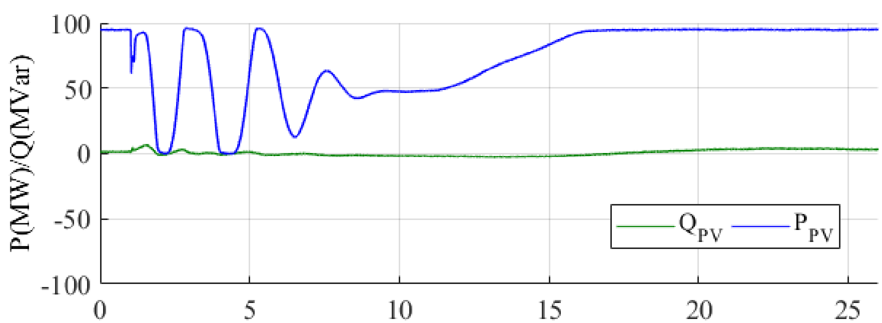
P(MW)/Q(MVar)
100
50
0
-50
-100
0
5
10
15
20
25
Q_PV
P_PV

(c)

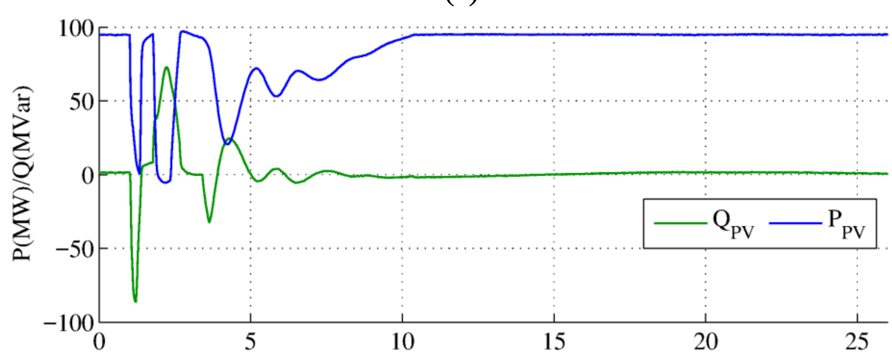
P(MW)/Q(MVar)
100
50
0
−50
−100
0
5
10
15
20
25
Q_PV
P_PV

(d)

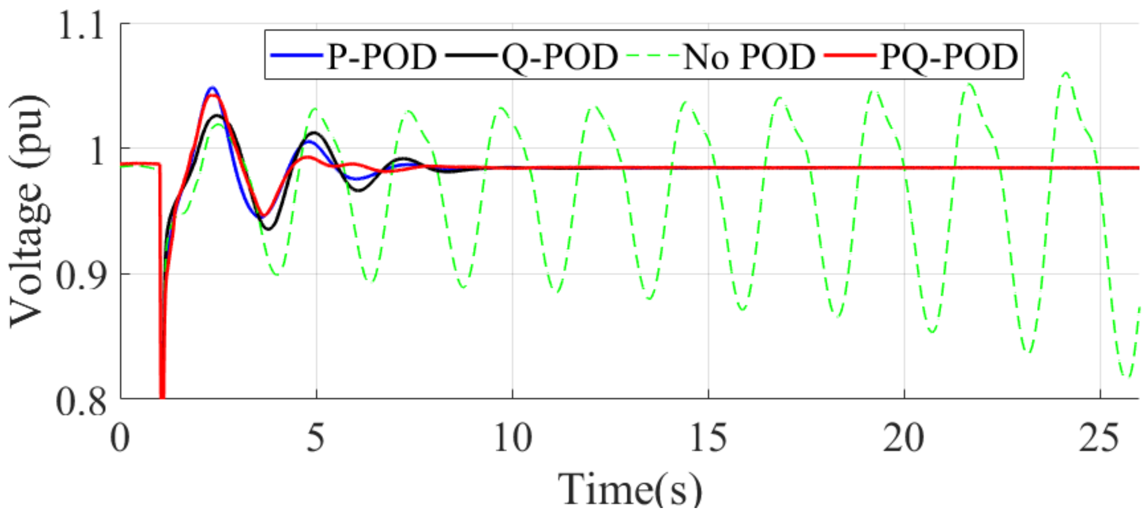

(e)

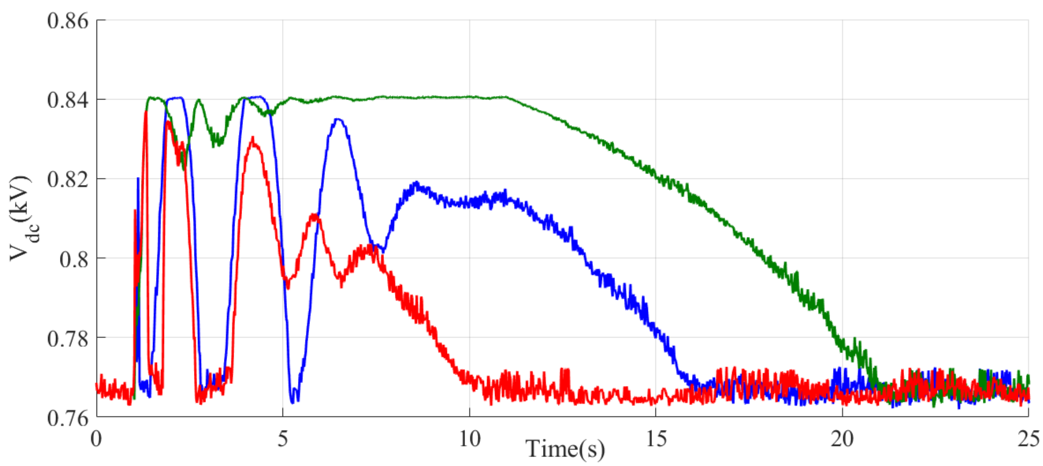

(f)

Figure 6.8 a) Midline real power for case study A, b) PV-STATCOM real and reactive power for Q-POD control technique, c) PV-STATCOM real and reactive power for P-POD control technique, d) PV-STATCOM real and reactive power for PQ-POD control technique, e) PCC Voltage in pu. f) PV-STATCOM DC voltage for Q-POD, P-POD, and PQ-POD controllers.

Figure 6.8 (b) presents the PV-STATCOM real and reactive power after the fault for Q-POD control. The PV real power is reduced to zero within 0.3 second after the fault initiation and the entire PV-STATCOM inverter capacity is made fully available for Q-POD control. The required modulation of reactive power of PV-STATCOM gets reduced to less than 5% by *t*=10 sec. Due to the decoupled P-Q control, the real power of the PV system continues to be at zero. Subsequently after the safety time of 2 seconds, at t = 12 *sec*, the PV real power is restored to P_{pr} = 100 MW with a ramp rate of 20 MW/sec Section 5.7.3.

Figure 6.8 (c) shows the PV-STATCOM real and reactive power after the fault for P-POD control. The PV system real power is reduced to half of its pre-fault value (50 MW) and P-POD control is performed by controlling the PV-STATCOM real power around 0 to 100 MW. The required modulation of midline real power decreases to less than 5% by *t*= 10 sec. Due to the decoupled control the reactive power of the PV system continues to be almost zero. Subsequently after the safety time of 2 seconds, at t = 12 *sec*, the PV real power is restored to P_{pr} = 100 MW with a ramp rate of 20 MW/sec. The effectiveness of P-POD control is observed to be similar to the Q-POD control.

Figure 6.8 (d) portrays the PV-STATCOM real and reactive power after the fault for PQ-POD control. Following the fault, the PV-STATCOM real power is reduced to half of its pre-fault value. Both P-POD and Q-POD controllers are activated. In this mode, P-POD is the primary control function and Q-POD is done with inverter remnant capacity. If the required attenuation of oscillations achieved and remain in 5% for duration of 2 sec, at *t* = 8 *sec*, the PV real power is restored to P_{pr} = 100 MW with 20 MW/sec ramp rate.

Figure 6.8 (e) depicts the voltage at the PCC. It is seen that none of the studied PV-STATCOM POD controllers have an adverse impact on the PCC voltage. In fact the bus voltage with all the POD controllers stays within utility specified limits. It is further observed that the voltage variation with PQ-POD control mode is much smaller than either P-POD and Q-POD acting alone.

Figure 6.8 (f) illustrates the PV-STATCOM DC voltage modulation based on the selected POD mode of operation. In Q-POD mode of operation, the DC voltage is controlled at 840 V to reduce the PV real power to zero based on VI characteristic of PV modules. In P-POD mode, PV-STATCOM DC voltage is controlled around 820 V (50 MW). This DC voltage variation results in 0 MW to 100 MW PV real power variation. In PQ-POD mode of operation, the DC voltage of the PV system is controlled around 830V to reduce the PV real power set point to 50 MW. It is shown that the DC voltage variation in PQ-POD control is smaller than both the Q-POD and P-POD control techniques. This reduces the stress on the DC link capacitor

6.6.1.1 The Effect of POD Controllers on Power System Frequency

Figure 6.9 illustrates the impact of the proposed POD control techniques on power system frequency after the fault. If no POD control is activated the power system frequency variation violates the standard limits set by Standards [44], in fact the system becomes unstable. None of the POD controls utilized in this study destabilize the frequency. It is seen that the largest frequency variation is experienced with the Q-POD control since the real power is suddenly reduced to zero to release the entire inverter capacity for reactive power modulation. P-POD causes lower frequency oscillation since power is reduced by only half (from 100 MW to 50 MW), while PQ-POD causes the lowest amount of frequency excursion.

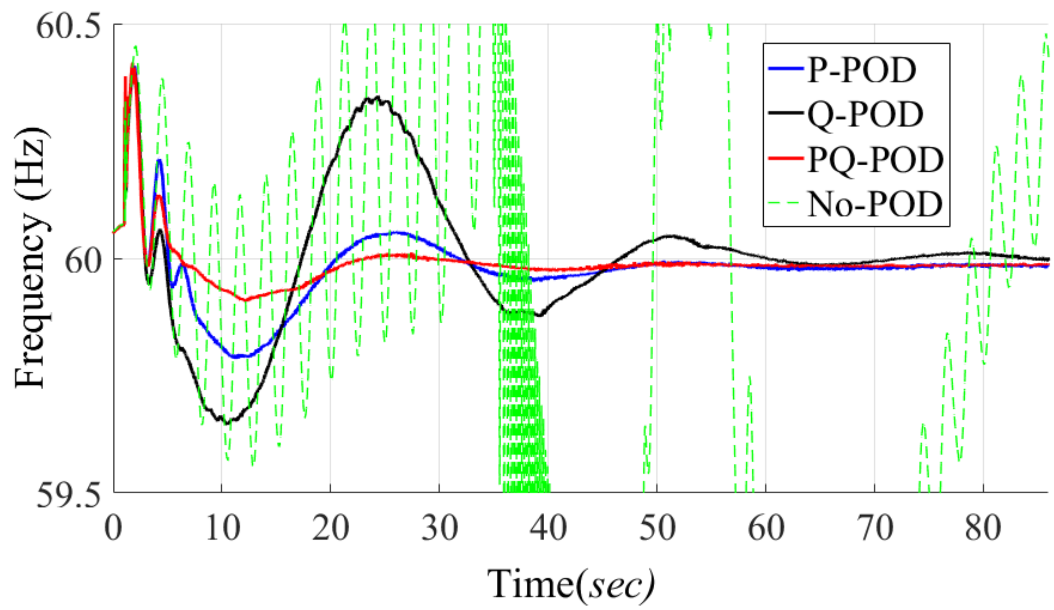

Figure 6.9 Power system frequency for No POD, Q-POD, P-POD and PQ-POD control techniques.

6.6.2 Effect of Available PV Real Power on Proposed Control Techniques

To evaluate the performance of PV-STATCOM POD controllers with respect to different PV real power injections, two case studies considering PV system is generating 60 MW and 20 MW are presented. Figure 6.10 and Figure 6.11 illustrate the result for P-POD, Q-POD, and PQ-POD control techniques for PV-STATCOM in which the PV system is generating 60 MW and 20 MW, respectively.

As shown in Figure 6.10 and Figure 6.11, the effectiveness of P-POD controller reduces due the lower available PV real power. The performance of Q-POD control technique is not affected by variation in PV system real power. This is quite expected. It is further noted that although the effectiveness of P-POD control technique is influenced by available PV system real power, the PQ-POD control provides the most effective damping in comparison to both Q-POD and P-POD control techniques.

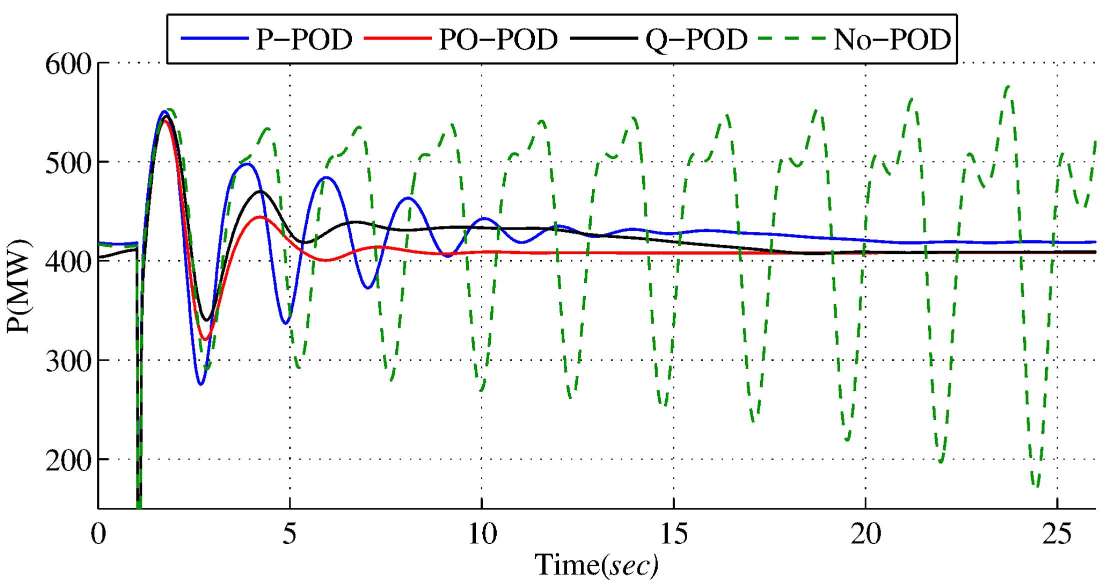

Figure 6.10 Midline real power for case study A, 430 MW power transfer, PV-STATCOM is connected at bus 10. PV system is operating at 60 MW.

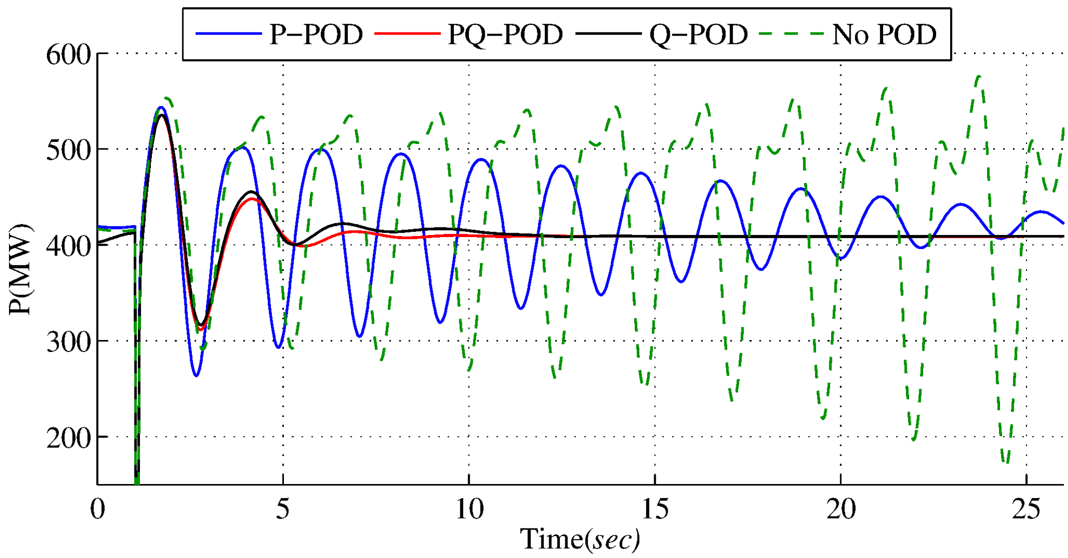

Figure 6.11 Midline real power for case study A, 430 MW power transfer, PV-STATCOM is connected at bus 10. PV system is operating at 20 MW.

6.6.3 Power Oscillation Damping by PV-STATCOM interconnected at other candidate busses

Similar studies as Case 1 considering PV-STATCOM is connected to bus 8 and 6 are performed in PSCAD/EMTDC for detailed model analysis to examine the correlation with residue analysis in the small signal model. As shown in Figure 6.12 and Figure 6.13, after three phase fault initiation at line 2 near the bus 9, same low-frequency power oscillations appear in power system. Figure 6.12 and Figure 6.13 illustrate the results for midline real power for all POD control techniques.

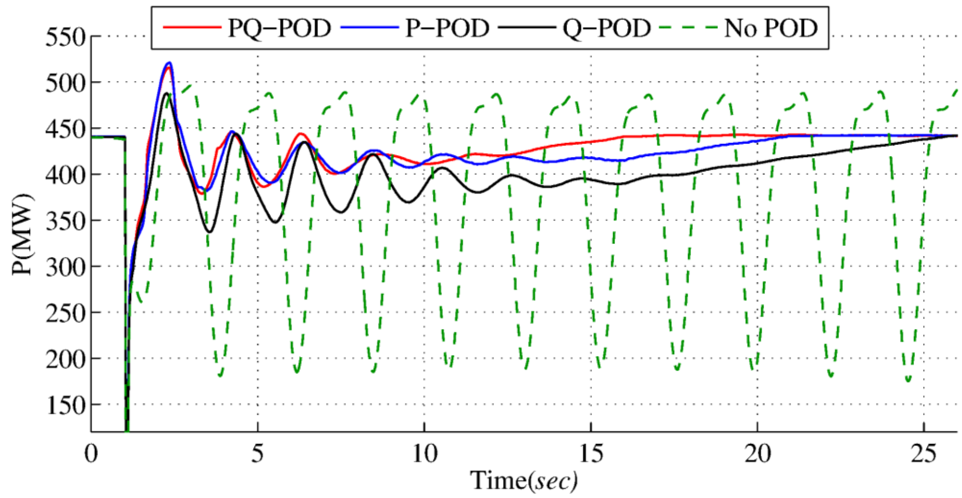

Figure 6.12 Midline real power for case study 2 with 430 MW power transfer while PV-STATCOM is connected at bus 8.

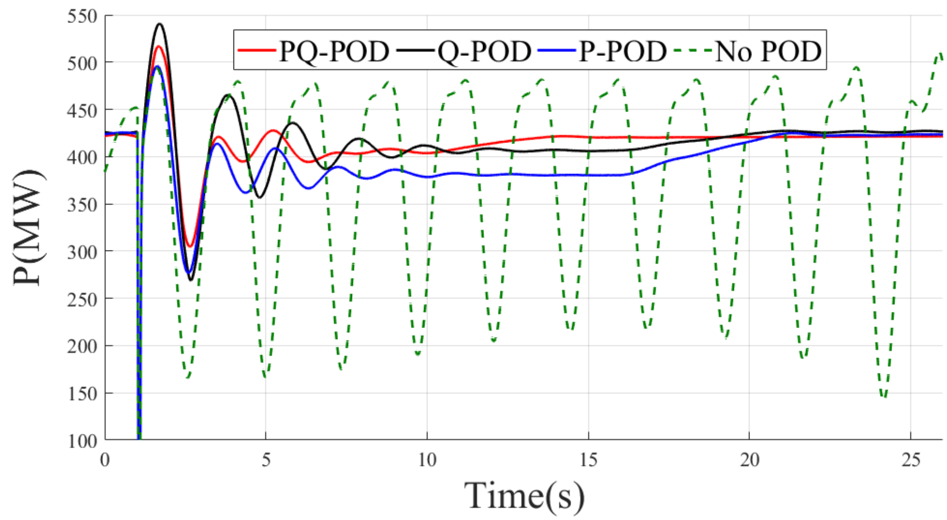

Figure 6.13 Midline real power for case study 2 with 430 MW power transfer while PV-STATCOM is connected at bus 6.

Table 6.1 illustrates the power oscillation settling times with regards to different PV-STATCOM locations and POD control techniques.

Table 6.1 Settling time of power oscillations with different PV-STATCOM locations and POD control techniques

PV-STATCOM Location	Settling time (*sec*)		
	Q-POD	**P-POD**	**PQ-POD**
Bus 6	13	15	9
Bus 8	15	15	12
Bus 10	10	10	6

It is shown that the effectiveness of both P-POD and Q-POD controls for PV-STATCOM on power oscillations are affected by the location of the PV-STATCOM. The fastest settling time is achieved if the PV-STATCOM is connected at bus 10 and PQ-POD controller is activated.

These results validate the residue analysis studies in *Section* 6.5 according to which the effectiveness of Q-POD and P-POD controllers is affected by changing the PV-STATCOM interconnection point to buses 8 and 6. Despite the adverse effect of the location of PV-STATCOM, the PQ-POD control provides the best power oscillation damping among all the POD controls.

6.7 Conclusion

Novel POD control technique with PV-STATCOM real and reactive power is presented based on patent [8]. The effectiveness of three power oscillation damping techniques – the Q-POD, P-POD and PQ-POD is compared in the Two-Area system for a three phase to ground fault for five cycles. This comparison is also made with respect to different levels of real power generation by the PV solar system. The POD controllers are designed using small signal analysis in Matlab and optimized controller tuning technique embedded in PSCAD/EMTDC software. Small signal and detailed electromagnetic transients studies are performed for the Two-Area power system with PV-STATCOM in Matlab and PSCAD/EMTDC software. The influence of the location of PV-STATCOM on the effectiveness of power oscillation damping is examined through small signal residue analysis, which is subsequently validated with EMTDC/PSCAD simulation studies. The following conclusions are made:

1) The best POD is achieved if PV-STATCOM real and reactive power are used together for damping power oscillations. Although P-POD controller is affected by the amount of PV real power availability, PQ-POD control results in best POD among all the three POD controls for all levels of power transfer.

2) The best location of P-POD and Q-POD is bus 10.

3) None of the three POD controls have any adverse impact on the system frequency.

4)The PQ-POD control technique has the smallest impact on power system frequency in comparison with the P-POD and Q-POD control techniques.

Chapter 7

7 Control of PV-STATCOM for Power Oscillation Damping in the 12 bus FACTS Power System

7.1 Introduction

In this chapter, the performance of the proposed Q-POD and PQ-POD control techniques for PV-STATCOM will be examined for power oscillation damping in the 12 bus FACTS power system in which different modes of oscillations are observed. According to [27, 120], the stability of the power system can be adversely affected by high real power injections from PV solar farms. It is argued that since PV solar systems do not have any inertia, the overall stability of the power system is negatively impacted by higher penetration levels of PV real power. In this chapter, the effect of PV real power injection with and without POD control techniques on power system stability is investigated. With regards to the different interarea modes of oscillation in the 12 bus FACTS power system, the aim of this chapter is to damp low-frequency oscillations of each mode by appropriate control signal selection. The effect of the location of PV-STATCOM with P-POD and Q-POD controller on damping the selected mode of oscillation is presented. In addition, the effect of delay on POD with PV-STATCOM is studied and a simple compensator design procedure is presented. The simulation studies are performed in Matlab Simulink software which are subsequently validated by PSCAD/EMTDC software simulations.

7.2 Study System

Figure 7.1 illustrates the 12 bus FACTS power system. This system is described in *Section* 2.3.3. A 100 MW solar system is connected at bus 4. This PV solar system is controlled as PV-STATCOM. In this system, the direction of power flow is defined based on the loads and power generations in different area. No PSS is assigned for synchronous generators. The power system exhibits low damping of oscillatory modes in the steady-state operation.

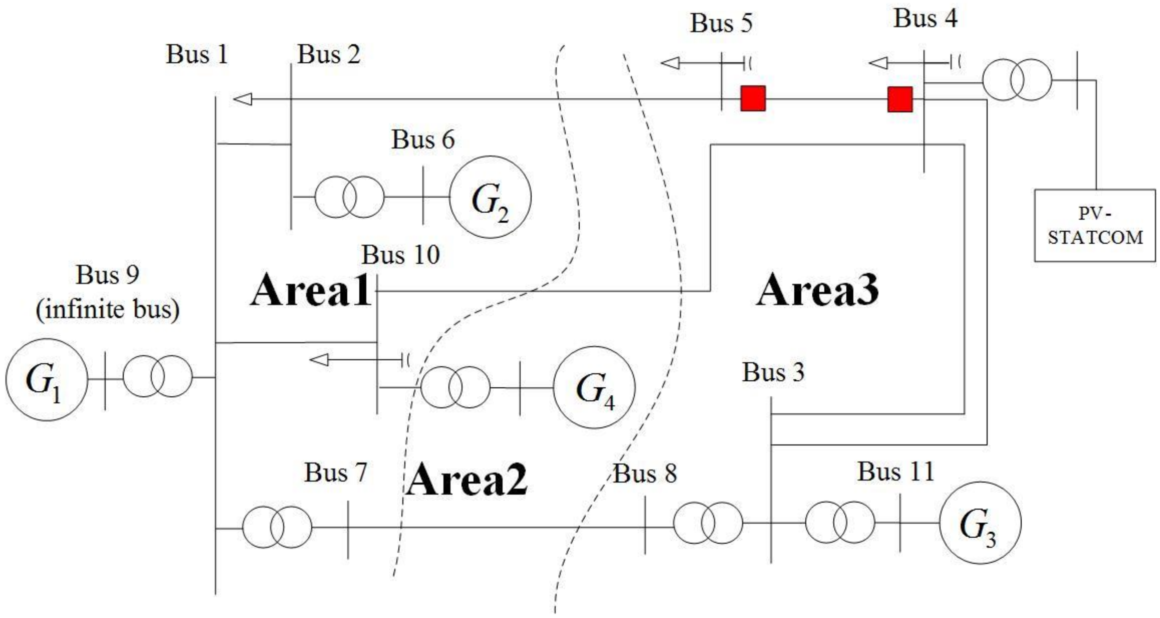

Figure 7.1 Twelve bus FACTS power system with 100 MW PV solar system at bus 4

7.3 PV-STATCOM Modeling

Figure 7.2 illustrates the single line diagram of the PV-STATCOM detail and small signal model in PSCAD/EMDTDC and Matlab Simulink.

7.3.1 PV-STATCOM EMT Model

The components modeling of the PV-STATCOM has been defined earlier in the thesis, i.e., PV solar panels (*Section* 2.5.1), Decoupled i_d/i_q controller (*Section* 2.5.2), LCL filter (*Section* 2.5.3), MPPT algorithm (*Section* 2.5.4), Conventional PV controller in real power controller (*Section* 2.5.5), Conventional PV controller in reactive power controller (*Section* 2.5.6), and Real power restoration controller (*Section* 5.4.2). The remaining constituents are described below:

A new PV-STATCOM operation controller is designed to damp different interarea modes of oscillation in 12 bus FACTS power system. In this context, new components including Q-POD and PQ-POD with

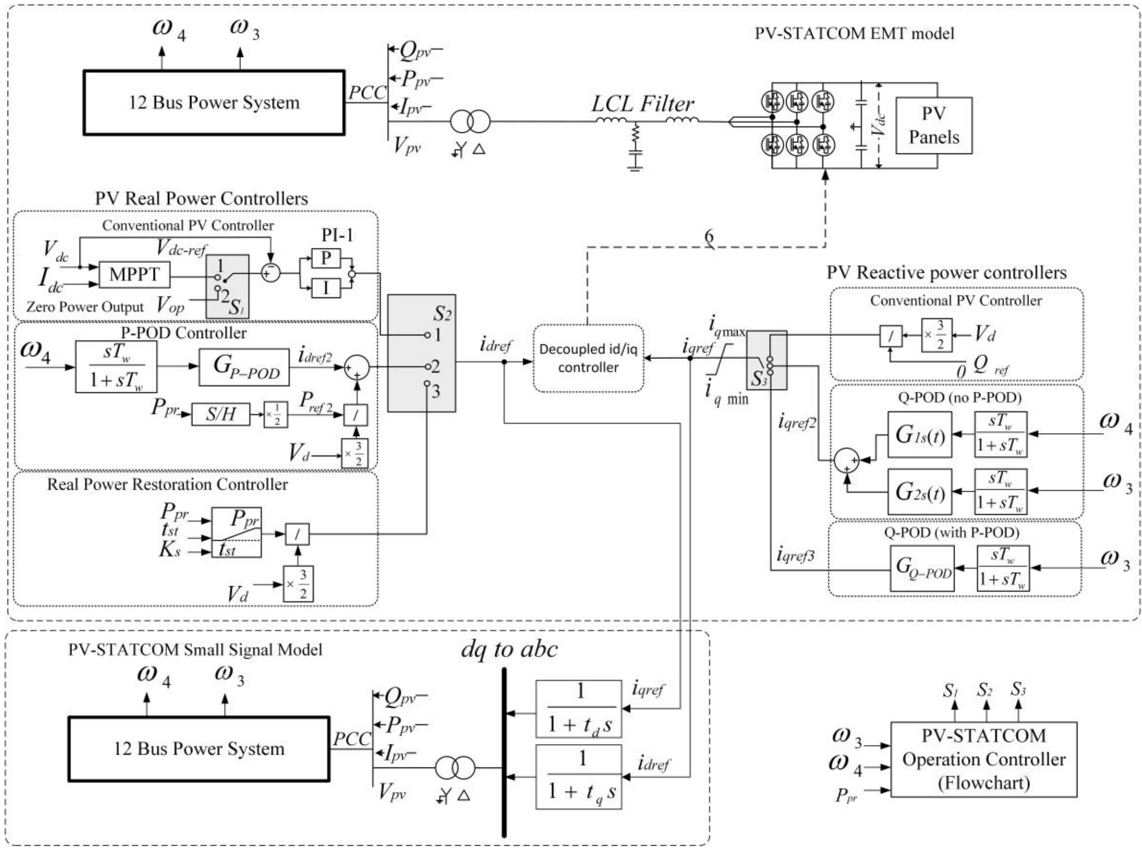

Figure 7.2 Detailed and Small signal Model of the PV-STATCOM

different generator speeds as control signals, and PV-STATCOM Operation controller are added to PV-STATCOM control units.

7.3.1.1 Q-POD Controller

In this mode of operation, the entire PV inverter capacity is released to perform POD with Full PV-STATCOM inverter capacity. The Q-POD controller in Full PV-STATCOM mode of operation is presented in Chapter 5. Speed deviation of G_3 and G_4 (ω_3 and ω_4) are selected as control signals and transferred to the Q-POD controller via Wide Area Measurements (WAM) technique. Control signals are selected based on PF analysis *Section* 2.7.2. The controllers are designed based on residue technique Section 2.7.3.

Q-POD controller is activated by switching i_{qref} to i_{qref2}. The DC voltage setpoint is changed from V_{mpp} to V_{op} by switching S_1 from position 1 to 2 to reduce the PV-STATCOM real power output to zero.

Figure 7.2 illustrates the Q-POD controllers for PV-STATCOM. Q-POD controller utilizes two control signals ω_3 and ω_4 as discussed earlier. The compensators for each controller are as:

$$G_{1Q-POD} = G_1 \frac{1 + sT_{1lead}}{1 + sT_{1lag}} \tag{7.1}$$

$$G_{2Q-POD} = G_2 \frac{1 + sT_{2lead}}{1 + sT_{2lag}} \tag{7.2}$$

where, G_1, T_{1lead} and T_{1lag} are the gain, lead and lag time constant for ω_3 compensator. G_2, T_{2lead} and T_{2lag} are the gain, lead and lag time constant for ω_4 compensator.

Since both ω_3 and ω_4 are used for Q-POD controllers, both Mode 1 and 3 can be damped with proposed control technique.

7.3.1.2 PQ-POD Controller

PQ-POD controller is designed to damp both G_3 and G_4 power oscillations by controlling PV-STATCOM real and reactive power outputs. ω_3 has been chosen as the control signal to control the PV-STATCOM reactive power output in PQ-POD control mode. Further, ω_4 is selected as the control signal to control the PV-STATCOM reactive power output in PQ-POD control mode. The signal selection is performed through Residue analysis and will be explained in *Section* 7.4.2.

In this mode of operation, i_{dref} changes to i_{dref2} by switching S_2 from position 1 to 2. ω_4 is used as the control signal. The control signal selection and the P-POD controller design is presented in *Section* 7.4.2.

The PQ-POD compensators as shown in Figure 7.2 are:

$$G_{3Q-POD} = G_3 \frac{1 + sT_{3lead}}{1 + sT_{3lag}} \tag{7.3}$$

$$G_{P-POD} = G \frac{1 + sT_{lead}}{1 + sT_{lag}} \tag{7.4}$$

where, G_3, T_{3lead} and T_{3lag} are the gain, lead and lag time constant for ω_3 compensator in Q-POD. G, T_{lead} and T_{lag} are the gain, lead and lag time constant for ω_4 compensator in P-POD controller. In order to provide the PQ-POD controller with maximum real power modulation ability, if the PQ-POD is activated, PV real power is reduced to half of its prefault value P_{pr}. This technique is described in detail in *Section* 6.4.1.2.

7.3.2 Selection of PV-STATCOM Controller Operation

Figure 7.3, depicts the flowchart for PV-STATCOM operation mode selection. As shown in Figure 7.3, if ω_3 or ω_4 speed deviation is greater than ε the PV-STATCOM changes its mode of operation to POD mode to damp the power oscillations. In this chapter ε is selected as 5%. The Q-POD and PQ-POD controllers are selected based on following criteria;

a. If the PV real power is less than the half of the PV power system maximum power (P_{av}=50 MW), PV real power reduces to zero and entire PV-STATCOM inverter capacity is used for Q-POD.

b. If the PV real power is greater than the half of the PV power system maximum power (P_{av}=50 MW), PV real power reduces to half of the PV real power pre-fault value P_{pr} and PQ-POD mode is activated. In this mode i_{qref} changes to i_{qref2} and i_{dref} changes to $i_{dref\,2}$.

c. The strategy of comparing with P_{av} is only to reduce the magnitude of change in real power with the objective of reducing a potential impact on the grid frequency.

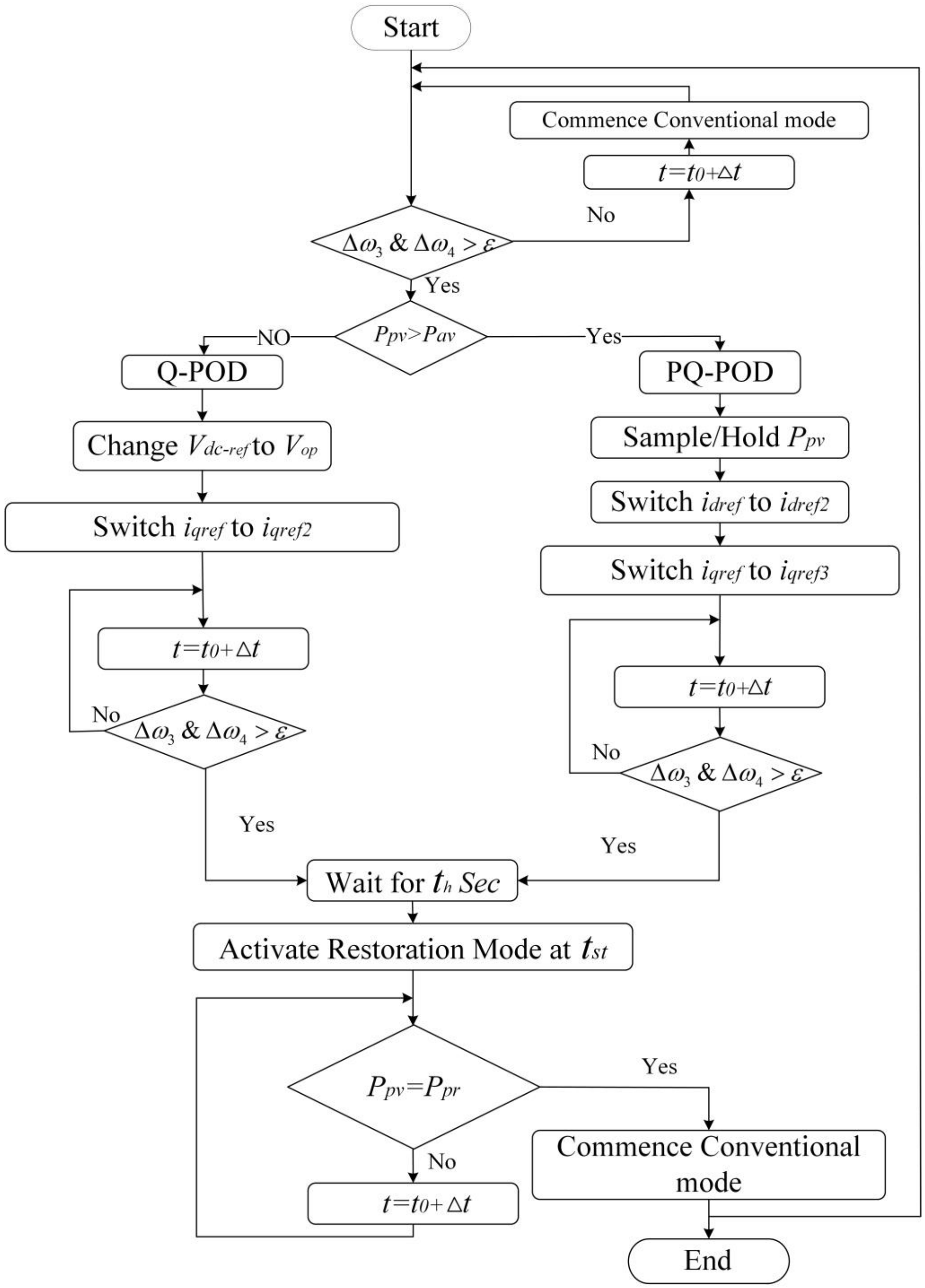

Figure 7.3 Flowchart for PV-STATCOM POD mode selection

d. If the oscillations in both ω_3 or ω_4 signals stabilize within 5% range, a waiting time period of t_h (selected as 2 sec) is utilized for safety. Subsequently at t = t_{st} , the PV real power is restored back to P_{pr} with a ramp function. When P_{pv} reaches P_{pr}, the conventional PV mode of operation is activated.

7.4 PV-STATCOM Small Signal Model

Although detailed simulation study can be performed in EMT-type simulation studies in PSCAD/EMTDC software, it is not so efficient for design of controllers. Since EMT-type simulations require small simulation step time (10-100μs depending on the application, the controller design could be very time-consuming procedure, especially when multiple controllers tuning is required. Hence, small signal studies are conducted for designing the POD controllers, using the PV-STATCOM small signal model. The small signal model of PV-STATCOM is presented in *Section* 2.9. The i_{dref} and i_{qref} signals are generated through the outer-loop controllers as illustrated in PV-STATCOM detail model.

7.4.1 Q-POD Controller Design

Since 12 bus power system has different interarea modes of oscillation, the first step in designing Q-POD controller is to find the controller signals in which the selected oscillatory modes have the highest participation factor.

7.4.1.1 Participation Factor analysis

Following a disturbance, three low-frequency electromechanical mode of oscillations as 1.21 Hz with a damping ratio of 11.4%, 1.002 Hz with a damping ratio of 9.7%, and 0.7624 Hz with a damping ratio of 4.1 % appear in the power system. In order to determine the state that has the highest participation in each mode of oscillation, PF analysis is performed through small signal studies in Matlab software.

Figure 7.4 illustrates the PF analysis for the three interarea modes of oscillations. The rotor speed and angle deviation of generator 3 have the highest participation in Mode 1. Generator 2 rotor speed and angle participate more in Mode 2 interarea oscillation. Furthermore, Generator 4 speed deviation and rotor angle are the main participants in Mode 3 interarea oscillation.

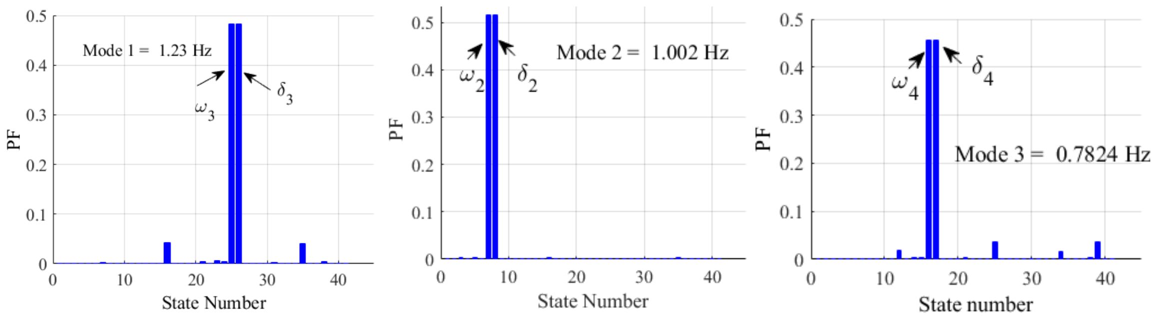

Figure 7.4 Participation Factor analysis for the critical modes of oscillations.

Based on the PF study, to damp the Mode 1 and 3, speed deviation signal from the generator 3 and 4 are the best control signals. It is noted that the PV-STATCOM does not have a significant damping effect on Mode 2 oscillation due to the long distance between generator 2 and PV-STATCOM location. This conclusion will further be justified in this chapter.

Although the Wide Area Measurement (WAM) technique contains a certain amount of delay, in this section to achieve POD controller which results in highest damping for critical modes of oscillations, no delay has been added to the WAMs signal. However, the effect of delay on the proposed controller is investigated in the *Section* 7.5.3, where new controller parameters are utilized to compensate the effect of delay. Since three interarea modes of oscillation exist in the 12 bus FACTS power system, POD controllers for an individual mode can have an adverse effect on other modes of oscillation. Hence, modal analysis is required to investigate the effect of POD feedback loop controllers on other modes of oscillation.

7.4.1.2 Modal Analysis for Q-POD Controller Design

Modal analysis based on small signal studies is performed in Matlab environment. A feedback signal from generator 3 (ω_3) is fed to the Q-POD controller of the 100 MW PV-STATCOM system. It is assumed that the PV system is generating 50 MW real power and 86.6 MVar inverter capacity is available for Q-POD. Figure 7.5 presents the root loci of the critical eigenvalues and the effect of the feedback gain of the POD controller on low-frequency modes of oscillation in the power system.

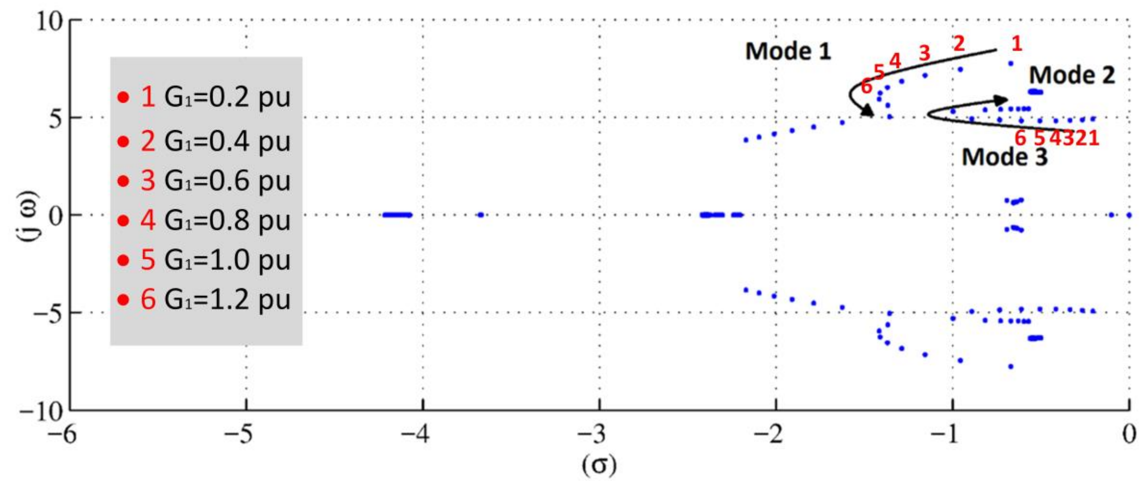

Figure 7.5 Eigenvalues of critical Modes with respect to different feedback gains of *G_3* without phase compensation.

It is seen that increasing the feedback gain of ω_3 from 0 to 2 pu, Mode 1 and Mode 3 start becoming more stable but maximum stability is achieved when the feedback gain reaches 1.2 pu. A Phase compensator $G_{1s}(t)$ is designed for small signal stability of the power system based on residue technique in *Section* 2.7.3 and presented in Appendix J.

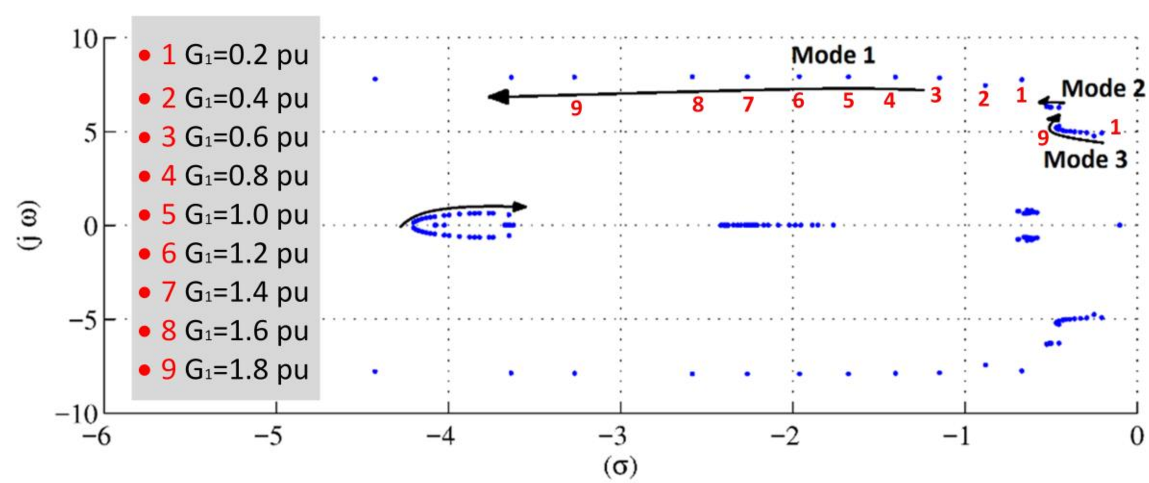

Figure 7.6 Eigenvalues of critical Modes with respect to different feedback gains of G_3 with phase compensation.

Figure 7.6 presents the root loci of the critical eigenvalues with changes in ω_3 feedback controller gain along with designed lead-lag controller. It is seen that by increasing the ω_3

feedback gain, Mode 3 moves towards $j\omega$ axis. After the feedback gain of ω_3 reaches 1.8 pu the damping of Mode 3 starts decreasing. Hence, the maximum feedback gain for ω_3 is selected as 1.8 pu. To increase the damping ratio of Mode 3, the ω_4 feedback gain is increased from 0 to 1.5 pu. Figure 7.7 portrays the mode shift due to ω_4 gain increment.

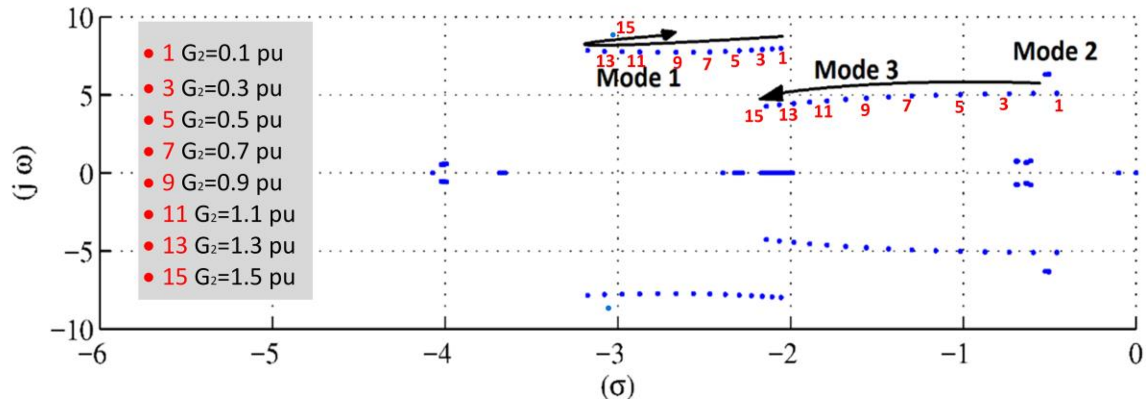

Figure 7.7 Eigenvalues of critical Modes with respect to different G_4 feedback gain with phase compensation.

It is observed that the maximum feedback gain must be set at 1.3 pu. If higher feedback gain is selected, according to Figure 7.7, Mode 1 moves back towards $j\omega$ axis which results in less damping of oscillations.

7.4.1.3 Effect of Delay Compensation on Response of Q-POD controller

The communication delay in transmitted signals varies with different data transmission techniques and distances [121]. The effect of different WAM delays on the PV-STATCOM POD is investigated and new controllers are designed to compensate the effect of delay caused by WAM signals. Figure 7.8 depicts the effect of WAM delay on the proposed POD controller for generator 3.

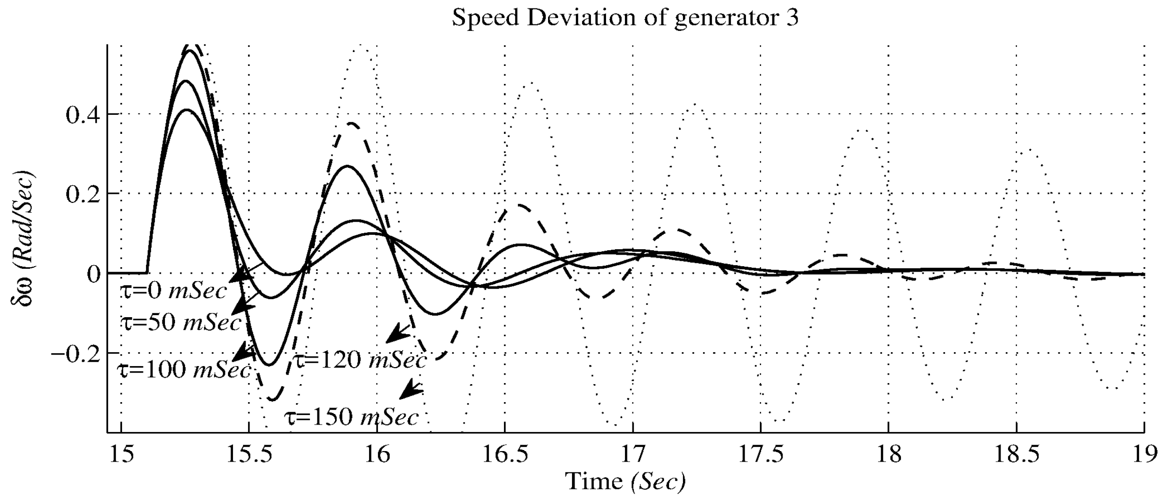

Figure 7.8 Effect of different delays on ω_3WAM signal

Since the PV-STATCOM has the same distance from generator 3 and 4, the same delay is considered for both WAM signals (ω_3 and ω_4). As shown in Figure 7.8, the effectiveness of POD controller for G_3 speed deviation is reduced as the delay increases from 0 to 150 *ms*.

Figure 7.9 illustrates the G_4 speed deviation with different WAM delays. In this case, ω_4 does not show significant change in damping as the delay is increased from 0 to 150 *ms* [122].

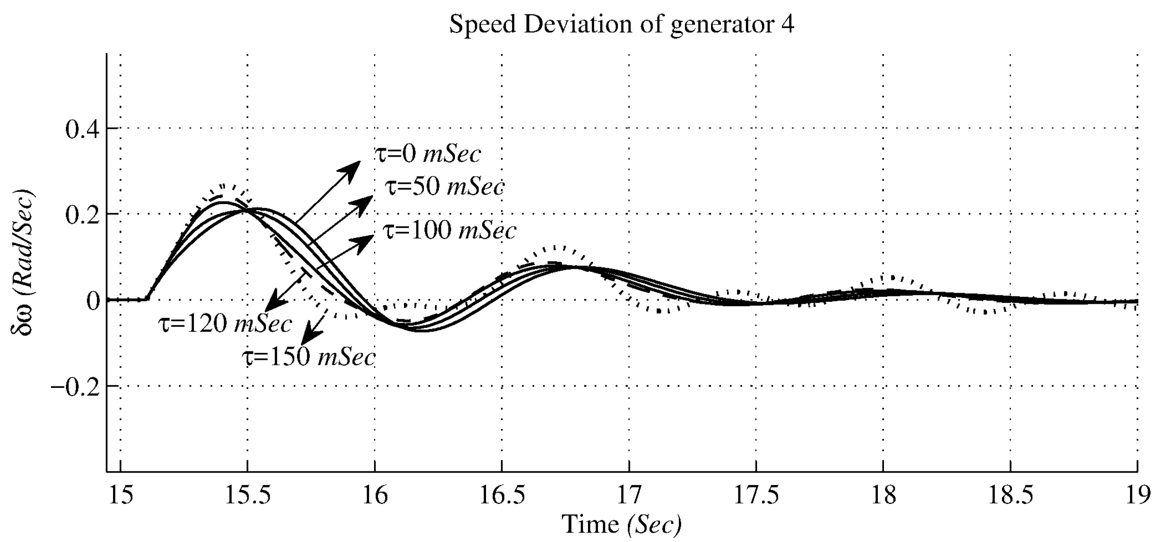

Figure 7.9 Effect of different delays on ω_4WAM signal

To compensate the effect of delay, a new POD controller based on the residue technique in *Section* 2.7.3 is presented and tested both in the small signal simulation and EMT-type simulation. In this study, a large delay time constant of 150 *ms* is considered which is compensated by a new Lead-Lag POD controller. The aim is to compensate the effect of delay on WAM signals to achieve the same damping ratio as if there is no delay in the WAM signals. Since the delay does not affect the ω_4 feedback gain POD controller, the gain for ω_4 remains the same as 0.8 pu. The parameters for the new ω_3 POD controller are given in Appendix J.

7.4.2 PQ-POD Controller Design

The proposed PQ-POD control technique described in *Section* 6.4.1.3 for PV-STATCOM during daytime is tested on the 12 Bus FACTS power system. Since this study system has different modes of interarea oscillations, signal selection for P-POD and Q-POD is done to achieve the highest POD effect. It is assumed that WAM measurements have a 150 ms delay. Residue analysis based on the technique in *Section* 2.8 describes how each P-POD and Q-POD controller can improve the stability of specific modes of oscillation with regard to the different possible locations of the PV power system. Figure 7.10 illustrates the residue analysis for PV-STATCOM interconnection to all the buses in 12 bus power system (except generator buses) for P-POD and Q-POD controllers.

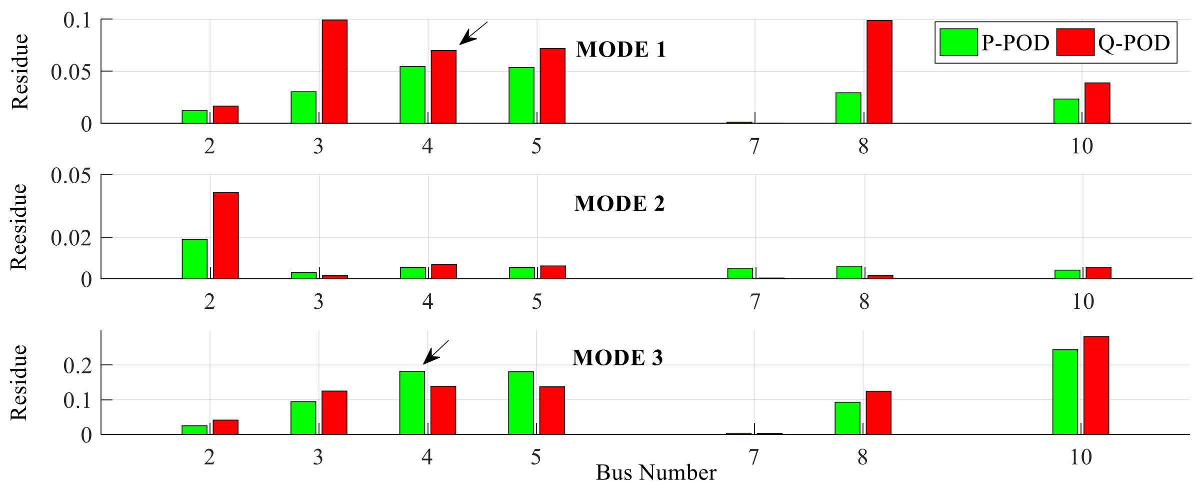

Figure 7.10 Residue analysis of 12 bus FACTS power system for Q-POD and P-POD controller

For residue analysis of P-POD, the input is selected as PV-STATCOM real power variation ΔP. For Q-POD residue analysis PV-STATCOM reactive power output variation ΔQ is selected as the input signal. The output signals for Mode 1, Mode 2, and Mode 3 are ω_3, ω_2, and ω_4, respectively. The output signals are selected based on PF analysis.

It is observed from Figure 7.10 that:

I. PV-STATCOM P-POD and Q-POD controllers have a high impact on Modes 1 and 3 oscillations except when they are connected at bus 2 and 7. The reason for this phenomenon is that the bus 2 and 7 are far from the generators 3 and 4. Further, the speed deviation of these generators have the highest participation in Modes 1 and 3.

II. Only at bus 2, the PV-STATCOM P-POD and Q-POD controllers have the highest effect on Mode 2 oscillation. This finding validates the assumption made in *Section* 7.4.1.1.

III. The highest effectiveness of Q-POD and P-POD control on Mode 3 damping is achieved at bus 10. This results also confirms the assumption that closeness of the PV-STATCOM to a specific generator results in highest POD effect on the oscillatory mode associated with that generator.

IV. Buses 4 and 5 are the best locations for PQ-POD control with PV-STATCOM due to the fact that magnitude of residue for Modes 1 and 3 are relatively high enough for P-POD and Q-POD controllers. Hence, both selected Mode of oscillations can be effectively damped by proposed Q-POD and/or P-POD controllers.

Based on the findings of the residue analysis, in order to damp the selected Modes of oscillation, the PV power system is considered to be connected to bus 4. According to Figure 7.10, the PV-STATCOM real power has the highest effect on Mode 3 and PV-STATCOM reactive power modulation has more effect on Mode 1. Hence, for PQ-POD controller design the P-POD controller is assigned to Mode 3 and Q-POD controller is allocated to damp Mode 1.

The controllers are designed based on residue technique in small signal analysis and optimized in PSCAD/EMTDC software for transient stability. These Controller parameters are listed in Appendix J.

7.5 Case Studies

To test the performance of the proposed controllers, a worst-case scenario is considered. The simulation results in small signal studies are compared with those obtained from EMT-detailed simulation.

7.5.1 Selection of Worst Case Scenario

Based on the modal analysis, four different case studies with regards to line outages near the PV-STATCOM interconnection are presented in Figure 7.11. This figure illustrates the shift in modes due to each line outage. The lowest damping ratio occurs if the line between bus 4 and 5 is disconnected. Hence, electromagnetic transients studies are performed considering the line between buses 4 and 5 is disconnected.

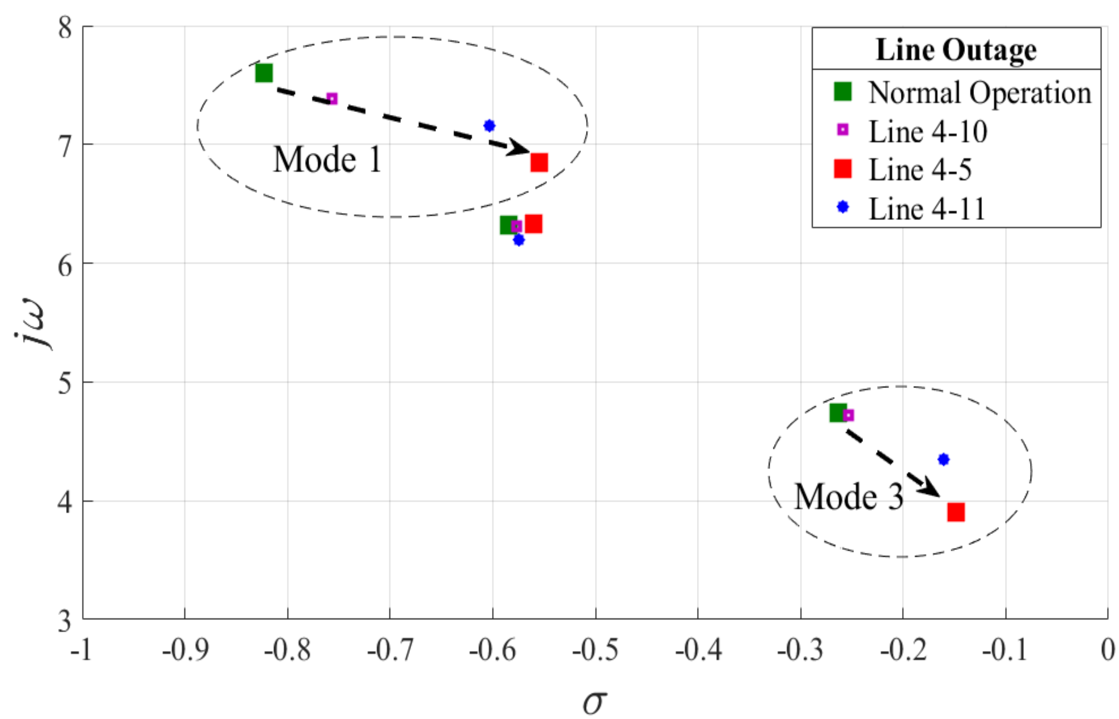

Figure 7.11 Modal analysis for 12 bus power system with respect to various contingencies

7.5.2 Comparison between Small Signal and EMT-Type Simulation

To validate the small signal model simulation, the results obtained in EMT-Type model simulation in PSCAD/EMTDC software is compared with that obtained in small signal simulation in Matlab. In this study, a permanent line outage between Bus 4 and Bus 5 is initiated at t=11.1 *Sec*. Figure 7.12 to Figure 7.14 respectively present the speed deviations of generators 2, 3, and 4 as obtained through PSCAD and Matlab simulations.

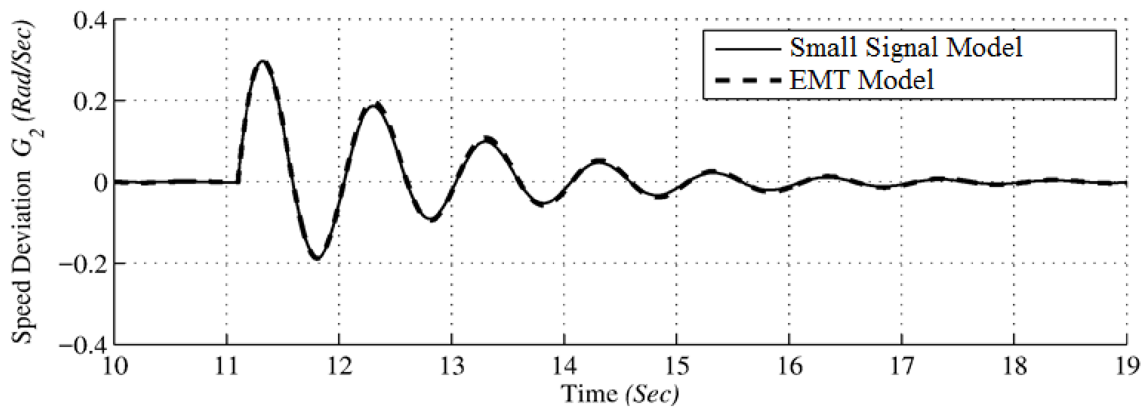

Figure 7.12 Generator 2 speed deviation for the permanent line outage at *t* = 11.1 sec in PSCAD/EMTDC and Matlab.

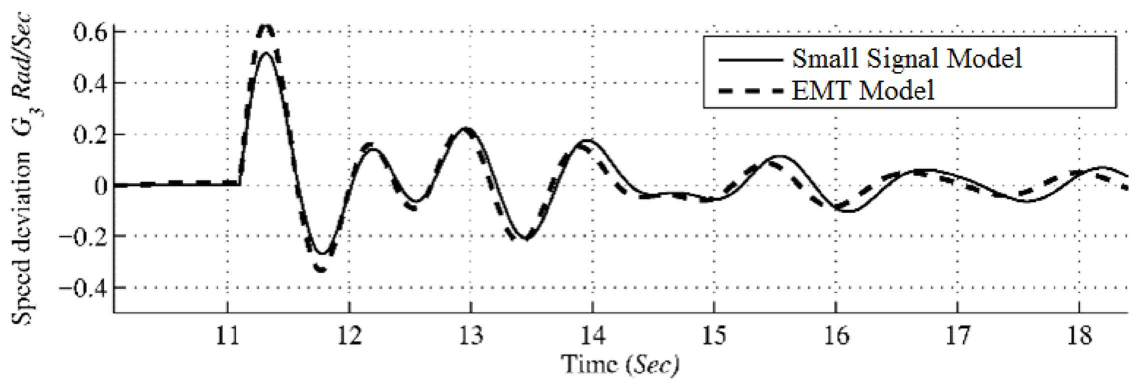

Figure 7.13 Generator 3 speed deviation for the line permanent outage at t= 11.1 sec in PSCAD/EMTDC and Matlab.

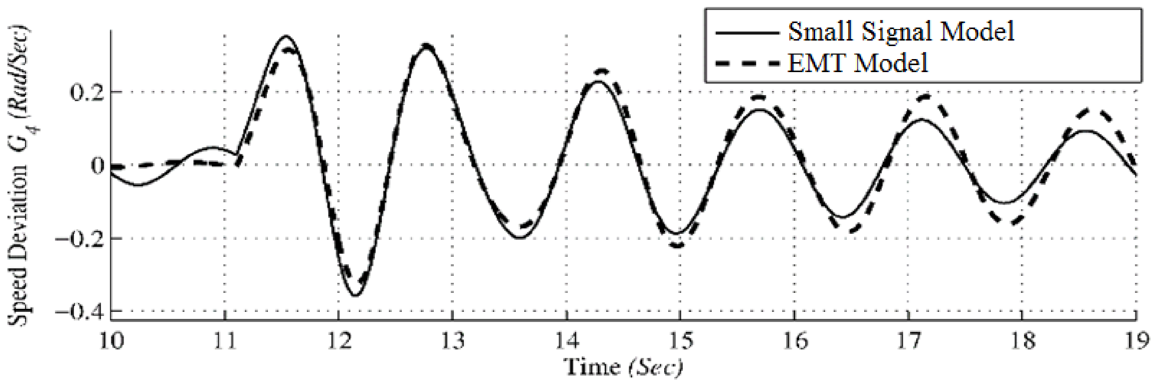

Figure 7.14 Generator 4 speed deviation for the line permanent outage at t = 11.1 sec in PSCAD/EMTDC and Matlab.

It is seen that the variations in generator speeds obtained through small signal simulation studies correlate well with those obtained through EMTDC/PSCAD studies.

7.5.3 Delay Compensation

The performance of the delay-compensated controllers in presence of the communication delays is examined in this study. In Figure 7.15 and Figure 7.16, the speed deviations of generator 3 and 4 are presented with No delay and 150 *ms* delay during Q-POD in Partial STATCOM mode.

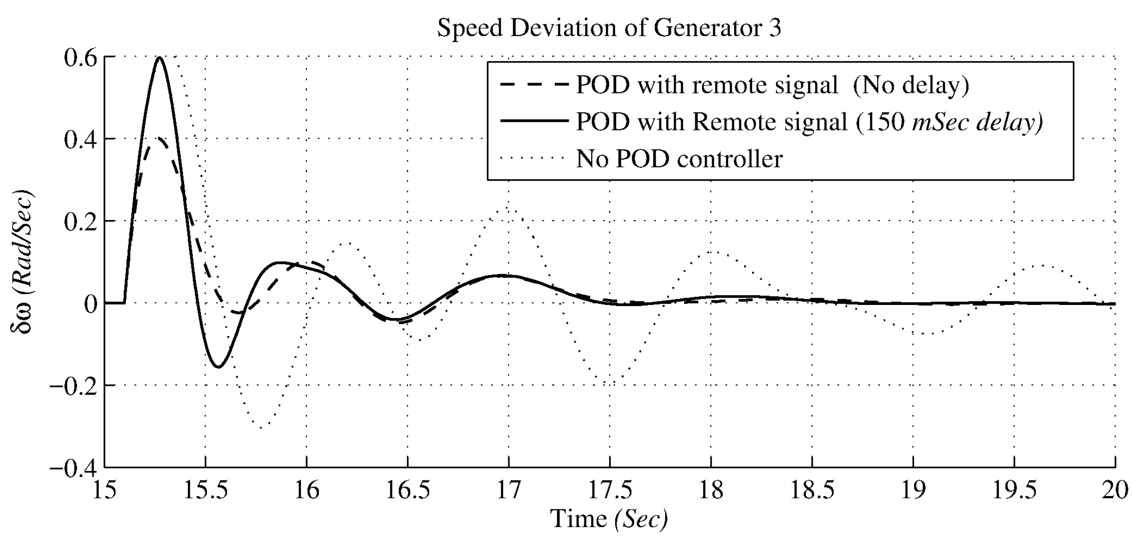

Figure 7.15 Generator 3 speed deviation for POD with and without 150 *ms* delay.

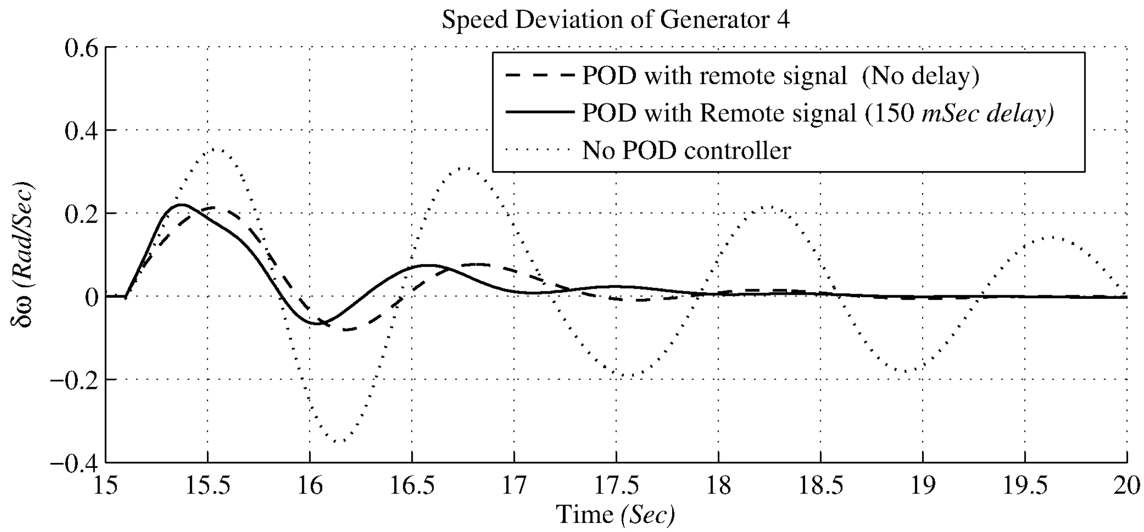

Figure 7.16 Generator 4 speed deviation for POD with and without 150 ms delay.

It is seen that a WAM delay of even 150 *ms* does not have any appreciable impact on the performance of the POD control provided by the PV-STATCOM. This demonstrates the successful compensation of the delays in the designed controllers.

7.5.4 PSCAD/EMTDC Simulation Studies

PSCAD/EMTDC simulation studies are performed to evaluate and compare the performance of the proposed Q-POD and PQ-POD controllers. A three phase to ground fault is initiated at line 4-5 near the bus 4. The fault is cleared after 5 cycles and the faulted line is permanently disconnected. Due to the fault and line outage, three electromechanical modes of oscillations appear in the power system. The PV-STATCOM changes its mode of operation to P-POD or PQ-POD mode of operation based on the Flowchart in Figure 7.3. Figure 7.17 illustrates the results for both Q-POD and PQ-POD control techniques of PV-STATCOM.

Figure 7.17 (a) depicts the results for G_4 speed deviation after the line outage considering PV-STATCOM operates based on No-POD, Q-POD, and PQ-POD controllers. Figure 7.17 (b) portrays the results for G_3 speed deviation after the contingency considering the same operating modes of PV-STATCOM as Figure 7.17 (a). It is shown that if No-POD control technique is applied for PV-STATCOM, the oscillations are poorly damped. On the other hand, by activation of Q-POD control or PQ-POD control, the settling time interval for both oscillatory modes are reduced significantly. It is evident from Figure 7.17 (a) and (b) that the fastest settling times for ω_3 and ω_4 are achieved through PQ-POD controller activation.

Figure 7.17 (c) illustrates the PV-STATCOM real and reactive power for Q-POD controller. As shown in Figure 7.17 (c), if the oscillations are detected in the power system, the PV real power reduces to zero to release the entire PV inverter capacity for Q-POD operation. The reactive power output of the PV-STATCOM is modulated to damp both selected modes of oscillation.

Figure 7.17 (d) portrays the PV-STATCOM real and reactive power output for PQ-POD control mode. As shown in Figure 7.17 (d), after detection of low frequency electro mechanical oscillations, PV real power reduces to half of its prefault value (P_{pr}) and POD is performed by controlling PV-STATCOM real and reactive power simultaneously. In both the controls, after the completion of POD, the PV-STATCOM changes its mode of operation to power restoration mode and PV real power restores back to the pre-disturbance power level P_{pr} in a ramped manner.

The following observations are made:

1. If no POD control is initiated, both oscillatory Modes 1 and 3 have unacceptable damping ratio (about 10%) [118].
2. The PQ-POD control results in faster damping than the Q-POD for speeds of both the generators 3 and 4.

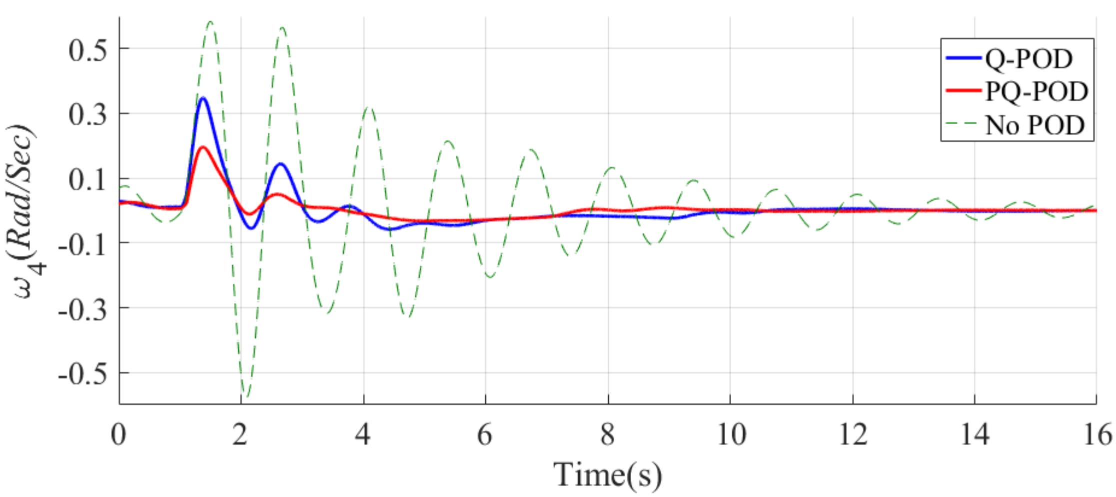

(a)

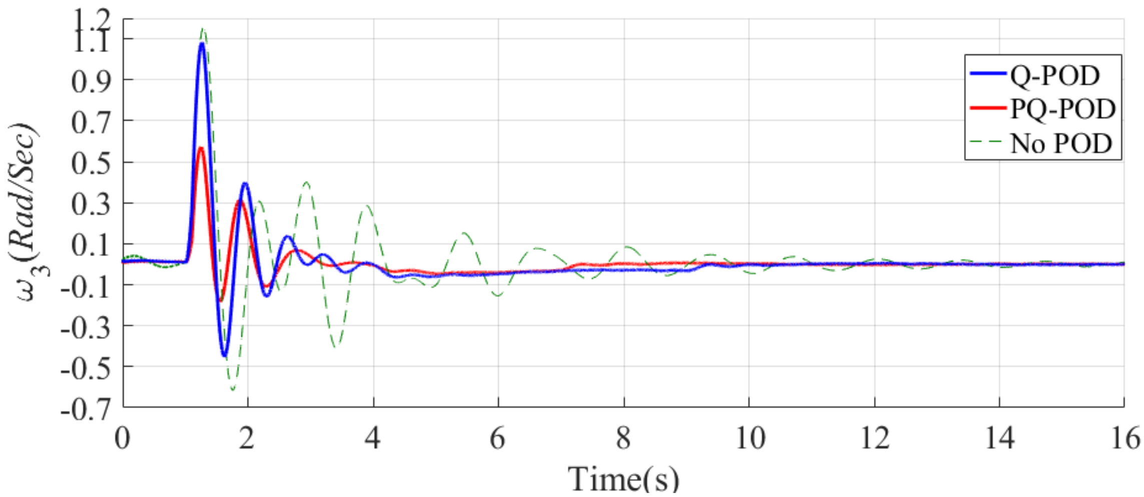

(b)

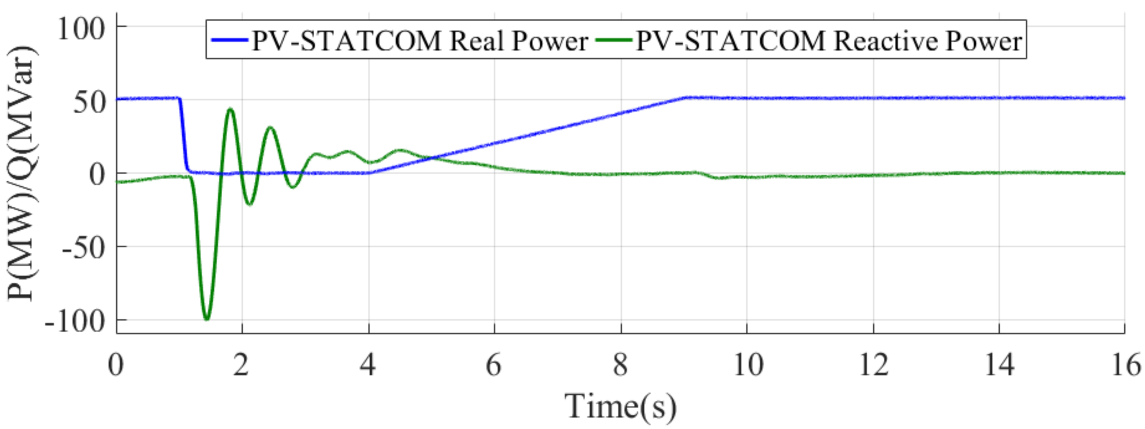

(c)

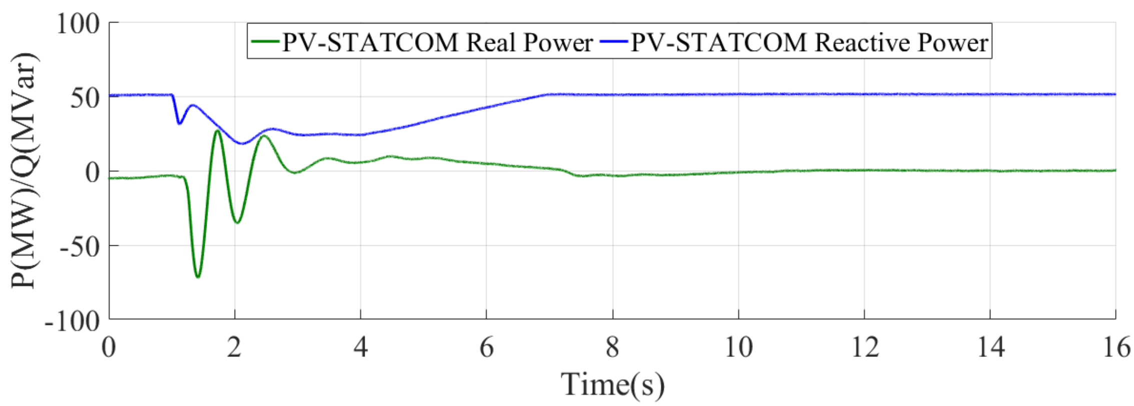

(d)

Figure 7.17 (a) Generator 4 speed deviation, (b) Generator 3 speed deviation, (c) PV-STATCOM real and reactive power in Q-POD mode of operation, (d) PV-STATCOM real and reactive power in PQ-POD mode of operation.

7.5.5 The Effect of PV Real Power Injection on Power System Stability

In this study, the effect of different levels of PV power injection on the 12 bus FACTS power system stability is studied. It is assumed that the 100 MW PV solar plant is connected to bus 4. The PV real power varies from 0 MW to 100 MW. Table 7.1 presents the damping ratio of critical modes of oscillations with respect to PV real power injection if no POD controller is activated. Table 7.1 demonstrates that by increasing the PV real power injection to the PCC, the damping ratio of Mode 1 and Mode 3 get reduced significantly from 11.4% to 9.72% for Mode 1 and 5.8% to 3.3 for Mode 3.

Table 7.1. Eigenvalues and damping ratio of critical modes of oscillation without Q-POD and PQ-POD controller

	Mode 1		Mode 2		Mode 3	
MW	λ	ζ	λ	ζ	λ	ζ
0	-0.88+j7.66	11.4	-0.62+j6.34	9.7	-0.28+j4.78	5.8
10	-0.87+j7.65	11.2	-0.62+j6.34	9.7	-0.27+j4.77	5.6
20	-0.86+j7.64	11.1	-0.62+j6.34	9.7	-0.27+j4.76	5.6
30	-0.84+j7.63	10.8	-0.62+j6.33	9.7	-0.27+j4.75	5.4
40	-0.83+j7.62	10.7	-0.62+j6.33	9.7	-0.26+j4.74	5.2
50	-0.81+j7.61	10.5	-0.61+j6.33	9.5	-0.26+j4.73	4.8
60	-0.80+j7.59	10.3	-0.61+j6.33	9.5	-0.25+j4.72	4.5
70	-0.79+j7.58	10.2	-0.61+j6.33	9.5	-0.25+j4.71	4.1
80	-0.77+j7.57	9.98	-0.61+j6.33	9.5	-0.24+j4.71	3.9
90	-0.76+j7.56	9.85	-0.61+j6.33	9.5	-0.24+j4.70	3.5
100	**-0.75+j7.5**	9.72	**-0.61+j6.34**	9.5	**-0.24+j4.70**	3.3

On the other hand, the damping ratio of Mode 2 does not change considerably. According to Residue analysis in Section 7.4.2, since generator 2 is far from the PV solar system its stability is not affected by the PV real power injection. It is noted that generators 3 and 4 are relatively closer to the PV system location, hence their stability is impacted by the increase of power injection from the PV solar system.

Table 7.2 depicts the results for PV real power penetration on the power system stability, considering that the Q-POD controller is activated. In this study, ω_3 and ω_4 are used as the reference signal for Q-POD controller. For this study, the PV-STATCOM does not select the PQ-POD mode after the PV real power generation exceeds 50 MW. To release the entire PV inverter capacity, PV real power injection function is disabled after the oscillations are detected. As shown in Table 7.2, the damping ratios of Modes 1 and 3 have significantly improved. In addition, it is observed that if the PV real power exceeds 50 MW, the damping ratio of Mode 3 starts reducing to 15.8 %. This damping ratio reduction is due to PV real power penetration level and sudden reduction in PV real power from 100 MW to 0.

Table 7.2 Eigenvalues and damping ratio of critical modes of oscillation with Q-POD

		Mode 1		**Mode 2**		**Mode 3**	
	MW	**λ**	**ζ**	**λ**	**ζ**	**λ**	**ζ**
Q-POD	0	-2.07+j7.85	25.3	-0.64+j6.38	9.9	-0.90+j4.72	18.7
	10	-2.07+j7.90	25.3	-0.64+j6.38	9.9	-0.90+j4.72	18.7
	20	-2.05+j7.89	25.1	-0.64+j6.38	9.9	-0.89+j4.71	18.5
	30	-2.02+j7.86	24.7	-0.64+j6.37	9.9	-0.89+j4.69	18.5
	40	-2.0+j7.84	24.4	-0.64+j6.37	9.9	-0.89+j4.67	18.5
	50	-2.0+j7.8	24.4	-0.63+j6.36	9.9	-0.88+j4.65	18.3
	60	-1.99+j7.8	24.3	-0.63+j6.36	9.8	-0.87+j4.5	18.1
	70	-1.99+j7.7	24.3	-0.63+j6.36	9.8	-0.85+j4.3	17.6
	80	-1.98+j7.86	24.2	-0.63+j6.36	9.8	-0.82+j4.1	17.0
	90	-1.98+j7.82	24.2	-0.63+j6.35	9.8	-0.81+j3.8	16.8
	100	-1.98+j7.6	24.2	**-0.63+j6.35**	9.8	-0.76+j3.1	15.8

Table 7.3 depicts the results for PQ-POD controller for PV-STATCOM considering the PV system real power varies from 0 to 100 MW. As illustrated in Figure 7.2, the ω_3 signal is utilized for Q-POD controller and ω_4 is selected as the control signal for P-POD controller. As shown in Table 7.3, the damping ratio of Mode 1 in which ω_3 has the highest participation is significantly increased regardless of the level of power generation. On the other hand, damping ratio of Mode 3 illustrates gradual improvement from 5.8% to 18.3%. This phenomenon is due to the gradual increase in PV-STATCOM available real power to perform POD with its real power.

Table 7.3 Eigenvalues and damping ratio of critical modes of oscillation with PQ-POD

	MW	Mode 1 λ	Mode 1 ζ	Mode 2 λ	Mode 2 ζ	Mode 3 λ	Mode 3 ζ
PQ-POD	0	-2.0+j7.85	24.6	-0.64+j6.38	9.9	-0.28+j4.78	5.8
	10	-2.0+j7.90	24.6	-0.64+j6.38	9.9	-0.35+j 4.77	7.3
	20	-2.05+j7.89	25.1	-0.64+j6.38	9.9	-0.41+j 4.6	8.3
	30	-2.02+j7.86	24.7	-0.64+j6.37	9.9	-0.62+j 4.6	12.5
	40	-2.0+j7.84	24.4	-0.64+j6.37	9.9	-0.83+j 4.6	16.9
	50	-2.01+j7.89	24.6	-0.63+j6.36	9.9	-0.91+j4.65	18.5
	60	-2.03+j7.7	24.8	-0.63+j6.36	9.8	-0.91+j4.63	18.5
	70	-2.05+j7.86	25.1	-0.63+j6.36	9.8	-0.91+j4.62	18.3
	80	-2.08+j7.86	25.4	-0.63+j6.36	9.8	-0.91+j4.60	18.3
	90	-2.08+j7.84	25.4	-0.63+j6.35	9.8	-0.91+j4.58	18.3
	100	-2.07+j7.8	25.3	**-0.63+j6.35**	9.8	**-0.91+j4.57**	18.3

Table 7.4 portrays the effect of PV real power penetration level on damping ratio of selected modes of oscillation considering Q-POD controller is activated if PV real power is less than 50 MW and PQ-POD controller is activated if the PV real power is more than 50 MW. As depicted in Table 7.4, despite the level of PV real power generation, the damping ratio of Mode 1 and Mode 3 have significantly improved from 9.7% to 25.3% and 3.3% to 18.3%, respectively.

Table 7.4 Eigenvalues and damping ratio of critical modes of oscillation with PQ-POD

	MW	Mode 1 λ	Mode 1 ζ	Mode 2 λ	Mode 2 ζ	Mode 3 λ	Mode 3 ζ
Q-POD	0	-2.07+j7.85	25.3	-0.64+j6.38	9.9	-0.90+j4.72	18.7
	10	-2.07+j7.90	25.3	-0.64+j6.38	9.9	-0.90+j4.72	18.7
	20	-2.05+j7.89	25.1	-0.64+j6.38	9.9	-0.89+j4.71	18.5
	30	-2.02+j7.86	24.7	-0.64+j6.37	9.9	-0.89+j4.69	18.5
	40	-2.0+j7.84	24.4	-0.64+j6.37	9.9	-0.89+j4.67	18.5
PQ-POD	50	-2.01+j7.89	24.6	-0.63+j6.36	9.9	-0.89+j4.65	18.5
	60	-2.03+j7.7	24.8	-0.63+j6.36	9.8	-0.89+j4.63	18.5
	70	-2.05+j7.86	25.1	-0.63+j6.36	9.8	-0.88+j4.62	18.3
	80	-2.08+j7.86	25.4	-0.63+j6.36	9.8	-0.88+j4.60	18.3
	90	-2.08+j7.84	25.4	-0.63+j6.35	9.8	-0.88+j4.58	18.3
	100	-2.07+j7.8	25.3	**-0.63+j6.35**	9.8	**-0.88+j4.57**	18.3

Hence, from Table 7.3 and Table 7.4, it is noted that proper switching between Q-POD and PQ-POD controller is required based on the level of PV real power generation.

7.1 Conclusion

In this chapter, the performances of Q-POD, P-POD and PQ-POD controllers of a PV-STATCOM on the 12 bus FACTS power system are investigated. Modal analysis is used to select a fault scenario that causes the highest level of damming for the different modes of oscillation. The results obtained with small signal simulation in Matlab are validated with those obtained with EMT-Type model simulation in PSCAD/EMTDC software. The various controllers are therefore designed using small signal model of the power system. Participation Factor analysis is performed to determine the appropriate control signal for power oscillation damping. In addition, the effect of various delays on WAM signals is studied and new compensators are designed to minimize the effect of delay. Modal analysis is used to compare the damping ratios of different oscillatory modes with and without the proposed POD controls for various levels of PV system real power generation from 0 to 100 MW. The following conclusions are drawn:

1) Each type of control at different locations has different levels of effectiveness in damping different modes of oscillations. Based on this study, the P-POD controller is assigned to Mode 3 and Q-POD controller is allocated to damp Mode 1.

2) Communication delays in the Wide Area Measurement signals adversely influence the damping performance of the various controllers. However, an appropriate controller design to compensate the delays mitigates this adverse impact.

3) The PQ-POD control is more effective than Q-POD control if the PV real power generation level is more than 50 MW or half of the inverter rating.

4) An increase in the PV penetration level is seen to reduce the stability of the study system. However, the proposed PV-STATCOM POD controllers significantly improve the stability of different oscillatory modes. Hence, higher level of PV penetration can be achieved with the use of proposed PV-STATCOM technology.

Chapter 8

8 Conclusion

8.1 Introduction

The number of large scale PV solar farm interconnections in power systems is rapidly increasing for environmental reasons. This is causing a growing apprehension that inertia-less real power injections from these inverters based generation units will result in a decline in power system stability. This thesis presents a novel 24/7 (night and day) control of a large-scale PV solar farm as STATCOM (PV-STATCOM) for damping low-frequency electromechanical power oscillations resulting in a significant improvement in power transfer capability of existing power systems. The proposed PV-STATCOM control techniques are tested on three power systems: Single Machine Infinite Bus SMIB system, Two-Area system, and the 12 bus FACTS power system. The effectiveness of the proposed Power Oscillation Damping (POD) control techniques based on reactive and real power modulation is evaluated in both small signal and EMT-Type simulations studies. The performance of the proposed control techniques for PV-STATCOM is compared with that of an actual BESS and actual STATCOM.

The broad overview of this thesis and the major contributions are presented below. Suggestions for future work based on the findings in this thesis are also provided.

8.2 Power System Modeling and Controller Design

In Chapter 2 the concept of PV-STATCOM in both Partial STATCOM mode and Full STATCOM mode are presented. In Partial STATCOM mode, the inverter capacity remaining after real power generation is used for reactive power control. This mode is available during early mornings and late afternoons. In the Full STATCOM mode of operation, the real power generation function of the PV solar farm is temporarily discontinued during a severe disturbance in the power system and the entire inverter capacity is released for reactive power modulation to support the grid. Simultaneously, the available real power is also modulated to provide enhanced grid support. After the need for system support is fulfilled, the PV solar system restores its real power output to the pre-disturbance level in a ramped manner, and the PV solar farm resumes its normal function of real power generation. In Full STATCOM mode during nighttime, the entire inverter capacity is utilized for reactive power control.

The Single Machine Infinite Bus (SMIB) system, Two-Area power system, and the 12 Bus FACTS power system which are used as study systems in this thesis are described. The models of different power system components i.e. generator, transmission lines, loads, etc. are presented. The modeling of an aggregated large-scale PV solar system is described. The design requirements for PV system controllers based on their required settling time and bandwidth are illustrated. Participation Factor analysis in POD control signal selection is presented. The design of power oscillation damping controllers through small signal Residue analysis and *Simplex* Optimization technique in electromagnetic transient simulations are exemplified.

The Residue analysis technique is utilized for selection of the appropriate location of PV-STATCOM POD controllers. The small signal simulations of POD controller performance of the proposed PV-STATCOM are presented and the results were compared with detailed EMT-Type simulation studies.

In order to compare the effectiveness of POD with PV-STATCOM real power modulation with a similar size Battery Energy Storage System (BESS), a detailed model of large scale BESS in PSCAD/EMTDC software is presented. The aggregated BESS model is based on a series and parallel interconnection of multiple single *Li-ion* battery system models. Furthermore, the effect of the battery State of Charge (SOC) on the behavior of internal variables is also illustrated.

8.3 Power Oscillation Damping in Single Machine Infinite Bus (SMIB) System with PV-STATCOM and Battery Energy Storage System (BESS)

This chapter presents a comparative study of Reactive power based Power Oscillation Damping Q-POD control with remnant PV inverter capacity of PV-STATCOM and real power based Power Oscillation Damping P-POD control with BESS of different sizes. To compare the effectiveness of the controllers, the POD controllers are first optimized in

EMT-type detailed simulation studies to achieve maximal damping for both P-POD and Q-POD controls.

It is shown that the effectiveness of P-POD control with BESS is dependent on the size of BESS. Further, the power oscillation damping achieved by Q-POD control of a PV-STATCOM can be accomplished by P-POD control of a BESS with just half size as the PV solar plant. This demonstrated that real power modulation based POD control can be effectively employed for damping electromechanical oscillations in PV solar plants.

Based on the above conclusions, a P-POD controller is implemented on a PV-STATCOM during daytime in Chapter 6 and Chapter 7.

8.4 Coordinated Control of PV Solar System as STATCOM (PV-STATCOM) and Power System Stabilizers for Power Oscillation Damping

One concern with POD controllers in FACTS devices is that these may adversely interact with other POD controllers such as Power System Stabilizer PSS in power systems. This chapter presents an optimized coordinated POD controller design for PV-STATCOMs considering PSSs are present in the power system. The Two-Area power system is selected as the study system and PSSs are introduced in all generators. The coordinated optimization of PV-STATCOM and PSSs is performed first through small signal analysis and subsequently tuned with detailed electromagnetic transients simulation studies. Three different POD scenarios were compared: i) PSSs present but no PV-STATCOM, ii) PV-STATCOM present but no PSSs, and iii) coordinated POD control with both PV-STATCOM and PSSs. It is concluded that a coordinated POD control provides a much superior performance than either of the two POD controls acting alone. The coordinated control results in considerably faster settling time and smaller oscillation magnitude during the power oscillations.

The performance of Q-POD with PV-STATCOM and that with an actual STATCOM at the same location is then compared. It is seen that Q-POD with PV-STATCOM remnant inverter capacity introduces no adverse effect on the PV system real power generation.

Further, the PV-STATCOM performance utilizing the remnant inverter capacity (after real power generation) is similar to that of an actual STATCOM with the same capacity.

8.5 Power Oscillation Damping with Reactive Power Control in Full PV-STATCOM

Although utilization of remnant PV inverter capacity for POD results in significant improvement of power system stability, the availability of this technique is limited during noon time (hours of full sun), since no PV inverter capacity is left for Q-POD operation. This chapter presents the application of a novel patented control technique for damping power oscillations with PV-STATCOM in Full-STATCOM mode utilizing the entire PV inverter capacity, even at noontime. As described earlier, in the Full-STATCOM mode, the PV system real power injection function is disabled and entire PV inverter capacity is made available for reactive power modulation to damp power oscillations.

In order to change the PV-STATCOM operation mode, an autonomous oscillation detection unit is designed in PSCAD/EMTDC software. If any low frequency electromechanical oscillations appear in the power system, the PV real power injection function is disabled and Q-POD is activated. It is shown that with the proposed Q-POD technique in Full STATCOM operation mode of the PV system, the power transfer capability of the power system is increased significantly both during night and day. A 100 MW PV solar system controlled as PV-STATCOM improves the power transfer capability by 230 MW in the SMIB power system and by 200 MW in the Two-Area power system on a 24/7 basis.

This chapter further presents a novel technique for restoration of power to its pre-disturbance level after the power oscillations are damped. Novel ramp and nonlinear PV real power restoration techniques are presented in which the Q-POD controller remains activated with the remaining inverter capacity, even during the restoration interval. Hence, the PV-STATCOM is able to prevent the recurrence of any power oscillations during the restoration process. These proposed restoration techniques decrease the restoration interval of 100 MW PV solar system to just 3 seconds. This technique is substantially faster than that required by various Grid Codes.

It is further demonstrated that despite the sudden discontinuation of real power from the PV system in the Full-STATCOM mode does not create any frequency stability issues in the two study systems.

8.6 Novel Combined Real and Reactive Power Control of PV Solar Farm as STATCOM (PV-STATCOM) for Power Oscillation Damping

This chapter presents the application of a novel patent-pending POD control utilizing combined real and reactive power modulation with a PV-STATCOM. Three controls are considered: i) reactive power modulation based POD control (Q-POD), ii) real power modulation based control (P-POD) and iii) combined real and reactive power modulation (PQ-POD) control. During a power system disturbance, the PV-STATCOM reduces its real power output from 100 MW to 50 MW and P-POD controller modulates the PV-STATCOM real power between 0 to 100 MW. In the Q-POD mode the entire 100 Mvar inverter capacity is utilized for POD. In the PQ-POD, the real power is reduced to half of its maximum power generation level at that time and modulated around the half level from zero to the maximum level. The remaining inverter capacity is utilized for Q-POD.

These different POD controllers are optimized in detailed simulation studies based on embedded *Simplex* optimization.

It is shown that during full noon hours, the 0-100 MW real power modulation based P-POD control results in the same damping as ±100 MVar Q-POD control with the PV-STATCOM. The combined real and reactive power modulation based PQ-POD control of a large scale PV solar farm control as PV-STATCOM is more effective than both Q-POD with Full PV-STATCOM and P-POD with BESS.

The effect of the location of the PV system and the magnitude of real power generation for P-POD and Q-POD control is investigated based on the small signal Residue analysis. The results of the Residue analysis are validated through detailed simulation studies in PSCAD/EMTDC software. It is seen that despite the location of PV-STATCOM, highest damping is achieved if PQ-POD controller is activated.

The effect of each controller (P-POD, Q-POD, and PQ-POD) on power system frequency is investigated. It is shown that the sudden reduction in PV-STATCOM real power to perform Q-POD results in a slightly lowered frequency stability of the power system. However, the PQ-POD controller has a minimal adverse effect on power system frequency.

8.7 Power Oscillation Damping for 12 bus FACTS Power system

The performances of different novel POD controls of a PV-STATCOM, i.e., Q-POD, P-POD and PQ-POD controls are investigated in the 12 bus FACTS power system which exhibits multiple interarea modes of oscillation. Modal analysis is used to justify the worst-case fault scenario that causes the highest level of undamping for selected oscillatory modes. The results of small signal simulations in Matlab Simulink are validated by EMT-simulations with PSCAD/EMTDC software. Participation Factor analysis is used to select the appropriate signal for POD controllers. After POD control signal selection, the effectiveness of P-POD and Q-POD controllers on selected mode of oscillations is examined. Based on the PV-STATCOM location in the power system, each POD controller (P-POD and Q-POD) has different effect on the modes of oscillations. Hence each mode of oscillation needs to be appropriately addressed by different controllers i.e., Q-POD or P-POD controller based on the findings of residue analysis.

The PV system real power penetration has an adverse effect on the power system stability if no POD controller is activated in the PV system.

It is observed that the effectiveness of P-POD controller on damping the selected mode of oscillation is affected by the level of PV system real power generation. The PQ-POD controller is more effective than Q-POD controller if the PV system is generating more than the half of its capacity (50 MW in this study).

However, through utilization of the proposed PQ-POD controller, not only the adverse effect of PV real power penetration is attenuated, but the overall power system stability is significantly improved.

The effect of communication delays in the Wide Area Measurement based control signals used for different POD controls is investigated. It is observed that the delays in communication system have an adverse effect on the POD with PV-STATCOM. However, with the design of delay-compensated controls, this adverse effect is obviated.

8.8 Contribution and Significance of this Thesis

This thesis presents the first time application of novel patented [1] and patent-pending [2] controls of PV solar farm as STATCOM (PV-STATCOM) for power oscillation damping in power systems. The resulting contributions of this thesis are as follows:

1) A novel reactive power modulation based control of PV solar farm as a STATCOM, termed PV-STATCOM, is demonstrated which provides a 24/7 (day and night) functionality of a STATCOM for power oscillation damping. This functionality is provided at a significantly lower cost than a STATCOM as the existing infrastructure of a PV system is utilized for STATCOM implementation.

2) The proposed Q-POD control on a PV-STATCOM reduces the need for installation of expensive Battery Energy Storage Systems for achieving similar levels of power oscillation damping.

3) Novel fast ramp and nonlinear PV real power restoration, in which the POD controller remains activated, has been proposed. This novel PV real power restoration technique can significantly reduce the restoration intervals even more than those specified by grid codes.

4) A method has been proposed in which the effectiveness of PV-STATCOM real and reactive power modulation on each mode of oscillations can be studied. This technique is useful for selecting an appropriate controller for POD for a given location of the PV-STATCOM in the power system.

5) Coordination of proposed PV-STATCOM controls with existing Power System Stabilizers (PSSs) on synchronous generators enhances the overall system damping.

6) A novel real and reactive power modulation based control of PV-STATCOM is demonstrated that combines the functionalities of both a STATCOM and a Battery Energy Storage System (during daytime) to provide significantly enhanced levels of power oscillation damping than that achieved by either a STATCOM or a BESS.

Such novel applications of a PV solar farm as STATCOM have been illustrated for the first time in literature.

8.9 Future Work

1) The PV inverters in large solar farms are considered as aggregated inverters. Studies need to be done to consider modeling of individual inverters and plant level controls in PV solar systems.

2) Control Hardware in loop studies based on Real Time Digital Simulator (RTDS) studies need to be conducted on Two-Area and 12 bus FACTS power systems power systems to demonstrate the benefit of the proposed novel Q-POD, P-POD, and PQ-POD PV-STATCOM control technologies in hardware.

3) Small signal and detailed simulation studies required to justify the restoration control technique in nonlinear manner to provide the restoration technique interval for various power systems based on the frequencies of different oscillatory modes.

4) Coordination between multiple PV-STATCOMs and other FACTS devices in the power systems needs to be investigated..

5) The effect of higher level of PV power penetration (20% to 50%) on the power system stability needs to be conducted based on implementation of PV-STATCOM controls on solar farms.

8.10 Publications from this Thesis

A. Refereed Journal Papers:

1) Rajiv K. Varma, **Hesamaldin Maleki** “PV-STATCOM: A Novel Smart PV Inverter for Power Oscillation Damping*” IEEE Trans on. Energy conversion* (Under review)

2) Rajiv K. Varma, **Hesamaldin Maleki** “Novel Combined Real and Reactive Power Control of PV Solar Farm as STATCOM (PV-STATCOM) for Power Oscillation Damping *IEEE Trans on. Power Systems* (Under review)

3) **Hesamaldin Maleki**, Rajiv K. Varma, “Fundamental Studies on Power Oscillation Damping with Large Scale PV Plant as PV-STATCOM” *IEEE Trans.* Power delivery. (To be submited as a Working Group Paper of the IEEE PES HVDC and FACTS Subcommittee).

4) **Hesamaldin Maleki**, Rajiv K. Varma, “Novel Combined Real and Reactive Power Control of PV Solar Farm as STATCOM (PV-STATCOM) for Power Oscillation Damping in the Twelve Bus FACTS System” (Ready for submission to IEEE Trans. On Smart Grid).

B. Refereed Conference Papers:

1) Rajiv K. Varma, Ehsan Siavashi, **Hesamaldin Maleki**, Reza Salehi, Sibin Mohan, Mahendra A.C., S. Arifur Rahman and T. Vanderheide, "PV-STATCOM: A Novel Smart Inverter for Transmission and Distribution System Applications", Poster at the 7th International Conference on Integration of Renewable and Distributed Energy Resources”, Niagara Falls, Canada, Oct. 24-28, 2016

2) Hesamaldin Maleki, Rajiv K. Varma, “Optimized coordination approach for power system stabilizer and PV-STATCOM tuning in electromagnetic transient study”, *Proc. IEEE Power & Energy Society General Meeting*, Boston, July 2016.

3) **Hesamaldin Maleki,** Rajiv K.Varma**, "**Comparative study for improving damping *oscillation of SMIB system with STATCOM and BESS using remote and local signal", IEEE Canadian Conference On Electrical And Computer Engineering (CCECE),* Halifax, 2015.

4) S. A. Rahman, **Hesamaldin Maleki,** S. Mohan, R. K. Varma, and W. H. Litzenberger, *"Bibliography of FACTS 2013;2014: IEEE working group report." Proc. 2015 IEEE Power & Energy Society General Meeting*, Denver.

5) S. Mohan, **Hesamaldin Maleki**, R. K. Varma, and W. H. Litzenberger, "Bibliography of HVDC Transmission 2013– 14 IEEE working group report." *Proc. 2015 IEEE Power & Energy Society General Meeting*, Denver, pp. 1-5.

C. PATENTS REFEREED

1) Rajiv K. Varma, Vinod Khadkikar and Shah Arifur Rahman, "Utilization of Distributed Generator Inverters as STATCOM" PCT Patent application PCT/CA2010/001419 filed on 15 September, 2010.

Patent granted in US and China

2) Rajiv K. Varma, "Multivariable Modulator Controller for Power Generation Facility", PCT Application (PCT/CA2014/051174) filed on December 6, 2014

Patent granted in Canada.

Appendices

Appendix A. SMIB power system data

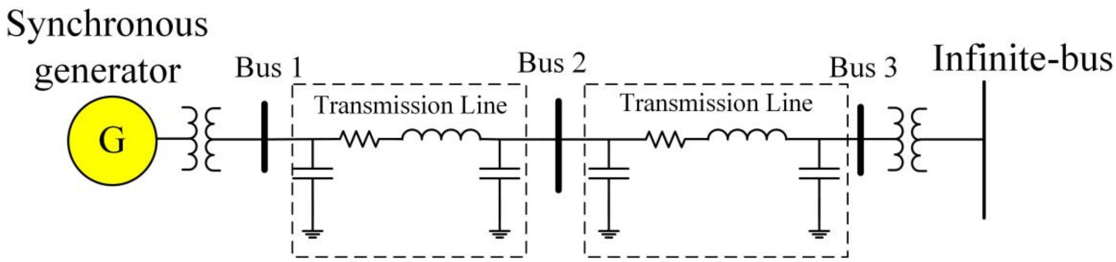

1) Generator parameters

S_n = 1110 MVA, V_n=22 kV, p.f.=0.9, R_a=0.0036 pu, X_1=0.21 pu, R_a=0, X_0=0.195 pu, T'_{d0}=6.66 sec, T'_{q0}=0.44 sec, T''_{d0}=0.032 sec, T''_{q0}=0.057 sec, X_d=1.933 pu, X_q=1.743 pu, X'_d=0.467 pu, X'_q=1.144, X'_q=1.144 pu, X''_d=0.312 pu, X''_q=0.312 pu.

2) Transformers Parameters (100 MVA and 400 kV)

R_T = 0.0 pu, X_t=0.15

3) DC-A1 Exciter parameters

T_R=0 sec, K_A= 400 pu, T_A=0.02 sec, K_E= 1.0 pu,

T_E=1.0 sec, K_F=0.06 pu, T_F=1.0 sec, S'_E=0

4) Transmission line parameters

R=0.055 ohm per phase per mile

X_L=0.52 ohm per phase per mile

B_C=5.92*10^{-6} Mho per phase per mile

5) Governor and turbine parameters

R=0.04 pu, T_f=0.05 sec, T_g=0.2 sec, r=1 pu, T_r=0.2 sec, T_w=2.0 sec

Appendix B.Two Area Power System data

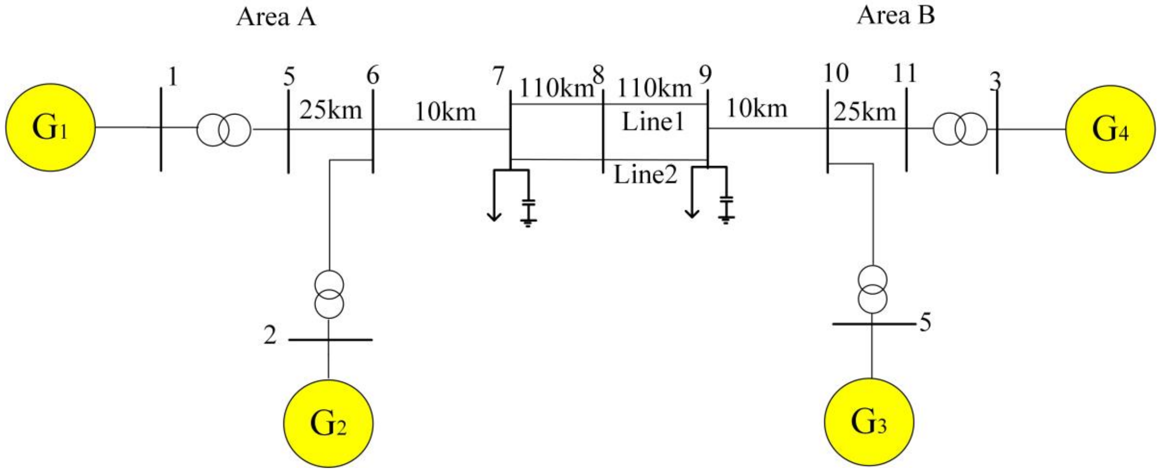

1) Generators and exciters parameters

H= 5 pu D= 1 T_{d0}'=8 s, T_{q0}'=0.4 s X_d= 1.8 pu $X'_{d'}$= 0.3 pu X_q=1.7 pu $X'_{q'}$= 0.55 pu
K_D=0 pu H=6.5 (for G1 and G2) H=6.175(for G3 and G4) K_A=20 TA =0.055 TE=0.36
K_F=0.125 T_F=1.8 A_{ex}=0.0056 B_{ex}=1.075 T_R=0.05

2) Lines

R=0.0001 pu/km x_L=0.001 pu/km b_c=0.00175pu/km

3) Loads

Bus 7:	P_L=967 MW	Q_L=100 MVar	Q_C=200 MVar
Bus 9:	P_L=1.767 MW	Q_L=100 MVar	Q_C=350 MVar

Appendix C 12 bus power system data

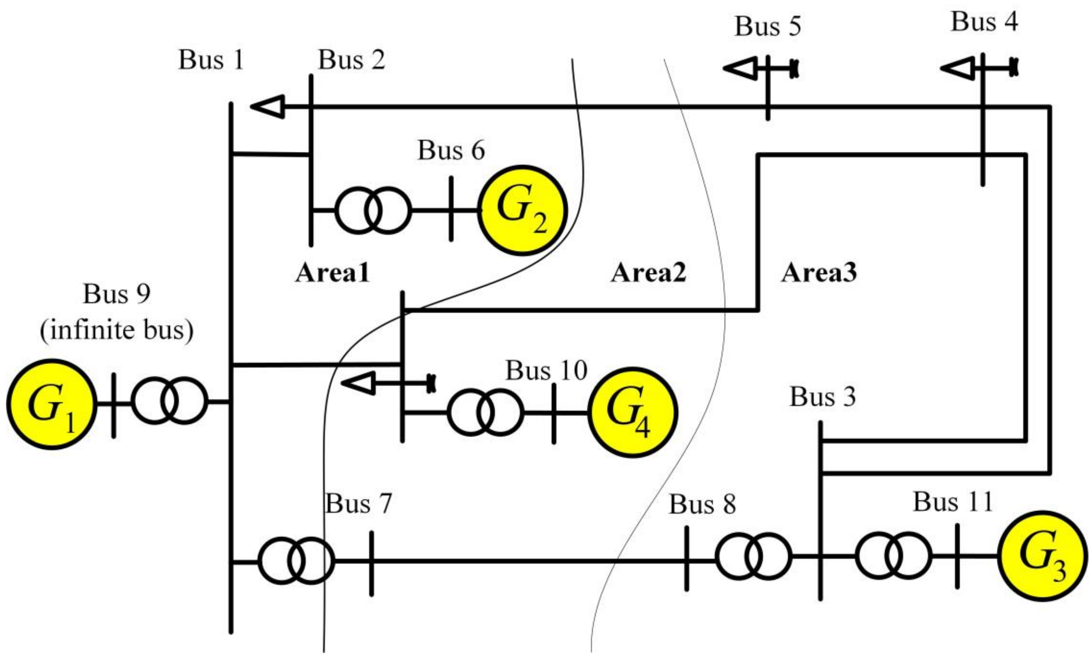

G2 *H*= *5* pu *D*= 1 T_{d0}'=5 pu X_d= 1.5 pu X'_d= 0.4 pu X_q=1.2 pu X'_q= 0.4 pu *Ta*=0.05 *K*a=20 pu

G3 *H*= *5* pu *D*= 0 T_{d0}'=6 pu X_d= 1.4 pu X'_d= 0.4 pu X_q=1.35 pu X'_q= 0.3 pu *Ta*=0.05 *K*a=20 pu

G4 *H*= *5* pu *D*= 1 T_{d0}'=5 pu X_d= 1.5 pu X'_d= 0.4 pu X_q=1.2 pu X'_q= 0.4 pu *Ta*=0.05 *K*a=20 pu

Transformer Data (S_{Base}=100 MVA)

From-to	Voltage (kV)	Leakage reactance(pu)	Rating (MVA)
1-7	230-345	0.01	1000
1-9	230-22	0.01	1000
2-10	230-22	0.01	1000
3-8	230-345	0.01	1000
3-11	230-22	0.01	1000
6-12	230-22	0.02	500

Lines

Line	**Voltage (kV)**	**Length (km)**	**R(pu)**	**X(pu)**	**B(pu)**	**Rating (MVA)**
1-2	230	100	0.0114	0.09111	0.18261	250
1-6	230	300	0.03356	0.26656	0.5547	250
2-5	230	300	0.03356	0.26656	0.5547	250
3-4(1)	230	100	0.0114	0.09111	0.18261	250
3-4(2)	230	100	0.0114	0.09111	0.18261	250
4-5	230	300	0.03356	0.26656	0.5547	250
4-6	230	300	0.03356	0.26656	0.5547	250
7-8	345	600	0.01595	0.17214	3.2853	500

Bus Data

Bus	Nominal Voltage	Specified Voltage kV	Load MVA	Shunt MVar	Generation MW
1	230				
2	230		280+j200		
3	230		320+j240		
4	230		320+j240	160	
5	230		100+j60	80	
6	230		440+j300	180	
7	345				
8	345				
9	22	1.040			
10	22	1.02			550
11	22	1.01			200
12	22	1.02			300

Appendix D FS 272 PV module electrical specification at STC* and at 45°C, 0.8 Sun

Table A. PV module electrical specification at STC* and at 45 oC, 0.8 Sun [23].

Item Description	Symbols	AT STC	At 45°C, 0.8 Sun
Nominal Power (±5%)	P_{MPP}(Watt)	72.5	54.4
Voltage at P_{MPP}	V_{mp}(Volt)	66.6	64.4
Current at P_{MPP}	V_{mp}(Amp)	1.09	0.87
Open Circuit Voltage	V_{oc}(Volt)	88.7	82.5
Short Circuit Current	I_{sc}(Amp)	1.23	1.01
Temperature Co-efficient	K_v(%/°C)	-0.25	-0.25
Series resistance	R_{sr} (Ω)	0.175	0.175
Shunt resistance	R_{sh}(Ω)	1000	1000

Appendix E Decoupled Controller Design Matlab Code

```
ti=0.002%settling time%
L=8.7093e-05%filter reactance%
R=0.002%the sum of R and ron resistances%
Ibase=150000000/208%base current calculation%
Rbase=208^2/100000000%base impidance calculation%
Lbase=Rbase/(2*pi*60)%base admitance calculation%
Rpu=R/Rbase%impidance in pu%
Lpu=L/Lbase%admitance in pu%
kp=Lpu/ti%kp%
Ki=Rpu/ti;%ki%
Ti=1/Ki%ti%
```

1) 100 MW_{pk} PV-STATCOM Connected to 400 kV Transmission line (SMIB)

C_f = 9.1183e-05 F --L_1 = 1.3064e-04 H --L_2 = 7.5118e-05 H-- R_f = 0.1203 Ω K_p=5.6918e+04 pu T_i=4.3264e-04 pu, K_{p_PLL}=900pu K_{i_PLL}=50pu K_{p_Vdc}=0.1 pu T_{i_Vdc}=10 pu

2) 150 MW_{pk} PV-STATCOM connected to 400 kV transmission line (SMIB)

C_f = 1.3677e-04 F--- L_1 = 8.7093e-05 H-- L_2 = 8.7093e-06 H--- R_f = 0.0802 Ω K_p= 3.7945e+04 pu T_i=4.3264e-04 pu, K_{p_PLL}=900pu K_{i_PLL}=50pu K_{p_Vdc}=0.1 pu T_{i_Vdc}=10 pu

3) 100 MW_{pk} PV-STATCOM connected to 230 kV transmission line (Two-Area and 12 bus power systems)

C_f = 2.7579e-04 *F* --L_1 = 7.5118e-05 *H* --L_2 = 7.5118e-06 *H*-- R_f = 0.0525 Ω K_p=3.2728e+04 pu T_i=4.3264e-04 pu, K_{p_PLL}=900pu K_{i_PLL}=50pu K_{p_Vdc}=0.1 pu T_{i_Vdc}=10 pu

Appendix F: LCL Filter Design Matlab Codes

```
%LCL Filter design%
clear all; close all;
s= sym('s');
fg=60; %system frequency%
VLL=400000;%Line Voltage%
Vph=VLL/sqrt(3);%phasevoltage
Pn=100000000; %max power%
Zb=VLL^2/Pn;%base impedance%
wn=2*pi*60;
landa=165;%landa%
Sw=5000;%switching frequency%
VDC=800;%DC voltage%
Imax=(Pn*sqrt(2))/(3*Vph);
Cb=1/(wn*Zb);
Cf=(landa*Pn/(6*pi*fg*Vph^2))/3 %for delta configuration you have to devide by 3
MRip=1; %maximum riple percentage
DeltaImax=MRip*Imax;
L1=VDC/(6*Sw*DeltaImax)
L2=0.1*L1
wres=(sqrt((L1+L2)/(L1*L2*Cf)));
fres=(sqrt((L1+L2)/(L1*L2*Cf)))/(2*pi);
Rf=1/(3*wres*Cf)
num1=[0 0 1];
den1=[L1*Cf*L2 0 (L1+L2) 0];
num2=[Cf*Rf 1];
den2=[L1*Cf*L2 Cf*(L1+L2)*Rf L1+L2 0];
sys1=tf(num1,den1);
sys2=tf(num2,den2);
bode (sys1);
hold on ;
bode (sys2);
```

Appendix G Numerical Example for Simplex Optimization Technique Imbedded in PSCAD/EMTDC.

To evaluate the performance of the *Simplex* Optimization technique in PSCAD/EMTDC software, consider a two-variable function *f* as:

$$f(x_1, x_2) = (x_1 - 1)^2 + (x_2 - 1)^2 + (\sin x_1)^2 . x_2$$

The function has a minimum of 0.38 at (0.79,0.69). $f(x_1, x_2)$ is simulated in PSCAD/EMTDC as *Slave* project. Figure bellow illustrates the simulated function in PSCAD software.

$f(x_1 + x_2)$

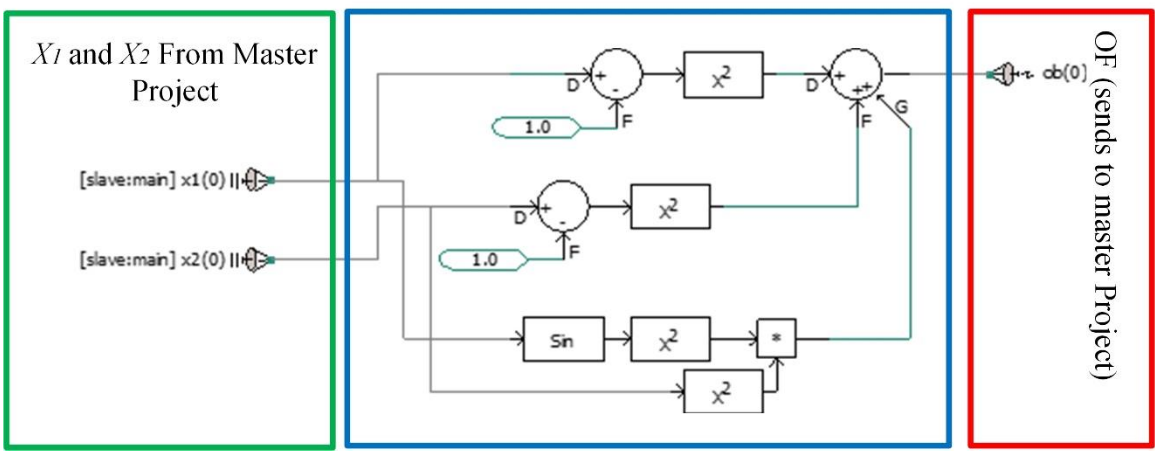

Simulation of $f(x_1, x_2)$ in PSCAD (Slave Project)

As shown in above figure, two variables x_1 and x_2 are received from the master project. After the simulation is done for $f(x_1, x_2)$, the objective function is sent to the slave project as shown below

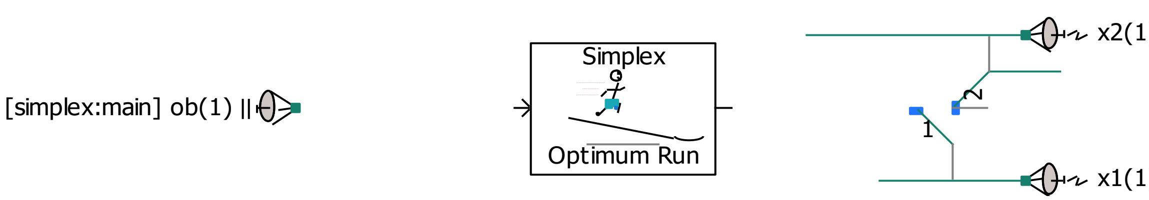

Master Project in PSCAD

It is illustrated the master project in which the Optimization block is placed. The Objective Function is received from *Slave* project and new variables x_1 and x_2 are generated and sent back to slave project.

Fiure below depicts the contour map of $f(x_1, x_2)$ in which the higher density represents the higher value of the function. It also depicts the evolution of x_1 and x_2 throughout the simulation study in PSCAD/EMTDC.

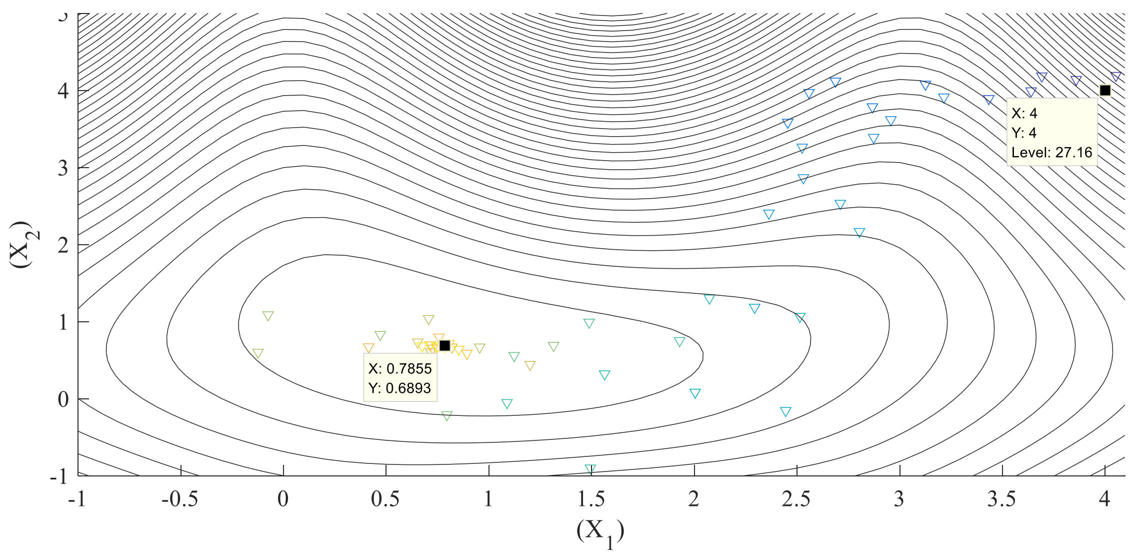

Contour map and OF for the optimization process of *F* (x_1,x_2) (MATLAB)

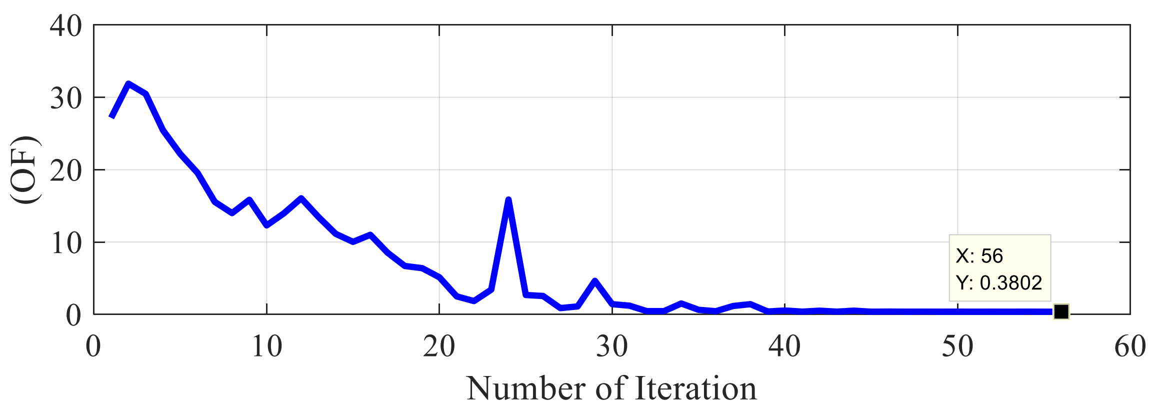

OF in PSCAD simulation to achieve the optimum values for variables

The objective function, which in this study is the value of $f(x_1, x_2)$, is shown. It is depicted that the OF has reached to 0.38 after 56 iterations. This technique is used to design optimized PV-STATCOM POD controllers.

To optimize the POD controllers, power system and PV-STATCOM are simulated in detail in the *slave* project. The simulation run time is set to cover at least 10 low-frequency oscillations (i.e. in a time period of 10-15*sec*). The OF is defined as the area bellow the oscillation. The objective function after each *Slave* project run is sent to *Master* project for the optimization process.

Appendix H BESS Fortran Code in PSCAD/EMTDC

```
$v=$n*(-1.03*EXP(-35*$SOC) + ( 0.2156*$SOC ) (0.1178*$SOC*$SOC) +
3.685+(0.3201*$SOC*$SOC*$SOC))
$rs=$n*(0.1562*EXP(-24.37*$SOC) + 0.07446)/$m
$rts=$n*(0.3208*EXP(-29.14*$SOC) + 0.04669)/$m
$rtl=$n*(6.603*EXP(-155.2*$SOC) + 0.04984)/$m
$tik=m*(-752.9*EXP(-13.15*$SOC) + 703.6)/$n
$lil=m*(-6056*EXP(-27.12*$SOC)+4475)/$n
```

where, v is the voltage output, n is the number of batteries in series, SOC represents the battery state of charge, m represents the number of batteries in parallel, rs is the series resistance, rts is the transient series resistance (short term), rtl is the transient series resistance (Long term). Is the transient capacitance (short term), and lil is the transient capacitance (Long term).

Appendix I P-POD, Q-POD, and PQ-POD Controller design for PV-STATCOM in Chapter 6

All controller parameters are presented in table below. The optimization process are given in following figures for each case study.

PCC	Controller Mode	*Gain* (pu)	T_{lead} *Gain* (sec)	T_{lag} *Gain* (sec)
10	P-POD	0.552	0.306	0.012
	Q-POD	0.509	0.1913	0.001984
8	P-POD	0.9196	0.046	0.1995
	Q-POD	0.5167	0.3121	0.0271
6	P-POD	0.5902	0.2195	0.0319
	Q-POD	0.5348	0.0002	0.2795

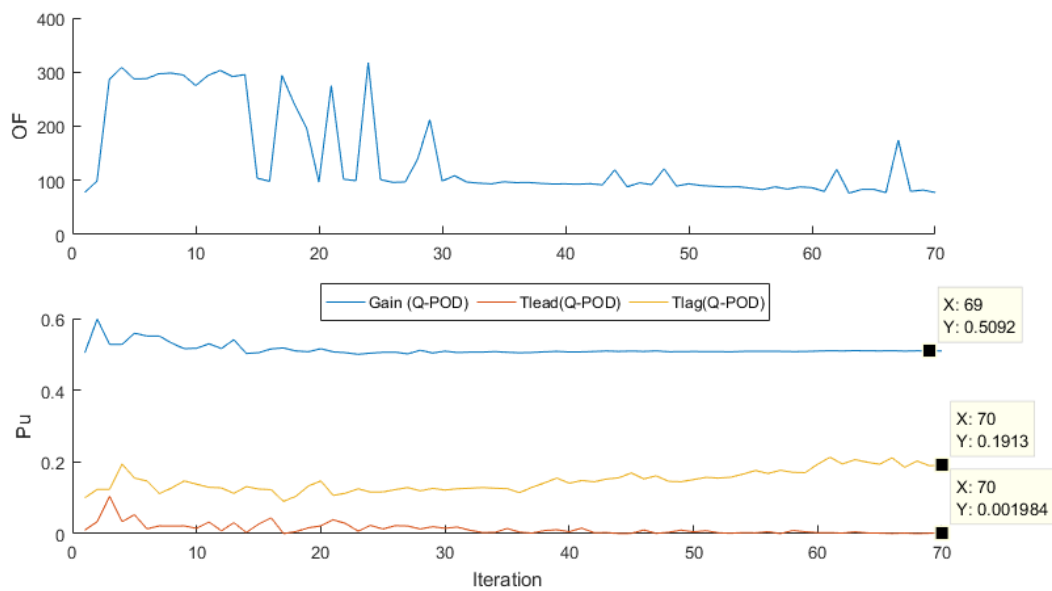

Optimization process for PV-STATCOM connected at bus 10, and Q-POD mode is activated

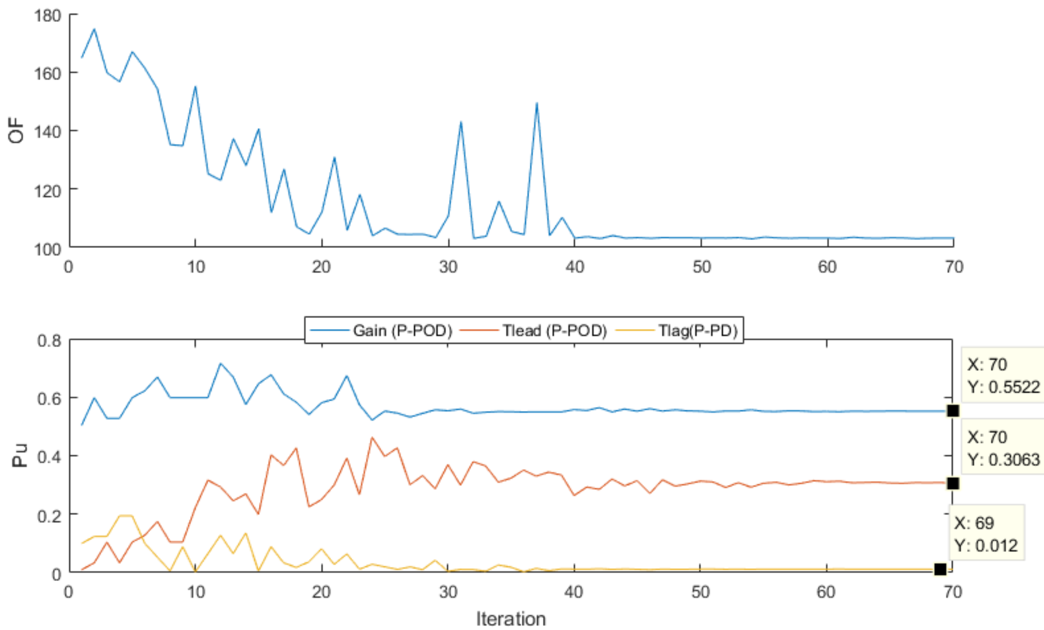

Optimization process for PV-STATCOM connected at bus 10, and P-POD mode is activated

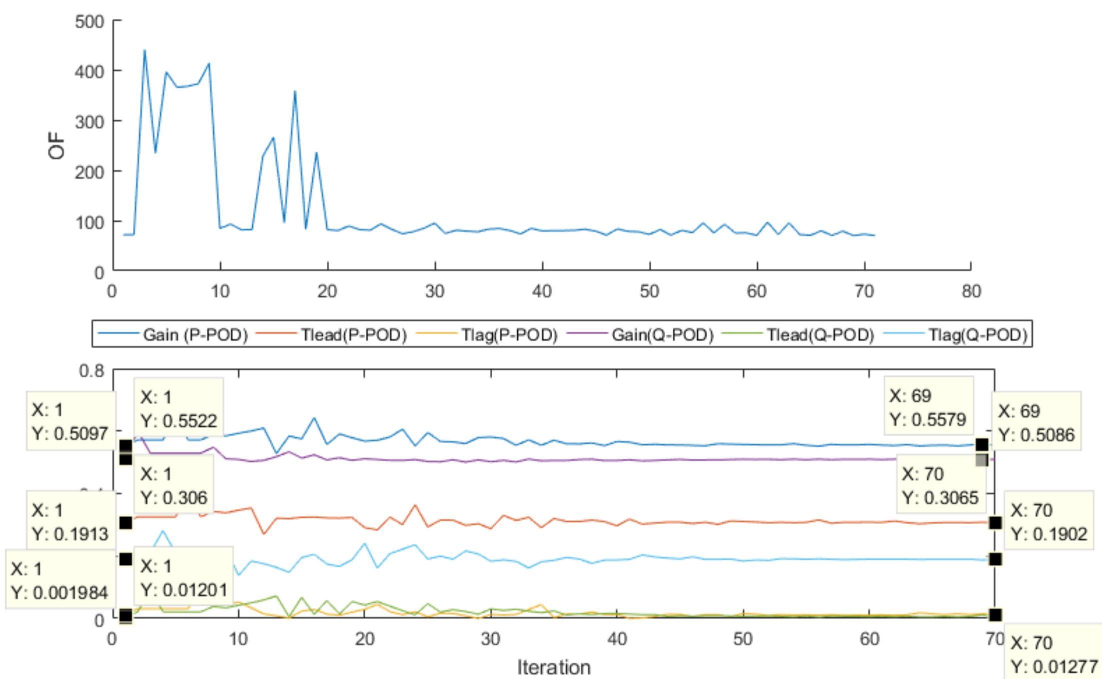

Optimization process for PV-STATCOM connected at bus 10, and PQ-POD mode is activated as shown in above figre, it is concluded that the controller parameter achieved for P-POD and Q-POD are very close to those achieved in PQ-POD optimization. Hence, controllers for PV-STATCOM interconnection at bus 8 and 6 are performed only for P-POD and Q-POD optimization process.

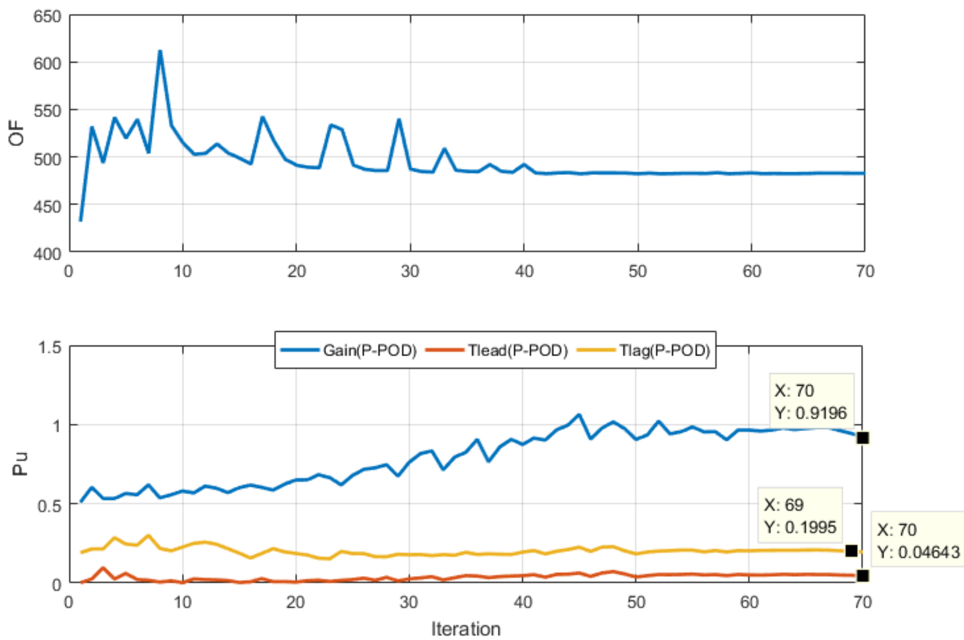

Optimization process for PV-STATCOM connected at bus 8, and P-POD mode is activated

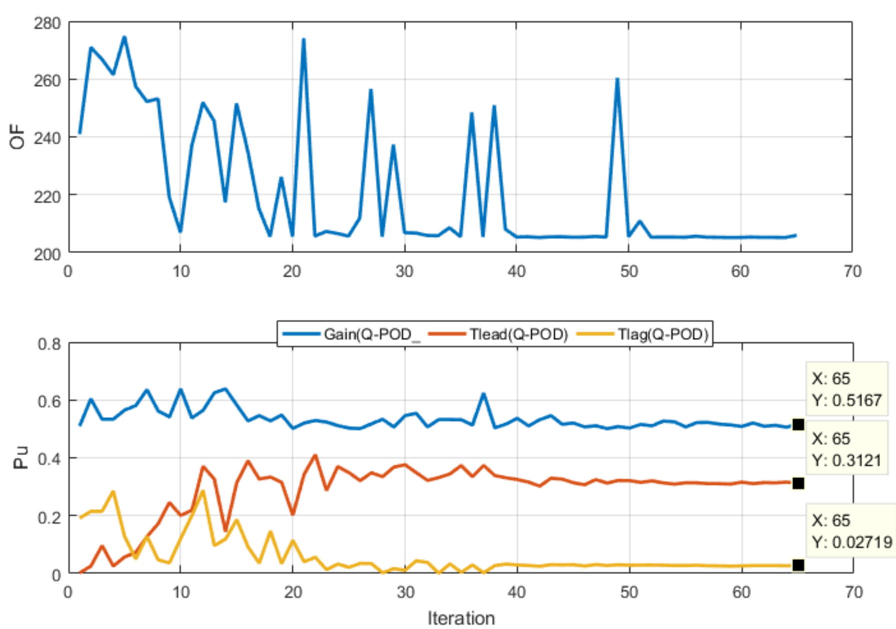

Optimization process for PV-STATCOM connected at bus 8, and Q-POD mode is activated

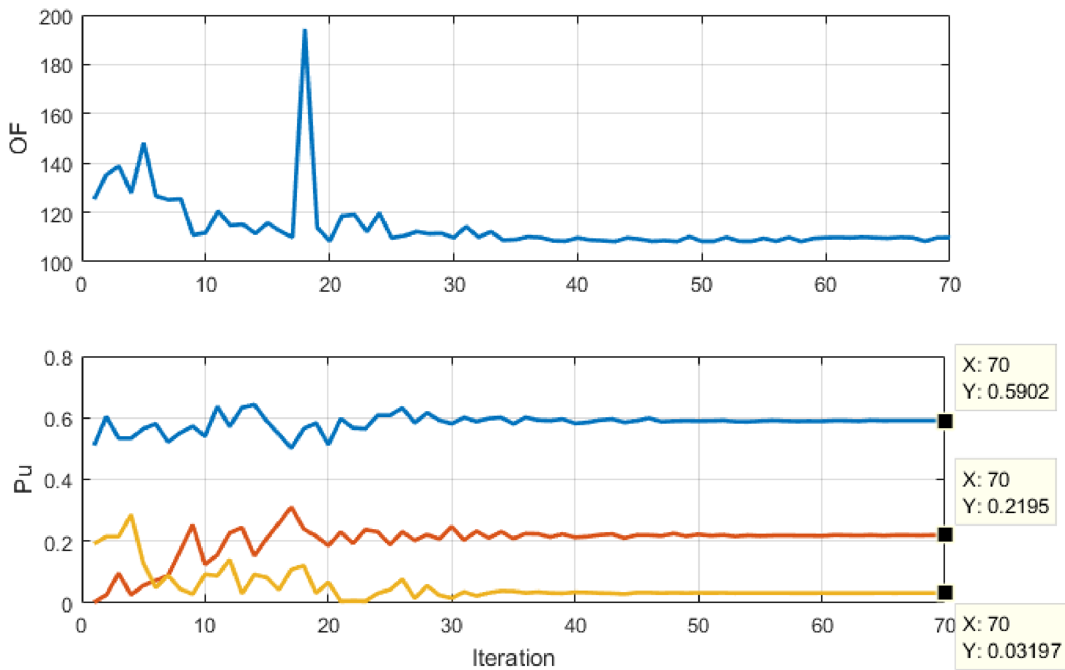

Optimization process for PV-STATCOM connected at bus 6, and P-POD mode is activated

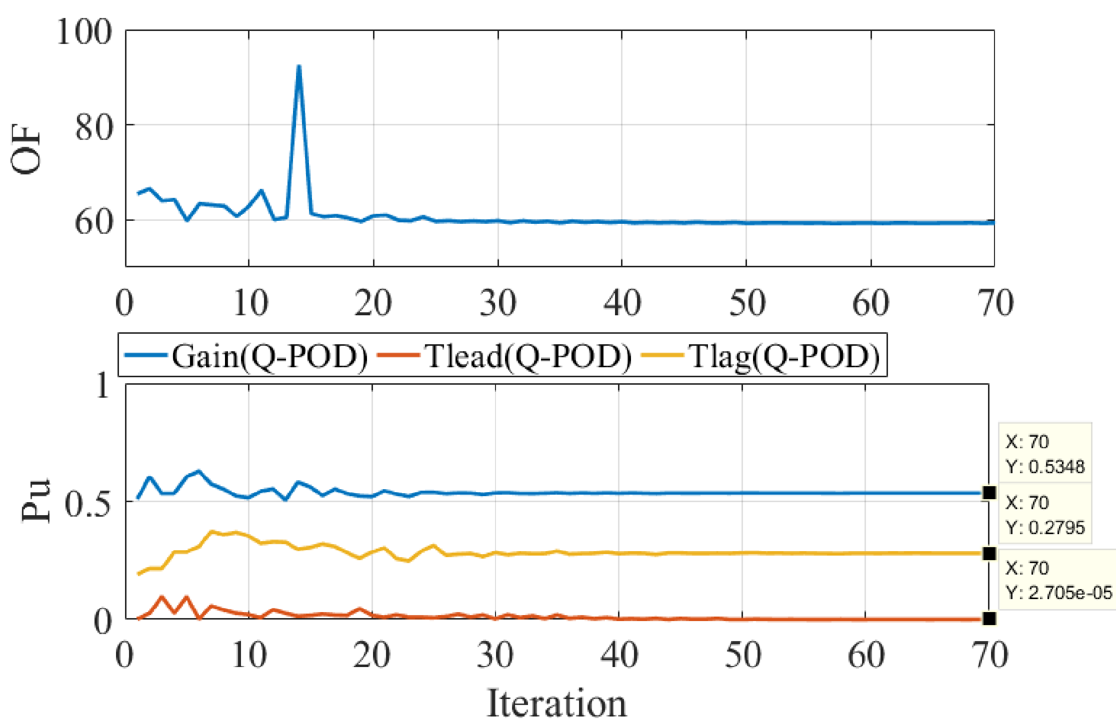

Optimization process for PV-STATCOM connected at bus 6, and Q-POD mode is activated

Appendix J Controller design for 12 bus FACTS power system

Residue Analysis for 12-Bus power systems based on different Pv-STATCOM Bus location and P-POD and Q-POD control mode. The Eigenvalue asociated with No POD controller (Eig no), Q-POD controller (Eig Q), and P-POD controller (Eig P) are illustrated in table below. The residue regarding Q-POD and P-POD control feedback closer are (RQ) and (RP) respectively.

Mode	Eig no	Eig Q	RQ	Eig P	RP
Bus 2					
1	8961 - 7.6927i	-0.8849 - 7.6879i	0.0122	9001 - 7.7089i	0.0166
2	5867 - 6.3514i	-0.5737 - 6.3652i	0.0189	5046 - 6.3140i	0.0414
3	2895 - 4.8177i	-0.3114 - 4.8058i	0.0249	2618 - 4.8481i	0.0411
Bus 10					
1	8560 - 7.6488i	-0.8506 - 7.6261i	0.0234	420 - 7.6126i	0.0389
2	5885 - 6.3345i	-0.5863 - 6.3309i	0.0042	5867 - 6.3293i	0.0056
3	2377 - 4.7020i	-0.4567 - 4.5941i	0.2441	4257 - 4.4920i	0.2818
Bus 5					
1	8281 - 7.6263i	-0.8706 - 7.6210i	0.0537	8382 - 7.6955i	0.072
2	5864 - 6.3341i	-0.5862 - 6.3322i	0.0054	5861 - 6.3272i	0.0062
3	2678 - 4.7673i	-0.4129 - 4.6725i	0.1808	3500 - 4.6555i	0.1373
Bus 4					
1	8281 - 7.6263i	-0.8806 - 7.6110i	0.0547	8382 - 7.6955i	0.07
2	5864 - 6.3341i	-0.5812 - 6.3322i	0.0054	5861 - 6.3272i	0.0069
3	2678 - 4.7673i	-0.4229 - 4.6725i	0.1818	3500 - 4.6555i	0.1387
Bus 3					
1	8287 - 7.6156i	-0.8586 - 7.6102i	0.0304	8360 - 7.7146i	0.0993
2	5874 - 6.3313i	-0.5843 - 6.3314i	0.0031	5869 - 6.3297i	0.0016
3	2720 - 4.7728i	-0.3546 - 4.7273i	0.0943	3506 - 4.6758i	0.1248
Bus 8					
1	8293 - 7.6156i	-0.8581 - 7.6100i	0.0294	8364 - 7.7142i	0.0988
2	5879 - 6.3364i	-0.5844 - 6.3314i	0.0061	5873 - 6.3349i	0.0016
3	2721 - 4.7728i	-0.3533 - 4.7284i	0.0926	3505 - 4.6763i	0.1243
Bus 7					
1	8980 - 7.6931i	-0.8969 - 7.6932i	0.0011	8978 - 7.6933i	0.0003
2	5932 - 6.3380i	-0.5935 - 6.3430i	0.0051	5929 - 6.3383i	0.0004
3	2917 - 4.8248i	-0.2888 - 4.8262i	0.0031	2933 - 4.8226i	0.0027

P-POD (green) Q-POD (red)

Compensator Controller design for G_3 Controller design

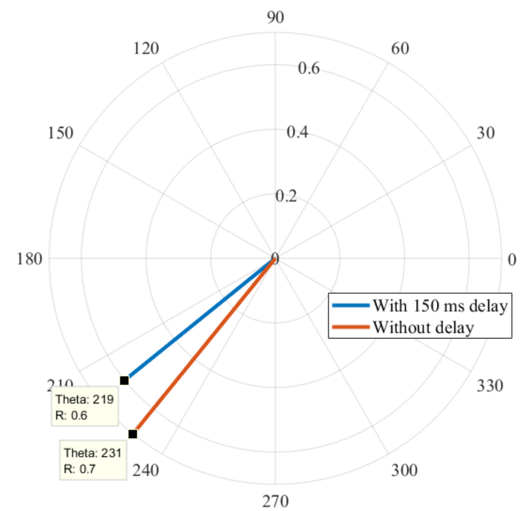

Residue analysis for ω_3

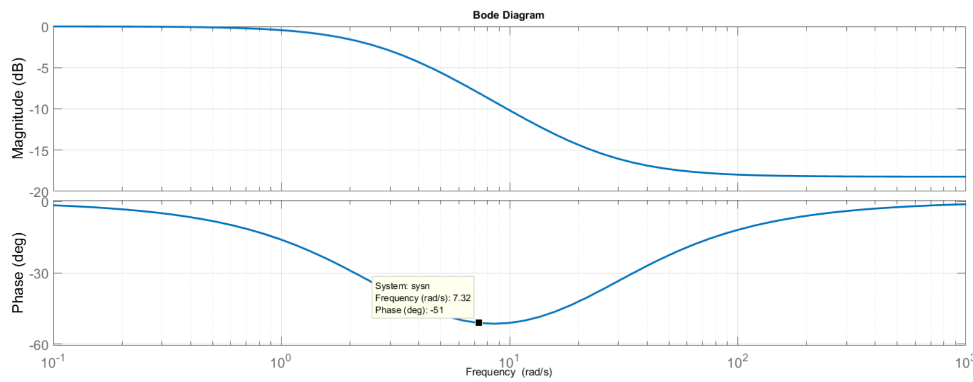

Bode plot for G3 compensator (No delay)

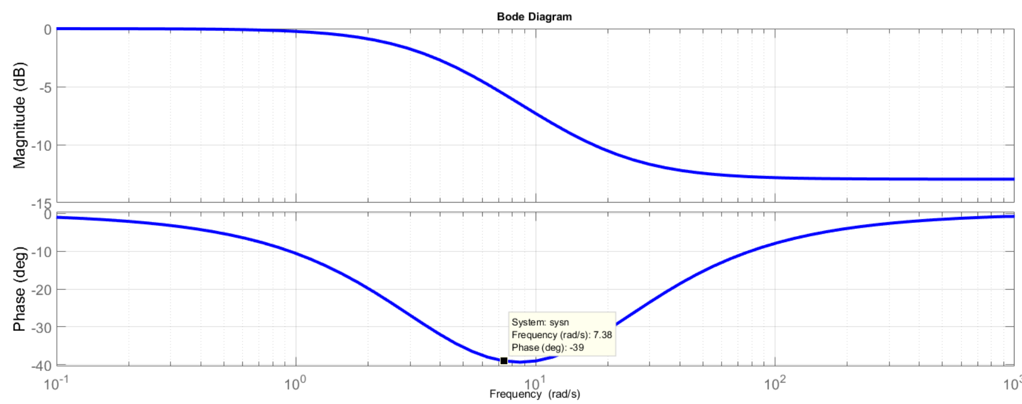

Bode plot for G3 compensator (150 ms delay)

PV-STATCOM controller parameters for Q-POD and P-POD in 12 bus FACTS power system

			$Gain$(pu)	$T_{lead}(s)$	$T_{lag}(s)$
Q-POD	ω_3	**No Delay**	1.8	0.041	0.55
		150 *ms* Delay	1.8	0.0334	0.245
	ω_4	**No Delay**	1.3	0	0
		150 *ms* Delay	1.3	0	0
P-POD	ω_4	**150 *ms* Delay**	0.7	0	0

References

[1] O. Ellabban, H. Abu-Rub, and F. Blaabjerg, "Renewable energy resources: Current status, future prospects and their enabling technology," *Renewable and Sustainable Energy Reviews,* vol. 39, pp. 748-764, 2014.

[2] G. W. E. Council, "Global Wind Report 2014: Annual Market Update," ed, 2014.

[3] D. Feldman, "Photovoltaic (PV) pricing trends: historical, recent, and near-term projections," 2014.

[4] D. Turney and V. Fthenakis, "Environmental impacts from the installation and operation of large-scale solar power plants," *Renewable and Sustainable Energy Reviews,* vol. 15, pp. 3261-3270, 2011.

[5] O. s. L.-T. E. Plan, "Achieving Balance Ontario's Long-Term Energy Plan," 2013.

[6] R. Adib, H. Murdock, F. Appavou, A. Brown, B. Epp, A. Leidreiter*, et al.*, "Renewables 2016 Global Status Report," *Global Status Report RENEWABLE ENERGY POLICY NETWORK FOR THE 21st CENTURY (REN21),* 2016.

[7] E. Romero-Cadaval, B. Francois, M. Malinowski, and Q. C. Zhong, "Grid-Connected Photovoltaic Plants: An Alternative Energy Source, Replacing Conventional Sources," *IEEE Industrial Electronics Magazine,* vol. 9, pp. 18-32, 2015.

[8] *The World's Largest Solar Plant Is Now Online in India*. Available: http://www.popularmechanics.com/science/green-tech/a24063/worlds-largest-solar-plant-india/

[9] *New French solar farm, Europe's biggest, cheaper than new nuclear*. Available: https://www.reuters.com/article/us-climatechange-summit-france-solar-idUSKBN0TK5GW20151201

[10] C. Tiba and E. d. A. Ricardo, "Siting PV plant focusing on the effect of local climate variables on electric energy production–Case study for Araripina and Recife," *Renewable Energy,* vol. 48, pp. 309-317, 2012.

[11] *Fact Sheet California Valley Solar Ranch*. Available: https://us.sunpower.com/sites/sunpower/files/media-library/fact-sheets/fs-california-valley-solar-ranch-factsheet.pdf

[12] A. Sharma, "A comprehensive study of solar power in India and World," *Renewable and Sustainable Energy Reviews,* vol. 15, pp. 1767-1776, 2011.

[13] *Neuhardenberg Solar Power Plant, Germany*. Available: http://www.power-technology.com/projects/neuhardenberg-solar-power-plant/

[14] P. Kundur, N. J. Balu, and M. G. Lauby, *Power system stability and control* vol. 7: McGraw-hill New York, 1994.

[15] P. Kundur, J. Paserba, V. Ajjarapu, G. Andersson, A. Bose, C. Canizares, *et al.*, "Definition and classification of power system stability IEEE/CIGRE joint task force on stability terms and definitions," *IEEE Transactions on Power Systems,* vol. 19, pp. 1387-1401, 2004.

[16] R. Preece, "A probabilistic approach to improving the stability of meshed power networks with embedded HVDC lines," 2013.

[17] N. S. Group, "Technical analysis of the August 14, 2003, blackout: What happened, why, and what did we learn," *report to the NERC Board of Trustees,* 2004.

[18] C. A. Canizares, C. Cavallo, M. Pozzi, and S. Corsi, "Comparing secondary voltage regulation and shunt compensation for improving voltage stability and transfer capability in the Italian power system," *Electric Power Systems Research,* vol. 73, pp. 67-76, 2005.

[19] D. N. Kosterev, C. W. Taylor, and W. A. Mittelstadt, "Model validation for the August 10, 1996 WSCC system outage," *IEEE Transactions on Power Systems,* vol. 14, pp. 967-979, 1999.

[20] O. B. Tor, C. Gencoglu, O. Yilmaz, E. Cebeci, and A. N. Guven, "Damping measures against prospective oscillations between Turkish grid and ENTSO-E System," in *2010 International Conference on Power System Technology*, 2010, pp. 1-7.

[21] H. Breulmann, E. Grebe, and M. Lösing, "Analysis and damping of inter-area oscillations in the UCTE/CENTREL power system," 2000.

[22] R. M. Mathur and R. K. Varma, *Thyristor-based FACTS controllers for electrical transmission systems*: John Wiley & Sons, 2002.

[23] S. A. Rahman, "Novel Controls of Photovoltaic (PV) Solar Farms," 2012.

[24] K. S. Tey and S. Mekhilef, "Modified incremental conductance MPPT algorithm to mitigate inaccurate responses under fast-changing solar irradiation level," *Solar Energy,* vol. 101, pp. 333-342, 2014.

[25] R. Shah, N. Mithulananthan, R. Bansal, and V. Ramachandaramurthy, "A review of key power system stability challenges for large-scale PV integration," *Renewable and Sustainable Energy Reviews,* vol. 41, pp. 1423-1436, 2015.

[26] B. Tamimi, C. Cañizares, and K. Bhattacharya, "System stability impact of large-scale and distributed solar photovoltaic generation: the case of Ontario, Canada," *IEEE transactions on sustainable energy,* vol. 4, pp. 680-688, 2013.

[27] S. Eftekharnejad, V. Vittal, G. T. Heydt, B. Keel, and J. Loehr, "Impact of increased penetration of photovoltaic generation on power systems," *IEEE Transactions on Power Systems,* vol. 28, pp. 893-901, 2013.

[28] S. Eftekharnejad, V. Vittal, G. T. Heydt, B. Keel, and J. Loehr, "Small Signal Stability Assessment of Power Systems With Increased Penetration of Photovoltaic Generation: A Case Study," *IEEE Transactions on Sustainable Energy,* vol. 4, pp. 960-967, 2013.

[29] H. Verdejo, L. Vargas, and W. Kliemann, "Fine Tuning of PSS Control Parameters under Sustained Random Perturbations," *IEEE Latin America Transactions,* vol. 9, pp. 1051-1059, 2011.

[30] G. Beck, D. Povh, D. Retzmann, and E. Teltsch, "Global blackouts–Lessons learned," in *Power-Gen Europe*, 2005, p. 30.

[31] *Boosting transmission capacity*. Available: https://library.e.abb.com/public/fdf0b019e1fe08a48325771f002dbfc5/A02-0158.pdf

[32] N. Mithulananthan, C. A. Canizares, J. Reeve, and G. J. Rogers, "Comparison of PSS, SVC, and STATCOM controllers for damping power system oscillations," *IEEE Transactions on Power Systems,* vol. 18, pp. 786-792, 2003.

[33] L. Wang, C. H. Chang, B. L. Kuan, and A. V. Prokhorov, "Stability Improvement of a Two-Area Power System Connected With an Integrated Onshore and Offshore Wind Farm Using a STATCOM," *IEEE Transactions on Industry Applications,* vol. 53, pp. 867-877, 2017.

[34] M. Furini, A. Pereira, and P. Araujo, "Pole placement by coordinated tuning of Power System Stabilizers and FACTS-POD stabilizers," *International Journal of Electrical Power & Energy Systems,* vol. 33, pp. 615-622, 2011.

[35] W. Qiao, R. G. Harley, and G. K. Venayagamoorthy, "Coordinated Reactive Power Control of a Large Wind Farm and a STATCOM Using Heuristic Dynamic Programming," *IEEE Transactions on Energy Conversion,* vol. 24, pp. 493-503, 2009.

[36] F. S. A.-. Ismail, M. A. Hassan, and M. A. Abido, "RTDS Implementation of STATCOM-Based Power System Stabilizers," *Canadian Journal of Electrical and Computer Engineering,* vol. 37, pp. 48-56, 2014.

[37] J. Kueck, B. Kirby, T. Rizy, F. Li, and N. Fall, "Reactive power from distributed energy," *The Electricity Journal,* vol. 19, pp. 27-38, 2006.

[38] A. M. Trzynadlowski, "An overview of modern PWM techniques for three-phase, voltage-controlled, voltage-source inverters," in *Industrial Electronics, 1996. ISIE '96., Proceedings of the IEEE International Symposium on*, 1996, pp. 25-39 vol.1.

[39] Y. Zhenyu, A. Mohammed, and I. Panahi, "A review of three PWM techniques," in *American Control Conference, 1997. Proceedings of the 1997*, 1997, pp. 257-261 vol.1.

[40] M. S. A. Dahidah and V. G. Agelidis, "Selective Harmonic Elimination PWM Control for Cascaded Multilevel Voltage Source Converters: A Generalized Formula," *Power Electronics, IEEE Transactions on,* vol. 23, pp. 1620-1630, 2008.

[41] N. N. V. S. Babu and B. G. Fernandes, "Cascaded Two-Level Inverter-Based Multilevel STATCOM for High-Power Applications," *Power Delivery, IEEE Transactions on,* vol. 29, pp. 993-1001, 2014.

[42] B. Gultekin and M. Ermis, "Cascaded Multilevel Converter-Based Transmission STATCOM: System Design Methodology and Development of a 12 kV ±12 MVAr Power Stage," *Power Electronics, IEEE Transactions on,* vol. 28, pp. 4930-4950, 2013.

[43] D. Soto and T. C. Green, "A comparison of high-power converter topologies for the implementation of FACTS controllers," *Industrial Electronics, IEEE Transactions on,* vol. 49, pp. 1072-1080, 2002.

[44] M. Klein, G. J. Rogers, and P. Kundur, "A fundamental study of inter-area oscillations in power systems," *IEEE Transactions on Power Systems,* vol. 6, pp. 914-921, 1991.

[45] ABB. *SVC Light® for grid code compliance of 220 kV steel plant connection*. Available: http://new.abb.com/facts/references/reference_zhangijagang

[46] ABB, "SVC Light for railway load balancing."

[47] M. S. El-Moursi, B. Bak-Jensen, and M. H. Abdel-Rahman, "Novel STATCOM Controller for Mitigating SSR and Damping Power System Oscillations in a Series Compensated Wind Park," *Power Electronics, IEEE Transactions on,* vol. 25, pp. 429-441, 2010.

[48] N. Thanh Hai and L. Dong-Choon, "Advanced Fault Ride-Through Technique for PMSG Wind Turbine Systems Using Line-Side Converter as STATCOM," *Industrial Electronics, IEEE Transactions on,* vol. 60, pp. 2842-2850, 2013.

[49] T. T. Nguyen and R. Gianto, "Optimisation-based control coordination of PSSs and FACTS devices for optimal oscillations damping in multi-machine power system," *IET Generation, Transmission & Distribution,* vol. 1, pp. 564-573, 2007.

[50] L.-J. Cai and I. Erlich, "Simultaneous coordinated tuning of PSS and FACTS damping controllers in large power systems," *IEEE Transactions on Power Systems*, vol. 20, pp. 294-300, 2005.

[51] N. Mithulananthan, C. A. Canizares, and J. Reeve, "Tuning, performance and interactions of PSS and FACTS controllers," in *Power Engineering Society Summer Meeting, 2002 IEEE*, 2002, pp. 981-987 vol.2.

[52] L. Xianzhang, E. N. Lerch, and D. Povh, "Optimization and coordination of damping controls for improving system dynamic performance," *Power Systems, IEEE Transactions on,* vol. 16, pp. 473-480, 2001.

[53] T. T. Nguyen and R. Gianto, "Optimisation-based control coordination of PSSs and FACTS devices for optimal oscillations damping in multi-machine power system," *Generation, Transmission & Distribution, IET,* vol. 1, pp. 564-573, 2007.

[54] R. A. Jabr, B. C. Pal, N. Martins, and J. C. R. Ferraz, "Robust and coordinated tuning of power system stabiliser gains using sequential linear programming," *Generation, Transmission & Distribution, IET,* vol. 4, pp. 893-904, 2010.

[55] H. Okamoto, A. Kurita, and Y. Sekine, "A method for identification of effective locations of variable impedance apparatus on enhancement of steady-state stability in large scale power systems," *IEEE Transactions on Power Systems,* vol. 10, pp. 1401-1407, 1995.

[56] E. Ghahremani and I. Kamwa, "Optimal placement of multiple-type FACTS devices to maximize power system loadability using a generic graphical user interface," *IEEE Transactions on Power Systems,* vol. 28, pp. 764-778, 2013.

[57] B. K. Kumar, S. N. Singh, and S. C. Srivastava, "Placement of FACTS controllers using modal controllability indices to damp out power system oscillations," *IET Generation, Transmission & Distribution,* vol. 1, pp. 209-217, 2007.

[58] B. C. Pal, A. H. Coonick, I. M. Jaimoukha, and H. El-Zobaidi, "A linear matrix inequality approach to robust damping control design in power systems with superconducting magnetic energy storage device," *IEEE Transactions on Power Systems*, vol. 15, pp. 356-362, 2000.

[59] N. Martins and L. T. G. Lima, "Determination of suitable locations for power system stabilizers and static VAR compensators for damping electromechanical oscillations in large scale power systems," *IEEE Transactions on Power Systems,* vol. 5, pp. 1455-1469, 1990.

[60] *Energy Storage Case Studies*. Available: http://energystorage.org/energy-storage/case-studies

[61] M. Beza and M. Bongiorno, "An Adaptive Power Oscillation Damping Controller by STATCOM With Energy Storage," *IEEE Transactions on Power Systems,* vol. 30, pp. 484-493, 2015.

[62] Y. Tang, C. Mu, and H. He, "SMES-Based Damping Controller Design Using Fuzzy-GrHDP Considering Transmission Delay," *IEEE Transactions on Applied Superconductivity,* vol. 26, pp. 1-6, 2016.

[63] J. Fang, W. Yao, Z. Chen, J. Wen, and S. Cheng, "Design of Anti-Windup Compensator for Energy Storage-Based Damping Controller to Enhance Power System Stability," *IEEE Transactions on Power Systems,* vol. 29, pp. 1175-1185, 2014.

[64] W. Du, H. Wang, and R. Dunn, "Power system small-signal oscillation stability as affected by large-scale PV penetration," in *Sustainable Power Generation and Supply, 2009. SUPERGEN'09. International Conference on*, 2009, pp. 1-6.

[65] R. Shah, N. Mithulananthan, and K. Y. Lee, "Large-scale PV plant with a robust controller considering power oscillation damping," *Energy Conversion, IEEE Transactions on,* vol. 28, pp. 106-116, 2013.

[66] R. K. Varma, S. A. Rahman, and T. Vanderheide, "New Control of PV Solar Farm as STATCOM (PV-STATCOM) for Increasing Grid Power Transmission Limits During Night and Day," *Power Delivery, IEEE Transactions on,* vol. 30, pp. 755-763, 2015.

[67] P. Chiradeja and R. Ramakumar, "An approach to quantify the technical benefits of distributed generation," *Energy Conversion, IEEE Transactions on,* vol. 19, pp. 764-773, 2004.

[68] Z. Ziadi, M. Oshiro, T. Senjyu, A. Yona, N. Urasaki, T. Funabashi, *et al.*, "Optimal Voltage Control Using Inverters Interfaced With PV Systems Considering Forecast Error in a Distribution System," *Sustainable Energy, IEEE Transactions on,* vol. 5, pp. 682-690, 2014.

[69] L. Yu-Kang, L. Ting-Peng, and W. Kuan-Hung, "Grid-Connected Photovoltaic System With Power Factor Correction," *Industrial Electronics, IEEE Transactions on,* vol. 55, pp. 2224-2227, 2008.

[70] L. Hassaine, E. Olias, J. Quintero, and M. Haddadi, "Digital power factor control and reactive power regulation for grid-connected photovoltaic inverter," *Renewable Energy,* vol. 34, pp. 315-321, 2009.

[71] T. S. Basso and R. DeBlasio, "IEEE 1547 series of standards: interconnection issues," *Power Electronics, IEEE Transactions on,* vol. 19, pp. 1159-1162, 2004.

[72] V. V. d. E. E. Informationstechnik, "eV: VDE-AR-N 4105: 2011-08: Power generation systems connected to the low-voltage distribution network Technical

minimum requirements for the connection to and parallel operation with low-voltage distribution networks," *English translation of the VDE application rule VDEAR-N-4105*.

[73] BDEW German Association of Energy and Water Industries. (2008, March). *BDEW Generating Plants Connected to the Medium-Voltage Network*. Available: https://www.bdew.de/internet.nsf/id/A2A0475F2FAE8F44C12578300047C92F/$file/BDEW_RL_EA-am-MS-Netz_engl.pdf

[74] D. S.-M. Luke Schwartfeger, "Review of Distributed Generation Interconnection Standards," presented at the EEA Conference & Exhibition 2014,, Auckland 2014.

[75] R. K. Varma, V. Khadkikar, and R. Seethapathy, "Nighttime Application of PV Solar Farm as STATCOM to Regulate Grid Voltage," *IEEE Transactions on Energy Conversion,* vol. 24, pp. 983-985, 2009.

[76] R. K. Varma, S. A. Rahman, and T. Vanderheide, "New Control of PV Solar Farm as STATCOM (PV-STATCOM) for Increasing Grid Power Transmission Limits During Night and Day," *IEEE Transactions on Power Delivery,* vol. 30, pp. 755-763, 2015.

[77] R. Shah, N. Mithulananthan, and K. Y. Lee, "Large-scale PV plant with a robust controller considering power oscillation damping," *IEEE Transactions on Energy Conversion,* vol. 28, pp. 106-116, 2013.

[78] R. G. Wandhare and V. Agarwal, "Novel Stability Enhancing Control Strategy for Centralized PV-Grid Systems for Smart Grid Applications," *IEEE Transactions on Smart Grid,* vol. 5, pp. 1389-1396, 2014.

[79] M. Zhu and F. Zhuo, "A novel method for low-frequency oscillation suppression based on PV system," in *2014 International Power Electronics and Application Conference and Exposition*, 2014, pp. 251-254.

[80] R. K. Varma, "Multivariable modulator controller for power generation facility," ed: Google Patents, 2014.

[81] K. Padiyar and R. Varma, "Damping torque analysis of static var system controllers," *IEEE Transactions on Power Systems,* vol. 6, pp. 458-465, 1991.

[82] X. Y. Bian, Y. Geng, K. L. Lo, Y. Fu, and Q. B. Zhou, "Coordination of PSSs and SVC Damping Controller to Improve Probabilistic Small-Signal Stability of Power System With Wind Farm Integration," *IEEE Transactions on Power Systems*, vol. 31, pp. 2371-2382, 2016.

[83] S. Jiang, U. Annakkage, and A. Gole, "A platform for validation of FACTS models," *IEEE Transactions on Power Delivery,* vol. 21, pp. 484-491, 2006.

[84] G. K. Venayagamoorthy and S. R. Jetti, "Dual-function neuron-based external controller for a static var compensator," *IEEE Transactions on Power Delivery,* vol. 23, pp. 997-1006, 2008.

[85] A. Adamczyk, M. Altin, O. Gosku, R. Teodorescu, and F. Iov, "Generic 12-bus test system for wind power integration studies-epe joint wind energy and t&d chapters seminar; aalborg denmark," 2012.

[86] *PSCAD Software*. Available: https://hvdc.ca/pscad/

[87] *Power Transmission System Planning Software*. Available: http://w3.siemens.com/smartgrid/global/en/products-systems-solutions/software-solutions/planning-data-management-software/planning-simulation/pages/pss-e.aspx

[88] I. C. Report, "Excitation System Models for Power System Stability Studies," *IEEE Transactions on Power Apparatus and Systems,* vol. PAS-100, pp. 494-509, 1981.

[89] "IEEE Recommended Practice for Excitation System Models for Power System Stability Studies," *IEEE Std 421.5-2005 (Revision of IEEE Std 421.5-1992),* pp. 1-93, 2006.

[90] D. Lee, "Ieee recommended practice for excitation system models for power system stability studies (ieee std 421.5-1992)," *Energy Development and Power Generating Committee of the Power Engineering Society,* vol. 95, p. 96, 1992.

[91] J. A. Short, D. G. Infield, and L. L. Freris, "Stabilization of Grid Frequency Through Dynamic Demand Control," *IEEE Transactions on Power Systems,* vol. 22, pp. 1284-1293, 2007.

[92] A. Adamczyk, M. Altin, G. Ö, R. Teodorescu, and F. Iov, "Generic 12-bus test system for wind power integration studies," in *2013 15th European Conference on Power Electronics and Applications (EPE)*, 2013, pp. 1-6.

[93] "Load representation for dynamic performance analysis [of power systems]," *IEEE Transactions on Power Systems,* vol. 8, pp. 472-482, 1993.

[94] S. A. Rahman, R. K. Varma, and T. Vanderheide, "Generalised model of a photovoltaic panel," *IET Renewable Power Generation,* vol. 8, pp. 217-229, 2014.

[95] K. Ding, X. Bian, H. Liu, and T. Peng, "A MATLAB-Simulink-Based PV Module Model and Its Application Under Conditions of Nonuniform Irradiance," *IEEE Transactions on Energy Conversion,* vol. 27, pp. 864-872, 2012.

[96] A. Chatterjee, A. Keyhani, and D. Kapoor, "Identification of Photovoltaic Source Models," *IEEE Transactions on Energy Conversion,* vol. 26, pp. 883-889, 2011.

[97] A. Yazdani and R. Iravani, *Voltage-sourced converters in power systems: modeling, control, and applications*: John Wiley & Sons, 2010.

[98] S. Jayalath and M. Hanif, "Generalized LCL-Filter Design Algorithm for Grid-Connected Voltage-Source Inverter," *IEEE Transactions on Industrial Electronics,* vol. 64, pp. 1905-1915, 2017.

[99] R. E. Best, *Phase locked loops: design, simulation, and applications*: McGraw-Hill Professional, 2007.

[100] M. H. Rashid, *Power electronics handbook: devices, circuits and applications*: Academic press, 2010.

[101] A. Reznik, M. G. Simões, A. Al-Durra, and S. M. Muyeen, "LCL filter design and performance analysis for small wind turbine systems," in *2012 IEEE Power Electronics and Machines in Wind Applications*, 2012, pp. 1-7.

[102] S. A. Rahman, "Novel Controls of Photovoltaic (PV) Solar Farms," The University of Western Ontario, 2012.

[103] K. Hussein, I. Muta, T. Hoshino, and M. Osakada, "Maximum photovoltaic power tracking: an algorithm for rapidly changing atmospheric conditions," *IEE Proceedings-Generation, Transmission and Distribution,* vol. 142, pp. 59-64, 1995.

[104] M. Gibbard, P. Pourbeik, and D. Vowles, *Small-signal stability, control and dynamic performance of power systems*: University of Adelaide Press, 2015.

[105] J. A. Nelder and R. Mead, "A simplex method for function minimization," *The computer journal,* vol. 7, pp. 308-313, 1965.

[106] A. M. Gole, S. Filizadeh, R. W. Menzies, and P. L. Wilson, "Optimization-enabled electromagnetic transient simulation," *Power Delivery, IEEE Transactions on,* vol. 20, pp. 512-518, 2005.

[107] N. Martins and L. T. Lima, "Determination of suitable locations for power system stabilizers and static var compensators for damping electromechanical oscillations in large scale power systems," *IEEE Transactions on Power Systems,* vol. 5, pp. 1455-1469, 1990.

[108] A. Ellis, M. Behnke, and C. Barker, "PV system modeling for grid planning studies," in *Photovoltaic Specialists Conference (PVSC), 2011 37th IEEE*, 2011, pp. 002589-002593.

[109] F. Fernandez-Bernal, L. Rouco, P. Centeno, M. Gonzalez, and M. Alonso, "Modelling of photovoltaic plants for power system dynamic studies," 2002.

[110] C. Min and G. A. Rincon-Mora, "Accurate electrical battery model capable of predicting runtime and I-V performance," *IEEE Transactions on Energy Conversion,* vol. 21, pp. 504-511, 2006.

[111] Z. Miao, L. Xu, V. R. Disfani, and L. Fan, "An SOC-based battery management system for microgrids," *Ieee transactions on smart grid,* vol. 5, pp. 966-973, 2014.

[112] *North American Electric Reliability Corporation Gtid Code*. Available: http://www.nerc.com/comm/PC/Integration%20of%20Variable%20Generation%20Task%20Force%20IVGT/Sub%20Teams/Interconnection/UK_Grid_Code.pdf

[113] *e.On Grid Code*. Available: http://www.nerc.com/docs/pc/ivgtf/German_EON_Grid_Code.pdf

[114] "Review of PREPA Technical Requirements for Interconnecting Wind and Solar Generation."

[115] *Common functions for smart inverters, version 3, EPRI Report 3002002233, Palo Alto, CA, 2013*. Available: https://www.epri.com/#/pages/product/3002002233/

[116] K. R. Padiyar and R. K. Varma, "Damping torque analysis of static VAR system controllers," *IEEE Transactions on Power Systems,* vol. 6, pp. 458-465, 1991.

[117] *Technical Guideline, "Generating Plants Connected to the Medium Voltage Network", BDEW, 2008,* . Available: https://www.bdew.de/internet.nsf/id/A2A0475F2FAE8F44C12578300047C92F/$file/BDEW_RL_EA-am-MS-Netz_engl.pdf

[118] T. CIGRE, "38.02. 16, Impact of the interactions among power system controls," Tech. Report 166, CIGRE2000.

[119] M. Morjaria, D. Anichkov, V. Chadliev, and S. Soni, "A Grid-Friendly Plant: The Role of Utility-Scale Photovoltaic Plants in Grid Stability and Reliability," *IEEE Power and Energy Magazine,* vol. 12, pp. 87-95, 2014.

[120] S. Achilles, S. Schramm, and J. Bebic, *Transmission system performance analysis for high-penetration photovoltaics*: National Renewable Energy Laboratory, 2008.

[121] L. Zeni, R. Eriksson, S. Goumalatsos, M. Altin, P. Sørensen, A. Hansen*, et al.*, "Power Oscillation Damping From VSC–HVDC Connected Offshore Wind Power Plants," *IEEE Transactions on Power Delivery,* vol. 31, pp. 829-838, 2016.

[122] W. Hongxia, K. S. Tsakalis, and G. T. Heydt, "Evaluation of time delay effects to wide-area power system stabilizer design," *IEEE Transactions on Power Systems,* vol. 19, pp. 1935-1941, 2004.

Curriculum Vitae

Name:	Hesamaldin Maleki
Post-secondary Education and Degrees:	Shahid Chamran University Ahwaz, Iran 2006-2010 B.A.
	The Tenaga Nasional University, Kajang, Selangor, Malaysia 2011-2013 M.A.
	The University of Western Ontario London, Ontario, Canada 2013-2017 Ph.D.
Honours and Awards:	Outstanding Presentation in Graduate Symposium 2017 2017
	Industrial Post Graduate Scholarship (NSERC) 2014-2017
	Western Graduate Research Scholarship (WGRS) 2013-2017
Related Work Experience	Teaching Assistant The University of Western Ontario 2013-2017
	Research Assistant The University of Western Ontario 2013-2017

Publications:

[1] Rajiv K. Varma, Ehsan Siavashi, **Hesamaldin Maleki**, Reza Salehi, Sibin Mohan, Mahendra A.C., S. Arifur Rahman and T. Vanderheide, "PV-STATCOM: A Novel Smart Inverter for Transmission and Distribution System Applications", Poster at the 7th International Conference on Integration of Renewable and Distributed Energy Resources", Niagara Falls, Canada, Oct. 24-28, 2016

[2] **Hesamaldin Maleki**, Rajiv K. Varma, "*Optimized coordination approach for power system stabilizer and PV-STACOM tuning in electromagnetic transient study*", Proc. IEEE Power & Energy Society General Meeting, Boston, July 2016.

[3] **Hesamaldin Maleki,** Rajiv K.Varma**, "***Comparative study for improving damping oscillation of SMIB system with STATCOM and BESS using remote and local signal",* Canadian Conference On Electrical And Computer Engineering (CCECE), Halifax, 2015.

[4] S. A. Rahman, **Hesamaldin Maleki,** S. Mohan, R. K. Varma, and W. H. Litzenberger, "*Bibliography of FACTS 2013;2014: IEEE working group report*." Proc. 2015 IEEE Power & Energy Society General Meeting, Denver.

[5] S. Mohan, **Hesamaldin Maleki**, R. K. Varma, and W. H. Litzenberger, "*Bibliography of HVDC Transmission 2013– 14 IEEE working group report*." Proc. 2015 IEEE Power & Energy Society General Meeting, Denver, pp. 1-5.

[6] **HesamAldin Maleki,** V. K. Ramachandaramurthy, M. Lak, *"Increase in Fault Ride Through Capability of 40 MW Wind Farm Connected to The Grid Using VSC-HVDC System"*, presented in UNITEN National Graduate Conference 2012 (NatGrad2012), 8 - 10 November 2012, Selangor, Malaysia

[7] H. Azad, V. Ramachandaramurthy, and H. Maleki, "*Voltage variation due to solar photovoltaic in distribution network,*" in *IOP Conference Series: Earth and Environmental Science*, 2013, p. 012092.

Awards:

1) Outstanding Presentation in Graduate Symposium 2017

2) Industrial Post Graduate Scholarship (NSERC) 2014-2017

3) Western Graduate Research Scholarship (WGRS) 2013-2017